RADIATIVE COOLING RATES IN THE PRESENCE OF ICE CRYSTAL AEROSOLS

A

DISSERTATION

Presented to the Faculty of the

University of Alaska in Partial Fulfillment

of the Requirements

for the Degree of

DOCTOR OF PHILOSOPHY

by

Sue Ann Bowling, A.B., M.S.

College, Alaska

May 1970

RADIATIVE COOLING RATES IN THE PRESENCE OF ICE CRYSTAL AEROSOLS

APPROVED:

Robert W. Brown

Norman D. Baker

Peter Allen

Wallace B. Hunsaker
Co-Chairman

Carl S. Benson
Co-Chairman

Roger Sheridan
Department Head

APPROVED: C. Blake DATE: May 7, 1970

Dean of the College of Mathematics, Physical Sciences and Engineering

E. A. Lee

Vice President for Research and Advanced Study

ABSTRACT

A method has been developed for computer calculation of radiative cooling rates within an ice fog (crystal radii 1 to 7μ, number density 100 to 1000 crystals cm^{-3}) or an ice crystal display (also called diamond dust; crystal radii 25 to 500μ, number density .01 to 1 crystals cm^{-3}). Mie scattering is assumed for the nearly spherical ice fog crystals, while diamond dust crystals,which are mainly flat plates, are considered black in the infrared. Elsasser's treatment is paralleled, with some modifications, for water vapor and carbon dioxide. The basic method is usable for almost any kind of cloud or fog, although the computer calculations become quite lengthy if both scattering and the dependence of the ice crystal parameters on wave number are considered.

Cooling rate profiles for ice crystal displays showed cooling rates, at the top of the displays, ranging from 4 to 6 °C $(12\ hr)^{-1}$ for displays having one 25μ radius crystal per cm^3 to nearly 100°C$(12\ hr)^{-1}$ for snow. Cooling rates decreased exponentially as they were calculated deeper in the display, and for snowfall even a 100 m thick layer was nearly black.

Cooling rate profiles in ice fog were computed both with the full scattering equation and with a gray-crystal approximation. Comparison of the results indicate that the small-crystal fogs typical of automobile exhaust behave similarly to a fog with crystals which are 25% black and 75% transmitting. Such thin fogs, in layers up to 20 m depth, produce a general enhancement of the cooling rate in the fog with

no particular tendency toward development of an adiabatic lapse rate. Deeper fogs with a size distribution more typical of downtown, mixed-origin ice fog gave cooling rate profiles which agreed in shape with a 75% black fog, but in magnitude with a 25% black fog. Fogs of this type with total ice contents greater than 1.4×10^{-4} gm cm^{-2} were found to produce convective lapse rates in the fog with inversions at the fog top even without considering man-made heating near the ground. If the man-made heating is considered, even thinner fogs will produce convective lapse rates.

The influence of ice fogs on radiative processes has a complex effect on the local climate of Fairbanks. The presence of ice fog enhances the heat island over the city. It also results in the development of an overall temperature structure which appears to be even more conducive to the concentration of air pollution than is the normal steep ground inversion. The result is the automatic development of the worst possible structure for air pollution at just the time when low temperatures cause peak fuel consumption.

ACKNOWLEDGEMENTS

This paper could not have been written without the help of many people. I would especially like to thank those listed here.

Mr. Wally Murcray read through each section as it was written as well as participating in many hours of discussion on how each problem that came up should be handled.

Dr. Carl Benson also went over the text in detail, and offered many suggestions for its improvement.

Dr. Robert Brown of the Mathematics department kindly took the time to check the derivations in Chapters II and III.

Dr. Tom Roberts and Dr. Gunter Weller also assisted in their capacity as committee members.

Mrs. Sharon Dean wrote the scattering program and provided much-needed assistance in writing and debugging the gray program.

Mrs. Helen Linde did an outstanding job of typing an extremely difficult manuscript. The entire Geophysical Institute steno section pitched in on the tables and corrections.

James S. Strandberg did the lettering on most of the figures, and Frank Daniels handled the photography.

Cy Backhaut "volunteered" to assist in proofreading the stencils for the entire thesis, and stuck to it even after he saw what he was getting into.

The research was supported initially by Grant 5-R01-AP-00449-03 from the National Center for Air Pollution Control, Department of Health, Education and Welfare, Public Health Service, and also by National Science Foundation Grant GA-900. Continuing support was provided by the National Air Pollution Control Administration through Grant 1-R01-AP00748-01-APC.

TABLE OF CONTENTS

TABLE OF CONTENTS (cont'd)

TABLE OF CONTENTS (cont'd)

TABLE OF CONTENTS (cont'd)

LIST OF FIGURES

LIST OF TABLES

LIST OF TABLES
(continued)

List of Symbols

This list includes most of the symbols used in this paper, together with short definitions and the page number of first use and/or full definition. It should be noted that the use of functional notation is highly variable; in order to keep the equations from becoming too cumbersome independent variables and subscripts are frequently dropped where they are not significant for a particular equation.

List of Symbols

		Page
$A(a,\theta)$	Scattering function of a single particle	34
a	Particle radius	33
B_ν, B	Blackbody flux	28
C	Dummy function	55
$\bar{C}(z_1,z_2)$	Mean cooling rate between z_1 and z_2	334
$c(z)$	Cooling rate at z	335
c	Speed of light	16
c_p	Specific heat of air at constant pressure	157
D	Defined constant	59
d_{vi}	Density of water vapor in air saturated over ice	158
E	Defined constant	59
E_ν	Monochromatic power input density	18
$\vec{E}'$	Electric field strength	339
Ei_3	Third exponential integral	28
F, $F_{\Delta\nu}$	Net flux, smoothed	27
F_ν	Net flux, monochromatic	16
$F_\int$, F	Integrated net flux	70
$F_{\nu+}$	Upward monochromatic half flux	26
$F_{\Delta\nu+}$, F_+	Upward smoothed half flux	27
$F_{\nu-}$	Downward monochromatic half flux	26
$F_{\Delta\nu-}$, F_-	Downward smoothed half flux	27
f	Dummy variable	40
$f(\phi_o, \psi_o, \phi, \psi)$	Volume scattering function	14

List of Symbols
(Continued)

		Page
G	Total smoothed flux	47
g	Dummy variable	40
H	Man-made heating	165
H'	Heat flux	161
H_F	Man-made heat term, flux units	165
h	Planck's constant	16
I_ν	Monochromatic intensity	12
$I_{\Delta\nu}$, I	Smoothed intensity	24
I_I	Integrated intensity	12
I_+, $I_{\nu+}$	Average upward intensity	20
I_-, $I_{\nu-}$	Average downward intensity	20
$I_{B\nu}$	Blackbody intensity	16
J_i	Constant of integration	49
J'_i	Constant of integration	49
K_i	Constant of integration	49
K'_i	Constant of integration	49
k	Boltzman constant (in blackbody equation only)	16
k	Volume absorption coefficient for ice crystals	237
k_a	Number absorption coefficient for ice fog size distribution a	138
k_b	Number absorption coefficient for ice fog size distribution b	138
k'	Thermal conductivity of air	161
k_ν	Monochromatic volume absorption coefficient	14
L	Generalized absorption coefficient	79
L, L_s	Latent heat of sublimation of ice	159

List of Symbols
(continued)

		Page
ℓ	Scalar distance	14
M	Ratio of ice crystal radiative to total radiative cooling	337
m	Complex refractive index	126
N	Index of top layer of atmosphere	51
n	Number density of ice crystals	33
n_a	Number density of ice crystals, distribution a	138
n_b	Number density of ice crystals, distribution b	138
n_i	Imaginary part of complex refractive index	114
n_r	Real part of complex refractive index	114
P	Pressure	89
P(a), p(a)	Normalized particle size distribution	33
$P_a(a)$	Size distribution a, auto-exhaust fog	138
$P_b(a)$	Size distribution b, mixed-origin fog	138
Q_{abs}	Mie efficiency factor for absorption	122
Q_{ext}	Mie efficiency factor for extinction	33
Q_{sca}	Mie efficiency factor for scattering	34
R	Elsasser integral	70
$\vec{r}$	Position vector	14
r	Reflectivity of ground or fog top	51
s	Smoothed volume single scattering albedo	45
s_ν	Monochromatic volume single scattering albedo	15
t	Time	157
t	Dummy variable	40

List of Symbols
(continued)

		Page
T	Temperature	16
T_g	Temperature of the ground	51
u	Amount of water vapor, liquid cm	45
u^*	Reduced amount of water vapor, liquid cm	45
V	Volume	14
V	Voltage	339
v	Amount of CO_2, cm STP	45
v^*	Reduced amount of CO_2, cm STP	45
x_ν	Optical depth	15
x_i	Value of x at lower boundary of ith layer	48
x_g	Value of x at ground	59
$\bar{x}_s$	Value of x at top of scattering layer	59
$\bar{x}$, $\bar{x}_N$	Value of x at top of atmosphere	59
y	Dummy variable	40
z	Height above ground	15
$z_g=0$	Height at ground	63
$\bar{z}_s$	Height of top of scattering layer	63
$\bar{z}$	Height of top of atmosphere	65
α	Angle between incoming ray and vertical	36
β	Volume flux backscatter	31
β_{SPP}	Fractional backscatter	22
$\beta(a)$	Monodisperse flux backscatter	33
β_a	Number flux backscatter, distribution a	145
β_b	Number flux backscatter, distribution b	145

List of Symbols
(continued)

		Page
γ	Angle from downward vertical	34
Δ	Difference	24
ϵ	A vanishingly small quantity	39
ϵ_o	Permittivity of free space	339
ϵ_ν	Monochromater volume emission rate	14
η	Dummy variable	28
θ	Scattering angle	15
κ	Smoothed volume extinction coefficient	45
κ_υ	Monochromatic volume extinction coefficient	15
λ	Wavelength	114
ν	Wave number	12
$\bar{\nu}$	Mean wave number in $\Delta\nu$	24
ν^*	Some wave number in $\Delta\nu$	73
ξ	Angle of incidence	12
ρ_{air}	Density of air	157
ρ_i	Density of pure water vapor in equilibrium with ice	159
σ	Stefan-Boltzman constant	70
σ'	Surface charge density	339
τ, $\tau_{\Delta\nu F}$	Smoothed flux transmissivity	27
τ_s, τ	Flux transmissivity modified for scattering	64
$\tau_{\Delta\nu}$	Smoothed transmissivity	24
$\left\lvert\frac{d \ln_\tau}{dz}\right\rvert$	Incremental absorptivity	25

List of Symbols

(continued)

		Page
Φ_ν, Φ	Indicatrix of scattering or phase function	15
Φ_{HG}	Henyey-Greenstein phase function	143
ϕ	Azimuthal angle	14
Ψ	Angle defined in figure II-4	36
ψ	Angle between direction of propagation and the vertical	14
Ω	Solid angle	12
$\tilde{\omega}_o$	Particle single scattering albedo	22

CHAPTER I

INTRODUCTION AND HISTORICAL BACKGROUND

Long wave or "terrestrial" radiation, with wavelengths greater than 4μ, has long been recognized as a major factor both in the total heat budget of the earth (where it must balance the absorbed portion of the incoming short wave (solar) radiation) and in the development of the temperature structure of the atmosphere (Simpson, 1927; Wexler, 1936). There are many techniques for computing radiative cooling rates in the atmosphere (Goody, 1964). But the standard computational methods do not allow consideration of cooling rates in atmospheres containing aerosols or thin clouds, as they are based entirely on radiation from water vapor, carbon dioxide and, to a lesser extent, ozone, with clouds (and usually the ground as well) considered as black bodies. Unfortunately, there are many cases, such as the ice crystal displays discussed by Gotaas and Benson (1965), which cannot be treated without considering the aerosol contribution to the atmospheric radiation. The purpose of this dissertation is to examine in detail two of these cases which are of particular importance in Interior Alaska: ice crystal displays and ice fog.

In order to provide some historical background for the mathematical treatment in Chapters II and III and for the meteorological situations in Chapter IV, the remainder of this chapter will be devoted to a qualitative discussion of some of the earlier basic literature. In section A the meteorological situations will be discussed and the problems defined. Section B will cover the development of radiative

transfer equations, while section C will cover their applications to problems in terrestrial radiation.

A. Effects of Aerosols on Cooling Rates

Dines (1931) observed that if a dense ground fog formed under strong inversion conditions, the lapse rate within the fog would be transformed to an essentially adiabatic one, with the inversion now appearing at the top of the fog layer. This phenomenon was explained by Brunt (1932) as being due to an upwards displacement of the effective radiating surface from the ground to the top of the fog layer. The same observation was made by Dobson (1948) in reference to air pollution studies.

Fleagle et al. (1952) used a greatly simplified model to calculate the effect of an essentially black ground fog on the local lapse rate. Their results confirmed Dines's suggestion. These investigators also pointed out that the type of temperature structure produced by this mechanism is one which is highly conducive to severe air pollution episodes, as the effective lifting of the inversion results in trapping of stack gases that would otherwise remain above the inversion, while still severely limiting the amount of air available for dilution. They suggested that this mechanism may have been involved in the air pollution disaster at Donora, Pennsylvania in October 1948.

Fleagle et al. (1952) pointed out that smokes, in which the particles are small compared with the peak wavelengths of the terrestrial infrared radiation at about 10-15μ would not be expected to produce as strong an effect on lapse rates as fogs with equal short wave

visibilities. In Fairbanks, Alaska, ice fogs with mean particle diameters around 5μ have been observed to develop normal lapse rates in their interiors and inversions above the fog (Robinson and Bell, 1956). Ice fog is itself a form of low-temperature air pollution, and any feedback effect affecting its severity is of great concern. Since the sizes of ice fog crystals are of the same order of magnitude as the wavelengths involved, a somewhat more complex treatment than that of Fleagle et al. (1952) must be used. Specifically, the effects of absorption and emission by water vapor, carbon dioxide and ice crystals must be considered, together with possible scattering by the ice crystals. Water droplets are generally not present in this aerosol (Ohtake, 1970) and will therefore not be considered, although an extension of the equations to cover water- or mixed-phase thin clouds would merely be a matter of recomputing coefficients. Absorption and scattering coefficients for the ice crystals will be computed (in Chapter 4) from data derived from the Mie theory (van de Hulst, 1957) for the scattering of electromagnetic radiation by uniform spheres.

Neither ice fog nor Mie scattering will be discussed extensively in this thesis; the reader desiring fuller background information on either is directed to Weller (1969) on ice fog and van de Hulst (1957) on scattering. Both works have excellent bibliographies.

A second type of radiative cooling in the presence of aerosol particles was first mentioned by Kraus (1947), who suggested that radiation from soot particles suspended in the air would increase the nocturnal cooling rate and thus enhance the probability of fog

formation in the sooty layer. Essentially the same argument was presented independently by Gotaas and Benson (1965) for ice crystal displays or "diamond dust", with plane ice crystals of radii $\sim$ 25μ and number densities $\sim$ 1 cm^{-3} replacing the soot particles and crystal growth replacing fog formation. In the usual treatment of the fog or cloud situation, radiative exchange is generally considered to be confined to the cloud boundaries. The individual crystals or droplets making up the cloud are either ignored completely or considered to be in radiative equilibrium with each other. In contrast to these assumptions, the two papers above consider particles to be mutually independent blackbody radiators, with the height of the upper boundary of the turbid layer not considered to be of any importance. As one result, the computed cooling rates in these papers are generally higher than those observed. This result is due to the neglect of overlapping of the crystals as seen from above, which for large enough thicknesses ($\sim$ 300 mb) leads to an effective radiating area greater than that of a horizontal surface. The treatment is valid for thin layers (< 500 m with the crystal sizes and densities used) where the overlap is negligible. It should be emphasized that Gotaas and Benson were considering an ice crystal display with visibility generally greater than 25 km (15 miles) not an ice fog. They did not attempt to discuss ice fog radiation.

In order to have a better idea of the extent to which ice crystal radiation actually affects cooling rates, a recomputation is needed which includes the effects of radiative interaction among crystals, and between crystals and the atmospheric gases. The ice crystal display

problem is a simplification of the one which includes ice fog, and can be handled by the same methods. Ice fog crystals are nearly spherical and have diameters in the range 2-15 μ. Mie scattering therefore applies, and as computation of the Mie efficiency factors in Chapter IV will show, scattering coefficients are similar to those for absorption.

Crystal display crystals, on the other hand, are generally well developed, symmetrical thin plates with diameters around 50 μ or more, which orient horizontally while falling slowly through the air. There is no theory available for the exact calculation of scattering and absorption coefficients, and in the absence of such a theory there is no justification for considering anything more complex than the first-order approximation of black, non-scattering crystals. This assumption is supported by the more nearly exact calculations for ice fog, which demonstrate the increasing approach to blackness of the larger crystals, and by the computations of Skekhter (1966) for cloud droplets. Again we will consider only water vapor, carbon dioxide and ice crystals, and assume that any water droplets present will either freeze or evaporate so quickly that their equilibrium concentration is negligible.

To recapitulate, our basic problem is to find or adapt a radiative transfer equation which will include the effects of absorption, emission and scattering of radiation, find the coefficients of absorption and scattering for ice fog, and solve this equation for the energy flux as a function of height both inside and outside of the layer containing ice crystals.

B. Equations of Radiative Transfer

There are at least two basic situations in which radiative transfer equations may be useful. In the first situation the composition, temperature and pressure are known functions of position, and the determination of the energy transfer, and specifically the cooling due to energy divergence owing to radiative processes is the result desired. This has generally been the situation of interest to the meteorologists, and more recently of those planetary astronomers interested in the meteorology of other planets (Sagan, 1969; Pollack, 1969A and 1969B). The main concern in this case is the energy transport, which involves integration over both wavelength and angle; furthermore the resulting equations should be applicable to a variety of situations. As a result, most of the meteorological radiative transfer equations are basically simplified applications of those developed for astrophysical purposes. Some of the history of these applied equations will be covered in section C.

The second situation, (and the one which produced the results which will be discussed in this section) is that in which the information received from some distant object consists largely or entirely of the spectral and spatial distributions of electromagnetic radiation. (The spatial distribution may imply an angular distribution if the shape of the object is known; e.g., Limb Darkening of the Sun.) Here the problem is to construct a model for the composition, temperature distribution, size etc. of the distant object, and use the equations of radiative transfer to compare the radiation which should be received from the model with that actually observed. Historically this has been the method of the astronomers, particularly the astrophysicists and planetary

astronomers; and more recently it has been the approach of those meteorologists whose primary interest is the interpretation of satellite data. As a general rule, this approach requires equations which are valid for a specific direction and wavelength (although boundary conditions may involve energy integrated over angles and/or wavelength) and it has produced most of the more nearly exact equations.

One of the early pioneers in radiative transfer equations was Schuster (1905), who derived a pair of one-dimensional transfer equations which included the effects of isotropic scattering, absorption and emission. He also solved these equations for the isothermal case (black-body emission invarient with height) and the special case in which the black-body emission varies linearly with height, (note this does not imply a linear variation of temperature) and used his results to explain the shapes of some of the lines in the solar spectrum.

Schuster's work is normally considered together with that of Schwarzschild (Milne, 1923) who made calculations for a pure scattering atmosphere. Milne (1923), using the work of both men, formulated the full equations of radiative transfer (neglecting the effects of polarization) for a plane-parallel, gray atmosphere with absorption, emission and isotropic scattering. He also provided approximate solutions for the full equation.

The culmination of this line of work, and the primary reference in the field today, is Chandrasekhar (1950). Additional basic references include Kourganoff (1952) and Sobolev (translation 1963); van de Hulst (1957) is the basic reference on scattering. King (1968 gives a historical outline of the development of radiative transfer equations.

Recent astronomical applications which bear on our problem include Sagan and Pollack (1967) and Potter (1969) on the possibility of ice clouds on Venus and Irvine (1965), who suggests that the errors involved in ignoring the effects of polarization may be neglected for particles of dimensions comparable to the wavelength. Studies aimed towards the interpretation of terrestrial satellite data include a simple treatment of cirrus clouds by Zoumkowski et al., (1965) as well as considerably more complex studies by Samuelson (1965) and Sekera (1968).

C. Studies of Radiative Cooling

The first investigators to attempt to use infrared fluxes to explain the observed temperature structure of the terrestrial atmosphere were Humphreys and Gold in 1909 (King, 1968). They assumed radiative equilibrium and a gray atmosphere and, although their computed vertical temperature gradient more or less agreed with observations, their latitudinal gradient had the wrong sign. They were followed by Emden (King 1968) and by Simpson (1927).

Simpson (1928a) first emphasized the importance of using at least an approximation of the water vapor and carbon dioxide spectra, as his 1927 computations with a gray atmosphere indicated that the atmosphere would be unable to adjust its radiative output to space in response to variations in the solar input. (Essentially the same result has recently been re-derived by Ingersoll (1969) for the case where the water vapor content and/or cloudiness is so great that the atmosphere is essentially opaque even in the 8-12 μ "window" region, and used to explain the apparent current shortage of water vapor on Venus.) Simpson's method

involved assuming that radiation from the earth to space was essentially directly from the ground in the 8½-11 μ window, from the stratosphere from 5 to 7 μ and at wavelengths beyond 14 μ. For the intervals 7-8½ μ and 11-14 μ the outgoing radiation is taken to be the average of that from the ground and that from the stratosphere. This scheme allowed computation of outgoing radiation as a function of latitude, and the first good estimate of the earth's heat balance (Simpson, 1928a).

These early papers were generally concerned with equilibrium temperature or (as in Simpson's heat balance study) with deducing the necessary heat transport when solar and terrestrial radiation did not balance locally. According to Möller (1951) Mügge and Möller developed a radiation chart as early as 1932. Wexler (1936) referenced Mügge and Möller but used Simpson's technique in his classic paper on the formation of continental polar air. He described the nocturnal cooling of an air column by radiation in wavelengths outside the "window" to an underlying snow surface which in turn was radiating to space through the window. Elsasser (1942) published the first detailed radiation chart available in English, while the version of Möllar's chart most often referenced was published (in Germany) in 1943 (Möller, 1951).

During the next twenty years a variety of computational methods for atmospheric radiation were derived (e.g., D. Brooks, 1950; F. Brooks, 1952; Yamamoto, 1952 and 1953; Elsasser and Culbertson, 1960). More recently, several papers and books have been published comparing the various methods in use and reconsidering the theories behind many of the simplifications (Goody, 1964; Kondrat'yev, 1965; Atwater, 1966; Rodgers and Walshaw, 1966). However, these authors are almost unanimous in their treatment of clouds (if at all) as black bodies.

Hewson (1943) had modified Schuster's equation to allow for absorption and scattering of visible light in clouds. Fleagle et al. (1952) treated the case of an absorbing and emitting layer under very simple assumptions (basically, a gray atmosphere and essentially black fog). But the first serious treatment of clouds as layers which might transmit and reflect, as well as absorb and emit, infrared radiation was by Havard (1960). Havard computed the effective reflectivity, transmissivity and absorptivity at several infrared wavelengths of water clouds of varying thicknesses with Mie-scattering droplets. He did not include emission, nor did he attempt to set up transfer equations which would be valid in the interiors of his reflecting and transmitting clouds.

Godson (1965) included the effect of a "turbid layer" with both scattering and absorption near the ground in a treatment otherwise similar to Simpson's (1928). His results were similar to those of Fleagle et al., (1952) with enhanced cooling near the top of the turbid layer. Zdunkowski et al. (1966) considered the effect of a thin haze layer near the ground, using spectrally averaged values of H_2O and haze transmissivities, and found only slight enhancement of cooling rates

In the Russian literature, Grosheva (1966) and Petrova and Feigelson (1966) have considered some of the effects of thermal radiation on low clouds, while Shekhter (1966) presents and solves equations for fluxes in the presence of emitting, absorbing and scattering clouds. Shekhter did not try to obtain flux divergences inside the clouds, but did compute the apparent emissivities, absorptivities and reflectivities of cloud layers.

On the basis of Shekhter's paper, it would seem that the Russian literature on practical equations for infrared transfer in cloudy atmospheres may be somewhat ahead of the English. Unfortunately, very little of it is available in translation, and the original Russian is difficult to follow at best, especially when symbols are used which appear to be standard in Russian (but not in English) without full definitions. Our flux backscatter (defined in Chapter II) appears to be different from anything used by Shekhter, although the incomplete definition of some key symbols in his derivation of coefficients make this section of his paper difficult to interpret.

Shekhter's basic equations are the same as those used in this paper and his method of solution is similar. We will apply our boundary conditions in a somewhat different manner, and since we are working entirely over snow surfaces, which are among the blackest of natural surfaces in the infrared, we will be able to neglect the infrared reflectivity of the ground. In addition, Shekhter used an exponential transmissivity curve for water vapor and neglected carbon dioxide; we will use Elsasser's (1960) smoothed absorption curves for both gases.

CHAPTER II

DERIVATION OF EQUATIONS AND COEFFICIENTS

In order to handle the general problem of radiative cooling in the presence of suspended ice crystals, we need an equation for the integrated flux divergence in a medium with absorption, emission and scattering, all varying with frequency. Several equations are available in the literature, although none are exactly suitable for our purposes as they stand. Rigorous derivations which are widely available in the literature will not be repeated but instead we confine ourselves to definition of the physical parameters and coordinate systems used and to brief discussions of the physical meaning behind each equation. We will then consider the requirements of our particular case in selecing and modifying an equation of transfer and deriving the coefficients we will need.

A. The Exact Equation

Consider a narrow pencil of radiation, confined to the very narrow wave number interval ν to $\nu + d\nu$, with directions of propagation confined within a small solid angle $d\Omega$, incident upon a unit area the normal to which is at an angle ξ to the direction of propagation (Figure II-1). The monochromatic intensity I_ν is then defined by setting the energy transport across the unit area per unit time equal to $I_\nu d\Omega d\nu \cos\xi$ (Chandrasekhar, 1950). I_ν has the dimensions of energy time^{-1} solid angle^{-1} area^{-1} wave number interval^{-1}, and we will express it in gcal (12 hr)$^{-1}$ stearadian^{-1} cm^{-1} (the area and wave number combine to give the last term). The integrated intensity $I_\int$ is given by $I_\int = \int_0^\infty I_\nu d\nu$.

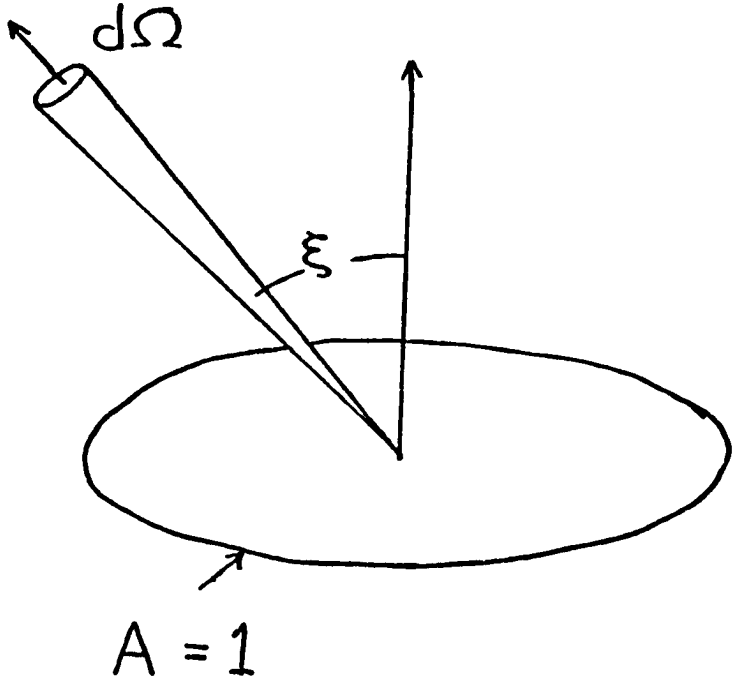

II-1 Geometry of the intensity definition. After Chandrasekhar (1950).

I_ν will in general be a function both of position in space, $\vec{r}$, and of direction. We will follow Irvine (1965) and neglect polarization. ϕ is the azimuthal angle (measured counterclockwise) of the direction of propagation, and ψ is the angle between the direction of propagation and the vertical.

Consider a beam of intensity $I_\nu(\vec{r}_o,\phi_o,\psi_o)$ as it traverses a small volume dV of thickness $d\ell$ and area $\frac{dV}{d\ell}$ centered at $\vec{r}_o$. An amount $I_\nu k_\nu dV$ of the incident radiation $I_\nu \frac{dV}{d\ell}$ will be absorbed, where k_ν is the absorption coefficient. In addition, an amount of radiation $I_\nu(\phi_o,\psi_o)dVf(\phi_o,\psi_o,\phi,\psi)d\Omega$ will be scattered out of the direction of incidence ϕ_o,ψ_o into the solid angle $d\Omega$ in the direction ϕ,ψ; while an amount $I_\nu(\phi,\psi)dVf(\phi,\psi,\phi_o\psi_o)d\Omega$ will be scattered from each $d\Omega$ into ϕ_o,ψ_o. Finally, the volume dV may contain radiation sources whose contribution we will denote by $\varepsilon_\nu(\vec{r}_o,\phi_o,\psi_o)dV$, where ε_ν is the volume emissivity for wave number ν to $\nu + d\nu$. Combining these terms and dividing by dV, we get the basic equation of radiative transfer:

$$\frac{dI_\nu}{d\ell} = - k_\nu I_\nu(\vec{r}_o,\phi_o,\psi_o) - I_\nu(\vec{r}_o,\phi_o,\psi_o) \int_{4\pi} f(\phi_o,\psi_o,\phi,\psi)d\Omega + \int_{4\pi} I_\nu(\vec{r}_o,\phi,\psi)\, f\,(\phi,\psi,\phi_o,\psi_o)d\Omega + \varepsilon_\nu(\vec{r}_o,\phi_o,\psi_o). \qquad (2\text{-}1)$$

We will refer to k_ν as the volume absorption coefficient*, and to $\int_{4\pi} f(\phi_o,\psi_o,\phi,\psi)d\Omega$ as the volume scattering coefficient. Both of these quantities will in the most general case (as in our horizontally oriented ice crystal display) depend on $\vec{r}_o$, ϕ_o,ψ_o and the polarization of the

*Note that in this definition we do not follow Chandrasekhar, whose absorption coefficient corresponds to our extinction coefficient. Nomenclature in radiative transfer problems is confused at best.

incident radiation. However, we will completely neglect the polarization (Irvine, 1965). For convenience we can define a volume extinction coefficient κ_ν, where $\kappa_\nu = k_\nu + \int f(\phi_o,\psi_o,\phi,\psi)d\Omega$. Simultaneously we define the volume single scattering albedo, s_ν, by the relationship $s_\nu = \frac{\int f_\nu(\vec{r},\phi_o,\psi_o,\phi,\psi)d\Omega}{\kappa_\nu}$, and the indicatrix of scattering (or phase function) by $\Phi_\nu(\vec{r},\phi_o,\psi_o,\phi,\psi) = \frac{f_\nu(\vec{r},\phi_o,\psi_o,\phi,\psi)}{\int_{4\pi} f_\nu(\vec{r},\phi_o,\psi_o,\phi,\psi)d\Omega}$. Note that from basic optics $\Phi_\nu(\phi_o,\psi_o,\phi,\psi) = \Phi_\nu(\phi,\psi,\phi_o,\psi_o)$. Finally, we define an optical depth x_ν by the relationship $dx_\nu = \kappa_\nu dz$, where z is the vertical coordinate. We can now rewrite (2-1) as

$$\cos\psi_o \frac{dI_\nu(\vec{r}_o,\phi_o,\psi_o)}{dx_\nu} = - I_\nu(\vec{r}_o,\phi_o,\psi_o,) + s_\nu (\vec{r}_o,\psi_o,\phi_o) \int_{4\pi} I_\nu(r_o,\phi,\psi)\Phi(\phi_o,\psi_o,\phi,\psi)d\Omega + \frac{\varepsilon_\nu(\vec{r}_o,\phi_o,\psi_o)}{\kappa_\nu}. \quad (2\text{-}2)$$

We can simplify this equation still further by introducing some assumptions about the physical problem, which up until now has been quite general. We will consider a plane parallel geometry, with spatial dependence on z only. In addition, we will assume that all incident light, and thus all light within our medium, is independent of ϕ. Finally, we will make an assumption which will not hold for the case of oriented scatterers such as plane snowflakes but will hold for spherical or randomly oriented particles, such as ice fog crystals, and require that both the absorption and scattering processes in an elementary volume are independent of direction of incidence. This last requirement means that $\Phi_\nu(\vec{r},\phi_o,\psi_o,\phi,\psi)$ becomes a function only of z and θ, where θ is the angle between the directions defined by ϕ_o,ψ_o, and by ϕ,ψ. θ is defined by

the spherical trigonometry relationship $\cos\theta = \cos\psi\cos\psi_o + \sin\psi\sin\psi_o\cos(\phi-\phi_o)$. If we assume that our medium is in local thermodynamic equilibrium, we can also say that $\varepsilon_\nu(\vec{r},\phi_o,\psi_o) = k_\nu I_{B\nu}(T(\vec{r}))$, where $T(\vec{r})$ is the temperature in °K at $\vec{r}$, and $I_{B\nu}$ is the blackbody intensity, $\frac{1}{\pi}\frac{2\pi hc^2\nu^3}{(\exp\frac{hc\nu}{kT}-1)}$ (h is Planck's constant, k is the Boltzman constant, and c is the speed of light). Equation (2-2) then simplifies to:

$$\frac{\cos\psi_o}{\kappa_\nu}\frac{dI_\nu(z,\psi_o)}{dz} = -I_\nu(z,\psi_o) + s_\nu(z)\int_{4\pi} I_\nu(z,\psi)\,\phi_\nu(\theta)d\Omega + (1-s)\,I_{B\nu}(T(z)) \quad (2\text{-}3)$$

What we wish to know is not the intensity as such, but the rate at which the combined intensities in all directions add energy to the medium (or remove it). Suppose we consider a horizontal, coin shaped volume dV of unit area and thickness dz, with its lower surface at $z = z_o$. The independence of I_ν from ϕ assures that the net energy transfer across the vertical sides is zero, so we need consider only the energy transfer across the two horizontal faces.

We will define the monochromatic net flux, F_ν as the energy transfer from the lower to the upper side of a horizontal unit area due to electromagnetic radiation in the wave number interval ν to $\nu + d\nu$, divided by $d\nu$. The energy transfer due to the incident radiation between the cones defined by ψ and $\psi + d\psi$, spanning a solid angle of $2\pi\sin\psi d\psi$, is (in our azimuth independent case) equal to $\int_0^{2\pi}(I_\nu(z,\psi)\cos\psi\sin\psi d\psi)d\phi = 2\pi I_\nu(z,\psi)\cos\psi\sin\psi d\psi d\nu$ (Fig. II-2). The monochromatic net flux F_ν is then

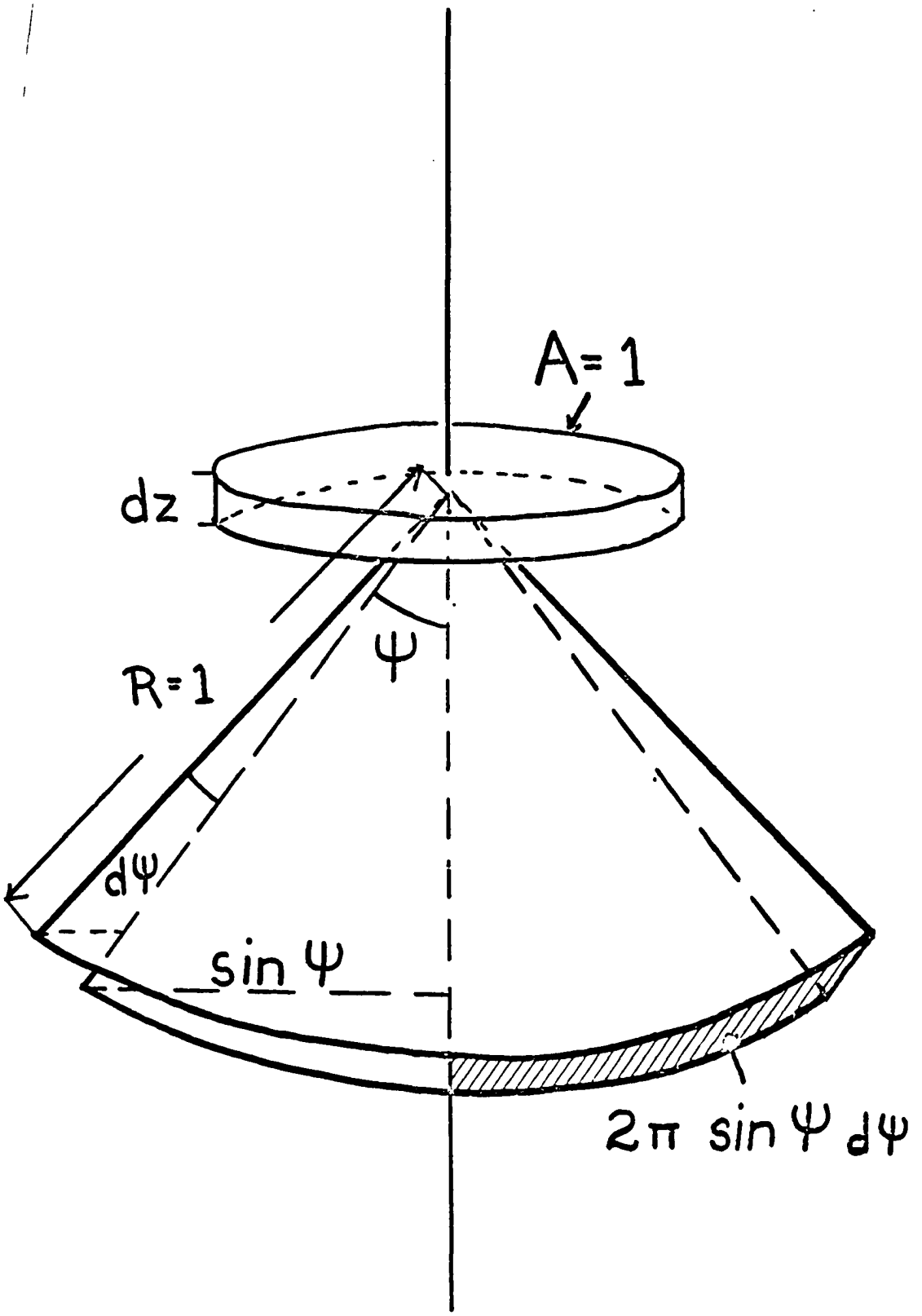

II-2 Geometry of the relationship between flux and intensity.

given by $F_\nu = 2\pi \int_0^\pi I_\nu(z,\psi)\cos\psi\sin\psi d\psi$.

The energy flux into the volume dV through the lower surface is then $\left\{\int_0^\pi 2\pi I_\nu(z_o,\psi)\cos\psi\sin\psi d\psi\right\}d\nu$ and that coming in through the upper surface is $-\left\{\int_0^\pi 2\pi I_\nu(z_o+dz,\psi)\cos\psi\sin\psi d\psi\right\}d\nu$. Dividing by $dvdz$ to obtain the energy input per unit volume per unit time per unit frequency interval, E_ν, we get

$$E_\nu = -\int_0^\pi 2\pi \frac{dI_\nu(z,\psi)}{dz}\sin\psi\cos\psi d\psi = -\frac{dF_\nu}{dz} \qquad (2\text{-}4)$$

Now if we similarly integrate equation (2-3) over solid angle, we get

$$-\int_0^\pi 2\pi \frac{dI_\nu(z,\psi_o)}{dz}\sin\psi_o\cos\psi_o d\psi_o = \kappa_\nu \int_0^\pi 2\pi\sin\psi_o\, I_\nu(z,\psi_o)d\psi_o$$

$$(2\text{-}5)$$

$$-\kappa_\nu s_\nu(z)2\pi \int_0^{2\pi}\int_0^\pi\int_0^\pi I_\nu(z,\psi)\Phi(\theta)\sin\psi_o d\psi_o \sin\psi d\psi d\phi - \kappa_\nu(1-s)I_{B\nu}(T(z))4\pi=k$$

The pair of equations (2-3) and (2-5) has the major advantage of being exact within the relatively non-restrictive physical limitations imposed during the derivation. Unfortunately, they are not practical to solve in any but a few, rather simple cases which are not of interest to us. Chandrasekhar (1950) has introduced a method of solving (2-3) by replacing I_ν as a continuous function of ψ by a discrete series of values for different directions. Equation (2-3) then becomes a series of simultaneous linear differential equations. In a case where the absorption and scattering coefficients either do not vary or vary quite slowly with frequency and height, this approach might be worthwhile. But in a case where these coefficients vary significantly with frequency (as is

true in the water vapor and carbon dioxide infrared spectra) the requirements that the solutions be made at frequency intervals which are small compared with the interval between spectral lines makes it highly impractical to use this nearly exact solution (which only neglects polarization effects). We will therefore confine ourselves to the types of approximate solutions known collectively as two-stream approximations. Chandrasekhar's multiple stream technique was based on the generalization of these early methods.

B. The Schuster-Schwarzschild and SPP Approximations

The two-stream approximation is the equation introduced in 1905 by Schuster and modified in 1906 by Schwarzschild (Chandrasekhar, 1950). We will refer to this approximation as the Schuster-Schwarzschild equation, leaving the term "two-stream approximation" to refer to the more general family of approximations which follow Schuster and Schwarzschild in splitting the radiation field into upward and downward streams. Only the principle of the Schuster-Swarzschild equation will be of interest to us.

The two-stream approximation as given by Chandrasekhar (1950) may be obtained by considering the simplest possible case of equation (2-3), with no emission, no absorption and isotropic scattering. In this case $s = 1$, and $\Phi = \frac{1}{4\pi}$, so that (2-3) becomes

$$\cos\psi_o \frac{dI_\nu(z,\psi_o)}{dx_\nu} = - I_\nu(z,\psi_o) + \frac{1}{2}\int_0^\pi I_\nu(z,\psi)\sin\psi d\psi \qquad (2\text{-}6)$$

We are not interested in knowing the angular distribution of radiation, but wish to know only the vertical flux. Assume average monochromatic

intensities $I_{\nu+}$ in the upward hemisphere (propagating upward from the lower hemisphere) and $I_{\nu-}$ in the lower hemisphere (propagating downward from the upper hemisphere). Exactly what relationship these "average intensities" have to the true intensity distribution is never clearly defined). We will assume that the average propagation law is the same as would be observed for a ray at the average angle ψ_o ($\cos\psi_o = \pm\frac{1}{2}$). We then have the Schuster-Schwarzschild equations,

$$\frac{1}{2}\frac{dI_{\nu+}(z)}{dx_\nu} = -I_{\nu+}(z) + \frac{1}{2}(I_{\nu+} + I_{\nu-}) = -\frac{1}{2}(I_{\nu+} - I_{\nu-})$$

$$-\frac{1}{2}\frac{dI_{\nu-}(z)}{dx_\nu} = -I_{\nu-}(z) + \frac{1}{2}(I_{\nu+} + I_{\nu-}) = \frac{1}{2}(I_{\nu+} - I_{\nu-}) \qquad (2\text{-}7)$$

from which $F_\nu = 2\pi I_{\nu+}\int_0^{\pi/2} \sin\psi\cos\psi d\psi + 2\pi I_{\nu-}\int_{\pi/2}^{\pi} \sin\psi\cos\psi d\psi = \pi(I_{\nu+} - I_{\nu-})$

and $\frac{1}{\kappa}\frac{dF_\nu}{dz} = -\frac{1}{2}(I_{\nu+} - I_{\nu-}) + \frac{1}{2}(I_{\nu+} - I_{\nu-}) = 0$. As a matter of fact this last result follows directly from the no absorption-no emission condition in the initial derivation. Obviously the restricted case considered by this equation is of no use in flux divergence calculations.

Schuster's original paper (1905) considered the more general case including absorption and emission, but with the scattered light equally divided between the forward and backward hemispheres. His derivation is as follows:

> 3. Let (Fig. I) S_1S_2 be a surface sending out the radiation S, and let this radiation after passing through part of the foggy atmosphere be reduced to a value A and fall on a thin layer of thickness dx. The effect of the layer is to absorb energy amounting to $\kappa A dx$, and additionally to reduce the incident light by a quantity $sAdx$, which is not absorbed, but sent in equal amounts backward and forward as scattered light. If the stream

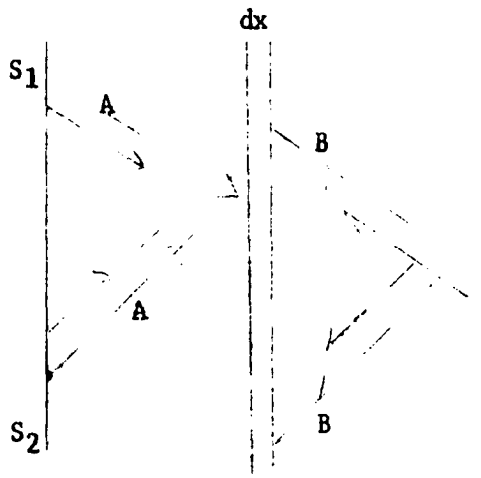

Fig. I.

of radiant energy in the opposite direction is B, we have similarly a diminution of energy equal to $(\kappa+s)$ B, of which, however, $\frac{1}{2}sB$ is sent both forward and backward as scattered light. The layer also radiates energy in both directions equal to $\kappa E dx$. Collecting these effects, we obtain the equations:

$$\frac{dA}{dx} = \kappa(E - A) + \frac{1}{2} s(B - A) \tag{1}$$

$$\frac{dB}{dx} = \kappa(B - E) + \frac{1}{2} s(B - A) \tag{2}$$

Combining (1) and (2) we find:

$$\frac{d(A + B)}{dx} = (\kappa + s)(B - A) \tag{3}$$

$$\frac{d(A - B)}{dx} = 2\kappa E - \kappa(A + B). \tag{4}$$

Differentiating (3) and with the help of (4)

$$\frac{d^2(A + B)}{dx^2} = \kappa(\kappa + s)(A + B - 2E) \tag{5}$$

If E is constant or varies uniformly with x, the last equation may be integrated, and we derive:

$$(A + B - 2E) = Ke^{(\kappa + s)ax} + K_1 e^{-(\kappa + s)ax} \tag{6}$$

where K and K_1 are two constants, (Shuster, 1905).

(In Schuster's notation κ is the absorption coefficient, s the scattering coefficient, and E the blackbody emission, and $a = \sqrt{\kappa/(\kappa + s)}$

The idea of splitting the flux into two streams has led to many of the theories in use today, and is particularly attractive where the objective is the flux divergence in a stratified medium. However, there are two problems in using exactly this set of equations for our purposes. First, scattering from particles of sizes comparable with the wavelength of the radiation has a pronounced forward peak. This problem was considered by Sagan and Pollack (1967) and will be discussed below. Second, the equations are of mixed form, the absorption and emission being set up as intensities while the scattering is realistic only for fluxes. Schuster was well aware of this problem, and even suggested that it might be taken care of by allowing the absorption coefficient to vary with distance. This is essentially what Elsasser does, and will be covered in section C.

Sagan and Pollack (1967) introduced a two-stream equation, based partly on previous work by Piotrowski, which will be of considerable use to us. This equation, referred to by Irvine (1968) as the SPP (Sagan-Pollack-Piotrowski) or modified two-stream approximation, has three departures from the original two-stream equation. (1) The average value of $\cos\psi$, given as $\frac{1}{2}$ in the Schuster-Schwarzschild equation, is corrected to Chandrasekher's (1950) value of $1/\sqrt{3}$. (This value allows for the weighting of $\cos\psi$ by the solid angle increment.) (2) Absorption is allowed for through the use of the single scattering albedo $\tilde{\omega}_o$, which gives the probability that a photon interacting with a particle will be scattered rather than absorbed. (3) Non-isotropic scattering is allowed through the use of a factor β_{SPP} which gives the fraction of the scattered light scattered into the hemisphere (upper or lower) from which the radiation is incident. Their equations are:

$$\frac{1}{\sqrt{3}} \frac{dI_{\nu+}}{dx_\nu} = - I_{\nu+} + I_{\nu+} \tilde{\omega}_o (1 - \beta_{SPP}) + I_{\nu-} \tilde{\omega}_o \beta_{SPP},$$

$$- \frac{1}{\sqrt{3}} \frac{dI_{\nu-}}{dx_\nu} = - I_{\nu-} + I_{\nu+} \tilde{\omega}_o (1-\beta_{SPP}) + I_{\nu+} \tilde{\omega}_o \beta_{SPP}, \qquad (2\text{-}8)$$

with $\beta_{SPP} = \frac{1}{2} - \frac{1}{2} \int_0^\pi \Phi(\theta) \cos\theta \sin\theta \frac{d\theta}{2}$.

This β_{SPP} was derived from approximate analogy with a case presented by Piotrowski for which the exact solution was known.

The final equation (2-8) appears quite useful in its intended field of planetary physics (Irvine, 1968). However, as it stands it is unsuitable for flux divergence calculations, as it does not allow for emission by the medium. Consequently, the flux divergence as calculated from (2-8) would always be ≤ 0, as may be seen by adding the two equations (2-8), remembering that by definition $\tilde{\omega}_o \leq 1$. It would be preferable to use upward and downward fluxes rather than the somewhat nebulous average intensities, which make the calculation of the correct form of β_{SPP} unnecessarily difficult. Finally, this equation is again accurate when used over a very narrow frequency interval, and the required numerical integration thus would require an extremely large number of steps.

In order to make use of this equation, we must combine it with techniques used when integrated flux divergence is the major consideration, and scattering may be neglected. With this in mind, let us consider Elsasser's (1942), and Elsasser and Culbertson's (1960) treatment of atmospheric fluxes.

C. Elsasser Approximation

Unlike the astrophysicists and planetary astronomers who developed most of the equations above, Elsasser was primarily interested in infrared transfer in the atmosphere of the earth. His treatment was thus

aimed at the computation of integrated fluxes, which is what we want, except that he considered only the non-scattering case, while we intend to include scattering. His methods of smoothing over frequency and handling flux transmission will be used, as well as his smoothed absorption parameters for water vapor and carbon dioxide and a good deal of his notation. First we will consider frequency smoothing.

One of the major problems with all of the approaches we have considered to this point is that they are valid only over frequency ranges within which the changes in the values of the optical properties of the medium are negligible. In order to obtain the integrated flux divergence, a complex numerical integration over several thousand or even tens of thousands of frequency intervals is required after solving the basic equations. In practice this is not feasible. Elsasser's approach was to perform the integration over wave number in two steps.

It is easy enough to show that in the absence of scattering and emission equation (2-3) has, for a vertical beam, the solution $I_\nu(z) = I_\nu(z_o)e^{-\left|\int_{z_o}^{z} k_\nu dz\right|}$. We are not interested in the monochromatic intensity I_ν, but rather an intensity $I_{\Delta\nu} = \frac{1}{\Delta\nu}\int_{\Delta\nu} I_\nu d\nu$, where $\Delta\nu$ is large compared with the line spacing in the spectral region considered, but small compared with major changes in the blackbody intensity. We will refer to $I_{\Delta\nu}$ as the "smoothed" intensity to distinguish it from the monochromatic and integrated quantities, and use the symbol $\bar{\nu}$ to indicate the mean value of ν in $\Delta\nu$. Let a beam of smoothed intensity $I_{\Delta\nu}(z_o)$ be incident at angle ψ from the vertical on a non-scattering, non-radiating layer of thickness $|z-z_o|$. We will then have emergent radiation

$$I_{\Delta\nu}(z) = \int_{\Delta\nu} \frac{I_\nu(z_o)e^{-\int_{z_o}^{z} k_\nu dz \sec\psi}}{\Delta\nu} d\nu = I_{\Delta\nu}(z_o)\,\tau_{\Delta\nu}(z,z_o,\psi), \qquad (2\text{-}9)$$

where τ is an as yet undefined function.

If our initial $I_{\nu o}$ is well defined over $\Delta\nu$, and if k_ν is a known function of z and ν, then $\tau_{\Delta\nu}(z)$ is a well defined function of $z, k_\mu(z)$, ψ, $\Delta\nu$, and $\mathfrak{V}$ even though it is no longer an exponential. Equation (2-9) may be considered the defining equation of $\tau_{\Delta\nu}$.

Since $\tau_{\Delta\nu}$ is well defined, we can define also an incremental absorptivity corresponding to the monochromatic real volume absorption coefficient, k_ν. The major difference between the incremental absorptivity and k_ν is that the incremental absorptivity depends directly on z as well as on the integrated absorber density. The upward intensity at z is $I_{\Delta\nu o}\tau_{\Delta\nu}(z,z_o)$, and at $z + \Delta z$ it is $I_{\Delta\nu o}\tau_{\Delta\nu}(z + \Delta z, z_o)$. Then the incremental absorptivity, defined as $\lim_{\Delta z \to o} \frac{I(z) - I(z + \Delta z)}{I(z)\Delta z}$ can be seen to be

$$\lim_{\Delta z \to o}\left\{ - \frac{I_{\Delta\nu o}[\tau_{\Delta\nu}(z + \Delta z, z_o) - \tau_{\Delta\nu}(z,z_o)]}{I_{\Delta\nu o}\,\tau_{\Delta\nu}(z,z_o)\Delta z} \right\} = - \frac{d \ln \tau_{\Delta\nu}}{dz} .$$

Similar computations for the downward case indicate that the simplest way to generalize this expression to both cases without a great deal of confusion on signs is to use absolute value brackets and state that the incremental absorptivity (corresponding to $k_{\Delta\nu}$) may be written as

$$\left| \frac{d \ln \tau_{\Delta\nu}}{dz} \right| .$$

The actual means of computation of $\tau_{\Delta\nu}(z,z_o)$ will be deferred to the last section of this chapter. For the present it will suffice to point out that Elsasser considered both theoretical and experimental means of obtaining $\tau_{\Delta\nu}(z,z_o)$, and presents in his more recent monograph (Elsasser and Culbertson, 1960) all necessary data for the computation of $\tau_{\Delta\nu}$ due either to water vapor or to carbon dioxide, under the

assumption that the incident radiation is independent of wave number. This last assumption may be questioned, particularly in the case of downward atmospheric radiation where the sources are the absorbing gases. Indeed, this assumption may be one of the major sources of error in this type of computation (see Goody, 1964). Since laboratory measurements are most easily made with frequency-independent sources, the transmissivity for a frequency-independent source is the one most often used for atmospheric computations. The presence of large number of ice crystals radiating without line structure will if anything tend to improve the approximation.

There is one further problem in that the path length actually traveled by a photon between two points in the presence of scattering will in general be increased over the straight-line distance. This will be discussed in Chapter III.

The second major point at which we find Elsasser's work helpful is in its treatment of the integration over solid angle. We have already made the assumption that I_ν is independent of ϕ, and have defined

$$F_\nu = 2\pi \int_0^{\pi/2} I_\nu(z,\psi)\sin\psi\cos\psi d\psi + 2\pi \int_{\pi/2}^{\pi} I_\nu(z,\psi)\sin\psi\cos\psi d\psi.$$

Let

$$2\pi \int_\nu^{\pi/2} I_\nu(z,\psi)\sin\psi\cos\psi d\psi = F_{\nu+}$$

and (2-10)

$$-2\pi \int_{\pi/2}^{\pi} I_\nu(z,\psi)\sin\psi\cos\psi d\psi = F_{\nu-}$$

The negative sign in the last equation is introduced solely to make $F_{\nu-}$ a positive quatity, as is customary in radiative transfer problems. Analogously, we can define

$$F_{\Delta\nu+} = 2\pi \int_0^{\pi/2} I_{\Delta\nu}(z,\psi)\sin\psi\cos\psi d\psi, \text{ etc.}$$

If we know how $I_{\Delta\nu}$ (or I_ν) depends on ψ at some height z, we can find $F_{\Delta\nu+}$ at z and at $z' > z$. We know

$$I_{\Delta\nu}(z',\psi) = I_{\Delta\nu}(z,\psi)\tau_{\Delta\nu}(z',z, \sec\psi)$$

$$F_{\Delta\nu+}(z) = 2\pi \int_0^{\pi/2} I_{\Delta\nu}(z,\psi)\sin\psi\cos\psi d\psi,$$

from which

$$F_{\Delta\nu+}(z') = 2\pi \int_0^{\pi/2} I_{\Delta\nu}(z,\psi)\tau_{\Delta\nu}(z',z,\sec\psi)\sin\psi\cos\psi d\psi$$

$$= F_{\Delta\nu+}(z)\ 2\pi \int_0^{\pi/2} \frac{I_{\Delta\nu}(z,\psi)}{F_{\Delta\nu+}(z)}\ \tau_{\Delta\nu}(z',z,\sec\psi)\sin\psi\cos\psi d\psi$$

$$= F_{\Delta\nu+}(z)\ \tau_{\Delta\nu F}(z',z),$$

where

$$\tau_{\Delta\nu F}(z',z) = \frac{2\pi}{F_{\Delta\nu+}(z)} \int_0^{\pi/2} I_{\Delta\nu}(z,\psi)\ \tau_{\Delta\nu}(z,z',\sec\psi)\ \sin\psi\cos\psi d\psi.$$

The above line contains the defining equation for $\tau_{\Delta\nu F}(z',z)$ which is called the flux transmissivity or slab transmissivity.

There are two obvious possibilities for the dependence of $2\pi \frac{I_{\Delta\nu}(z,\psi)}{F_{\Delta\nu+}(z)}$ on ψ, both of which were considered by Elsasser. The first, mentioned only in his 1947 paper, considered the angular distribution of $I_{\Delta\nu}$ to be that emitted by a thin horizontal sheet. This solution was not applied in practice. The second distribution, and the one actually used by Elsasser, was the hemi-isotropic flux, in which $I_{\Delta\nu}$ is independent of ψ within a hemisphere and allowed to vary only as ψ passes through $\pi/2$. In this case we have already shown (see equation immediately following (2-7)) that $F_{\nu+} = \pi I_{\nu+}$ and $F_{\nu-} = \pi I_{\nu-}$, so we have

$$\tau_{\Delta\nu F}(z,z') = 2\int_0^{\pi/2} \tau_{\Delta\nu}(z,z', \sec\psi)\sin\psi\cos\psi d\psi \qquad (2\text{-}11)$$

If $\tau_{\Delta\nu}(z,z')$ happens to be exponential, this may be written as

$$2\int_0^{\pi/2} e^{-\left|\int_z^{z'} k dz \sec\psi\right|} \sin\psi\cos\psi d\psi = 2\int_1^{\infty} e^{-\left|\int_z^{z'} k dz\right| \eta \frac{d\eta}{\eta^3}} = 2Ei_3\left(\left|\int_{z'}^{z} k dz\right|\right).$$

$Ei_3(x)$ is called the third exponential integral, and is roughly equal to $e^{-1.6x}$ & $e^{-\sqrt{3}x}$. (The coefficient 1.6 in Elsasser's exponent corresponds to the $\sqrt{3}$ in the SPP approximation.) If $\tau_{\Delta\nu}$ is not exponential a numerical integration is necessary and has been carried out by Elsasser and Culbertson (1960) for the water vapor and carbon dioxide transmissivities. $\tau_{\Delta\nu F}(z,z')$ is still found to be nearly equal to $\tau_{\Delta\nu}\left(1.6\left|\int_z^{z'} k dz\right|\right)$. The presence of scatterers should improve this approximation by making the incident radiation more nearly isotropic.

Before leaving Elsasser there is one further point to discuss. We have derived the quantity $\left|\frac{1}{\tau_{\Delta\nu}} \frac{d\tau_{\Delta\nu}}{dz}\right|$ as an analogue to k_ν. However, since it was derived for absorption of radiation emitted from $z = z_o$, it is not immediately apparent that it is appropriate for radiation omitted elsewhere and absorbed at $z = z_o$. Let us consider a vertical beam emitted at z and find its intensity at z_o. We will use the incident frequency-independent case, with $\tau_{\Delta\nu} = \frac{1}{\Delta\nu} \int_{\Delta\nu} e^{-\left|\int_z^{z_o} k_\nu dz\right|} d\nu$. From the exact theory, the intensity emitted by a layer of thickness Δz is $I_\nu = k_\nu B_\nu(T)\Delta z$ (where T is also a function of z and B_ν is the blackbody flux, $\pi I_{B\nu}$, the transmitted intensity is $k_\nu e^{-\left|\int_z^{z_o} k_\nu dz\right|} B_\nu(T)\Delta z$ and the smoothed intensity observed at z_o is

$\frac{1}{\Delta\nu} \int_{\Delta\nu} k_\nu e^{-\left|\int_z^{z_o} k_\nu dz\right|} B_\nu(T(z))\Delta z d\nu$. From the approximate theory, the emitted smoothed intensity is $\frac{1}{\tau_{\Delta\nu}} \frac{d\tau_{\Delta\nu}}{dz} B_\nu(T)\Delta z$, and the transmitted smoothed intensity is $\frac{d\tau_{\Delta\nu}}{dz} B_\nu(T)\Delta z = \Delta z B_\nu(T(z)) \frac{1}{\Delta\nu} \int_{\Delta\nu} k_\nu e^{-\left|\int_z^{z_o} k_\nu dz\right|} d\nu$. If the $\Delta\nu$'s are small enough so that the variation of $B_\nu(T)$ in $\Delta\nu$ may be neglected, (and $\Delta\nu$ can always be chosen to fulfill this condition) the agreement is exact. Likewise, the absorptivity for frequency independent radiation of a thickness Δz at $z = z_o$ is $\frac{\Delta z}{\Delta\nu} \int_{\Delta\nu} k_\nu d\nu \Big|_{z=z_o}$ by exact theory, and $\left.\frac{\frac{\Delta z}{\Delta\nu} \int_{\Delta\nu} k_\nu(z) e^{-\left|\int_z^{z_o} k_\nu dz\right|} d\nu}{\frac{1}{\Delta\nu} \int_{\Delta\nu} e^{-\left|\int_z^{z_o} k_\nu dz\right|} d\nu}\right|_{z=z_o} = \frac{\Delta z}{\Delta\nu} \int k_\nu d\nu \Big|_{z=z_o}$ for the

approximation. The integration over angle gives no particular difficulties in this regard.

Putting all this together, we come out with Elsasser's equation for flux transfer:

$$dF_{\Delta\nu+} = -\left|\frac{1}{\tau_{\Delta\nu F}}\frac{d\tau_{\Delta\nu F}}{dz}\right|\left[F_{\Delta\nu+} - B_{\Delta\nu}(T)\right]dz$$

$$dF_{\Delta\nu-} = \left|\frac{1}{\tau_{\Delta\nu F}}\frac{d\tau_{\Delta\nu F}}{dz}\right|\left[F_{\Delta\nu-} - B_{\nu}(T)\right]dz \qquad (2\text{-}12)$$

z is positive upward in both equations, and $\tau_{\Delta\nu F}$ is measured from the point at which the flux is to be computed.

We will accept Elsasser and Culbertson's (1960) linear pressure reduction without comment, as our primary interest is in the lower atmosphere and in the difference in radiative fluxes with and without suspended ice crystals. Since the pressure variations in the part of the lower atmosphere considered here are small the recent criticisms by Goody (1964, p. 234-236) concerning complexities of correcting for pressure variations do not apply in our case.

Having reviewed some of the pertinent equations in the literature, we are now ready to derive the equation we will use.

D. Derivation of Final Equation

Elsasser's equation (2-12) would be suitable for our use if it included scattering. (For some simple solutions, to be discussed in Chapter III, it is suitable as it stands.) The SPP equations (2-8) include scattering in a manageable form, but are not in an appropriate form for the computation of flux divergence, as they do not include emission. If both these equations are considered as improvements on

the original Schuster equation, and both are applied to it at once, an equation suitable for our purpose is obtained.

Start by defining a new quantity, $\beta = \beta(\nu,z)$ the volume flux backscatter. This β is <u>not</u> the same as the β_{SPP} of equation (2-8), although there are some analogies. β is defined by the following procedure: Let an upward flux $F_{\Delta\nu+}$ be incident upon a layer Δz. An amount $\beta F_{\Delta\nu+}\Delta z$ will be scattered from the incident flux $F_{\Delta\nu+}$ at such angles that it returns to the lower hemisphere. The actual computation of β will be considered in the next section.

A slight change in nomenclature is convenient at this point. Until now we have used subscripts to specify monochromatic, smoothed, or integrated quantities, and whether beam or flux transmissivities were being considered. From this point to the final integrations over ν in the next chapter, the subscripts will be dropped when speaking of any smoothed flux quantity. If the dependence on $\bar{\nu}$ is important for the particular equation under consideration, it will be written out as a functional dependence on ν. Thus $F_{\Delta\nu F}$ becomes F_+ or $F_+(\nu)$; $\tau_{\Delta\nu F}$ becomes τ or (ν), etc.

With this change of notation, Schuster's, Elsasser's and the SPP equations may be combined to give

$$\frac{dF_+}{dz} = -\left|\frac{d\ln\tau}{\phi\zeta}\right|\left[F_+ - B\right] - \beta F_+ + \beta F_- \qquad (2\text{-}13)$$

$$\frac{dF_-}{dz} = \left|\frac{d\ln\tau}{dz}\right|\left[F_- - B\right] + \beta F_- - \beta F_+$$

These equations may be simplified by defining $k = \beta + \left|\frac{d\ln\tau}{dz}\right| = \kappa(\nu,z,(z_o))$, $s = \beta/\kappa$, and $dx = \kappa dz$,

Then,

$$\frac{dF_+}{dx} = -F_+ + sF_- + (1-s)B$$

$$\frac{dF_-}{dz} = F_- - sF_+ - (1-s)B \qquad (2\text{-}14)$$

By making suitable assumptions these equations are solved, and the solutions integrated over ν, in the next chapter. This chapter concludes with a description of the procedures used in the computation of τ and β.

E. Computation of Coefficients

In order to use (2-14) it is necessary to know how τ and β are related to the properties of an atmosphere with three absorbers--ice crystals, water vapor and carbon dioxide--and one scatterer, ice crystals. As pointed out in the first chapter, water droplets are being neglected in this case; in a temperate atmosphere they would also have to be considered. We will assume that stratospheric ozone contributes downward radiation between 9.5 and 10 microns wavelength, and has no significant effect outside that range, or in the troposphere.

Consider first the transmissivity of a mixture of gases, (or other absorbers), with absorption coefficients k_1, k_2 etc.

$\tau = \int_{\Delta\nu} e^{\int k_1(\nu)dz + \int k_2(\nu)dz + \int k_3(\nu)dz} d\nu$. In our case, with low water vapor content and low temperature, there is never more than one absorber in a particular spectral range $\Delta\nu$ with strong line structure. Therefore, in a given spectral region the variability of only one k needs to be considered, and terms containing the others may be considered constants with respect to ν and taken out of the integral to give

$\tau = \tau_{H_2O}\, \tau_{co_2}\, \tau_{ice}$, and

$$\frac{1}{\tau}\frac{d\tau}{dz} = \frac{1}{\tau_{H_2O}}\frac{d\tau_{H_2O}}{dz} + \frac{1}{\tau_{co_2}}\frac{d\tau_{co2}}{dz} + \frac{1}{\tau_{ice}}\frac{d\tau_{ice}}{dz} \qquad (2\text{-}15)$$

Both τ_{H_2O} and τ_{co_2} may readily be obtained from Elsasser and Culbertson (1960); the procedure used is given in Chapter IV below.

τ_{ice} may be obtained from Irvine and Pollack (1968), who give single scattering albedos ($\tilde{\omega}_o$ in our notation, a in theirs) and extinction coefficients for ice spheres of .3μ, 1μ, 3μ and 10μ radius. These coefficients are probably safe to use directly for ice fog, which is composed largely of nearly spherical crystals of radii 1-7μ. For plate crystals or snowflakes in a crystal display, an exact treatment is impossible at this level of approximation and we will assume blackbody plates. In ice fog,

$$\tau_{ice}(z_1,z_2) = 2Ei_3 \left(\left| \int_{z_1}^{z_2} \int_{0}^{\infty} (1-\tilde{\omega}_o)\, Q_{ext}\, \pi a^2 n P(a) da dz \right| \right) \qquad (2\text{-}16)$$

Here a is the particle radius (cm), n is the number of particles cm^{-3}, z is altitude (cm), P(a) is the normalized particle size distribution and Q_{ext} is the Mie efficiency factor for extinction. For flat plates, $2Ei_3$ ( ) is replaced by exp ( ). (See Chapter IV, section C.)

The derivation of the correct form for β is considerably more complicated. β as defined in the second paragraph of section D is a function of P(a), n, Q_{ext}, $\tilde{\omega}_o$ and the phase function, $\Phi(\theta)$. It is convenient to define the monodisperse flux backscatter, β(a) as the fraction of the flux incident on a unit area scattered into the hemisphere of incidence by a single particle of radius a. β then becomes

$$\beta = n \int P(a)\, \beta(a) da \qquad (2\text{-}17)$$

and the problem of computing β reduces to that of computing the flux backscatter of a single particle.

The usual problems of converting from intensities to fluxes in our transfer equations are here included in the coefficient β, as β has been defined throughout as the relationship between incident and

backscattered fluxes. Lavard (1960) derived a β similar to this one, but his procedure of calculation required a separate double integration for each size-wavelength pair used. We will use a somewhat different procedure which will require a final integration only over the scattering angle θ.

Consider a horizontal layer of unit thickness with one spherical scatterer of radius $\underline{a}$ per unit volume. We know from Mie scattering theory (van der Hulst, 1957) that the power scattered per unit solid angle at an angle θ from the direction of an incoming beam with intensity I_o is given by

$$I_{sca}\, r^2 = I_o A(\theta) = I_o Q_{sca} \Phi(\theta) \pi a^2$$

$A(\theta)$ is the scattering function and $Q_{sca} = \tilde{\omega}_o Q_{ext}$ is the Mie efficiency factor for scattering. This equation holds for scattering by each particle in our layer. Assume a hemi-isotropic flux, F_+ incident from below. This flux is composed of radiation of intensity $I = F_+/\pi$ from all directions below the horizontal, and is incident equally on each particle in the layer.

We will assume that this flux gives rise to a scattered flux, with intensity $I_{sca}(\gamma)$ at an angle γ from the downward vertical. In order to transform this intensity to flux, consider the power per unit area crossing a plane parallel to our scattering layer. Assume that each unit area of the scattering layer has one scatterer which scatters $r^2 I_{sca}\, d\Omega$ into the angle $d\Omega$. This same cone of rays must cross the reference plane (Figure II-3P) giving a local flux of $r^2 I_{sca}\, d\Omega / (r^2 d\Omega/\cos\gamma)$. This must be multiplied by the fraction of the unit area covered by the cone of rays, $r^2 d\Omega/\cos\gamma$, in order to give the average

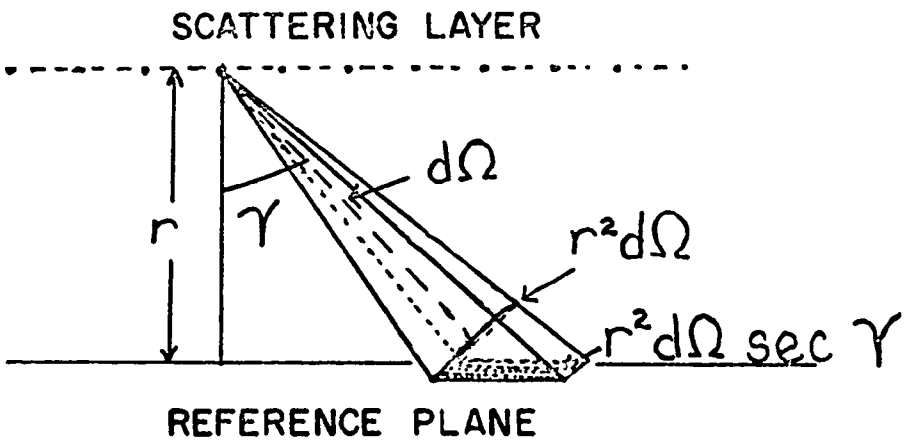

II-3 Scattering and reference planes for computation of β.

contribution to the flux from $d\Omega$. We get $dF_{sca} = r^2 I_{sca}\, d\Omega$ so our total downward scattered flux is given by $F_{sca} = \int r^2 I_{sca}\, d\Omega$ where the integral is over the lower hemisphere.

Consider next the computation of F_{sca}. Let α be the angle between the incoming ray and the vertical, and θ be the scattering angle (Figure II-4). The scattering particle constitutes the origin of this coordinate system. We will consider five cases, each valid for a different range of α and θ. 1. $0 < \theta < \frac{\pi}{2}$, $\alpha < \frac{\pi}{2} - \theta$. With this geometry all scattered light is scattered upward, and there is no contribution to the flux backscatter. 2. $0 < \theta < \pi/2$, $\alpha > \pi/2 - \theta$. An amount of radiation (F_+/π) $2\pi \sin\alpha\, d\alpha$ is incident from the cone at angle α, of which

$$A(\theta)\, 2\pi \sin\theta\, d\theta\, (F_{+o}/\pi)\, 2\pi \sin\alpha\, d\alpha$$

is scattered into the series of cones of scattering angle θ. (Figure II-4 shows the incident radiation as a single ray rather than as a cone for the sake of clarity.) Of this scattered radiation, a fraction Ψ/π is scattered into the lower hemisphere. The angle Ψ is defined in Figure II-4. In order to evaluate Ψ in terms of α and θ, consider Figure II-5. We see from the left side of Figure II-5, drawn in the plane of the incident ray that $a = r \tan\theta$, $b = r \tan(\pi/2 - \alpha)$, and from the right side that $b/a = \cos\Psi$. So for this case $\Psi = \cos^{-1}(\tan(\frac{\pi}{2} - \alpha)/\tan\theta)$, and the contribution to the total backscattered flux is

$$dF_{sca} = 4F_{+o}\, A(\theta) \sin\theta d\theta \cos^{-1}\left[\frac{\tan(\pi/2-\alpha)}{\tan\theta}\right] \sin\alpha d\alpha \qquad (2\text{-}18a)$$

3. $\theta = \pi/2$ This is similar to the above, except $\Psi = \pi/2$ for all α, giving

$$dF_{sca} = 4F_{+o}\, A(\theta) \sin\theta d\theta\, \frac{\pi}{2} \sin\alpha d\alpha \qquad (2\text{-}18b)$$

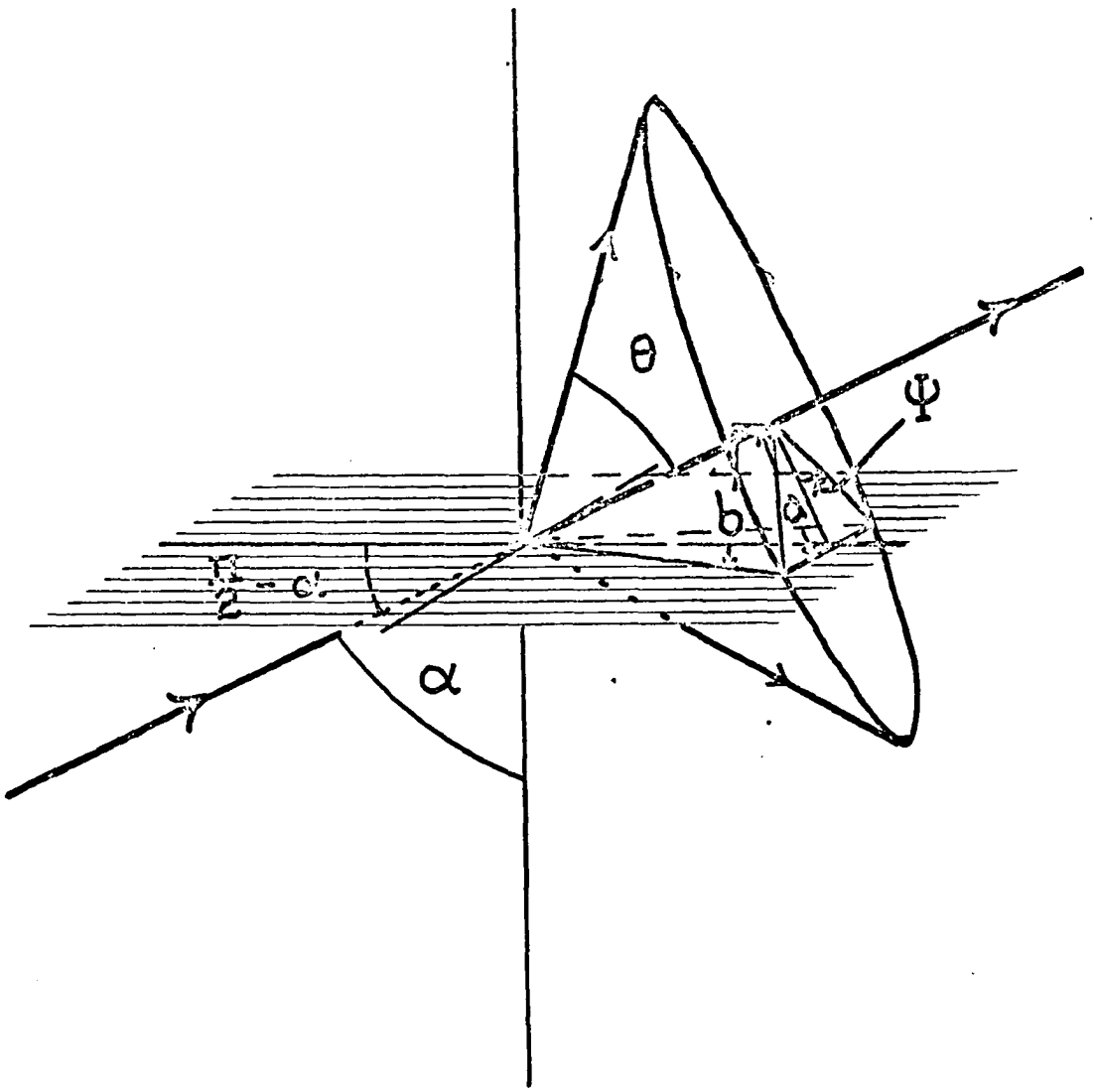

II-4 Solid geometry for the computation of ß.

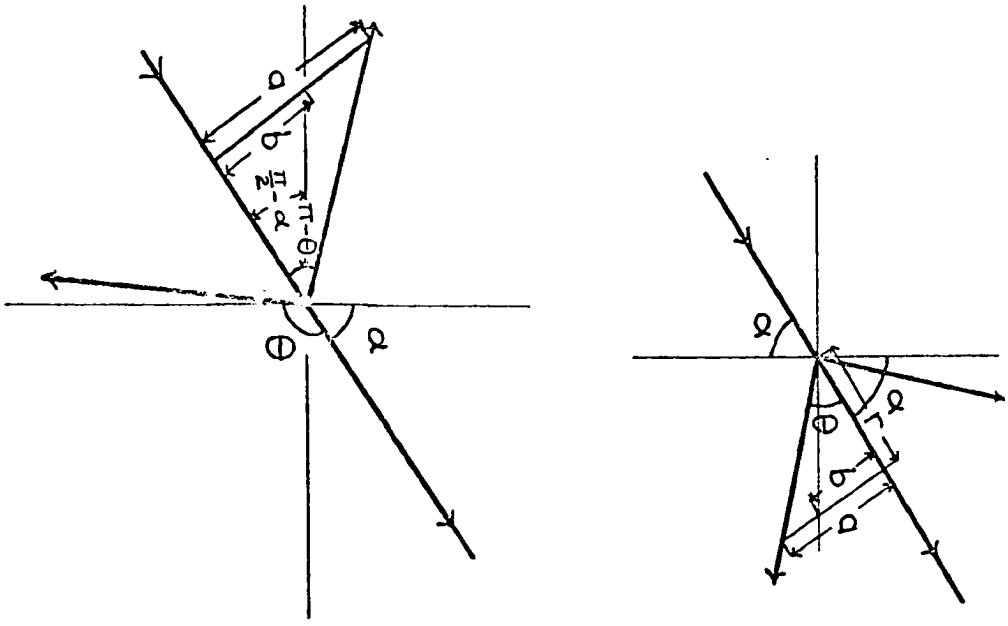

II-5 Computation of Ψ for $0 < \theta < \pi/2$.

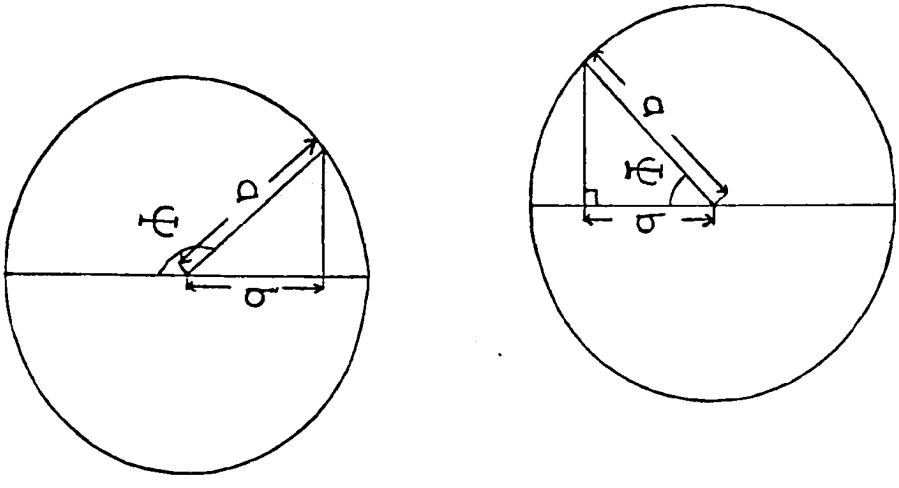

II-6 Computation of Ψ for $\frac{\pi}{2} < \theta < \pi$.

4. $\pi/2 < \theta < \pi$, $\theta - \pi/2 < \alpha$. The basic equations are the same as case 2, but the derivation of Ψ is somewhat different. Following Figure II-6 we see that now $b = r \tan(\frac{\pi}{2} - \alpha)$, $a = r \tan(\pi-\theta)$, and $\cos\Psi = -b/a = -\tan(\pi/2 - \alpha)/\tan(\pi-\theta)$

$$\Psi = \cos^{-1}\left(\frac{-\tan(\pi/2-\alpha)}{\tan(\pi-\theta)}\right) = \cos^{-1}\left(\frac{-\cot\alpha}{\tan(\pi-\theta)}\right).$$

So

$$dF_{sca} = 4F_o\, A(\theta)\, \sin\theta d\theta \cos^{-1}\left(\frac{-\cot\alpha}{\tan(\pi-\theta)}\right)\sin\alpha d\alpha \qquad (2\text{-}18c)$$

5. $\pi/2 < \theta \leq \pi$, $\alpha < \theta - \pi/2$. The entire scattering cone is below the horizontal, so Ψ can be set equal to the limiting value, ie $\psi = \pi$, and $dF_{sca} = 4F_o A(\theta)\, \sin\theta d\theta\, \pi \sin\alpha d\alpha$. (2-18d)

Utilizing the fact that the problem was defined in such a way that $\beta(a) = F_{sca}/F_+$, we can now write out the equation for $\beta(a)$ by adding together the 5 cases discussed above:

$$\beta(a) = 4\Bigg\{\int_0^{\varepsilon} 0\,d\theta + \int_{\varepsilon}^{\pi/2-\varepsilon} A(\theta)\sin\theta \int_{\pi/2-\theta}^{\pi/2-\varepsilon} \cos^{-1}\left[\frac{\tan(\frac{\pi}{2} - \alpha)}{\tan\theta}\right] \sin\alpha d\alpha d\theta$$

$$+ \int_{\pi/2-\varepsilon}^{\pi/2+\varepsilon} \frac{\pi}{2}\, A(\theta)\sin\theta \int_0^{\pi/2} \sin\alpha d\alpha d\theta + \int_{\pi/2+\varepsilon}^{\pi-\varepsilon} A(\theta)\sin\theta \int_0^{\pi} \pi\sin\alpha d\alpha \qquad (2\text{-}19)$$

$$+ \int_{\theta-\pi/2}^{\pi/2-\varepsilon} \cos^{-1}\left[\frac{-\cot\alpha}{\tan(\pi-\theta)}\right] \sin\alpha d\alpha\Bigg] d\theta + \int_{\pi-\varepsilon}^{\pi} \pi A(\theta)\sin\theta \int_0^{\pi/2} \sin\alpha d\alpha d\theta\Bigg\}$$

Here ε is a vanishingly small number used to eliminate those values of θ from the integrals for which the argument of the $\cos^{-1}$ is undefined.

The first term, $\int_0^{\varepsilon} 0 d\theta$, results from the limiting value, $\theta = 0$, in case 1.

Note that in the third and last terms the integral $\int_0^{\pi/2} \sin\alpha d\alpha$ is equal to 1.

It proves convenient to rewrite the parenthesis in the fourth term by adding and subtracting $\int_{\theta-\frac{\pi}{2}}^{\pi/2-\varepsilon} \pi \sin\alpha d\alpha$. This gives

$$\int_0^{\pi/2-\varepsilon} \pi \sin\alpha d\alpha - \int_{\theta-\pi/2}^{\pi/2-\varepsilon} \left(\pi - \cos^{-1}\left[\frac{-\cot\alpha}{\tan(\pi-\theta)}\right]\right) \sin\alpha d\alpha \qquad (2\text{-}20)$$

The first term of this is equal at once to π. The part of the second term in parentheses may be written as $\pi - \cos^{-1}\left[\frac{-\cot\alpha}{\tan(\pi-\theta)}\right] = y$.

Then $\cos^{-1}\left[\frac{-\cot\alpha}{\tan(\pi-\theta)}\right] = \pi - y, \left[\frac{-\cot\alpha}{\tan(\pi-\theta)}\right] = \cos(\pi-y) = -\cos y,$

$$\cos y = \left|\frac{+\cot\alpha}{\tan(\pi-\theta)}\right|, \quad y = \cos^{-1}\left|\frac{\cot\alpha}{\tan(\pi-\theta)}\right|,$$

and the fourth term of (2-19) may be rewritten as

$$\int_{\pi/2+\varepsilon}^{\pi-\varepsilon} A(\theta)\sin\theta \left(\pi - \int_{\theta-\pi/2}^{\pi/2-\varepsilon} \cos^{-1}\left[\frac{\cot\alpha}{\tan(\pi-\theta)}\right] \sin\alpha d\alpha\right) d\theta . \qquad (2\text{-}21)$$

Equation (2-19) now can be rewritten in the more symmetrical form

$$\beta(a) = 4 \int_0^{\varepsilon} 0 d\theta + \int_{\varepsilon}^{\pi/2-\varepsilon} A(\theta)\sin\theta \int_{\pi/2-\theta}^{\pi/2-\varepsilon} \cos^{-1}\left|\frac{\cot\alpha}{\tan\theta}\right| \sin\alpha d\alpha d\theta + \int_{\pi/2-\varepsilon}^{\pi/2+\varepsilon} \frac{\pi}{2} A(\theta)\sin\theta d\theta$$

$$+ \int_{\pi/2+\varepsilon}^{\pi-\varepsilon} A(\theta)\sin\theta \left(\pi - \int_{\theta-\pi/2}^{\pi/2-\varepsilon} \cos^{-1}\left|\frac{\cot\alpha}{\tan(\pi-\theta)}\right| \sin\alpha d\alpha\right) d\theta + \int_{\pi-\varepsilon}^{\pi} \pi A(\theta)\sin\theta d\theta .$$

(2-19')

In order to complete the integration over α, we now need only to evaluate the integral

$$\lim_{\varepsilon \to 0} \int_{f}^{\pi/2-\varepsilon} \cos^{-1}\left|\frac{\cot \alpha}{\tan g}\right| \sin\alpha d\alpha$$

for the two sets of values of f, g, $f = \pi/2 - \theta$, $g = \theta$ and $f = \theta - \pi/2$, $g = \pi - \theta$. The first set of valuees applies for $\theta < \pi/2$, the second set for $\theta > \pi/2$. Let us make the substitution $t = \cot \alpha$. We then have $\sin \alpha = \frac{1}{\sqrt{1+t^2}}$, $dt = -\frac{1}{\sin^2\alpha} d\alpha$, $d\alpha = -\sin^2\alpha dt = -\frac{dt}{1+t^2}$ and $\sin\alpha d\alpha = -\frac{dt}{\sqrt{1+t^2}^3}$. Then

$$\lim_{\varepsilon \to 0} \int_{f}^{\pi/2-\varepsilon} \cos^{-1}\left|\frac{\cot \alpha}{\tan g}\right| \sin\alpha d\alpha = \lim_{\varepsilon \to 0}\left(-\int_{\cot f}^{\cot(\frac{\pi}{2}-\varepsilon)} \cos^{-1}\left|\frac{t}{\tan g}\right| \frac{dt}{\sqrt{1+t^2}^3}\right)$$

$$= \lim_{\varepsilon \to 0}\left(-\int_{\cot f}^{\cot(\frac{\pi}{2}-\varepsilon)} \cos^{-1}\left|\frac{t}{\tan g}\right| d\left|\frac{t}{\sqrt{1+t^2}}\right|\right) \qquad (2\text{-}22)$$

$$= -\cos^{-1}\left|\frac{\cot \alpha}{\tan g}\right| \cos \alpha \Big|_{f}^{\pi/2} - \lim_{\varepsilon\to 0} \int_{\cot f}^{\cot(\pi/2-\varepsilon)} \frac{t}{\sqrt{1+t^2}} \frac{1}{\sqrt{\tan^2 g - t^2}} dt .$$

Evaluating the first term and making the substitution $u = t^2$ in the second, this becomes

$$\cos f \cos^{-1} \frac{\cot f}{\tan g} - \lim_{\varepsilon\to 0} \frac{1}{2} \int_{\cot^2 f}^{\cot^2(\pi/2-\varepsilon)} \frac{du}{\sqrt{-u^2+(\tan^2 g - 1)u + \tan^2 g}}$$

The second term may be evaluated from any standard integral table; it is

$$\lim_{\varepsilon \to 0} \left(-\frac{1}{2} \sin^{-1} \frac{2t^2 - \tan^2 g + 1}{\tan^2 g + 1} \Bigg|_{\cot f}^{\cot(\pi/2-\varepsilon)} \right) =$$

$$= \frac{1}{2} \sin^{-1} \frac{\tan^2 g - 1}{\tan^2 g + 1} - \frac{1}{2} \sin^{-1} \frac{-2\cot^2 f + \tan^2 g - 1}{\tan^2 g + 1}$$

and 2-22 becomes

$$\lim_{\varepsilon \to 0} \int_{f}^{\pi/2-\varepsilon} \cos^{-1} \left| \frac{\cot \alpha}{\tan g} \right| \sin\alpha d\alpha \qquad (2\text{-}23)$$

$$= \cos f \cos^{-1} \frac{\cot f}{\tan g} + \frac{1}{2} \sin^{-1} \frac{\tan^2 g - 1}{\tan^2 g + 1} - \frac{1}{2} \sin^{-1} \frac{-2\cot^2 f + \tan^2 g - 1}{\tan^2 g + 1} .$$

For each set of f, g, we have $f = \pi/2 - g$, so $\cot f = \tan g$. This allows simplification of Eq. 2-23 because $\cos^{-1}(\cot f/\tan g) = 0$, and $\sin^{-1}((-2\cot^2 f + \tan^2 g - 1)/\tan^2 g + 1)) = \sin^{-1}(-1) = -\pi/2$. Inserting these values, (2-23) becomes

$$\lim_{\varepsilon \to 0} \int_{f}^{\pi/2-\varepsilon} \cos^{-1} \left| \frac{\cot \alpha}{\tan g} \right| \sin\alpha d\alpha = \frac{1}{2} \sin^{-1} \frac{\tan^2 g - 1}{\tan^2 g + 1} + \frac{\pi}{4} \qquad (2\text{-}24)$$

Using the fact that $\frac{\tan^2 g - 1}{\tan^2 g + 1} = -\cos 2g, = -\sin(\frac{\pi}{2} \pm 2g)$ $= -\sin(-\frac{3\pi}{2} \pm 2g)$ etc.,

and noting that we want $-\pi/2 < \sin^{-1} \leq \frac{\pi}{2}$,

$$\sin^{-1} \frac{\tan^2 g - 1}{\tan^2 g + 1} \Bigg|_{0<g<\pi/2} = 2g - \pi/2 = \begin{cases} 2\theta - \pi/2 & 0<\theta<\pi/2 \\ \frac{3\pi}{2} - 2\theta & \pi/2 <\theta<\pi, \end{cases}$$

and we have

$$\lim_{\varepsilon \to 0} \int_{f}^{\pi/2-\varepsilon} \cos^{-1}\left|\frac{\cot \alpha}{\tan g}\right| \sin\alpha d\alpha = \begin{cases} \theta, & 0 < \theta < \pi/2 \\ \pi - \theta, & \pi/2 < \theta < \pi \end{cases} \tag{2-25}$$

(2-19') now simplifies to

$$\beta(a) = \lim_{\varepsilon \to 0} 4 \left\{ \int_{0}^{\varepsilon} 0 \sin\theta d\theta + \int_{\varepsilon}^{\pi/2-\varepsilon} A(\theta)\, \theta \sin\theta d\theta + \int_{\pi/2-\varepsilon}^{\pi/2+\varepsilon} \pi/2\, A(\theta) \sin\theta d\theta \right.$$

$$\left. + \int_{\pi/2+\varepsilon}^{\pi-\varepsilon} \left|\pi - (\pi-\theta)\right| A(\theta) \sin\theta d\theta + \int_{\pi-\varepsilon}^{\pi} \pi A(\theta) \sin\theta d\theta = 4 \int_{0}^{\pi} A(\theta)\theta \sin\theta d\theta \right\} \tag{2-26}$$

from which, referring back to (2-17),

$$\beta = n4 \int_{0}^{\infty} \int_{0}^{\pi} A(\theta,a)\, \theta \sin\theta\, P(a) d\theta da. \tag{2-27}$$

This is the volume flux backscatter coefficient we need.

It may be noted that if isotropic scatterers are considered in equation 2-26, we find that the backscattered flux, which in this case is half the total scattered energy, is equal not to $\frac{1}{2} Q_{sca} \pi a^2$, but rather to $Q_{sca} \pi a^2$. This result, implying as it does that the scattering cross section of a sphere for fluxes is twice that for intensities, is physically sound. A sphere of radius a exposed to a hemi-isotropic flux F will intercept a total energy $\int_{0}^{2\pi} \int_{0}^{\pi/2} \frac{F}{\pi} \pi a^2 \sin\psi d\psi d\phi = 2F \pi a^2$, twice the energy which would be incident on a flat horizontal plate of the same radius. For absorption, this is the situation that gives $\tau_F(x) \approx \tau\,(1.6\, x)$. In the case of

scattering, no energy is actually lost and we will consider that equation 2-26 as it stands provides the proper correction for the intensity-to-flux transfer

F. Review of Assumptions

Before attempting to solve the equations (2-14), let us review the assumptions made in their derivation, with special emphasis on their application to our particular requirements.

The validity of any two stream approximation can be questioned. In our particular case, the goodness of the approximation depends on two factors: the horizontal homogeneity of that portion of the atmosphere under consideration and the approach of the angular intensity distribution to the hemi-isotropic case. True ice fog has horizontal inhomogeneities ranging in scale from the eddies in single auto exhaust plumes through buildings and gravity waves to the thinning of the fog layer towards its boundaries. In general inhomogeneities lasting long enough to affect cooling rates have horizontal scales at least an order of magnitude larger than vertical scales (with the exception of downtown buildings) and it seems safe to assume that for computation of cooling over several hours the ice fog may be treated as if it were smeared out into a uniform horizontal layer. The true angular distribution is harder to take into consideration, but the presense of scatterers will if anything improve the approximation over what is normally observed in atmosphere radiation problems. Since we are interested primarily in the difference between cases with and without ice crystals, it is sufficient that our approximations have at least the same validity as Elsasser's.

The operation of smoothing over frequency gives rise to inaccuracies both in Elsasser's formulae and in our own. Unavoidable errors arise from the fact that smoothed transmissivities vary with source as well as path. The dependence of line width on pressure and temperature affects the smoothed transmissivity in a manner which varies with the frequency range considered (Goody, 1964). Since our principal interest is in the lower troposphere in near-isothermal conditions this variation is not critical, and we will use Elsasser's -40°C transmissivity curves and linear pressure reduction, defining an effective $u = \int (P/1013\ mb)\ du$ and $v = \int (P/1013\ mb)\ dv$ for use in place of u and v, where u is the amount of water vapor in cm precipitable water and v is the amount of CO_2 in cm at STP. In addition to these standard difficulties, the presence of scattering will increase the effective vertical path length between layers. Since $\frac{d\ln\tau}{dz}$ will not in general be constant with z, and since the true variation is with the (unknown) scattered path length rather than geometrical distance, we do not know the correct value for $\frac{d\ln\tau}{dz}$. This situation is eased considerably by the near equality of scattering and essentially exponential absorption by the ice crystals, which will become apparent when these quantities are calculated in Chapter IV. At frequencies where scattering is of overall significance variation in $\frac{d\ln\tau}{dz}$ will be small, while the presence of strong line structure, and hence non-uniform $\frac{d\ln\tau}{dz}$, will be accompanied by small values of s. A partial correction will be considered in Chapter III.

The third major potential source of error is in the computation of coefficients. The optical constants of ice as given by Irvine and

Pollack (1968) are probably the best available, but they are based on very scanty data and do not include $\phi(\theta)$. Actual computation of β will be based on tabulated values of $< \cos\theta > = 2\pi \int \Phi(\theta) \cos\theta \sin\theta d\theta$, as was β_{SPP}, but through a somewhat improved formula.

CHAPTER III

MATHEMATICAL SOLUTIONS

Equations (2-14) are in theory solvable as they stand, but in practice we will need to make one further assumption about the scattering layers, and divide our scattering atmosphere into N layers each of which has a uniform scattering ratio, s. Once this is done we can obtain analytical solutions for each layer. The solutions thus obtained may then be particularized for various cases of interest, and set up for computer calculation.

A. The General Solution for N Scattering Layers

In the notation of Chapter II, we have

$$\frac{dF_+}{dx} = -F_+ + sF_- + (1-s)B$$

$$\frac{dF_-}{dx} = F_- - sF_+ - (1-s)B \qquad (2\text{-}14)$$

Define G as the total energy incident on both top and bottom of a horizontal thin plate of unit area, and call it the total flux. Thus $G = F_+ + F_-$, whereas $F = F_+ - F_-$. First subtracting and then adding the two equations of (2-14), we have

$$\frac{dF}{dx} = -G(1-s) + 2(1-s)B \qquad (3\text{-}1a)$$

$$\frac{dG}{dx} = -F(1+s) \qquad (3\text{-}1b)$$

Differentiating,

$$\frac{d^2F}{dx^2} = -\frac{dG}{dx}(1-s) + \frac{ds}{dx}G + 2(1-s)\frac{dB}{dx} - 2B\frac{ds}{dx} \qquad (3\text{-}2a)$$

$$\frac{d^2G}{dx^2} = -\frac{dF}{dx}(1+s) - \frac{ds}{dx}F \qquad (3\text{-}2b)$$

Substituting from (3-1) for F, G, $\frac{dF}{dx}$ and $\frac{dG}{dx}$, we have

$$\frac{d^2F}{dx^2} + \frac{1}{1-s}\frac{ds}{dx}\frac{dF}{dx} - F(1-s^2) = 2(1-s)\frac{dB}{dx} \qquad (3\text{-}3a)$$

$$\frac{d^2G}{dx^2} - \frac{1}{1+s}\frac{ds}{dx}\frac{dG}{dx} - (1-s^2)G = -2(1-s^2)B \qquad (3\text{-}3b)$$

Up until now we have assumed that s is a variable. Suppose instead we divide our medium into N layers and hold s constant within each layer. We will number our layers 1, 2,....N from the bottom up, with scattering ratios s_1, s_2,..., s_N and lower boundaries $\underline{x}_1$, $\underline{x}_2$, ... $\underline{x}_N$, and match solutions at the layer boundaries. x is the optical depth, defined by $dx = \kappa dz$. Its use allows considerable simplification in the mathematics of the problem over what would be the case if z, the vertical coordinate, were used as the independent variable. The equations for the $\underline{i}$th layer are then

$$\frac{d^2F_i}{dx^2} - (1-s_i^2)F_i = 2(1-s_i)\frac{dB}{dx} \qquad (3\text{-}4a)$$

$$\frac{d^2G_i}{dx^2} - (1-s_i^2)G_i = -2(1-s_i^2)B \qquad (3\text{-}4b)$$

which have the solutions (Ford, 1955, p. 73)

$$F_i = J_i\, e^{\sqrt{1-s_i^2}x} + K_i\, e^{-\sqrt{1-s_i^2}x} + \sqrt{\frac{1-s_i}{1+s_i}} \int_{\underline{x}_i}^{x} \left| e^{\sqrt{1-s_i^2}(x-y)} - e^{-\sqrt{1-s_i^2}(x-y)} \right| \frac{dB}{dy}\, dy$$

$$G_i = J_i'\, e^{\sqrt{1-s_i^2}x} + K_i'\, e^{-\sqrt{1-s_i^2}x} - \sqrt{1-s_i^2} \int_{\underline{x}_i}^{x} \left| e^{\sqrt{1-s_i^2}(x-y)} - e^{-\sqrt{1-s^2}(x-y)} \right| B\, dy.$$

where J_i, K_i, J_i', and K_i' are constants to be evaluated, and y is a dummy variable replacing x in the integration procedure.

Integrating the last term of the second equation by parts, we have

$$F_i = J_i\, e^{\sqrt{1-s_i^2}x} + K_i\, e^{-\sqrt{1-s_i^2}x} + \sqrt{\frac{1-s_i}{1+s_i}} \int_{\underline{x}_i}^{x} \left| e^{\sqrt{1-s_i^2}(x-y)} - e^{-\sqrt{1-s_i^2}(x-y)} \right| \frac{dB}{dy}\, dy \qquad (3\text{-}5a)$$

$$G_i = J_i'\, e^{\sqrt{1-s_i^2}x} + K_i'\, e^{-\sqrt{1-s_i^2}x} + 2B(x) - B(\underline{x}_i)\left[e^{\sqrt{1-s_i^2}(x-\underline{x}_i)} + e^{-\sqrt{1-s_i^2}(x-\underline{x}_i)} \right] - \int_{\underline{x}_i}^{x} \left| e^{\sqrt{1-s_i^2}(x-y)} + e^{-\sqrt{1-s_i^2}(x-y)} \right| \frac{dB}{dy}\, dy \qquad (3\text{-}5b)$$

2N of the 4N constants in this set of equations arise from the differentiations between (3-1) and (3-2) and will be eliminated by application of (3-1). Dividing (3-1a) by $\sqrt{1-s_i}$ and (3-1b) by $\sqrt{1+s_i}$, and substituting from (3-5), we have

$$e^{\sqrt{1-s_i^2}x} \left[\sqrt{1+s_i}\, J_i + \left(J_i' - B(\underline{x}_i)\, e^{-\sqrt{1-s_i^2}\underline{x}_i} \right) \sqrt{1-s_i} \right] - e^{-\sqrt{1-s_i^2}x} \left[K_i \sqrt{1+s_i} - \left(K_i' - e^{\sqrt{1-s_i^2}\underline{x}_i} B(\underline{x}_i) \right) \sqrt{1-s_i} \right] = 0 \qquad (3\text{-}1a')$$

and

$$e^{\sqrt{1-s_i^2}x}\left[J_i\sqrt{1+s_i}+\left(J_i'-B(\underline{x}_i)\,e^{-\sqrt{1-s_i^2}\underline{x}_i}\right)\sqrt{1-s_i}\right] \tag{3-1b'}$$

$$+\,e^{-\sqrt{1-s_i^2}x}\left[K_i\sqrt{1+s_i}-\left(K_i'-B(\underline{x}_i)\,e^{\sqrt{1-s_i^2}\underline{x}_i}\right)\sqrt{1-s_i}\right]=0$$

from which

$$J_i'=e^{-\sqrt{1-s_i^2}\underline{x}_i}\,B(\underline{x}_i)-\sqrt{\frac{1+s_i}{1-s_i}}\,J_i$$

$$K_i'=e^{\sqrt{1-s_i^2}\underline{x}_i}\,B(\underline{x}_i)+\sqrt{\frac{1+s_i}{1-s_i}}\,K_i$$

and we can rewrite our solution as

$$F_i=J_ie^{\sqrt{1-s_i^2}x}+K_i\,e^{-\sqrt{1-s_i^2}x}+\sqrt{\frac{1-s_i}{1+s_i}}\int_{\underline{x}_i}^{x}\left(e^{\sqrt{1-s_i^2}(x-y)}-e^{-\sqrt{1-s_i^2}(x-y)}\right)\frac{dB}{dy}\,dy \tag{3-6a}$$

$$G_i=-\sqrt{\frac{1+s_i}{1-s_i}}\,J_i\,e^{\sqrt{1-s_i^2}x}+\sqrt{\frac{1+s_i}{1-s_i}}\,K_i\,e^{-\sqrt{1-s_i^2}x}+2B(x) \tag{3-6b}$$

$$-\int_{\underline{x}_i}^{x}\left(e^{\sqrt{1-s_i^2}(x-y)}+e^{-\sqrt{1-s_i^2}(x-y)}\right)\frac{dB}{dy}\,dy\ .$$

The remaining 2N constants are connected by N-1 equations for the continuity of F of the form

$$J_i\,e^{\sqrt{1-s_i^2}\underline{x}_i}+K_i\,e^{-\sqrt{1-s_i^2}\underline{x}_i}=J_{i-1}\,e^{\sqrt{1-s_{i-1}^2}\underline{x}_i}+K_{i-1}\,e^{-\sqrt{1-s_{i-1}^2}\underline{x}_i} \tag{3-7a}$$

$$+\sqrt{\frac{1-s_i}{1+s_{i-1}}}\int_{\underline{x}_{i-1}}^{\underline{x}_i}\left(e^{\sqrt{1-s_{i-1}^2}(\underline{x}_i-y)}-e^{-\sqrt{1-s_{i-1}^2}(\underline{x}_i-y)}\right)\frac{dB}{dy}\,dy$$

and N-1 equations for the continuity of G of the form

$$-\sqrt{\frac{1+s_i}{1-s_i}}\ J_i\ e^{\sqrt{1-s_i^2}\,\underline{x}_i} + \sqrt{\frac{1+s_i}{1-s_i}}\ K_i\ e^{-\sqrt{1-s_i^2}\,\underline{x}_i} = -\sqrt{\frac{1+s_{i-1}}{1-s_{i-1}}}\ J_{i-1}\ e^{\sqrt{1-s_{i-1}^2}\,\underline{x}_i} \tag{3-7b}$$

$$+\sqrt{\frac{1+s_{i-1}}{1-s_{i-1}}}\ K_{i-1}\ e^{-\sqrt{1-s_{i-1}^2}\,\underline{x}_i} - \int_{\underline{x}_i}^{\underline{x}_i}\left[e^{\sqrt{1-s_{i-1}^2}\,(\underline{x}_i-y)} + e^{-\sqrt{1-s_{i-1}^2}\,(\underline{x}_i-y)}\right]\frac{dB}{dy}\,dy$$

The two remaining conditions for evaluation of the constants involve the downward flux at the top of the atmosphere, $F_-(\bar{x}_N)$ and the upward flux at the bottom, $F_+(\underline{x}_1)$. $\bar{x}_N$ is the value of x at the top of the atmosphere. The equations are

$$-\frac{1+\sqrt{\frac{1+s_N}{1-s_N}}}{2}\ J_N\ e^{\sqrt{1-s_N^2}\,\bar{x}_N} + \frac{\sqrt{\frac{1+s_N}{1-s_N}}-1}{2}\ K_N\ e^{\sqrt{1-s_N^2}\,x_N}$$

$$+ B(\bar{x}_N) - \frac{1}{2}\int_{\underline{x}_N}^{\bar{x}_N}\left[\left(1+\sqrt{\frac{1-s_N}{1+s_N}}\right)e^{\sqrt{1-s_N^2}(\bar{x}_N-y)}\right. \tag{3.7c}$$

$$\left.+\left(1-\sqrt{\frac{1-s_N}{1+s_N}}\right)e^{-\sqrt{1-s_N^2}(\bar{x}_N-y)}\right]\frac{dB}{dy}\,dy = F_-(\bar{x}_N)$$

and

$$\frac{1-\sqrt{\frac{1+s_1}{1-s_1}}}{2}\ e^{\sqrt{1-s_1^2}\,\underline{x}_1}\ J_1 + \frac{1+\sqrt{\frac{1+s_1}{1-s_1}}}{2}\ e^{-\sqrt{1-s_1^2}\,\underline{x}_1}\ K_1 + B(\underline{x}_1) = F_+(\underline{x}_1) \tag{3-7d}$$

If the lower boundary is the ground, with temperature T_g and reflectivity r, we have also

$$F_+(\underline{x}_1) = (1-r)\ B(T_g) + r\left\{J_1\left(\frac{-1-\sqrt{\frac{1+s_1}{1-s_1}}}{2}\right)e^{\sqrt{1-s_1^2}\,\underline{x}_1} + K_1\left(\frac{-1+\sqrt{\frac{1+s_1}{1-s_1}}}{2}\right)\right.$$

$$\left.e^{-\sqrt{1-s_1^2}\,\underline{x}_1} + B(\underline{x}_1)\right\} \tag{3-7e}$$

Equations (3-6) and (3-7) will, when their solutions are integrated over ν, give the required integrated flux. Although flux divergences calculated at the mathematically sharpened boundaries do not exist, as the flux divergence has a discontinuity at the boundary, the flux differences are still usable across these boundaries provided the distance over which they are taken is comparable to the true physical transition distance for the scattering ratio change.

The N-layer solution is a useful conceptual generalization, but both ice fog and ice crystal displays are, so far as we presently know, uniform vertically. Therefore in our particular case one scattering layer is adequate. Furthermore, the reflectivity of almost any surface except desert sand is negligible in the infrared (Griggs, 1968), and snow is even less reflective than normal ground. Thus, our problem is greatly simplified because we may set $r = 0$, and consider only one scattering layer.

B. One Scattering Layer with Frequency-Dependent Multiple Scattering

Let the atmosphere have only three layers. The middle layer will contain scatterers and have a scattering ratio $s = s_2$; the upper and lower layers will be free of scatterers, with $s_1 = s_3 = 0$. We will neglect the reflectivity of the ground, and assume that the downward radiation at the top of the atmosphere is $\bar{F}_-$. Our boundary equations now become

$$J_3 e^{\underline{x}_3} + K_3 e^{-\underline{x}_3} = J_2 e^{\sqrt{1-s^2}\,\underline{x}_3} + K_2 e^{-\sqrt{1-s^2}\,\underline{x}_3} + \sqrt{\frac{1-s}{1+s}} \int_{\underline{x}_2}^{\underline{x}_3} \left| e^{\sqrt{1-s^2}(\underline{x}_3 - y)} - e^{-\sqrt{1-s^2}(\underline{x}_3 - y)} \right| \frac{dB}{dy}\, dy \tag{3-8a}$$

$$-J_3 e^{\underline{x}_3} + K_3 e^{-\underline{x}_3} = -\sqrt{\frac{1+s}{1-s}}\ J_2 e^{\sqrt{1-s^2}\underline{x}_3} + \sqrt{\frac{1+s}{1-s}}\ K_2 e^{-\sqrt{1-s^2}\underline{x}_3}$$

$$-\int_{\underline{x}_2}^{\underline{x}_3}\left(e^{\sqrt{1-s^2}(\underline{x}_3-y)} + e^{-\sqrt{1-s^2}(\underline{x}_3-y)}\right)\frac{dB}{dy}\,dy\ , \tag{3-8b}$$

$$\bar{F}_- = -J_3 e^{\bar{x}_3} + B(\bar{x}_3) - \int_{\underline{x}_3}^{\bar{x}_3} e^{(\bar{x}_3-y)}\frac{dB}{dy}\,dy, \tag{3-8c}$$

$$J_2 e^{\sqrt{1-s^2}\underline{x}_2} + K_2 e^{-\sqrt{1-s^2}\underline{x}_2} = J_1 e^{\underline{x}_2} + K_1 e^{-\underline{x}_2}$$

$$+\int_{\underline{x}_1}^{\underline{x}_2}\left(e^{(\underline{x}_2-y)} - e^{-(\underline{x}_2-y)}\right)\frac{dB}{dy}\,dy, \tag{3-8d}$$

$$\sqrt{\frac{1+s}{1-s}}\left(-J_2 e^{\sqrt{1-s^2}\underline{x}_2} + K_2 e^{-\sqrt{1-s^2}\underline{x}_2}\right) = -J_1 e^{\underline{x}_2} + K_1 e^{-\underline{x}_2}$$

$$-\int_{\underline{x}_1}^{\underline{x}_2}\left(e^{(\underline{x}_2-y)} + e^{-(\underline{x}_2-y)}\right)\frac{dB}{dy}\,dy\ , \text{ and} \tag{3-8e}$$

$$K_1 e^{-\underline{x}_1} + B(\underline{x}_1) = B(T_g)\ . \tag{3-8f}$$

Subtracting (3-8b) from (3-8a) and applying (3-8c) to eliminate J_3, and then adding (3-8d) and (3-8e) and applying (3-8f) to eliminate K_1, we have:

$$J_2 e^{\sqrt{1-s^2}\underline{x}_3}\left[1+\sqrt{\frac{1+s}{1-s}}\right]+K_2 e^{-\sqrt{1-s^2}\underline{x}_3}\left[1-\sqrt{\frac{1+s}{1-s}}\right]=-2e^{-(\bar{x}_3-\underline{x}_3)}\Bigg[\bar{F}-$$

$$B(\bar{x}_3)+\int_{\underline{x}_3}^{\bar{x}_3} e^{(\bar{x}_3-y)}\frac{dB}{dy}\,dy\Bigg]-\int_{\underline{x}_2}^{\underline{x}_3}\Bigg[\left[1+\sqrt{\frac{1-s}{1+s}}\right]e^{\sqrt{1-s^2}(\underline{x}_3-y)}$$

$$+\left[1-\sqrt{\frac{1-s}{1+s}}\right]e^{-\sqrt{1-s^2}(\underline{x}_3-y)}\Bigg]\frac{dB}{dy}\,dy,$$

and

$$J_2\left[1-\sqrt{\frac{1+s}{1-s}}\right]e^{\sqrt{1-s^2}\underline{x}_2}+K_2\left[1+\sqrt{\frac{1+s}{1-s}}\right]e^{-\sqrt{1-s^2}\underline{x}_2}$$

$$=2\Big[B(T_g)-B(\underline{x}_1)\Big]e^{-(\underline{x}_2-\underline{x}_1)}-2\int_{\underline{x}_1}^{\underline{x}_2} e^{-(\underline{x}_2-y)}\frac{dB}{dy}\,dy\,.$$

Combining these equations gives J_2 and K_2 in the following forms:

$$J_2=\left\{\frac{-2}{\left[1+\sqrt{\frac{1+s}{1-s}}\right]^2 e^{\sqrt{1-s^2}(\underline{x}_3-\underline{x}_2)}-\left[1-\sqrt{\frac{1+s}{1-s}}\right]^2 e^{-\sqrt{1-s^2}(\underline{x}_3-\underline{x}_2)}}\right\}$$

$$\left\{e^{-\sqrt{1-s^2}\underline{x}_3}\left[1-\sqrt{\frac{1+s}{1-s}}\right]\Bigg[\Big[B(T_g)-B(\underline{x}_1)\Big]e^{-(\underline{x}_2-x_1)}\right.$$

$$\left.-\int_{\underline{x}_1}^{\underline{x}_2} e^{-(\underline{x}_2-y)}\frac{dB}{dy}\,dy\Bigg]+e^{-\sqrt{1-s^2}\underline{x}_2}\left[1+\sqrt{\frac{1+s}{1-s}}\right]\Bigg[\Big[\bar{F}-B(\bar{x}_3)\Big]e^{-(\bar{x}_3-\underline{x}_3)}\right.$$

$$\left.+\int_{\underline{x}_3}^{\bar{x}_3} e^{-(y-\underline{x}_3)}\frac{dB}{dy}\,dy\Bigg]+e^{-\sqrt{1-s^2}\underline{x}_2}\int_{\underline{x}_2}^{\underline{x}_3}\Bigg[\left[1+\frac{1}{\sqrt{1-s^2}}\right]e^{\sqrt{1-s^2}(\underline{x}_3-y)}\right.$$

$$\left.+\frac{+s}{\sqrt{1-s^2}}\,e^{-\sqrt{1-s^2}(\underline{x}_3-y)}\Bigg]\frac{dB}{dy}\,dy\right\} \qquad (3\text{-}9a)$$

and

$$K_2 = \left\{ \frac{2}{\left(1+\sqrt{\frac{1+s}{1-s}}\right)^2 e^{\sqrt{1-s^2}(\underline{x}_3-\underline{x}_2)} - \left(1-\sqrt{\frac{1+s}{1-s}}\right)^2 e^{-\sqrt{1-s^2}(\underline{x}_3-\underline{x}_2)}} \right\} \left\{ e^{\sqrt{1-s^2}\underline{x}_3} \right.$$

$$\left(1+\sqrt{\frac{1+s}{1-s}}\right)\left[\left(B(T_g) - B(\underline{x}_1)\right) e^{-(\underline{x}_2-\underline{x}_1)} - \int_{\underline{x}_1}^{\underline{x}_2} e^{-(\underline{x}_2-y)} \frac{dB}{dy}\, dy \right]$$

$$+ e^{\sqrt{1-s^2}\underline{x}_2}\left(1-\sqrt{\frac{1+s}{1-s}}\right)\left[\left(\bar{F}_- - B(\bar{x}_3)\right) e^{-(\bar{x}_3-\underline{x}_3)} + \int_{\underline{x}_3}^{\bar{x}_3} e^{-(y-\underline{x}_3)} \frac{dB}{dy}\, dy \right]$$

$$\left. + e^{\sqrt{1-s^2}\underline{x}_2} \int_{\underline{x}_2}^{\underline{x}_3} \left[\frac{-s}{\sqrt{1-s^2}} e^{\sqrt{1-s^2}(\underline{x}_3-y)} + \left(1-\frac{1}{\sqrt{1-s^2}}\right) e^{-\sqrt{1-s^2}(\underline{x}_3-y)} \right] \frac{dB}{dy}\, dy \right\}. \qquad (3\text{-}9b)$$

Noting that

$$F_+(\underline{x}_2) = \left(B(T_g) - B(\underline{x}_1)\right) e^{-(\underline{x}_2-\underline{x}_1)} + B(\underline{x}_2) - \int_{\underline{x}_1}^{\underline{x}_2} e^{-(\underline{x}_2-y)} \frac{dB}{dy}\, dy,$$

and

$$F_-(\underline{x}_3) = \left(\bar{F}_- - B(\bar{x}_3)\right) e^{-(\bar{x}_3-\underline{x}_3)} + \int_{\underline{x}_3}^{\bar{x}_3} e^{-(y-\underline{x}_3)} \frac{dB}{dy}\, dy + B(\underline{x}_3),$$

we see that the first two terms in the second curly brackets in equations (3-9) arise from the physical radiative inputs at the boundaries of the scattering layer, while the third term in each case comes from the arbitrary selection of $\underline{x}_1$ as a lower bound in the integrals of (3-6). Let us write

$$C = C(s, \underline{x}_3-\underline{x}_2) = \frac{2}{\left(1+\sqrt{\frac{1+s}{1-s}}\right)^2 e^{\sqrt{1-s^2}(\underline{x}_3-\underline{x}_2)} - \left(1-\sqrt{\frac{1+s}{1-s}}\right)^2 e^{-\sqrt{1-s^2}(\underline{x}_3-\underline{x}_2)}}.$$

We then have

$$J_2 = -C\left\{e^{-\sqrt{1-s^2}\underline{x}_3}\left(1-\sqrt{\frac{1+s}{1-s}}\right)\left[F_+(\underline{x}_2)-B(\underline{x}_2)\right]+e^{-\sqrt{1-s^2}\underline{x}_2}\left[\left(1+\sqrt{\frac{1+s}{1-s}}\right)\right.\right. \tag{3-10a}$$

$$\left.\left.\left[F_-(\underline{x}_3)-B(\underline{x}_3)\right]+\int_{\underline{x}_2}^{\underline{x}_3}\left[\left(\frac{+s}{\sqrt{1-s^2}}\right)e^{-\sqrt{1-s^2}(\underline{x}_3-y)}+\left(1+\frac{1}{\sqrt{1-s^2}}\right)e^{\sqrt{1-s^2}(\underline{x}_3-y)}\right]\frac{dB}{dy}\,dy\right]\right\}$$

and,

$$K_2 = C\left\{e^{\sqrt{1-s^2}\underline{x}_3}\left(1+\sqrt{\frac{1+s}{1-s}}\right)\left[F_+(\underline{x}_2)-B(\underline{x}_2)\right]+e^{\sqrt{1-s^2}\underline{x}_2}\left[\left(1-\sqrt{\frac{1+s}{1-s}}\right)\right.\right. \tag{3-10b}$$

$$\left.\left.\left[F_-(\underline{x}_3)-B(\underline{x}_3)\right]+\int_{\underline{x}_2}^{\underline{x}_3}\left[\left(\frac{-s}{\sqrt{1-s^2}}\right)e^{\sqrt{1-s^2}(\underline{x}_3-y)}+\left(1-\frac{1}{\sqrt{1-s^2}}\right)e^{-\sqrt{1-s^2}(\underline{x}_3-y)}\right]\frac{dB}{dy}\,dy\right]\right\}$$

Using these expressions for J_2 and K_2, together with equations 3-8, yields the following expressions for J_1, K_1, J_3, and K_3:

$$J_1 = e^{-\underline{x}_2}\left\{C\left\{-\frac{s}{1-s}\left[e^{\sqrt{1-s^2}(\underline{x}_3-\underline{x}_2)}-e^{-\sqrt{1-s^2}(\underline{x}_3-x_2)}\right]\left[\left[B(T_g)-B(\underline{x}_1)\right]e^{-(\underline{x}_2-\underline{x}_1)}\right.\right.\right.$$

$$\left.\left.\left.-\int_{\underline{x}_1}^{\underline{x}_2}e^{-(\underline{x}_2-y)}\,dB(y)\right]-2\sqrt{\frac{1+s}{1-s}}\left[\left[\bar{F}_--B(\bar{x}_3)\right]e^{-(\bar{x}_3-\underline{x}_3)}+\int_{\underline{x}_3}^{\bar{x}_3}e^{-(y-\underline{x}_3)}\,dB(y)\right]\right.\right.$$

$$\left.\left.-\int_{\underline{x}_2}^{\underline{x}_3}\left[\left(1+\sqrt{\frac{1+s}{1-s}}\right)e^{\sqrt{1-s^2}(\underline{x}_3-y)}-\left(1-\sqrt{\frac{1+s}{1-s}}\right)e^{-\sqrt{1-s^2}(\underline{x}_3-y)}\right]dB(y)\right\}-\int_{\underline{x}_1}^{\underline{x}_2}e^{(\underline{x}_2-y)}dB\right\}, \tag{3-11a}$$

$$K_1 = e^{\underline{x}_1}\left[B(T_g)-B(\underline{x}_1)\right], \tag{3-11b}$$

$$J_3 = \left[-\bar{F}_- + B(\bar{x}_3) - \int_{\underline{x}_3}^{\bar{x}_3} e^{(\bar{x}_3 - y)} \frac{dB}{dy}\, dy\right] e^{-\bar{x}_3}, \text{ and} \tag{3-11c}$$

$$K_3 = 2\left[F_+(\underline{x}_2) - B(\underline{x}_2)\right] C e^{\underline{x}_3} \sqrt{\frac{1+s}{1-s}} + \left[F_-(\underline{x}_3) - B(\underline{x}_3)\right] e^{\underline{x}_3} \left\{ 1 \right.$$

$$\left. + C\left[\left(1 - \sqrt{\frac{1+s}{1-s}}\right) e^{-\sqrt{1-s^2}(\underline{x}_3 - \underline{x}_2)} - \left(1 + \sqrt{\frac{1+s}{1-s}}\right) e^{\sqrt{1-s^2}(\underline{x}_3 - \underline{x}_2)}\right]\right\}$$

$$+ e^{\underline{x}_3} \int_{\underline{x}_2}^{\underline{x}_3} \left[-C \frac{s}{\sqrt{1-s^2}} e^{\sqrt{1-s^2}(y - \underline{x}_2)} - C \frac{s}{\sqrt{1-s^2}} e^{-\sqrt{1-s^2}(y - \underline{x}_2)}\right.$$

$$-C\left(1 + \frac{1}{\sqrt{1-s^2}}\right) e^{\sqrt{1-s^2}(2\underline{x}_3 - \underline{x}_2 - y)} + C\left(1 - \frac{1}{\sqrt{1-s^2}}\right) e^{-\sqrt{1-s^2}(2\underline{x}_3 - \underline{x}_2 - y)}$$

$$\left. + \sqrt{\frac{1-s}{1+s}}\, e^{\sqrt{1-s^2}(\underline{x}_3 - y)} - \sqrt{\frac{1-s}{1+s}}\, e^{-\sqrt{1-s^2}(\underline{x}_3 - y)}\right] \frac{dB}{dy}\, dy\,. \tag{3-11d}$$

This can be further simplified by observing that we can always add a non-absorbing, non-scattering layer with a temperature gradient from $T(\underline{x}_1)$ to T_g at the lower boundary of the atmosphere and from $T(\bar{x}_3)$ to 0°K (or the effective radiating temperature of stratospheric ozone between 9.5 and 10 μ), to allow for that gas at the top. Mathematically this corresponds to defining

$T(\underline{x}_1) = T_g$ and $B\,(T(\bar{x}_3)) = \bar{F}_-$, and gives:

$$B(T_g) - B(\underline{x}_1) = 0, \quad \bar{F}_- - B(\bar{x}_3) = 0, \text{ and}$$

$$F_+(\underline{x}_2) - B(\underline{x}_2) = -\int_{\underline{x}_1}^{\underline{x}_2} e^{-(\underline{x}_2 - y)} \frac{dB}{dy}\, dy\,.$$

With these values substituted in (3-10) and (3-11) equation (3-6) should give satisfactory results for thin stratus cloud and, aside from the pressure reduction problem which may be handled by proper choice of τ, for cirrus clouds and contrails. In the case of ice fog, fog, or an ice crystal display the lowest layer is degenerate, with $\underline{x}_1 = \underline{x}_2$. $F_+(\underline{x}_2) - B(\underline{x}_2)$ also becomes zero, and the constants become,

$$J_2 = -Ce^{-\sqrt{1-s^2}\underline{x}_2}\left[\left(1+\sqrt{\frac{1+s}{1-s}}\right)\int_{\underline{x}_3}^{\bar{x}_3} e^{-(y-\underline{x}_3)}\frac{dB}{dy}dy+\int_{\underline{x}_2}^{\underline{x}_3}\left[\frac{+s}{\sqrt{1-s^2}}\ e^{-\sqrt{1-s^2}(\underline{x}_3-y)}\right.\right.$$

$$\left.\left.+\left(1+\frac{1}{\sqrt{1-s^2}}\right)e^{\sqrt{1-s^2}(\underline{x}_3-y)}\right]\frac{dB}{dy}\ dy\right],$$

$$K_2 = Ce^{\sqrt{1-s^2}\underline{x}_2}\left[\left(1-\sqrt{\frac{1+s}{1-s}}\right)\int_{\underline{x}_3}^{\bar{x}_3} e^{-(y-\underline{x}_3)}\frac{dB}{dy}\,dy+\int_{\underline{x}_2}^{\underline{x}_3}\left[\frac{-s}{\sqrt{1-s^2}}\ e^{\sqrt{1-s^2}(\underline{x}_3-y)}\right.\right.$$

$$\left.\left.+\left(1-\frac{1}{\sqrt{1-s^2}}\right)\ e^{-\sqrt{1-s^2}(\underline{x}_3-y)}\right]\frac{dB}{dy}\,dy\right],$$

$$J_3 = -e^{-\underline{x}_3}\int_{\underline{x}_3}^{\bar{x}_3} e^{-(y-\underline{x}_3)}\frac{dB}{dy}\,dy, \quad \text{and}$$

$$K_3 = e^{\underline{x}_3}\left[1+C\left[\left(1-\sqrt{\frac{1+s}{1-s}}\right)e^{-\sqrt{1-s^2}(\underline{x}_3-\underline{x}_2)}-\left(1+\sqrt{\frac{1+s}{1-s}}\right)e^{\sqrt{1-s^2}(\underline{x}_3-\underline{x}_2)}\right]\right]$$

$$\int_{\underline{x}_3}^{\bar{x}_3} e^{-(y-\underline{x}_3)}\frac{dB}{dy}\,dy + e^{\underline{x}_3}\int_{\underline{x}_2}^{\underline{x}_3}\left[\frac{-Cs}{\sqrt{1-s^2}}\left(e^{\sqrt{1-s^2}(y-\underline{x}_2)}+e^{-\sqrt{1-s^2}(y-\underline{x}_2)}\right)\right.$$

$$-\left(1+\frac{1}{\sqrt{1-s^2}}\right)C\,e^{\sqrt{1-s^2}(2\underline{x}_3-\underline{x}_2-y)}+\left(1-\frac{1}{\sqrt{1-s^2}}\right)C\,e^{-\sqrt{1-s^2}(2\underline{x}_3-\underline{x}_2-y)}$$

$$\left.+\sqrt{\frac{1-s}{1+s}}\left(e^{\sqrt{1-s^2}(\underline{x}_3-y)}-e^{-\sqrt{1-s^2}(\underline{x}_3-y)}\right)\right]\frac{dB}{dy}\,dy\,. \qquad (3\text{-}12)$$

Let $\underline{x}_g$ be the ground level, $\bar{x}_s$ be the top of the scattering layer, $\bar{x}$ be the top of the atmosphere, and use subscript s for constants in the scattering layer and c for those in the clear air. Then we define

$$D = \frac{2\int_{\bar{x}_s}^{\bar{x}} e^{-(y-\bar{x}_s)}\,dB(y) + \int_{\underline{x}_g}^{\bar{x}_s}\left[\left(1+\sqrt{\frac{1-s}{1+s}}\right)e^{\sqrt{1-s^2}(\bar{x}_s-y)} + \left(1-\sqrt{\frac{1-s}{1+s}}\right)e^{-\sqrt{1-s^2}(\bar{x}_s-y)}\right]dB}{\left(1+\sqrt{\frac{1+s}{1-s}}\right)^2 e^{\sqrt{1-s^2}(\bar{x}_s-\underline{x}_g)} - \left(1-\sqrt{\frac{1+s}{1-s}}\right)^2 e^{-\sqrt{1-s^2}(\bar{x}_s-\underline{x}_g)}} \tag{3-13}$$

and

$$E = \frac{\left(1+\sqrt{\frac{1+s}{1-s}}\right)e^{\sqrt{1-s^2}(\bar{x}_s-\underline{x}_g)} - \left(1-\sqrt{\frac{1+s}{1-s}}\right)e^{-\sqrt{1-s^2}(\bar{x}_s-\underline{x}_g)}}{\left(1+\sqrt{\frac{1+s}{1-s}}\right)^2 e^{\sqrt{1-s^2}(\bar{x}_s-\underline{x}_g)} - \left(1-\sqrt{\frac{1+s}{1-s}}\right)^2 e^{-\sqrt{1-s^2}(\bar{x}_s-\underline{x}_g)}},$$

after which

$$J_s = -e^{-\sqrt{1-s^2}\underline{x}_g}\left(1+\sqrt{\frac{1+s}{1-s}}\right)D, \quad \text{and}$$

$$K_s = e^{\sqrt{1-s^2}\underline{x}_g}\left(1-\sqrt{\frac{1+s}{1-s}}\right)D$$

for the scattering layer, and

$$J_c = -\int_{\bar{x}_s}^{\bar{x}} e^{-y}\,dB(y),$$

$$K_c = e^{\bar{x}_s}\left\{(1-2E)\int_{\bar{x}_s}^{\bar{x}} e^{-(y-\bar{x}_s)}\,dB(y) - \int_{\underline{x}_g}^{\bar{x}_s}\left[\left(E+E\sqrt{\frac{1-s}{1+s}}-\sqrt{\frac{1-s}{1+s}}\right)\right.\right.$$

$$\left.\left. e^{\sqrt{1-s^2}(\bar{x}_s-y)} + \left(E-E\sqrt{\frac{1-s}{1+s}}+\sqrt{\frac{1-s}{1+s}}\right)e^{-\sqrt{1-s^2}(\bar{x}_s-y)}\right]dB(y)\right\}. \tag{3-14}$$

If we combine equations (3-13) and (3-14) with equations (3-6) we get the final forms for F_s, $\frac{dF_s}{dz}$, F_c and $\frac{dF_c}{dz}$:

$$F_s = -D\left[\left(1+\sqrt{\frac{1+s}{1-s}}\right)e^{\sqrt{1-s^2}(x-\underline{x}_g)} - \left(1-\sqrt{\frac{1+s}{1-s}}\right)e^{-\sqrt{1-s^2}(x-\underline{x}_g)}\right] \tag{3-15a}$$

$$+\sqrt{\frac{1-s}{1+s}}\int_{\underline{x}_g}^{x}\left(e^{\sqrt{1-s^2}(x-y)} - e^{-\sqrt{1-s^2}(x-y)}\right)dB(y),$$

$$\frac{dF_s}{dz} = \kappa\left\{\sqrt{1-s^2}\;D\left[-\left(1+\sqrt{\frac{1+s}{1-s}}\right)e^{\sqrt{1-s^2}(x-\underline{x}_g)} - \left(1-\sqrt{\frac{1+s}{1-s}}\right)e^{-\sqrt{1-s^2}(x-\underline{x}_g)}\right]\right. \tag{3-15b}$$

$$\left.+(1-s)\int_{\underline{x}_g}^{x}\left(e^{\sqrt{1-s^2}(x-y)} + e^{-\sqrt{1-s^2}(x-y)}\right)dB(y)\right\},$$

$$F_c = -\int_{\bar{x}_s}^{\bar{x}} e^{(x-y)}\,dB(y) + e^{-(x-\bar{x}_s)}\left[(1-2E)\int_{\bar{x}_s}^{\bar{x}} e^{-(y-\bar{x}_s)}\,dB(y)\right.$$

$$\left.-\int_{\underline{x}_g}^{\bar{x}_s}\left[\left(E+E\sqrt{\frac{1-s}{1+s}}-\sqrt{\frac{1-s}{1+s}}\right)e^{\sqrt{1-s^2}(\bar{x}_s-y)} + \left(E-E\sqrt{\frac{1-s}{1+s}}+\sqrt{\frac{1-s}{1+s}}\right)e^{-\sqrt{1-s^2}(\bar{x}_s-y)}\right]dB(y)\right]$$

$$+\int_{\bar{x}_s}^{x}\left(e^{(x-y)} - e^{-(x-y)}\right)dB(y), \quad \text{and} \tag{3-15c}$$

$$\frac{dF_c}{dz} = \kappa \left\{ - \int_{\bar{x}_s}^{\bar{x}} e^{(x-y)}\, dB(y) - e^{-(x-\bar{x}_s)}(1-2E) \int_{\bar{x}_s}^{\bar{x}} e^{-(y-\bar{x}_s)}\, dB(y) \right.$$

$$+ e^{-(x-\bar{x}_s)} \int_{\bar{x}_c}^{\bar{x}_s} \left[\left(E + E\sqrt{\frac{1-s}{1+s}} - \sqrt{\frac{1-s}{1+s}} \right) e^{\sqrt{1-s^2}(\bar{x}_s - y)} \right. \tag{3-15d}$$

$$\left. \left. + \left(E - E\sqrt{\frac{1-s}{1+s}} + \sqrt{\frac{1-s}{1+s}} \right) e^{-\sqrt{1-s^2}(\bar{x}_s - y)} \right] dB(y) + \int_{\bar{x}_s}^{x} e^{(x-y)} + e^{-(x-y)}\, dB(y) \right\}.$$

We will now consider some of the practical details of computing these values.

C. Some Considerations on the Assignment of Numerical Values and Setting up the Computer Program

Up until now we have left both the zero level for x and the initial level for the computation of τ undefined. It is evident from equation (3-15) that the zero level of x has no significance, as only differences in x appear in the final equations. The level from which τ is computed will, on the other hand, have a definite effect on the value of $\frac{d\ln\tau}{dz}$ and hence on dx, especially in those regions of the spectrum where line structure is strong and τ deviates considerably from an exponential. κ is of course computed as close as possible to the level at which the flux divergence is wanted. There are several ways of evaluating a term such as $e^{-\sqrt{1-s^2}(x_2-x_1)}$, $x_2 > x_1$. We may compute $x_2 - x_1$, using the level at which the flux is to be computed as the zero level for computing τ,

or we may use x_2 or x_1 as the zero level for computing τ. We may also observe that

$$e^{-\sqrt{1-s^2}(x_2-x_1)} = \exp\left(-\sqrt{1-s^2}\int_{z_1}^{z_2}\left|\frac{d\ln\tau}{dz}\right| + \beta\, dz\right) = \exp - \sqrt{\frac{1+s}{1-s}}\int_{z_1}^{z_2}\left|d\ln\tau\right|dz$$

If τ is measured from z_o, $z_2 > z_o > z_1$, this is

$$\exp\left(-\sqrt{\frac{1+s}{1-s}}\int_{z_1}^{z_2}\left|d\ln\tau\right|dz\right) = \left|\tau(z_o,z_1)\right|^{\sqrt{\frac{1+s}{1-s}}}.$$ The extension to the positive exponential or to cases where z_o is outside the range of z_2 to z_1 is obvious.

In all these cases we need a way of evaluating s. In those cases where z, the level at which the flux is to be computed, is used as the base level for computation of τ, the logical procedure is to take

$$\int_{-\underline{z}_g}^{\bar{z}_s}\left|\frac{d\ln\tau}{dz}\right| + \beta\, dz = \frac{1}{1-s}\int_{-\underline{z}_g}^{\bar{z}_s}\left|\frac{d\ln\tau}{dz}\right| dz$$

from which it follows that

$$s = \left(\int_{-\underline{z}_g}^{\bar{z}_s}\beta dz\right)\Big/\left(-\ln(\tau(\bar{z}_s,z)\tau(z,\underline{z}_g)) + \int_{-\underline{z}_g}^{\bar{z}_s}\beta dz\right) \quad z<\bar{z}_s,$$

and (3-16)

$$s = \int_{-\underline{z}_g}^{\bar{z}_s}\beta dz\Big/\left(-\ln(\tau(z,z_g)/\tau(\bar{z}_s,z)) + \int_{\underline{z}_g}^{\bar{z}_s}\beta dz\right) \quad z>\bar{z}_s .$$

If the computation is made with transmissivity measured from $\underline{z}_g$ or $\bar{z}_s$, we have

$$s = \frac{\int_{-\underline{z}_g}^{\bar{z}_s} \beta dz}{-\ln\tau(\bar{z}_s, \underline{z}_g) + \int_{\underline{z}_g}^{\bar{z}_s} \beta dz}$$

The first method is more nearly accurate; the second has the advantage that s is the same for all computational heights, varying only with frequency.

Considering the number of times $e^{\sqrt{1-s^2}(x_2-x_1)}$, etc. appear in our equations, it is of considerable interest to determine how much error would be introduced by computing these quantities once and for all in each frequency interval for each sounding. As a check, suppose we compare the values we get, neglecting scattering, in a relatively non-exponential absorption region. We will use the carbon dioxide band at about 14.3 μ wavelength (700 cm^{-1}) and consider how $\tau(\bar{z}_s,\underline{z}_g)$ differs from $\tau(\bar{z}_s,z)\tau(z,\underline{z}_g)$ for $\bar{z}_s > z > \underline{z}_g$ and from $\tau(z,\underline{z}_g)/\tau(z,\bar{z}_s)$ for $z > \bar{z}_s > \underline{z}_g$. Assume the carbon dioxide content of the air is .03% by volume in which case v will be about .03 cm/m. If $\bar{z}_s$ = 10 m and z_g = 0 we have from Elsasser and Culbertson (1960) $\tau(\bar{z}_s,\underline{z}_g)$ = .49. If we let z vary we get $\tau(\bar{z}_s,z_g)$ = .35 for z=5, and τ=.52 for z=100. It appears advisable to compute τ (and s) from z for each level considered, especially as the numbers obtained are often subtracted from numbers of comparable magnitude. Another consideration is that in the course of manipulating exponentials in the derivation we may have formed terms of the form $e^{(x-x_1)}\ e^{-(x_3-x_1)}$ where the physical meaning is $e^{-(x_3-x)}$. If the x's are all calculated from z the resulting τ's will not be affected by this type of manipulation.

Returning to (3-13) and (3-15) we find three basic types of term in algebraic combination. The first and simplest family is an assortment of irrational algebraic functions of s. These should give no difficulty to a computer. The second group of terms is of the form $e^{\pm \sqrt{1-s^2}(x_2-x_1)}$, which we have already shown to be equal to $\left[\tau(z_2,z)\right]^{\pm\sqrt{\frac{1+s}{1-s}}} \left[\tau(z,z_1)\right]^{\pm\sqrt{\frac{1+s}{1-s}}}$. The plus and minus signs in the exponent of τ depend on the relative magnitude of z_2, z, and z_1 as well as on the sign of the original exponent of e.

In the scattering layers, $s \neq 0$ and we have already discussed the inaccuracy in our basic equations from the effect of scattering on $\frac{d\ln\tau}{dz}$ at a fixed distance. In this connection it is interesting to note that if τ were an exponential, the effective transmissivities as defined above are the same as would be obtained by lengthening each dz to $\sqrt{\frac{1+s}{1-s}}\,dz$. It seems logical to assume that this mathematical lengthening reflects the physical lengthening of the path by scattering. We will adopt this viewpoint and replace

$$\left[\tau(z_2,z)\right]^{\pm\sqrt{\frac{1+s}{1-s}}}$$

by $\tau_s(z_2,z)$ with the understanding that values of Δu and Δv in the scattering layer, as well as the number densities of ice crystals used in computing τ_s, will be multiplied by $\sqrt{\frac{1+s}{1-s}}$ before computing $\tau(H_2O)\tau(CO_2)$ and τ (ice).

The third set of terms is of the form $\pm \int_{x_1}^{x_2} e^{\pm\sqrt{1-s^2}(y-x_2)}\, dB =$ $\pm \int_{z_1}^{z_2} \tau_s(y,z_0)^{\pm 1}\, \tau_s(z,z)^{\pm 1}\, dB(y)$, each of which will require a

numerical integration. (Note that we continue to use y as a dummy variable, although it now stands for z instead of x.) As a further bit of shorthand, write $\tau_s(z_i)$ for $\tau_s(z,z_i)$ where z is the height of computation.

In order to compute flux divergences directly, we will also need to know κ very near the point of computation. This will be further discussed in Chapter IV.

The τ_s values are to be computed from the value of z at which the flux and/or flux divergence is desired. The following expressions may be written for D, E, F_s, $\frac{dF_s}{dz}$, Fc and $\frac{dF_c}{dz}$:

$$D = \left\{ 2 \int_{\bar{z}_s}^{\bar{z}} \frac{\tau_s(y)}{\tau_s(\bar{z}_s)} dB(y) + \int_0^z \left[\frac{\left| 1+\sqrt{\frac{1-s}{1+s}} \right|}{\tau_s(\bar{z}_s)\tau_s(y)} + \left| 1 - \sqrt{\frac{1-s}{1+s}} \right| \tau_s(\bar{z}_s)\tau_s(y) \right] dB(y) \right.$$

$$\left. + \int_z^{\bar{z}_s} \left[\left| 1 + \sqrt{\frac{1-s}{1+s}} \right| \frac{\tau_s(y)}{\tau_s(\bar{z}_s)} + \left| 1-\sqrt{\frac{1-s}{1+s}} \right| \frac{\tau_s(\bar{z}_s)}{\tau_s(y)} \right] dB(y) \right\} \left\{ \left\{ \frac{\left| 1 + \sqrt{\frac{1+s}{1-s}} \right|^2}{\tau_s(0)\tau_s(\bar{z}_s)} \right.\right.$$

$$\left.\left. - \left| 1 - \sqrt{\frac{1+s}{1-s}} \right|^2 \tau_s(0)\tau_s(\bar{z}_s) \right\}^{-1}, \qquad (3\text{-}17a)$$

$$E = \frac{\left| 1+\sqrt{\frac{1+s}{1-s}} \right| \frac{\tau_s(\bar{z}_s)}{\tau_s(z_g)} - \left| 1 - \sqrt{\frac{1+s}{1-s}} \right| \frac{\tau_s(z_g)}{\tau_s(\bar{z}_s)}}{\left| 1 + \sqrt{\frac{1+s}{1-s}} \right|^2 \frac{\tau_s(\bar{z}_s)}{\tau_s(z_g)} - \left| 1 - \sqrt{\frac{1+s}{1-s}} \right|^2 \frac{\tau_s(z_g)}{\tau_s(\bar{z}_s)}}, \qquad (3\text{-}17b)$$

$$F_s = -D\left[\left(1+\sqrt{\frac{1+s}{1-s}}\right)\frac{1}{\tau_s(0)} - \left(1-\sqrt{\frac{1+s}{1-s}}\right)\tau_s(0)\right]$$

$$+\sqrt{\frac{1-s}{1+s}}\int_{z_g}^{z}\left(\frac{1}{\tau_s(y)} - \tau_s(y)\right)dB\nu(y)\ , \tag{3-17c}$$

$$\frac{dF_s}{dz} = \kappa\left\{\sqrt{1-s^2}\ D\left[-\left(1+\sqrt{\frac{1+s}{1-s}}\right)\frac{1}{\tau_s(0)} - \left(1-\sqrt{\frac{1+s}{1-s}}\right)\tau_s(0)\right]\right.$$

$$\left.+(1-s)\int_{0}^{z}\left(\frac{1}{\tau_s(y)}+\tau_s(y)\right)dB_\nu(y)\right\}\ , \tag{3-17d}$$

$$F_c = -\int_{\bar{z}_s}^{z}\frac{1}{\tau_s(y)}\,dB(y) - \int_{z}^{\bar{z}}\tau_s(y)\,dB_\nu(y) + \tau(\bar{z}_s)\left[(1-2E)\left(\int_{\bar{z}}^{z}\frac{\tau_s(\bar{z}_s)}{\tau_s(y)}\,dB_\nu(y)\right.\right.$$

$$\left.+\int_{z}^{\bar{z}}\tau_s(\bar{z}_s)\tau_s(y)dB_\nu(y)\right)$$

$$-\int_{0}^{\bar{z}_s}\left[\left(E+E\sqrt{\frac{1-s}{1+s}}-\sqrt{\frac{1-s}{1+s}}\right)\frac{\tau_s(\bar{z}_s)}{\tau_s(y)}+\left(E-E\sqrt{\frac{1-s}{1+s}}+\sqrt{\frac{1-s}{1+s}}\right)\frac{\tau_s(y)}{\tau_s(\bar{z}_s)}\right]dB\ (y)\Bigg]$$

$$+\int_{z}^{z}\left(\frac{1}{\tau_s(y)}-\tau_s(y)\right)dB_\nu(y),\quad \text{and} \tag{3-17e}$$

$$\frac{dF_c}{dz} = \kappa \left\{ - \int_{\bar{z}_s}^{z} \frac{1}{\tau_s(y)}\, dB(y) - \int_{z}^{\bar{z}} \tau_s(y)\, dB(y) - \tau(\bar{z}_s)(1-2E) \left(\int_{\bar{z}_s}^{z} \frac{\tau_s(\bar{z}_s)}{\tau_s(y)}\, dB(y) \right.\right.$$

$$\left. + \int_{z}^{\bar{z}} \tau_s(\bar{z}_s)\tau_s(y)\, dB(y) \right) + \tau(\bar{z}_s) \int_{0}^{\bar{z}_s} \left[\left(E + E\sqrt{\frac{1-s}{1+s}} - \sqrt{\frac{1-s}{1+s}} \right) \frac{\tau_s(\bar{z}_s)}{\tau_s(y)} \right.$$

$$\left.\left. + \left(E - E\sqrt{\frac{1-s}{1+s}} + \sqrt{\frac{1-s}{1+s}} \right) \frac{\tau_s(y)}{\tau_s(\bar{z}_s)} \right] dB(y) + \int_{\bar{z}_s}^{z} \left(\frac{1}{\tau_s(y)} + \tau_s(y) \right) dB(y) \right\} . \qquad (3\text{-}17f)$$

By carrying out all the multiplications and defining a new pair of constants,

$$A' = \frac{1}{(1 + \sqrt{1-s^2}) - (1 - \sqrt{1-s^2})\tau_s^2(0)\tau_s^2(\bar{z}_s)}$$

$$A'' = \frac{1}{(1 + \sqrt{1-s^2}) - (1 - \sqrt{1-s^2})\dfrac{\tau_s^2(0)}{\tau_s^2(\bar{z}_s)}} \quad ,$$

and $C' = A''\, s(\tau_s^2(\bar{z}_s) - \tau_s^2(0))$,

it becomes possible to write

$$F_s = A' \Bigg\{ -\left[\tau_s^2(0)\left(s\sqrt{\frac{1-s}{1+s}} - (1-s-\sqrt{\frac{1-s}{1+s}})\tau_s^2(\bar{z}_s)\right)\right] \int_0^z \frac{1}{\tau_s(y)}\, dB(y)$$

$$-\left[\left(1-s+\sqrt{\frac{1-s}{1+s}}\right) - s\sqrt{\frac{1-s}{1+s}}\,\tau_s^2(\bar{z}_s)\right] \int_0^z \tau_s(y)\, dB(y)$$

$$-\left[\tau_s^2(\bar{z}_s)\left(s\sqrt{\frac{1-s}{1+s}} + \left(1-s-\sqrt{\frac{1-s}{1+s}}\right)\tau_s^2(0)\right)\right] \int_z^{\bar{z}_s} \frac{1}{\tau_s(y)}\, dB(y) \qquad (3\text{-}17c^1)$$

$$-\left[1-s+\sqrt{\frac{1-s}{1+s}} + s\sqrt{\frac{1-s}{1+s}}\,\tau_s^2(0)\right] \int_z^{\bar{z}_s} \tau_s(y)\, dB(y)$$

$$-\left[(1-s+\sqrt{1-s^2}) - (1-s-\sqrt{1-s^2})\tau_s^2(0)\right] \int_{\bar{z}_s}^{\bar{z}} \tau_s(y)\, dB(y) \Bigg\},$$

$$\frac{dF_s}{dz} = A'\kappa \Bigg\{ \tau_s^2(0)\left[s(1-s)-(1-s-(1-s)\sqrt{1-s^2})\tau_s^2(\bar{z}_s)\right] \int_0^z \frac{1}{\tau_s(y)}\, dB(y)$$

$$+\left[(1-s+(1-s)\sqrt{1-s^2})-s(1-s)\tau_s^2(\bar{z}_s)\right] \int_0^z \tau_s(y)\, dB(y) - \tau_s^2(\bar{z}_s)\left[s(1-s)-(1-s-(1-s)\sqrt{1-s^2})\tau_s^2(0)\right]$$

$$\int_z^{\bar{z}_s} \frac{1}{\tau_s(y)} dB(y) - \left[(1-s+(1-s)\sqrt{1-s^2})-s(1-s)\tau_s^2(0)\right] \int_z^{\bar{z}_s} \tau_s(y)\, dB(y) \qquad (3\text{-}17d^1)$$

$$-\left[1-s^2+(1-s)\sqrt{1-s^2} + (1-s^2-(1-s)\sqrt{1-s^2})\,\tau_s^2(0)\right] \int_{\bar{z}_s}^{\bar{z}} \tau_s(y)\, dB(y) \Bigg\},$$

$$F_c = A''\tau_s^2(0)(1-s-\sqrt{1-s^2}) \int_0^{\bar{z}_s} \frac{1}{\tau_s(y)} dB(y)$$

$$- A''(1-s+\sqrt{1-s^2}) \int_0^{\bar{z}_s} \tau_s(y)\, dB(y) \qquad (3\text{-}17e^1)$$

$$+ C \int_{\bar{z}_s}^{z} \frac{1}{\tau_s(y)}\, dB(y) - \int_{\bar{z}_s}^{z} \tau_s(y)\, dB(y) - (1-C) \int_z^{\bar{z}} \tau_s(y)\, dB(y)$$

and

$$\frac{dF_c}{dz} = \kappa \Bigg\{ - A'' \, (1-s-\sqrt{1-s^2})\tau_s^2(0) \int_0^{\bar{z}_s} \frac{1}{\tau_s(y)} \, dB(y) \qquad (3\text{-}17\text{?})$$

$$+ A'' \, (1-s+\sqrt{1-s^2}) \int_0^{\bar{z}_s} \tau_s(y) dB(y) - C \int_{\bar{z}_s}^{z} \frac{1}{\tau_s(y)} \, dB(y) + \int_{\bar{z}_s}^{z} \tau_s(y) dB(y)$$

$$- (1+C) \int_z^{\bar{z}} \tau_s(y) dB(y) \Bigg\} .$$

Although we will not go deeply into the actual computer work until Chapter V, we can already make some statements about general strategy. The first step is to provide the computer with a subroutine for evaluating $\tau(z_i)$ when it is given the wave number, ν, the height, z, at which the flux is to be computed and the water vapor, carbon dioxide and ice crystal concentrations as functions of height; and $\tau_s(z_i)$ if it is given s in addition. A second subroutine would allow computation of s from τ. A third subroutine should be written for the computation of

$$\int_{z_1}^{z_2} \tau_s(z_2)^{\pm 1} \tau_s(y)^{\pm 1} \frac{dB}{dy} \, dy, \qquad \text{or rather of} \qquad \int_{z_1}^{z_2} \tau_s(y)^{\pm 1} \frac{dB}{dy} \, dy$$

as the first factor may always be taken outside the integral. Once this is done the smoothed fluxes become algegraic functions and the integrated fluxes merely require adding the resulting smoothed fluxes, with appropriate wave number interval weighting. We now have an equation which includes both absorption and scattering by ice crystals and gases.

D. The Non-scattering Case

Suppose we know very little about the scattering properties of the crystals, as is the case in an ice crystal display. Then an elaborate computation to determine the effects of scattering is hardly justified, and we may just as well let s = 0. If we do this we have

$$F_s = -\int_{\bar{x}_s}^{\bar{x}_c} e^{-(y-\bar{x}_s)} \frac{dB}{dy}\, dy\left[e^{-(\bar{x}_s-x)}\right] - e^{-(\bar{x}_s-x)} \int_{\underline{x}_g}^{\bar{x}_s} e^{(\bar{x}_s-y)} \frac{dB}{dy}\, dy$$

$$+ \int_{\underline{x}_g}^{x} \left\{e^{(x-y)} - e^{-(x-y)}\right\} \frac{dB}{dy}\, dy = -\int_{\underline{x}_g}^{\bar{x}_c} e^{-|x-y|} \frac{dB}{dy}\, dy = -\int_{\underline{z}_g}^{\bar{z}_c} \tau(z,z_o) \frac{dB}{dz}\, dz, \tag{3-18a}$$

and

$$F_c = -\int_{\bar{x}_s}^{\bar{x}_c} e^{-(y-\bar{x}_s)} \frac{dB}{dy}\, dy\, e^{(x-\bar{x}_s)} - \int_{\underline{x}_g}^{\bar{x}_s} e^{(y-x)} \frac{dB}{dy}\, dy + \int_{\bar{x}_s}^{x} \left\{e^{(x-y)} - e^{-(x-y)}\right\} \frac{dB}{dy}\, dy$$

$$= -\int_{\underline{z}_g}^{\bar{z}_c} \tau(z,z_o) \frac{dB}{dz}\, dz = F_s \tag{3-18b}$$

which may also be readily derived from Elsasser and Culbertson's (1960) equation 78. The expression for $F_s = F_c$ may be used in its present form, with integration over z and ν. If we make the further assumption that the ice particles behave as gray bodies in the infrared, we have

$$\tau = \tau(\text{ice})\tau(H_2O)\tau(CO_2) \text{ and } F_f = -\int_{T(\underline{z}_g)}^{T(\bar{z})} \tau(\text{ice}) \int_0^{\infty} \tau(H_2O)\tau(CO_2) \frac{dB}{dT}\, d\nu dT.$$

The integral over ν is now identical to Elsasser's, and we can use his tabulated values for $R = \int \frac{dB_\nu}{dt} (1-\tau(\nu))d\nu$ in evaluating it. The

Elsasser integral will actually be used in the computations for ice crystal displays, and it is convenient to consider here the carbon dioxide-water vapor overlap correction.

We have assumed throughout and will continue to assume that the smoothed transmissivity of a mixture of absorbers is equal to the product of the smoothed transmissivities of the individual absorbers. (This is the same approximation used by Elsasser and Culbertson (1960) and Yamamoto (1952) in correcting for the water vapor-carbon dioxide overlap.) Then for the black-crystal case, we have

$$F = -\int_{T(z_g)}^{T(\bar{z})} \tau(\text{ice}) \int_0^\infty \tau(H_2O)\tau(CO_2) \frac{dB}{dT} \, d\nu \, dT \tag{3-19}$$

Considering only the integral over ν,

$$-\int_0^\infty \tau(H_2O)\tau(CO_2) \frac{dB}{dT} \, d\nu = -\int_0^\infty \frac{dB}{dT} \, d\nu + \int_0^\infty \frac{dB}{dT} (1-\tau(H_2O)\tau(CO_2)) \, d\nu \tag{3-20}$$

The range of ν may be divided into four regions. In region 1, there is no absorption by either water or carbon dioxide. Water alone absorbs in region 2, carbon dioxide alone absorbs in region 3 and both gases absorb in region 4. The second integral on the right of (3-20) may then be written as

$$\begin{aligned}\int_0^\infty \frac{dB}{dT} (1-\tau(H_2O)\tau(CO_2))d\nu &= \int_1 \frac{dB}{dT} (1-1)d\nu + \int_2 \frac{dB}{dT} (1-\tau(H_2O)) \, d\nu \\ &+ \int_3 \frac{dB}{dT} (1-\tau(CO_2)) \, d\nu + \int_4 \frac{dB}{dT} (1-\tau(H_2O)\tau(CO_2))d\nu.\end{aligned} \tag{3-21}$$

Elsasser's tabulated values are

$$R_{H_2O} = \int_2 \frac{dB}{dT}(1-\tau(H_2O))d\nu + \int_4 \frac{dB}{dT}(1-\tau(H_2O))d\nu,$$

$$R_{CO_2} = \int_3 \frac{dB}{dT}(1-\tau(CO_2))d\nu + \int_4 \frac{dB}{dT}(1-\tau(CO_2))d\nu, \qquad (3\text{-}22)$$

$$\Delta' R_{H_2O} = \int_4 \frac{dB}{dT}\tau(H_2O)(1-\tau(CO_2))d\nu$$

and

$$\Delta' R_{CO_2} = \int_4 \frac{dB}{dT}\tau(CO_2)(1-\tau(H_2O))d\nu$$

Using (3-22), (3-21) may be rewritten

$$R_{H_2O} - \int_4 \frac{dB}{dT}(1-\tau(H_2O))d\nu + R_{CO_2} - \int_4 \frac{dB}{dT}(1-\tau(CO_2))d\nu + \int_4 \frac{dB}{dT}(1-\tau(H_2O)\tau(CO_2))d\nu$$

$$= R_{H_2O} + R_{CO_2} - \int_4 \frac{dB}{dT}(1-\tau(H_2O)-\tau(CO_2)+\tau(H_2O)\tau(CO_2))d\nu$$

$$= R_{H_2O} + R_{CO_2} - \int_4 \frac{dB}{dT}(1-\tau(H_2O))(1-\tau(CO_2))d\nu$$

$$= R_{H_2O} + R_{CO_2} - \int_4 \frac{dB}{dT}(1-(CO_2))d\nu - \Delta R_{H_2O} \qquad (3\text{-}23)$$

Now in checking the wave numbers used by Elsasser to determine the limits of the various integrals, it becomes apparent that his region 4, from 540 cm^{-1} to 820 cm^{-1} includes the entire region for which he gives values of $\tau(CO_2)$ and is thus equal to region 3 plus region 4. So region 3 is

degenerate and

$$R_{CO_2} = \int_4 \frac{dB}{dT}\,(1-\tau(CO_2))\,d\nu$$

Also $\int_\infty \frac{dB}{dT}\,d\nu = \frac{dB}{dT} = 4\sigma T^3 = 4.678 \times 10^{-7}\,T^3$ from which, with (3-23) and (3-19),

$$F = \int_{T(z_g)}^{T(\bar{z})} \tau_{ice} \left| R_{H_2O} - \Delta R_{H_2O} - 4.678\times 10^{-7} T^3 \right| dT \qquad (3\text{-}24)$$

One further correction is necessary. Elsasser's ΔR_{H_2O} which we will designate as $\Delta' R_{H_2O}$ was computed for a constant T = +20°C. Our computations will be made for much lower values of T. The appropriate values of $\frac{dB}{dT}$ from Elsasser and Culberson's (1960) table 1 are given in table III-1. The correction of Elsasser's tabulation so that it applies to a temperature T is made by observing that

$$\int_{\nu_1}^{\nu_2} \frac{dB}{dT}(T)\,\tau(H_2O)(1-\tau(CO_2))\,d\nu$$

$$\cong \int_{\nu_1}^{\nu_2} \frac{\frac{dB}{dT}(T)}{\frac{dB}{dT}(20°)}\,\frac{dB}{dT}(20°)\,\tau(H_2O)(1-\tau(CO_2))\,d\nu$$

$$\cong \left.\frac{\frac{dB}{dT}(T)}{\frac{dB}{dT}(20°)}\right|_{\nu^*} \Delta R_{H_2O}, \text{ where } \nu^* \text{ is some value of } \nu \text{ betseen } \nu_1 \text{ and } \nu_2.$$

Furthermore, from table III-1 $\frac{dB}{dT}$ varies only slightly with ν while $\tau(H_2O)(1-\tau(CO_2))$ varies by orders of magnitude. The major contribution

to the integral will then be in the narrow peak of $\tau(H_2O)(1-\tau(CO_2))$ in the neighborhood of 680 cm^{-1}, and the appropriate value of ν^* will be near this.

$$\left.\frac{\frac{dB}{dT}(T)}{\frac{dB}{dT}(20°)}\right|_{680\ cm^{-1}} = .64 \text{ for } T = -40°C;$$

.705 for T = -30°C and .77 for T = -20°C.

To a good approximation, we can write at least for the range $-45°C < T < -15°C$

$$\Delta R_{H_2O} = (.90 + .0065T(°C))\Delta' R_{H_2O}$$

As Elsasser uses units of cal $cm^{-2}day^{-1}$,

$$F = \frac{1}{2}\int_{T(0)}^{T(\bar{z})} \tau_{ice}\left[R_{H_2O} - (.90 + .0065T)\Delta' R_{H_2O} - 4.678 \times 10^{-7}T^3\right]dT \text{ in}$$

cal $cm^{-2}(12\ hr)^{-1}$.

Table III-1.

$\nu \backslash T$	-40	-30	-20	$\frac{dB\nu}{dT} \times 10^6$ +20
560	6763	7240	7694	9290
600	6865	7411	7937	9820
640	6866	7478	8073	10242
680	6778	7449	8107	10555
720	6612	7333	8047	10760
760	6379	7141	7904	10860
800	6094	6887	7688	10861

CHAPTER IV

PHYSICAL SITUATIONS OF INTEREST

We will examine typical soundings simulating conditions at varying times during an ice fog event and consider how the flux divergence and cooling rates vary with such parameters as the complexity of the equations used, the fog height, crystal number density and crystal size distribution. This chapter will be concerned with specifying the soundings to be used, and determining the numerical values for most of the coefficients in the flux equations. The actual application of computer techniques, and discussion of the possible significance of the results, will be reserved for chapters V and VI.

A. The Meteorological Situation

A typical ice fog event is preceded by cloud cover and cold air advection aloft. As the air above about 900 mb becomes colder and dryer, the cloud cover thins until it is visually transparent. The air near the ground is now free to cool radiatively. As it cools, the moisture initially present forms numerous tiny (25μ - 100μ) ice crystals, or in some cases snowflakes. These crystals fall out very slowly, and during their period of semi-suspension they are effective radiators, collecting heat from the air by conduction and radiating it away. Gotaas and Benson (1965) studied this effect but did not take into account the radiation exchanged among the crystals.

As the crystals fall out, radiative cooling directly from the snow surface becomes increasingly important, and a steep surface

inversion develops. The cold air layer produced will drain from higher to lower-lying areas, at first thickening the cold air layer in the valley bottoms, but later flowing across the tops of the low lying pools of intensely cold air. Wind speeds are generally less than 2 m sec^{-1} in the lowlands, although hilltop stations (such as Birch Hill, 200 m above the flats) normally record measureable to strong winds (20 m sec^{-1}) throughout an ice fog event. On the slopes, katabatic flow may be of considerable importance. In the densely inhabited valley bottom of the Chena-Tanana confluence (Fairbanks), the water vapor produced by heating and power plants and by automobiles becomes trapped in the cold, stagnant layer of air near the ground. The saturation vapor pressure of ice is rapidly exceeded, and fog normally becomes visible in downtown Fairbanks at in-town ground temperatures of around -30°C. Temperatures usually continue to drop, and the ice fog continues to thicken (Benson, 1965; Benson and Rogers, 1965). The fog crystals are now participating in the radiative exchange.

While surface temperatures are decreasing and ice fog is forming, the continuing cold air advection aloft is being increasingly balanced by warming due to subsidence (Bowling et al., 1968). In most cases, the temperature of the warmest air aloft begins to increase from minimum values near or below -30°C within 24 hours after the sky clears. During the time temperatures at the ground are at their lowest level (-40° to -50°C), the air aloft may have warmed up to temperatures near or even above -20°C. However, this relatively warm air will also be quite dry, and will thus remain fairly transparent except in the carbon dioxide band. Radiosonde humidities usually range from 15% to 60% in the warm layer.

Eventually the combination of cold advection and subsidence warming is replaced by advection of warm, moist air, and a dense cloud cover returns to the area. Back radiation from the clouds causes rapid warming at ground level, and the fog evaporates.

The radiative balance under thick clouds can be determined by using conventional flux computation techniques with the cloud layer considered as a block body at the temperature of its lower boundary. From the time the cloud cover thins to infrared semi-transparency to just before the advection of fresh dense clouds, the presence of ice crystal displays and/or ice fog requires the use of a treatment of the type developed in the preceding chapter. These are the situations to be examined.

The first subject will be the initial cooling in the presence of suspended ice crystals or light snow, as studied by Gotaas and Benson (1965). Since the majority of the crystals in these displays are neither spherical nor randomly oriented, the use of Mie theory is not justified and only black crystals will be considered. The exact numbers to be used are considered in the sections B and C of this chapter.

The second subject will be ice fog, in which the crystals are nearly spherical and randomly oriented, and Mie scattering must be considered.

Ice fog occurs under a succession of conditions, of which we will consider the two extremes. The formation of a sounding typical of the onset of ice fog, with cold, relatively moist air aloft, together with the terminal phase of an ice fog event, with relatively

warm but dry air aloft, will be considered in section L. Available experimental data will be discussed in section E. The transition from flux divergence to temperature change, as well as energy transfer processes other than radiation, will be discussed in section F.

B. The Absorbing Gases

Water vapor, carbon dioxide and ozone, in that order, are the significant infrared absorbers in most lower atmospheric work. In the case of ice fog and ice crystal displays the total atmospheric precipitable water is extremely small (under 2 mm in most of the cases considered here and at the temperatures involved the peak of the blackbody curve approaches the CO_2 15μ band. CO_2 thus becomes a significant absorber, while water vapor becomes much less important than it is in more temperate climates. Tropospheric ozone will be neglected, but the radiation from stratospheric ozone approximates the blackbody curve for -40°C in the 10μ region (Murcray 1963), and will be considered in computing the downward flux from the stratosphere.

Elsasser and Culbertson's (1960) figures for the transmissivities of water vapor and carbon dioxide will be used. Elsasser (1942) observed that although the values of the smoothed transmissivity for a given optical thickness of absorbing gas varied by orders of magnitude with changing wave number, the shapes of the curves of transmissivity versus optical thickness remained remarkably consistent for any given gas. In fact, in a transmissivity versus log-optical thickness (log u) plot, the curves could be brought into near agreement by shifting them along the log u axis.* This fact suggested the

*Note "log" is used for base 10 logarithms; the alternate ln notation is used for base e logarithms.

definition of a generalized absorption coefficient, L (=L(ν)) such that log L gives the necessary shift along the log u axis for overlap of the various transmissivity curves. It is then possible to define the flux transmissivity τ as a function of a single variable, τ(log L + log u). Thus, instead of tabulating τ as a two dimensional array of optical thickness and wave number, we may tabulate the two one dimensional functions log L(ν) and τ(log L + log u).

Elsasser and Culbertson (1960) present tabulations of τ_F (our τ) for water vapor and carbon dioxide which are reproduced in Tables IV-1 and IV-2.

Table IV-1

Water Vapor Flux Transmissivity

$\tau(\log L_{H_2O} + \log u)$

	-4	-3	-2	-1	0	1
0.0		95.22	83.04	54.52	15.54	0.45
0.1		94.39	81.09	50.67	12.45	0.19
0.2		93.50	78.95	46.71	9.73	0
0.3	99.32	92.55	76.61	42.67	7.41	
0.4	98.98	91.53	74.06	38.59	5.50	
0.5	98.54	90.42	71.30	34.50	3.98	
0.6	98.01	89.21	68.33	30.44	2.81	
0.7	97.40	87.88	65.15	26.46	1.93	
0.8	96.73	86.42	61.78	22.61	1.28	
0.9	96.00	84.81	58.23	18.95	0.80	
1.0	95.22	83.04	54.52	15.54	0.45	

Their tables of log L are all valid for T = +20C; however, they give curves for +20C, -10C, -40C and -70C. Their curves for water vapor and carbon dioxide were scaled for -40C, and the results are given in Table IV-3. Since the flux transmissivity for the entire depth of the wettest atmosphere considered here will be unity over most of the

Table IV-2

Carbon Dioxide Flux Transmissivity

$\tau(\log L_{CO_2} + \log v)$

	-6	-5	-4	-3	-2	-1	0	1
0.0		99.52	96.62	90.24	77.93	53.83	20.67	2.19
0.1		99.37	96.15	89.35	76.14	50.69	17.73	1.63
0.2		99.18	95.65	88.40	74.22	47.46	15.00	1.23
0.3		98.97	95.12	87.39	72.17	44.13	12.51	0.94
0.4		98.72	94.55	86.30	69.97	40.74	10.28	0.73
0.5		98.45	93.94	85.14	67.64	37.31	8.30	0.57
0.6		98.14	93.29	83.90	65.15	33.87	6.58	0.43
0.7		97.81	92.60	82.57	62.53	30.44	5.12	0.31
0.8	99.74	97.44	91.86	81.13	59.76	27.07	3.91	0.19
0.9	99.65	97.04	91.08	79.59	56.86	23.80	2.94	0.10
1.0	99.52	96.62	90.24	77.93	53.83	20.67	2.19	0.02

water vapor window, the water vapor coefficients in this region have been approximated by putting a lower limit of -4 on log L. (This makes $\tau = 1$, see Table IV-1.) In order to give the values in these tables more meaning, Figure IV-1 shows the absorption curves ($1-\tau$) for the full height of a rather wet ice fog atmosphere.

As mentioned during the derivation of equations for the scattering case, the upper boundary for these equations can be controlled most easily by an artificial extension of the sounding above the stratosphere to 0°K without absorbers for all except the ozone band. The ozone band will be considered to cover the wave number intervals centered at 1000 cm^{-1} and 1040 cm^{-1}, and our soundings in these intervals will be extended to -40C.

The downward flux from the stratosphere provides some information on the significance of various spectral regions for ice crystal radiation. Since most of the ice fog and ice crystal soundings considered will have tropopause heights below 300 mb and tropopause

Table IV-3

Generalized Absorption Coefficients for T = -40°C
Values in Parentheses are Interpolated;
Others are Scaled from Elsasser and Culbertson (1960)

I	ν	dν	λ (microns)	Log L_{H_2O}	Log L_{CO_2}
1	10	20	1000	.35 + 1	-10
2	40	40	250	.15 + 2	-10
3	80	40	125	.53 + 2	-10
4	120	40	83.3	.73 + 2	-10
5	160	40	62.5	.70 + 2	-10
6	200	40	50.0	.60 + 2	-10
7	240	40	41.7	.42 + 2	-10
8	280	40	35.7	.13 + 2	-10
9	320	40	31.2	.80 + 1	-10
10	360	40	27.8	.35 + 1	-10
11	400	40	25.0	+ 1	-10
12	440	40	22.71	.54	-10
13	480	40	20.81	.10	-10
14	520	40	19.25	.61-1	-7
15	560	25	17.85	.15-1	.67-6
16	570	10	17.55	(.02-1)	.0-5
17	580	10	17.25	(.90-2)	.84-5
18	590	10	16.95	(.77-2)	.68-4
19	600	10	16.65	.65-2	.50-3
20	610	10	16.40	(.50-2)	.11-2
21	620	10	16.12	(.35-2)	.80-2
22	630	10	15.88	(.20-2)	.38-1
23	640	10	15.61	.05-2	.79-1
24	650	10	15.39	(.90-3)	.25
25	660	10	15.15	(.75-3)	.45
26	670	10	14.91	(.60-3)	.52
27	680	10	14.70	.46-3	.41
28	690	10	14.50	(.30-3)	0
29	700	10	14.30	(.14-3)	.64-1
30	710	10	14.09	(.98-4)	.22-1
31	720	10	13.89	.83-4	.70-2
32	730	10	13.70	(.66-4)	.19-2
33	740	10	13.51	(.49-4)	.70-3
34	750	10	13.32	(.32-4)	.18-3
35	760	10	13.16	.15-4	.57-4
36	770	10	12.99	-4	-4
37	780	10	12.82	-4	.44-5

Table IV-3 (Continued)

Generalized Absorption Coefficients for T = -40°C
Values in Parentheses are Interpolated;
Others are Scaled from Elsasser and Culbertson (1960)

I	ν	dν	λ (microns)	Log L_{H_2O}	Log L_{CO_2}
38	790	10	12.66	-4	.75-6
39	800	10	12.50	-4	.18-6
40	810	15	12.33	-4	.25-7
41	840	40	11.90	-4	-10
42	880	40	11.37	-4	-10
43	920	40	10.87	-4	-10
44	960	40	10.40	-4	-10
45	1000	40	10.00	-4	-10
46	1040	40	9.61	-4	-10
47	1080	40	9.26	-4	-10
48	1120	40	8.93	.09-4	-10
49	1160	40	8.62	.85-4	-10
50	1200	40	8.33	.55-3	-10
51	1240	40	8.06	.40-2	-10
52	1280	40	7.81	.21-1	-10
53	1320	40	7.57	0	-10
54	1360	40	7.35	.59	-10
55	1400	40	7.14	.15+1	-10
56	1440	40	6.94	.62+1	-10
57	1480	40	6.75	.07+2	-10
58	1520	40	6.58	.52+2	-10
59	1560	40	6.41	.15+2	-10
60	1600	120	6.25	.65+1	-10
61	1800	200	5.55	.32+1	-10
62	2000	200	5.00	.10-1	-10
63	2200	200	4.54	.25-4	-10

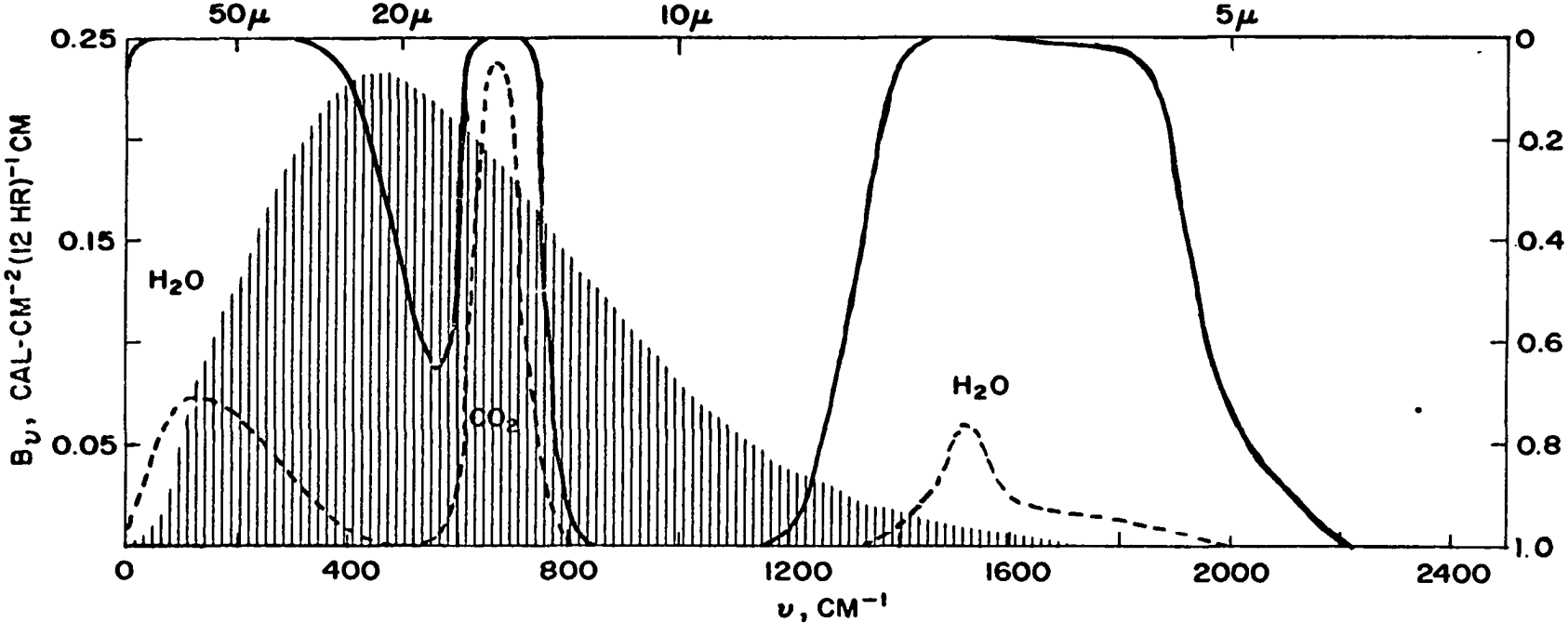

IV-1 Absorption by a saturated atmosphere with temperatures typical of ice fog. Solid curve is for the entire atmosphere with total precipitable water 0.2 cm and total carbon dioxide 240 cm at STP; dashed curve for a 50 m layer ice-saturated at 1013 mb and -40°C. Both refer to right hand scale. The blackbody curve at -40°C is shaded for reference (left hand scale).

temperatures around -55°C, we will for the purposes of estimating the stratospheric contribution consider the stratosphere above 300 mb to be an isothermal layer extending to 50 mb and having a temperature of -55°C (218°K).

The water vapor content of the stratosphere is difficult to estimate, and has been the subject of some controversy (Murcray et al., 1966; Houghton, 1966). Furthermore, none of the measurements alluded to have been made in a winter subpolar or polar atmosphere. The ice saturated case gives an upper limit to the mixing ratio of 4.3×10^{-5} x (300/P) g/g*(P = pressure in millibars). Houghton (1966) suggests a constant mixing ratio of 2×10^{-6} g/g, while Murcray et al. (1966) give values varying with height and ranging from 10^{-4} to 10^{-6} g/g. Pick and Houghton (1969) give 3×10^{-6} g/g, while Kuhn et al. (1969) emphasize the variability of stratospheric water vapor with time and place. Kuhn and London (1969) use extreme values of 10^{-4} and 10^{-6} g/g in the 30-110 km region. On the basis of the available data, we will use a value of 4×10^{-6} g/g for the winter arctic case, corresponding to about 10% relative humidity over ice at the tropopause, and obtain an error estimate by computing a few points for mixing ratios of 10^{-4} and 10^{-6} g/g. Elsasser's linear pressure reduction has been used. The reduced optical depths of water vapor for the central and extreme mixing ratios are then 1.8×10^{-4} cm, 4.4×10^{-3} cm and 4.4×10^{-5} cm. The corresponding reduced value for carbon dioxide is 10.6 cm (STP).

The transmissivity of the stratosphere is given by $\tau(H_2O)\tau(CO_2)$; the corresponding emissivity (= absorptivity) is $1-\tau(H_2O)\tau(CO_2)$ and the emitted flux intensity is given by $\left[B_\nu(218°K)\right]\left[1-\tau(H_2O)\tau(CO_2)\right]$. The

*Mixing ratios are expressed in g H_2O/g air.

results of these calculations for the 63 wave number intervals of Table IV-3 are given in Table IV-4. The resulting flux is shown in Figure IV-2. It is apparent that back radiation in the carbon dioxide and ozone bands will effectively cancel tropospheric radiation, while the windows on both sides of the carbon dioxide band will be of considerable importance in considering radiation to space from the troposphere.

Finally, it is necessary to consider the influences of water vapor and carbon dioxide on κ, the extinction coefficient needed for computation of the flux divergence in the ice fog case. By definition

$$\kappa = \left| \frac{d\ln\tau}{dz} \right| + \beta = \left| \frac{d\ln\tau(H_2O)}{dz} \right| + \left| \frac{d\ln\tau(CO_2)}{dz} \right| + \left| \frac{d\ln}{dz}\,\tau(\text{ice}) \right| + \beta.$$

Considering first the water vapor contribution, and letting $\tau = \tau(H_2O)$,

$$\left| \frac{1}{\tau} \frac{d\tau}{dz} \right| \approx \frac{2}{\tau(z_2)+\tau(z_1)} \left| \frac{\tau(z_2)-\tau(z_1)}{z_2-z_1} \right| .$$

$\tau(z')$ was defined in Chapter III as a shorthand notation for $\tau_s(z,z')$, where z is the height at which the flux is to be computed. This is also the height at which the derivative is to be evaluated. Setting $z_2 = z$ and $z_1 = z + \Delta z$, we have

$$\left| \frac{d\ln\tau}{dz} \right| \approx \frac{2}{\tau(z)+\tau(z+\Delta z)} \quad \frac{\tau(z)-\tau(z+\Delta z)}{|\Delta z|}$$

Now if $z' = z$, $\tau(z') = \tau_s(z,z)$, which, as the transmissivity of a layer of zero thickness, equals unity. In order to make Δz as small as possible, $\tau(z+\Delta z)$ should be the first value in Table IV-1 which differs from 1. (This happens to be .9932, for log u + log L_{H_2O} = -4 + .3).

Table IV-4 Downward Flux at 300 mb

ν	τ (50 mb - 300 mb)	cal/cm^2 day cm^{-1} $(1-\tau)B_\nu$	cal/cm^2 day $(1-\tau)B_\nu d_\nu$
10	.8921	1.20×10^{-4}	2.4×10^{-3}
40	.7406	4.17×10^{-3}	1.67×10^{-1}
80	.6245	2.09×10^{-2}	8.36×10^{-1}
120	.5526	4.83×10^{-2}	1.93
160	.5637	7.00×10^{-2}	2.80
200	.60	8.72×10^{-2}	3.49
240	.6610	9.03×10^{-2}	9.03
280	.7457	7.70×10^{-2}	3.08
320	.8207	6.00×10^{-2}	2.40
360	.8921	3.85×10^{-2}	1.54
400	.9302	2.52×10^{-2}	1.01
440	.9680	1.16×10^{-3}	4.64×10^{-1}
480	.9915	3.02×10^{-3}	1.21×10^{-1}
520	1.0000	0	0
560	.9781	7.07×10^{-3}	1.27×10^{-1}
570	.9649	1.13×10^{-2}	1.13×10^{-2}
580	.9131	2.72×10^{-2}	2.72×10^{-1}
590	.8376	5.04×10^{-2}	5.04×10^{-1}
600	.6611	1.03×10^{-1}	1.03
610	.4940	1.53×10^{-1}	1.53
620	.2609	2.16×10^{-1}	2.16
630	.1008	2.57×10^{-1}	2.57
640	.0370	2.67×10^{-1}	2.67
650	.0100	2.72×10^{-1}	2.72
660	.0060	2.66×10^{-1}	2.66
670	.0050	2.59×10^{-1}	2.59
680	.0067	2.48×10^{-1}	2.48
690	.0202	2.41×10^{-1}	2.41
700	.0556	2.26×10^{-1}	2.26
710	.1375	2.02×10^{-1}	2.02
720	.2943	1.61×10^{-1}	1.61
730	.4679	1.18×10^{-1}	1.18
740	.6169	8.32×10^{-2}	8.32×10^{-1}
750	.7402	5.5×10^{-2}	5.5×10^{-1}
760	.8390	3.3×10^{-2}	3.3×10^{-1}
770	.8997	2.2×10^{-2}	2.2×10^{-1}
780	.9412	1.14×10^{-2}	1.14×10^{-1}
790	.9751	4.70×10^{-3}	4.70×10^{-2}
800	.9916	1.53×10^{-3}	1.53×10^{-2}
810	1.0000	0	0
840	1.0000	0	0
880	1.0000	0	0
920	1.0000	0	0

Table IV-4 Downard Flux at 300 mb (Continued)

ν	τ (50 mb - 300 mb)	cal/cm2 day cm^{-1} $(1-\tau)B_\nu$	cal/cm^2 day $(1-\tau)B_\nu d_\nu$
960	1.0000	0	0
1000	0 (0_3)	1.6×10^{-1}	6.4
1040	0 (0_3)	1.4×10^{-1}	5.16
1080	1.0000	0	0
1120	1.0000	0	0
1160	1.0000	0	0
1200	1.0000	0	0
1240	1.0000	0	0
1280	1.0000	0	0
1320	.9950	1.25×10^{-4}	5.00×10^{-3}
1360	.9643	8.07×10^{-4}	3.23×10^{-2}
1400	.9153	1.50×10^{-3}	6.00×10^{-2}
1440	.8529	2.12×10^{-3}	8.48×10^{-2}
1480	.7610	2.88×10^{-3}	1.15×10^{-1}
1520	.6279	3.74×10^{-3}	1.49×10^{-1}
1560	.7406	2.15×10^{-3}	8.60×10^{-2}
1600	.8481	1.04×10^{-3}	1.25×10^{-1}
1800	.8957	2.70×10^{-4}	5.40×10^{-2}
2000	1.0000	0	0
2200	1.0000	0	0

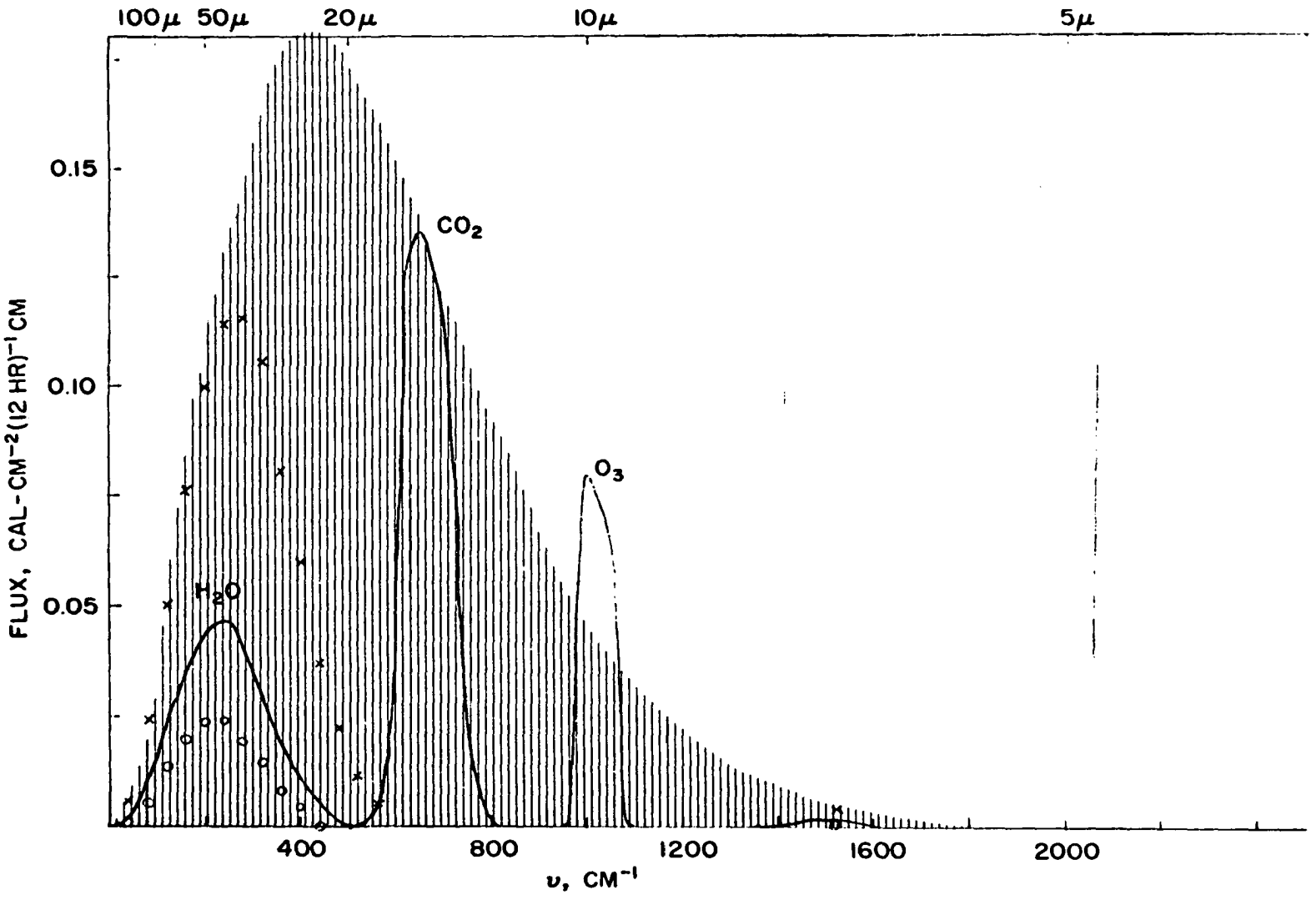

IV-2 Sky radiation at the tropopause for a -55°C stratosphere with a water vapor mixing ratio of 4 x 10^{-6} g/g. x's show a mixing ratio of 10^{-4}; circles, 10^{-6}. The -55°C blackbody curve is shaded.

Since $u = \frac{du}{dz}\Delta z$, (where $\frac{du}{dz}$ is the water vapor density in gm $cm^{-2}m^{-1}$) $u = 10^{(-4+.3-\log L_{H_2O})}$, and $\tau(z) = 1$,

$$\left|\frac{d\ln\tau}{dz}\right| \approx \frac{2}{1+.9932}\left|\frac{1-.9932}{\frac{1}{\frac{du}{dz}}10^{(-4+.3-\log L_{H_2O})}}\right| ,$$

or

$$\left|\frac{1}{\tau_{(H_2O)}}\frac{d\tau_{(H_2O)}}{dz}\right| \approx \frac{2L}{1.9932}\frac{.0068}{2\times10^{-4}}\frac{du}{dz} = 34L_{H_2O}\frac{du}{dz} \qquad (4\text{-}1)$$

For practical purposes $\frac{du}{dz}$ may be considered to be the sum of the u's in the layers above and below the level at which the flux divergence is being calculated, divided by the sum of their thickness.

By similar processes,

$$\left|\frac{1}{\tau(CO_2)}\frac{d\tau(CO_2)}{dz}\right| = 4.1\, L_{CO_2}\frac{dv}{dz} \times 10^2$$

Since $\frac{dv}{dz} = .0003\frac{P}{1013}\frac{273}{T} \times 10^2$ for z in meters (where P is pressure in millibars and T is temperature in °K), this can be rewritten as

$$\left|\frac{d\ln\tau(CO_2)}{dz}\right| = 3.3\, L_{CO_2}\frac{P}{T} . \qquad (4\text{-}2)$$

C. Physical Parameters of an Ice Crystal Display

Ice crystals suspended in otherwise clear air may radically change the radiative cooling rate of the air even when actively growing and releasing latent heat*, as demonstrated by Gotaas and Benson (1965).

*Note that in the free air the direction of the latent heat term always opposes that of all other processes combined. In other words, latent heat is added only if the air is cooling and the ice crystals growing. If the air is warming, the crystals will evaporate and remove latent heat from the air.

In order to obtain the energy flow to or from the air containing ice crystals it is necessary to consider both the energy emitted by the crystals and the energy absorbed from the radiation incident on the crystals. This energy will consist of that originally emitted by the ground, atmospheric gases and other crystals. For a first approximation, which is valid if the total optical depth of the crystal display is significantly less than unity, the radiation from other crystals may be ignored, as was done by Gotaas and Benson (1965). But if the display is very deep or dense, the crystals, especially those in the lower parts of the display, will clearly be affected by radiation from higher crystals.

The calculation of the heat balance including the effects of interaction among crystals will be carried out in Chapters V and VI. The remainder of this chapter will be concerned with the definition and numerical computation of the quantities to be used in the final computer calculations.

Assume that an ice crystal display contains one horizontally oriented thin plane crystal, of radius 25μ, per cm^3 (Gotaas and Benson, 1965).* Three sets of initial conditions of temperature and humidity will be considered. Two of Gotaas and Benson's (1965) soundings are used here to allow comparison with their results: 1400 14 December 1961 and 1400 24 January 1962, both times being Alaska Standard Time (AST) = GMT-10 hours. The significant levels of these soundings are given in Table IV-5, and the soundings are shown in Figure IV-3. On these two soundings radiosonde humidities are accepted to facilitate comparison with the previous study, although the accuracy of the sensing elements is highly questionable at the temperatures involved.

*This is, of course, a simplification; individual ice crystals will oscillate about the stable horizontal orientation, and there will be a range of radii from 10μ to several hundred μ

Table IV-5

Significant Points of Soundings from Gotaas and Benson (1965)

P(mb)	h(m above msl)	z(m above ground)	T(°C)
a) 1400 14 December 1961			
993	135	0	-18.2
876	1050	915	-24.5
766	2050	1915	-24.5
738	2300	2165	-21.2
669	3020	2885	-21.9
500	5118	4973	-33.7
400	6644	6509	-46.7
348	7540	7405	-54.4
100	15669	15534	-47.2
50	20219	19074	-51.3
18	26794	26659	-57.4
b) 1400 24 January 1962			
1005	135	0	-30.4
978	340	205	-29.1
945	590	455	-25.1
895	980	845	-27.4
853	1320	1185	-26.4
768	2060	1925	-30.7
724	2490	2355	-31.0
400	6530	6395	-49.1
289	8660	8525	-54.4
100	15473	15138	-51.0
50	19967	19832	-52.3
39	21571	21436	-52.9

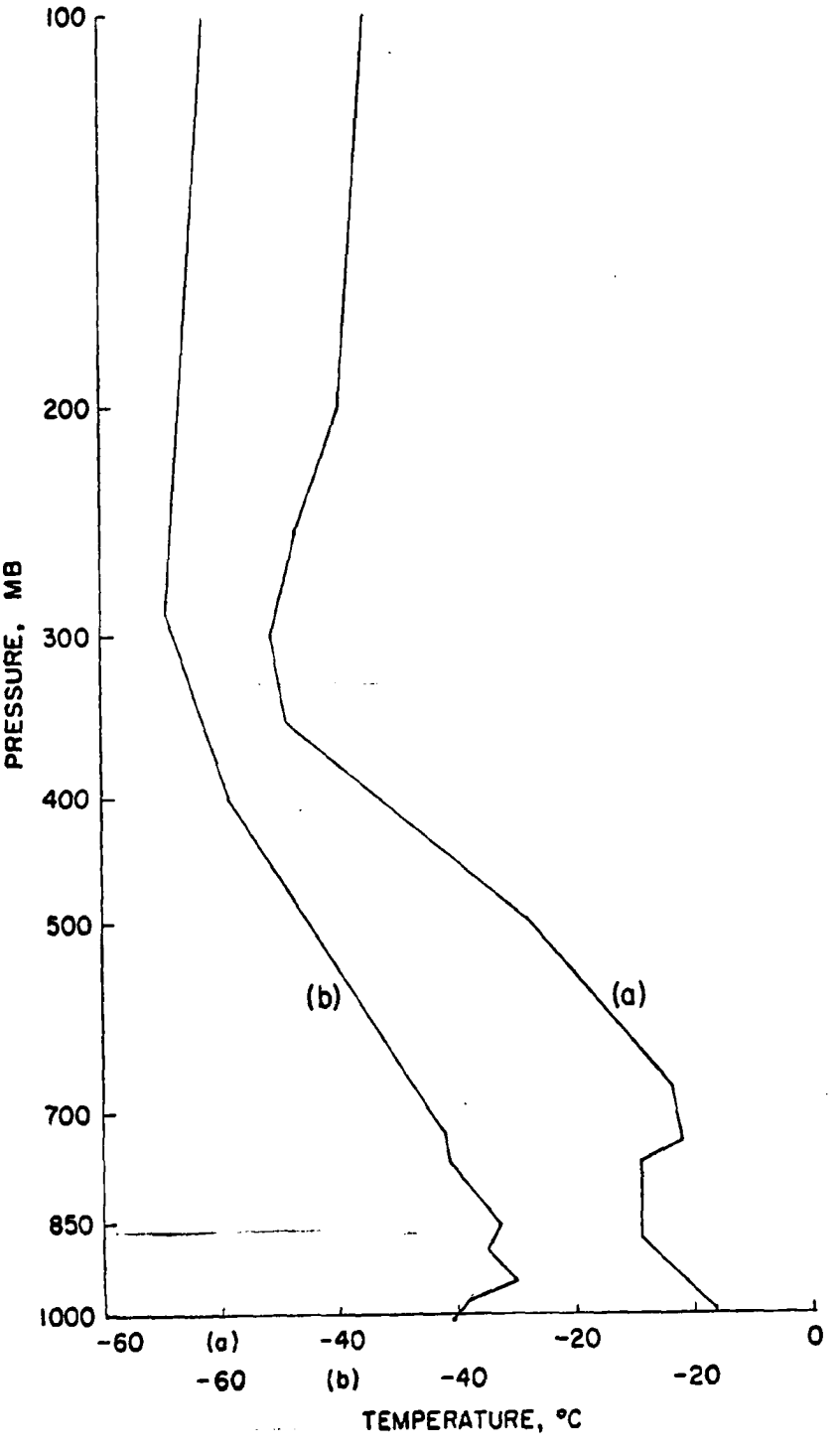

IV-3 Soundings from Gotaas and Benson (1965); (a) 1400 14 Dec 1961 local time, lower temperature scale; (b) 1400 24 Jan 1962, upper temperature scale.

The third sounding is an abstraction for purposes of discussion. It was based on soundings preceding nine of the ice fog events or sub-events listed in Bowling (1967) (Fig. IV-4). The purpose of this composite sounding was to provide the simplest possible sounding which showed the general temperature structure typical of an ice crystal display. With it we can test the effect of varying both such computational parameters as the number of subdivisions used in the integrations, and such purely physical parameters as the height and density of the crystal display.

The significant points in this composite are the features common to most or all of the soundings. These include: (1) a highly variable lapse rate from the ground to about 700 mb. The most common form appeared to be a succession ot normal and inverted lapse rates, with the most common temperatures being between about -30°C and -25°C. This region was approximated by an isothermal layer at -28°C, extending from 1000 mb to 720 mb. (2) A fairly constant normal lapse rate from around 720 mb to the tropopause. A constant lapse was used from -28°C at 720 mb to -55°C at 360 mb. (3) Above the tropopause the stratosphere was again very weakly inverted in most cases. A temperature of -48°C at 100 mb was selected and the sounding was extended above that level with an even weaker inversion to give a temperature of -47°C at 50 mb. Contributions to the near-ground flux from levels above 50 mb were neglected.

For the two soundings from Gotaas and Benson (1965), the crystal densities and radii will in all cases be held to $1/cm^3$ and 25μ respectively. We will consider cases where the upper surfaces of the crystal

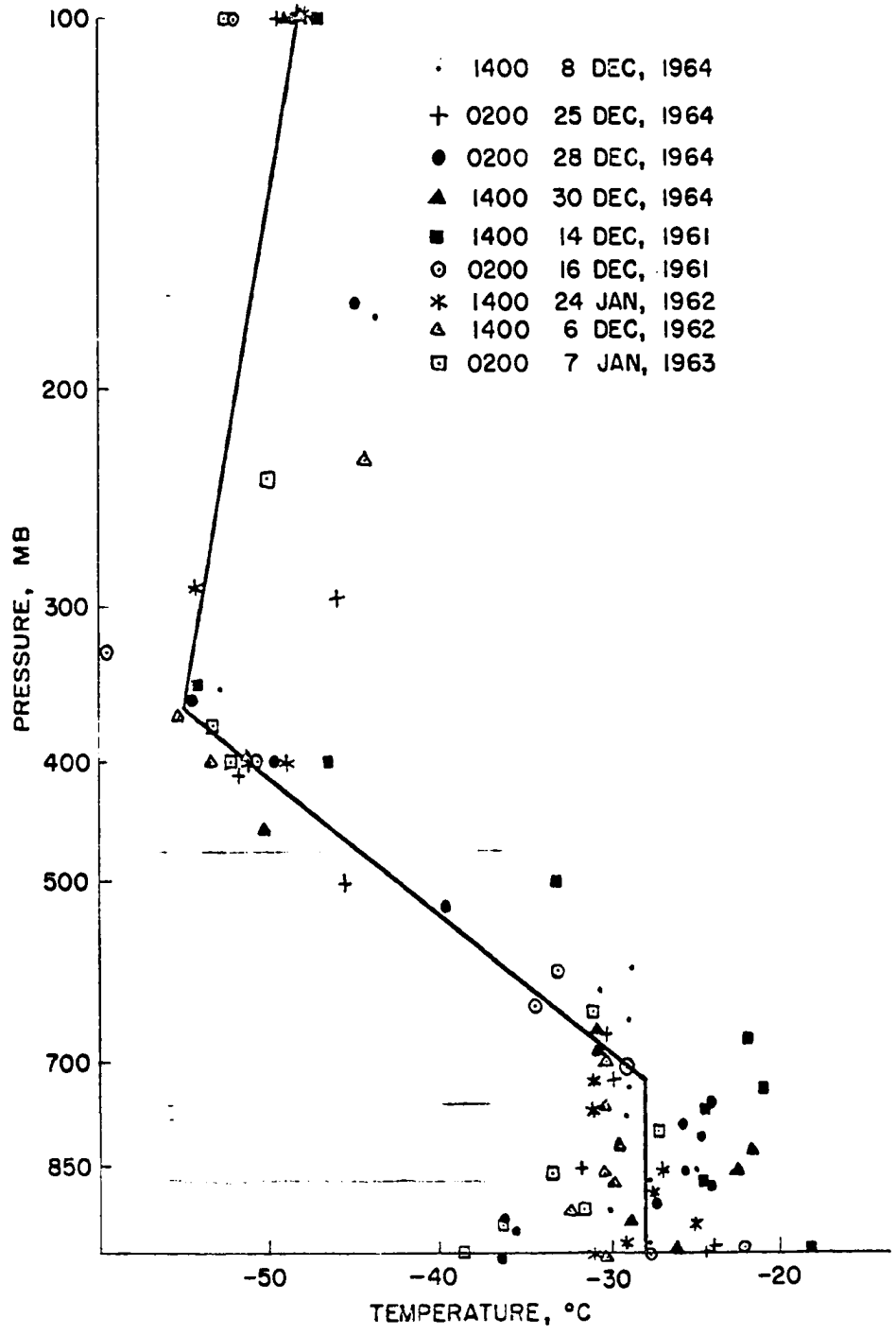

IV-4 Component and final soundings for the composite ice crystal display sounding. The component soundings were those closest to the time the cloud cover disappeared before the ice fog events discussed in Bowling (1967).

displays are 100 m, 600 m and the top of the isothermal layer (2165 m and 1185 m). This includes cases where crystal displays are controlled by power plant plumes, local topography or regional cooling respectively.

Black, thin, horizontal crystals can be shown to give a vertical flux transmissivity which is a true exponential rather than an exponential integral. Consider the situation shown in Figure IV-5. The heavy horizontal line represents a plane, black ice crystal, seen edge-on. A sub-parallel beam of radiation of intensity I is incident on the crystal at an angle γ from the vertical. The beam carries energy $Id\Omega\cos\gamma$ per unit horizontal area vertically. If the crystal is considered to be a black disc of radius a, it will intercept and absorb an amount of energy $\pi a^2 Id\Omega\cos\gamma$. Assume n crystals per unit volume, with a normalized size distribution P(a). Then the energy absorbed per unit vertical distance per unit horizontal area from the angle $d\Omega$ is $n\int p(a)\pi a^2 da Id\Omega\cos\gamma$, and the fraction of the incident radiation absorbed is $n\int p(a)\pi a^2 da$. The vertical transmissivity of a beam at angle γ from the vertical is then $\exp(-\int n\int p(a)\pi a^2 da dz)$. The total energy transmitted by a layer of vertical extent z from an indicent hemi-isotropic flux $F_o=\pi I$, is then

$$F(z) = \int_{2\pi} (F_o/\pi)\cos\gamma d\Omega \exp(-\int n\int p(a)\pi a^2 da dz) = F_o \exp(-\int n\int p(a)\pi a^2 da dz),$$

so $\tau = \exp(-\int n\int p(a)\pi a^2 da dz)$.

For the crystal display considered in Gotaas and Benson (1965), the flux transmissivity is $\tau(ice) = \exp(-1.96 \times 10^{-3} z)$, z being in meters.

We will consider also two other types of "crystal display" (or light snowfall) in connection with the composite sounding. The first

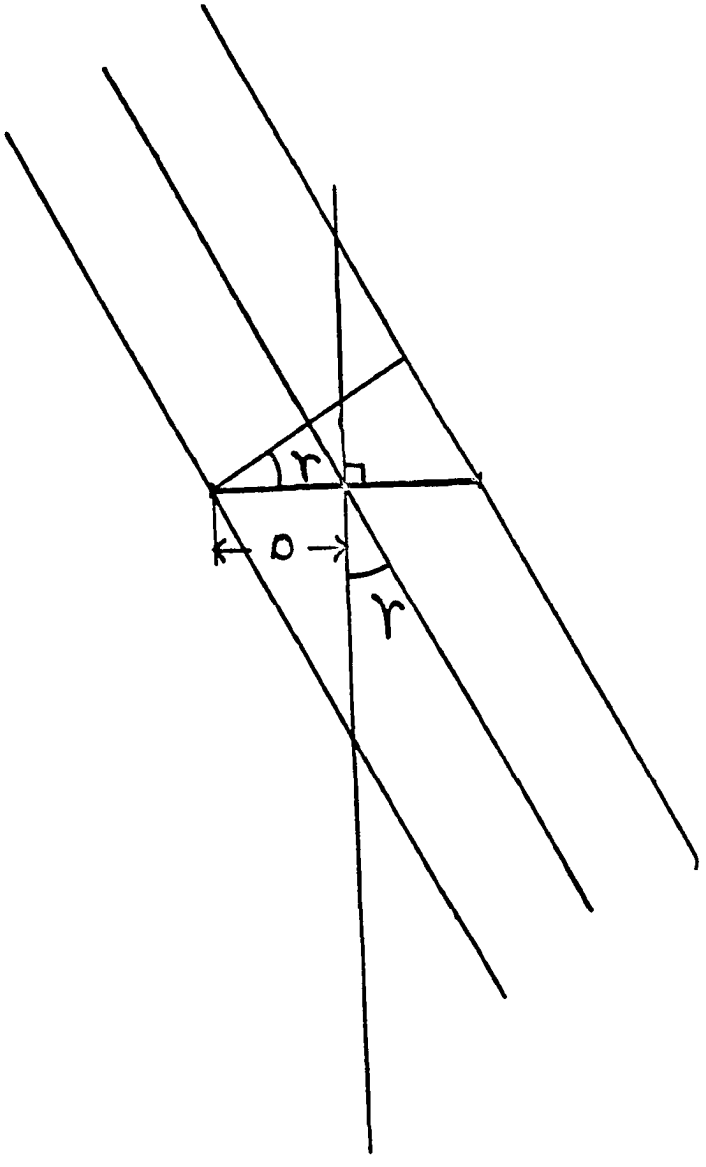

IV-3 Geometry of interception of radiation by a plane crystal, seen edge on.

may be considered either as a coarse crystal display or as fine snowflakes, with 10% of the crystal radii = .5 mm and 90% of them = .05 mm. This type of display not infrequently leaves a deposit of crystals just visible as hexagonal plates on cars, etc. after a clear night in early winter. Total densities expressed in crystals per liter, of 1000 ($\tau(ice) = \exp(-8.55 \times 10^{-2} z)$) and 100 ($\tau(ice) = \exp(-8.55 \times 10^{-3} z)$) will be considered. A density of 20 per liter would give the same transmissivity as the 25μ crystals above. Light snowfall, with plane dendritic crystals falling out of a clear sky, may consist of crystals with radii of about 1.5 mm. A density of 10 crystals/liter will give $\tau(ice) = \exp(-7.06 \times 10^{-2} z)$, roughly the same as the .5 mm-.05 mm case with n=1000/liter, while 1 crystal/liter will give $\tau(ice) = \exp(-7.06 \times 10^{-3} z)$. Snowfall and coarse displays will be lumped, and the final flux transmissivities will be taken as $\exp(-8 \times 10^{-2} z)$ for snow and $\exp(-8 \times 10^{-3} z)$ for large-crystal displays. $\tau(ice) = \exp(-1.96 \times 10^{-3} z)$ will be used for thin large-crystal displays as well as moderate small-crystal displays. Relative humidity will be assumed to be 80% over ice through the troposphere, while carbon dioxide content will be assumed to be .03% by volume throughout the atmosphere. Stratospheric water vapor was discussed in section B; a mixing ratio of 4×10^{-6} g/g will again be assumed. Tables IV-6, IV-7 and IV-8 summarize the ice crystal soundings.

D. Ice Fog

1. Soundings

Composite soundings for the initial and terminal stages of an ice fog event were manufactured in precisely the same manner as were

Table IV-6

Ice Crystal Sounding, 1400 AST 14 December 1961

Average over layer from z(J) to z(J+1)

J	Z	P	T	r.h.(ice)	u x 10^3	ν
1	0	993	-18.2	59	1.51	.78
2	25	989.75	-18.4	59	1.49	.78
3	50	986.5	-18.6	60	1.48	.78
4	75	983.25	-18.8	60	1.47	.78
*5	100	980	-18.9	64	6.06	3.12
6	200	967	-19.6	67	11.81	6.24
7	400	941	-21.0	73	11.19	6.00
*8	600	916	-22.4	82	16.40	9.60
*9	915	876	-24.5	89	51.20	26.64
*10	1910	765	-24.5	94	.544	.24
*11	1920	764	-24.5	93	4.66	2.16
12	2000	755	-23.4	93	5.03	1.92
13	2080	747	-22.3	93	5.45	1.92
*14	2160	739	-21.2	92	.73	.24
*15	2170	738	-21.2	94	28.20	9.12
16	2561	700	-21.7	95	38.15	12.06
17	3106	650	-23.0	96	34.00	12.00
18	3690	600	-25.2	100	25.55	12.00
19	4310	550	-29.8	102	19.95	12.00
20	4983	500	-33.7	88	26.80	24.00
21	6509	400	-46.7	65	2.08	12.00
22	7380	350	-54.0	40	.817	12.00
23	8363	300	-55.4	∿10	1.02	60.00
24	19074	50	-50.0	-	0	0
25	19074	50	-273	-		

Table IV-7

Ice Crystal Sounding, 1400 AST 24 January 1962

	Point			Layer Above Point		
J	Z	P	T°C	r.h.(ice)	$ux10^3$	ν
1	0	1005	-30.4	79	.643	.84
2	25	1001.5	-30.2	76	.630	.84
3	50	998	-30.0	74	.627	.84
4	75	994.5	-29.8	72	.615	.84
*5	100	991	-29.7	62	2.20	3.36
6	200	977	-29.1	61	1.172	1.68
7	250	970	-28.3	65	2.82	3.12
8	350	957	-26.7	70	3.54	3.12
9	450	944	-25.1	74	.404	.48
10	460	942	-25.2	76	1.630	1.20
11	500	937	-25.3	72	3.68	3.12
*12	600	924	-26.0	80	7.49	6.00
13	800	899	-27.1	85	3.72	3.12
14	900	886	-27.3	83	9.54	7.20
*15	1150	856	-26.4	80	2.24	1.44
*16	1208	850	-26.4	77	26.18	24.00
17	2103	750	-30.8	75	11.01	12.00
18	2592	700	-32.0	80	18.40	24.00
19	3667	600	-36.9	80	12.28	24.00
20	4911	500	-42.5	80	7.49	24.00
21	6395	400	-49.1	80	4.77	24.00
22	8262	300	-53.8	60	.371	2.64
23	8525	289	-54.4	∿10	.98	57.6
24	19832	50	-51.0	0	0	0
25	19832	50	-273			

Table IV-8

Composite Ice Crystal Sounding

J	Z	P	T(°C)	r.h.(ice)	$ux10^3$	ν
1	0	1000	-28	80%	.825	.84
2	25	996.5	-28	80%	.825	.84
3	50	993	-28	80%	.825	.84
4	75	989.5	-28	80%	.825	.84
*5	100	986	-28	80%	3.30	2.22
6	200	972	-28	80%	6.60	6.24
7	400	946	-28	80%	6.60	6.24
*8	600	920	-28	80%	13.20	12.00
*9	1000	870	-28	80%	5.52	4.80
10	1167	850	-28	80%	14.39	12.00
11	1602	800	-28	80%	15.27	12.00
12	2065	750	-28	80%	8.00	6.00
13	2308	725	-28	80%	1.65	1.20
*14	2358	720	-28	80%	1.65	1.20
15	2408	715	-28.6	80%	4.76	3.60
16	2560	700	-29.3	80%	14.33	12.00
17	3036	650	-32	80%	10.69	12.00
18	3649	600	-35.2	80%	7.92	12.00
19	4250	550	-38.3	80%	6.49	12.00
20	5402	500	-42.5	80%	6.83	24.00
21	6883	400	-51.2	80%	1.38	8.40
22	7478	365	-54.5	54%	.20	2.40
23	7656	355	-55	20%	.45	13.20
24	8731	300	-54	~10%	1.02	60
25	20466	50	-47	0	0	0
26	20466	50	-273			

those for ice crystal displays. The major differences between the initial and terminal ice fog cases are (1) the terminal sounding is considerably warmer above 100 m (especially around 800 mb) and colder near the ground, and (2) the terminal soundings tend to be dryer than the initial ones. The data points and composite soundings for the two cases are shown in Figures IV-6 and IV-7, and the numberical data on the composite soundings are given in Tables IV-9 and IV-10. It should be noted that the soundings on which these composite soundings are based were taken at the Fairbanks airport rather than downtown, and all precede the sharp increase in airport activity since about 1968 with the resulting increase in airport fog density.

The humidity within the ice fog layer was chosen to be 100% relative to ice. This is a physically reasonable assumption for a stable fog layer; measurements in areas where the fog is in the process of thickening or dissipating could be expected to give higher or lower humidities respectively. Hennni (1969) found the water vapor content in the presence of ice fog to lie between ice and water saturation, while Thuman and Robinson (1954) found water vapor contents generally below ice saturation.

The humidities above the ice fog layer are harder to define. Radiosonde measurements of humidity with respect to water vary from less than 20% to 100% in both initial and terminal soundings. Although the accuracy of radiosonde data at the temperatures involved (often below -30°C) is highly questionable, we note that the humidity values for the initial stages of ice fog seem to cluster around 60% over water, while the corresponding values for terminal ice fog are frequently less than 40%. The relatively low humidities of terminal ice fog conditions are

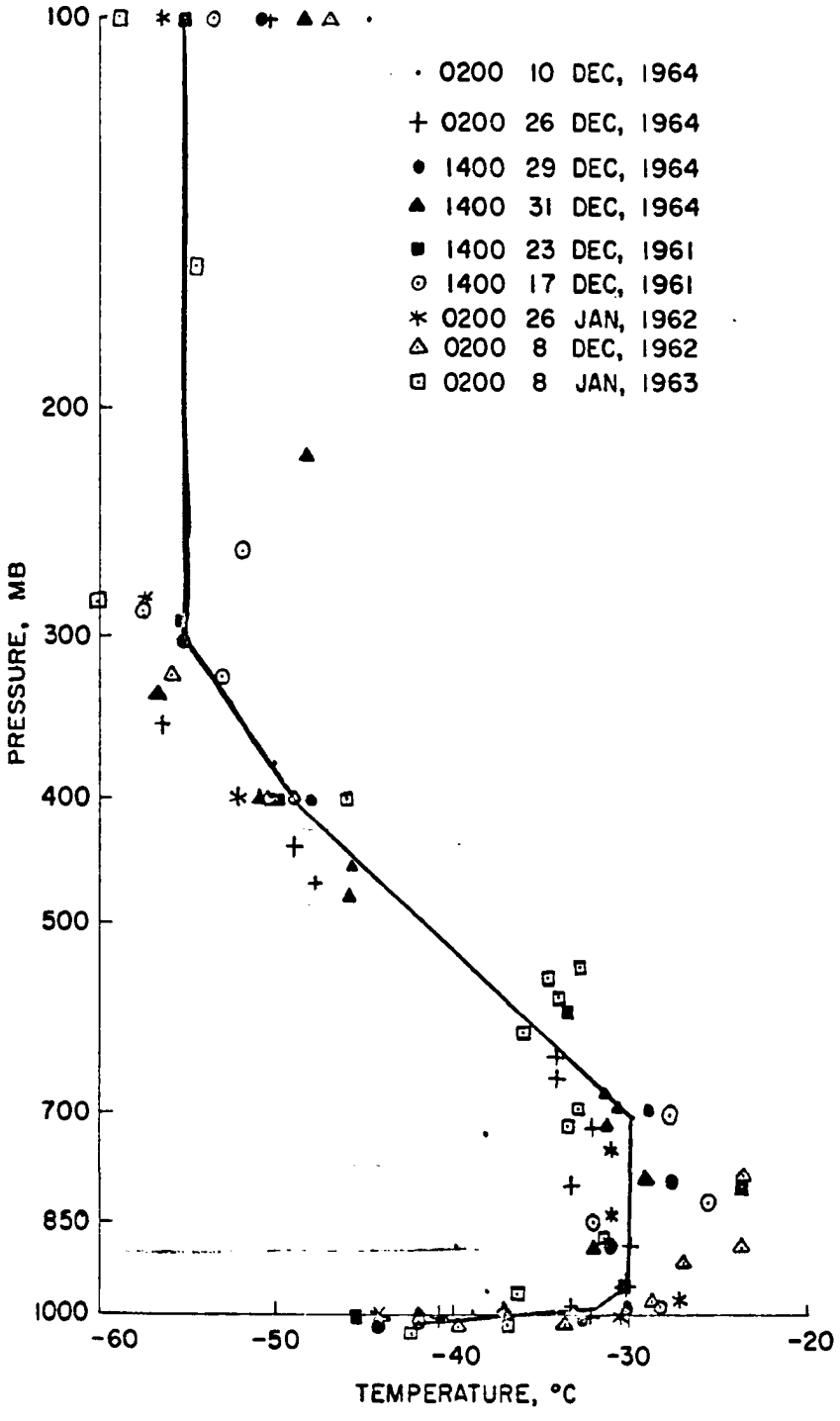

IV-6 Component and composite soundings for the composite initial phase ice fog sounding. The component soundings are in each case the first soundings in which the ground temperature was less than -40°C.

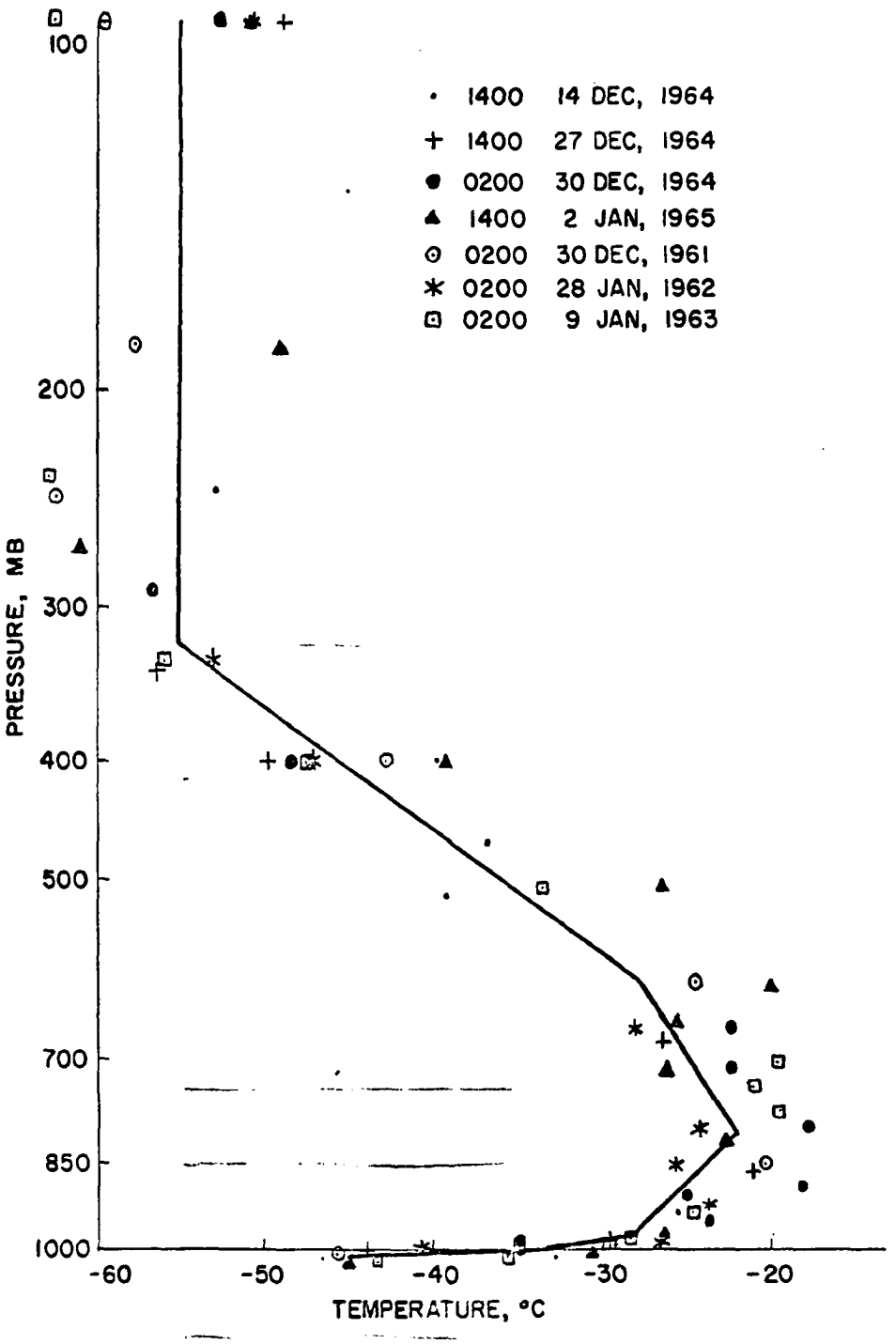

IV-7 Component and composite soundings for the typical terminal ice fog sounding. The component soundings are in each case the last before the development of a cloud cover.

Table IV-9

Initial Ice Fog Sounding

	At Z(J)				Layer above Z (J)	
J	Z	P	T	r.h.(ice)	ux10^3	V
1	0	1010.0	-44	100	.0038	.0192
2	.5	1009.92	-43	100	.0043	.0168
3	1	1009.85	-42.5	100	.0096	.0360
4	2	1009.70	-42	100	.0287	.1008
5	5	1009.28	-41.5	100	.048	.1776
6	10	1008.54	-41	100/80	.0534/.0426	.1776
7	15	1007.8	-40.5	100/80	.0534/.0426	.168
8	20	1007.1	-40	100/80	.1192/.0955	.360
9	30	1005.6	-39.5	100/80	.1329/.1061	.360
10	40	1004.1	-39	100/80	.1329/.1061	.336
11	50	1002.7	-38	100/80	.4115/.329	.888
12	75	999.0	-36	100/80	.564/.451	.864
13	100	995.4	-34	80	.759	1.296
14	138	990	-32	80	1.585	2.4
15	210	980	-31.3	80	1.760	2.4
16	283	970	-30.7	80	3.65	4.8
17	433	950	-30	80	10.40	12.0
18	818	900	-30	80	11.02	12.0
19	1225	850	-30	80	11.69	12.0
20	1657	800	-30	80	12.49	12.0
21	2117	750	-30	80	13.29	12.0
22	2608	700	-30	80	21.7	24.0
23	3692	600	-35.3	80	14.88	24.0
24	4948	500	-41.4	80	8.16	24.0
25	6439	400	-49	80	2.51	12.0
26	7310	350	-52	80	1.985	12.0
27	8302	300	-55	∿10	1.02	60.0
28	19751	50	-55	0	0	0
29	19751	50	-273			

Table IV-10

Terminal Ice Fog Sounding

	At Z(J)			Layer above Z(J)		
J	Z	P	T	r.h.(ice)	ux10^3	v
1	0	1010	-50	100	.0019	.0192
2	.5	1009.92	-47	100	.0027	.0168
3	1	1009.85	-45	100	.0068	.036
4	2	1009.70	-44	100	.0230	.108
5	5	1009.25	-43.5	100	.0428	.177
6	10	1008.51	-43	100/50	.0479/.0239	.177
7	15	1007.77	-42	100/50	.0479/.0239	.177
8	20	1007.03	-41	100/50	.1069/.0535	.348
9	30	1005.58	-40	100/50	.1329/.0664	.346
10	40	1004.14	-38	100/50	.1646/.0823	.343
11	50	1002.71	-36	100/50	.2032/.1016	.338
12	60	1001.3	-34	100/50	.4996/.2498	.672
13	80	998.5	-33	100/50	.5534/.2767	.672
14	100	995.7	-32	50	.566	1.37
15	139	990	-30.6	50	1.381	2.4
16	213	980	-28	50	1.53	2.4
17	287	970	-27.6	50	3.44	4.8
18	438	950	-27	50	9.8	12.0
19	829	900	-25.3	50	12.6	12.0
20	1246	850	-23.6	50	14.8	12.0
21	1690	800	-22	50	16.6	12.0
22	2164	750	-23.3	50	15.3	12.0
23	2667	700	-26.6	50	27.5	24.0
24	3783	600	-28	50	17.8	24.0
25	5071	500	-36	50	8.1	24.0
26	6588	400	-45.7	50	2.79	19.2
27	8047	320	-55	20	.427	4.8
28	8459	300	-55	∿10	1.02	60.0
29	19908	50	-55	0	0	0
30	19908	50	-273			

also indicated by the independent evidence for strong subsidence warming at this stage (Bowling et al., 1968). Also, radiant sky temperatures normally remain constant almost to the end of an ice fog event (Murcray, personal communication in 1969 on observations made circa 1955), even though it has been shown that air temperatures aloft normally increase through most of an ice fog period (Bowling et al., 1968). On the basis of these observations tropospheric humidities were assumed to be 80% over ice in the initial ice fog case and 50% over ice in terminal ice fog.

2. Thickness

Ice fog height may vary considerably. Benson (1965) gives thicknesses ranging from 10 m for normal light ice fog and outlying areas to 40 m for the city center under dense ice fog. During the extreme cold spell in late 1968 and early 1969, heights approaching 100 m were estimated (Weller, 1969). We will consider heights of 10, 20, 50 and 100 m.

3. Size Distribution of Ice Fog Crystals

Particle size distributions and number densities of the crystals in ice fog have recently been presented in two master's theses. Hemmi (1969) based his observations entirely on precipitated particle samples, a procedure which, as Huffman (1968) indicated, is subject to errors not only from the Stoke's law variation of falling speed with size (which can at least in theory be corrected for), but also from microturbulence and possible updrafts in the downtown area. This last source of error was also pointed out by Benson (1965). Huffman used some precipitation data, but also collected fog crystals by an impaction technique. The impaction samples showed significantly more small

crystals ($a < 5\mu$) than precipitation samples taken simultaneously. Only five of his impaction distributions were taken at temperatures near or below -40°C. Of these, one was taken at Eielson Air Force Base and appears similar in its main features to another sample taken at the Fairbanks Airport 15 February 1967 at -38.5°C. The airport sample, shown in Figure IV-8, provided distribution a in Table IV-11. In the absence of other data, this distribution is considered typical of thin, widespread ice fog due almost entirely to auto exhaust and will be used for 10 and 20 m fog heights.

Two of the five samples were taken at an open water site. They were similar to each other and showed a considerable shift towards larger crystal sizes. These distributions were not used, as they are representative of such a limited area with dense but localized fog that the assumption of horizontal homogeneity is questionable.

The final distribution, taken in downtown Fairbanks 23 December 1965 at -40°C (Fig. IV-9), is presented as distribution b in Table IV-11. It will be considered typical of the downtown area and dense ice fog derived from multiple sources. It will be used for 20 m, 50 m and 100 m thicknesses.

4. Number Density of Ice Fog Crystals.

Huffman (1968) gives particle concentrations n, (crystals per cm^3) from 27 to 90 for the airport-Eielson samples at -38 to -40°C, and from 101 to 656 in downtown Fairbanks at temperatures of -32 to -34°C. These estimates are based on visibility. Hemmi (1969) showed that numerical precipitation rates increase exponentially with decreasing temperatures. He also presents evidence that the fraction of very small particles

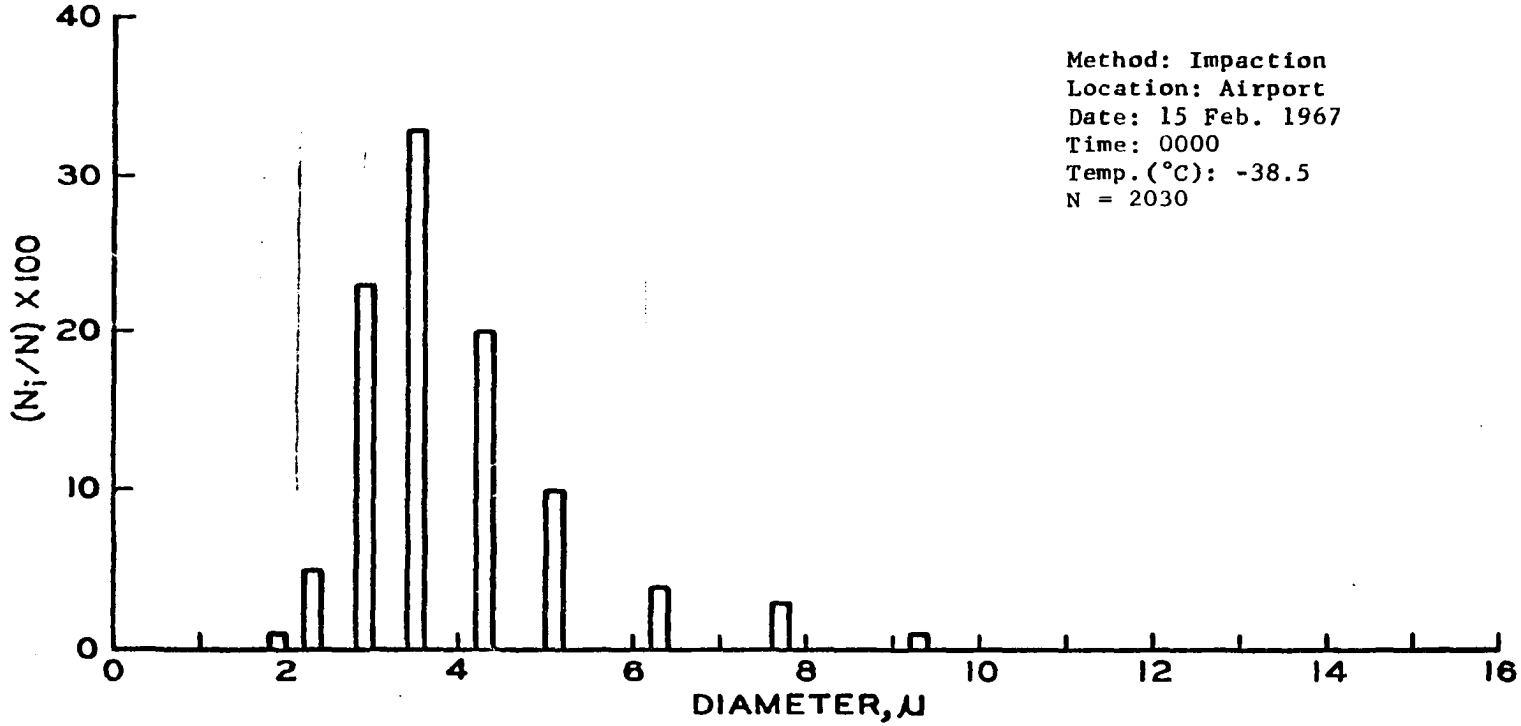

App. II. Ice fog particle size distribution.

IV-8 Ice fog size distribution a; thin fog (from Huffman, 1968).

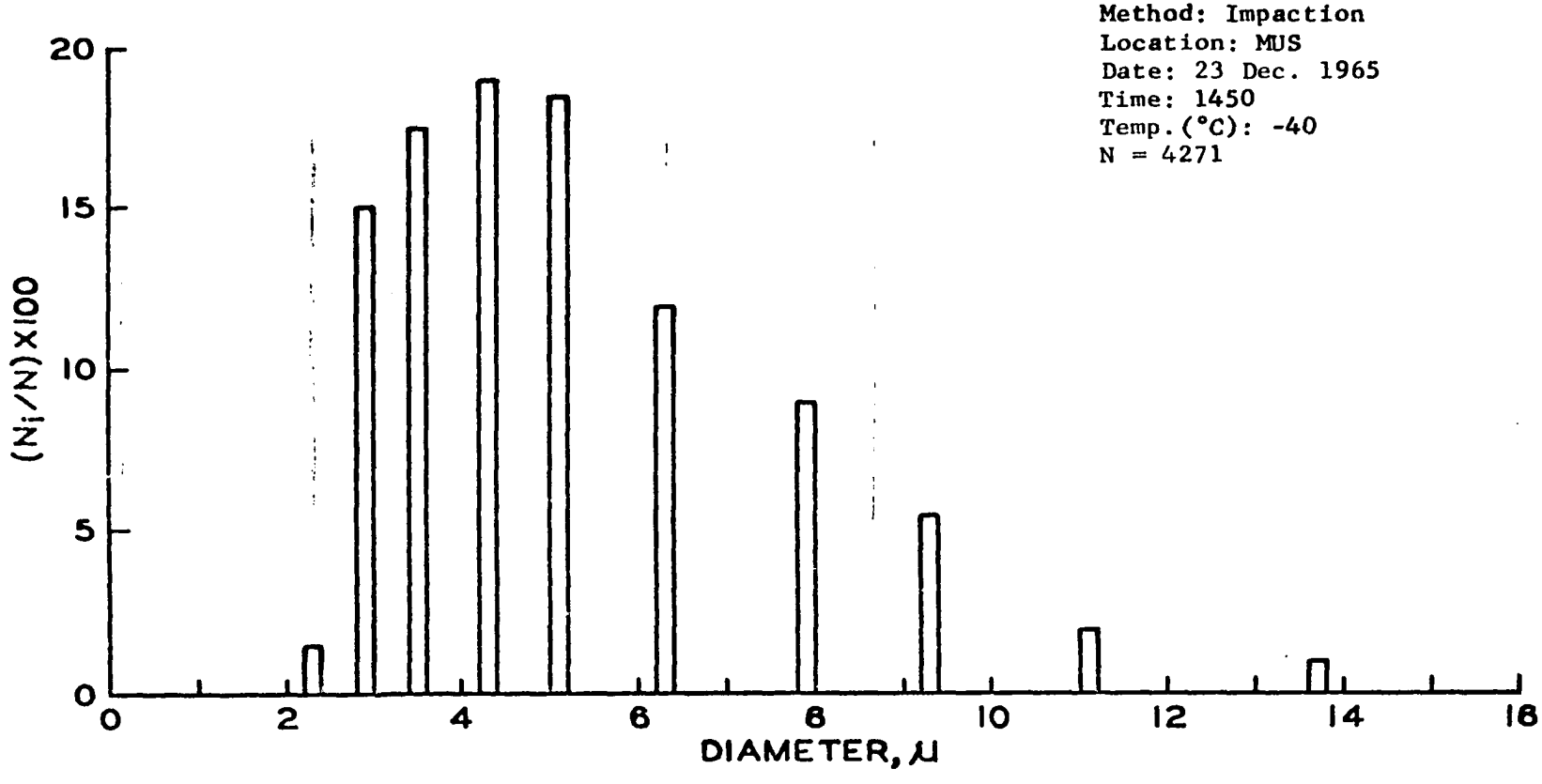

App. II. Ice fog particle size distribution.

IV-9 Ice fog size distribution b; downtown fog (from Huffman, 1968).

Table IV-11

Ice Fog Size Distributions

Radius, a	Distribution a Thin, auto-exhaust type fog $P_a(a) = p_a(a)da$	Distribution b Thick, mixed-origin fog $P_b(a) = p_b(a)da$
1	.03	.005
1.5	.27	.15
2	.40	.18
2.5	.12	.18
3	.06	.13
3.5	.05	.11
4	.05	.09
4.5	.02	.065
5		.04
5.5		.02
6		.01
6.5		.01
7		.005
7.5		.005

increases with decreasing temperature. Thus, the trend of the number density is opposite to the bias expected due to the precipitation sampling. This may be expected to reflect a real exponential increase in n with decreasing temperature.* His precipitation data suggest concentrations as high as n = 1000 at -40°C. Attempts to fit Huffman's impaction values at -32°C and -34°C to Hemmi's curve lead to even higher values of n, as high as 4000 or more at -40°C. As there is no other evidence for such extremely high values for the number density, we will consider n = 100 and 200 for the thin-fog size distribution a, and n = 200, 500 and 1000 for thick fog (distribution b. The combinations of size distribution, fog height, and number density to be

*Although this occurs over the temperature range in which measurements were made, it is clear that the exponential trend cannot continue indefinitely as temperatures continue to drop, or an atmosphere of solid ice would soon result.

used, together with the solid water content of each combination, are given in table IV-12.

5. Computation of Ice Fog Absorption and Flux Backscattering Coefficients

Ice fog crystals, unlike the crystals of an ice crystal display, are equant, randomly oriented, and in many cases almost spherical. This allows the use of Mie theory to compute the flux backscatter and transmissivity. It also affects the form of the transmissivity curve. A solid crystal will not have the complex line structure of a gas, and the beam transmissivity will be an exponential, $\exp(-(n\int p(a)Q_{ext}(a)(1-\tilde{\omega}_o(a))\pi a^2 da)\ |\vec{r}|)$. Here n is the number density of the crystals, a is crystal radius, p(a) is the normalized size distribution, $Q_{ext}(a)$ is the Mie extinction efficiency factor (the ratio of the cross section of the particle as measured by the amount of radiation scattered and absorbed from a beam to the geometrical cross section of the particle), $\tilde{\omega}_o(a)$ is the single scattering albedo (the ratio of scattered energy to the total scattered plus absorbed energy due to a single scattering center) and $|\vec{r}|$ is distance. Note that this "transmissivity" is defined as if the scattering did not exist, and that it depends on ν through Q_{ext} and $\tilde{\omega}_o$. From Elsasser (1942) we know that the flux transmissivity $\tau(x)$ for a locally isotropic beam transmissivity $\exp(x)$ is given by twice the third exponential integral,

$$\tau(x) = 2Ei_3(x) = 2\int_1^\infty e^{-x\eta}\frac{d\eta}{\eta^3} .$$

For the black case, $Q_{ext} = 1$, $\tilde{\omega}_o = 0$ and the quantity of interest in each size distribution is $\int_0^\infty p(a)\pi a^2 da$. The results are shown

Table IV-12

Summary of Ice Fog Situations

height / Number and Size Distribution	10 m	20 m	50 m	100 m
n = 100 Distr. a SWC = .0057 g/m^3	thin, low widespread fog	widespread fog, thicker layer	-	-
n = 200 Distr. a SWC = .0114 g/m^3	denser widespread fog	relatively thick, dense widespread fog	-	-
n = 200 Distr. b SWC = .028 g/m^3	-	thin city fog	thin but deep fog	-
n = 500 Distr. b SWC = .07 g/m^3	-	dense, low-lying city fog	moderately dense city fog	moderately dense city fog, very thick layer
n = 1000 Distr. b SWC = .14 g/m^3	-	-	very dense city fog	very dense city fog, very thick layer

in table IV-13, together with the factors $n\int_0^\infty p(a)\pi a^2 da$ for each of the 5 combinations of n and p(a) to be used.

Table IV-13

Absorption Parameters for Black Ice Fog

		Distribution a	Distribution b
Effective crystal area		$16.8 \times 10^{-8} cm^2$	$33.3 \times 10^{-8} cm^2$
Effective crystal radius		2.3 μ	3.25 μ
Absorption Coefficient,	n = 100	$1.68 \times 10^{-3} m^{-1}$	-
	n = 200	$3.36 \times 10^{-3} m^{-1}$	$6.66 \times 10^{-3} m^{-1}$
	n = 500	-	$1.665 \times 10^{-2} m^{-1}$
	n = 1000	-	$3.33 \times 10^{-2} m^{-1}$

For the more realistic approximate Mie case, Irvine and Pollack (1968) present values of Q_{ext}, $\tilde{\omega}_o$ (their a) and $\langle \cos\theta \rangle = 2\pi\int\Phi(\theta)\cos\theta\sin\theta d\theta$ for ice (and water) spheres of radii 1, 3 and 10μ. They also summarize what they believe to be the best available values of the optical constants of ice and water. Their results for ice are reproduced in Tables IV-14, IV-15, IV-16 and IV-17. They have made a thorough search of the literature on the optical constants of ice, and find that available values in the 200 to 2000 cm^{-1} region often show 5 to 10% variation from their selected values. Under these circumstances the five place accuracy of their results seems somewhat optimistic, and in rescaling their values to fit our wavelength intervals no attempt has been made to retain more than slide rule accuracy.

Table Iv-14

Ice: Absorption Coefficient k and Real (n_r) and Imaginary (n_i) Parts of Index of Refraction versus Wavelength λ after Irvine and Pollack, 1968

$\nu(cm^{-1})$	(λ)	n_r	k, cm^{-1}	n_i
2500	4.0	1.327	389	0.0124
2439	4.1	1.315	459	0.0150
2381	4.2	1.307	525	0.0175
2326	4.3	1.299	636	0.0210
2273	4.4	1.288	806	0.0282
2222	4.5	1.280	921	0.0330
2174	4.6	1.273	783	0.0287
2128	4.7	1.266	576	0.0215
2083	4.8	1.258	454	0.0173
2041	4.9	1.252	377	0.0147
2000	5.0	1.247	334	0.0133
1961	5.1	1.241	321	0.0130
1923	5.2	1.236	322	0.0133
1887	5.3	1.231	360	0.0152
1852	5.4	1.227	408	0.0175
1818	5.5	1.226	479	0.0210
1786	5.6	1.226	548	0.0244
1754	5.7	1.226	690	0.0313
1724	5.8	1.227	918	0.0424
1695	5.9	1.232	1120	0.0526
1667	6.0	1.235	1293	0.0617
1653	6.05	1.235	0341	0.0646
1639	6.1	1.234	1325	0.0643
1613	6.2	1.232	1248	0.0616
1587	6.3	1.228	1164	0.0584
1563	6.4	1.226	1090	0.0555
1538	6.5	1.225	1065	0.0551
1515	6.6	1.223	1065	0.0559
1504	6.65	1.222	1065	0.0564
1493	6.7	1.222	1039	0.0554
1471	6.8	1.221	988	0.0535
1449	6.9	1.221	925	0.0508
1429	7.0	1.221	881	0.0491
1408	7.1	1.221	837	0.0473
1389	7.2	1.221	790	0.0453
1333	7.5	1.220	669	0.0399
1250	8.0	1.219	580	0.0369
1176	8.5	1.217	520	0.0352
1111	9.0	1.210	510	0.0365
1053	9.5	1.192	410	0.0310
1000	10	1.152	520	0.0413
952	10.5	1.195	720	0.0602

Table IV-14
(continued)

$\nu(cm^{-1})$	(λ)	n_r	k, cm^{-1}	n_i
909	11	1.290	1090	0.0954
870	11.5	1.393	1240	0.0114
833	12	1.480	1260	0.0120
800	12.5	1.565	1190	0.0119
769	13	1.612	1040	0.0108
741	13.5	1.613	870	0.0935
667	15	1.550	640	0.0762
571	17.5	1.486	250	0.0347
500	20	1.455	160	0.0255
400	25	1.425	150	0.0298
333	30	1.427	220	0.0525
286	35	1.440	400	0.111
250	40	1.460	560	0.178
230	43.4	1.49	930	0.321
223	44.8	1.49	1630	0.581
215	46.5	1.50	1170	0.433
192	52	1.530	650	0.269
179	56	1.545	340	0.152
161	62	1.57	580	0.286
120	83	1.620	330	0.22
100	100	1.650	100	0.08
85	117	1.690	32	0.03
67	150	1.722	25	0.03
66	152	1.730	25	0.03

Table IV-15

Q_{ext} for Ice Spheres after Irvine and Pollack, 1968

ν (cm^{-1})	λ	a = 1μ	3μ	10μ
2500	4 000	0.41089	3.27865	2.64357
2439	4.10	0.37619	3.04390	2.43268
2381	4.20	0.34957	2.84437	2.30208
2326	4.30	0.33535	2.66589	2.15927
2273	4.40	0.32718	2.46297	2.11202
2222	4.50	0.31939	2.30783	2.09771
2174	4.60	0 28042	2.17039	2.09618
2128	4.70	0.23324	2.02251	2.06310
2083	4.80	0.19859	1.86074	2.16270
2041	4.90	0.17425	1.72722	2.27418
2000	5.000	0.15664	1.61334	2.39254
1961	5.10	0.14328	1.49870	2.58912
1923	5.20	0.13389	1.40261	2.73445
1887	5.30	0.13068	1.31887	2.85172
1852	5.40	0.13000	1.25170	2.95456
1818	5.50	0.13534	1.22135	2.98646
1786	5.60	0.14085	1.20125	2.98993
1754	5.70	0.15689	1.20055	2.94923
1724	5 80	0.18533	1.22923	2.86444
1695	5.90	0.21197	1.28060	2.78483
1667	6.000	0.23336	1.31047	2 73194
1653	6.05	0.23840	1.30807	2.72223
1639	6.10	0.23401	1.28562	2.73611
1613	6.20	0.21984	1.23219	2.77696
1587	6.30	0.20410	1 16515	2.82259
1563	6.40	0.19062	1.11292	2.86402

Table Iv-15 (Continued)

Q_{ext} for Ice Spheres after Irvine and Pollack, 1968

$\nu(cm^{-1})$	λ a =	1μ	3μ	10μ
1538	6.50	0.18456	1.08019	2.8807
1515	6.60	0.18152	1.04927	2.88099
1504	6.65	0.18033	1.03494	2.87810
1493	6.70	0.17571	1.01872	2.89054
1471	6.80	0.16667	0.98209	2.91088
1449	6.90	0.15628	0.94735	2.94115
1429	7.000	0.14866	0.91845	2.96145
1408	7.10	0.14106	0.88963	2.98223
1389	7.20	0.13326	0.86029	3.00347
1333	7.50	0.11255	0.77351	3.03995
1250	8.000	0.09507	0.67259	3.01342
1176	8.50	0.08285	0.58483	2.92431
1111	9.000	0.07765	0.50939	2.73760
1053	9.50	0.06105	0.38686	2.41170
1000	10.000	0.07204	0.33056	1.75928
952	10.50	0.09865	0.46534	2.18902
909	11.000	0.14617	0.77347	2.78996
870	11.50	0.16331	1.05026	3.01376
833	12.000	0.16066	1.25005	3.00211
800	12.50	0.14904	1.42773	2.89169
769	13.000	0.12817	1.43721	2.87530
741	13.50	0.10647	1.27268	2.98623
667	15.000	0.07611	0.80472	3.58427
571	17.50	0.03049	0.36587	3.73704
500	20.000	0.01924	0.20961	3.06167
400	25.000	0.01693	0.11253	1.99812
333	30.000	0.02394	0.10803	1.57165
286	35.000	0.04235	0.15628	1.40262
250	40.000	0.05822	0.20037	1.36663
230	43.40	0.09423	0.31478	1.64259
223	44.80	0.16336	0.54005	2.07899
215	46.50	0.11715	0.38556	1.77753
192	52.000	0.06377	0.20842	1.24798
179	56.000	0.03312	0.10860	0.82405
161	62.000	0.05495	0.17580	1.02083
159	63.000	0.05669	0.18088	1.02615
120	83.000	0.03032	0.09469	0.51317
100	100.000	0.00895	0.02790	0.17105
85	117.000	0.00277	0.00874	0.06770
67	150.000	0.00210	0.00650	0.03733
66	152.000	0.00206	0.00637	0.03635

Table IV-16

$\tilde{\omega}_o$ for Ice Spheres after Irvine and Pollack 1968

ν	λ	a = 1μ	3μ	10μ
2500	4.00	0.84733	0.93014	0.76471
2439	4.10	0.80727	0.91469	0.72841
2381	4.20	0.76772	0.89994	0.67962
2326	4.30	0.71024	0.87564	0.62953
2273	4.40	0.63161	0.83867	0.56903
2222	4.50	0.57414	0.80973	0.54763
2174	4.60	0.58796	0.82383	0.57509
2128	4.70	0.63608	0.85598	0.63888
2083	4.80	0.66403	0.87478	0.70437
2041	4.90	0.68198	0.88700	0.75188
2000	5.00	0.68743	0.89271	0.78817
1961	5.10	0.67412	0.89004	0.81008
1923	5.20	0.65178	0.88301	0.82018
1887	5.30	0.60241	0.86264	0.81522
1852	5.40	0.55103	0.83905	0.80609
1818	5.50	0.49484	0.80914	0.78478
1786	5.60	0.44901	0.78203	0.76615
1754	5.70	0.38139	0.73372	0.72958
1724	5.80	0.30984	0.66989	0.67950
1695	5.90	0.27002	0.62734	0.64136
1667	6.00	0.24072	0.59311	0.61542
1653	6.05	0.23032	0.58106	0.60956
1639	6.10	0.22652	0.57857	0.61312
1613	6.20	0.22409	0.58108	0.62619
1587	6.30	0.22049	0.58258	0.64207
1563	6.40	0.21939	0.58697	0.65630
1538	6.50	0.21315	0.58331	0.66134
1515	6.60	0.20255	0.57294	0.66191
1504	6.65	0.19718	0.56733	0.66169
1493	6.70	0.19696	0.56962	0.66650
1471	6.80	0.19509	0.57217	0.67597
1449	6.90	0.19704	0.58044	0.68852
1429	7.00	0.19655	0.58465	0.69737
1408	7.10	0.19661	0.58959	0.70651
1389	7.20	0.19758	0.59582	0.71646
1333	7.50	0.19922	0.61158	0.74449
1250	8.00	0.18443	0.60714	0.76331
1176	8.50	0.16604	0.59304	0.77317
1111	9.00	0.13467	0.54949	0.76308
1053	9.50	0.11680	0.52898	0.77414
1000	10.00	0.05367	0.34444	0.65360
952	10.50	0.05423	0.35561	0.64180
909	11.00	0.06689	0.40822	0.62529
870	11.50	0.08763	0.47925	0.60930
833	12.00	0.10664	0.53451	0.58702
800	12.50	0.12844	0.58637	0.55944
769	13.00	0.14478	0.62649	0.55853

Table IV-16
(continued)

$\nu(cm^{-1})$	$\lambda(\mu)$	a = 1μ	3μ	10μ
741	13.50	0.14910	0.65112	0.59469
667	15.00	0.11300	0.63331	0.71541
571	17.50	0.12102	0.70132	0.86357
500	20.00	0.09989	0.68024	0.89496
400	25.00	0.04128	0.48288	0.85822
333	30.00	0.01435	0.25185	0.75194
286	35.00	0.00484	0.10470	0.55727
250	40.00	0.00242	0.05638	0.43627
230	43.40	0.00151	0.03629	0.34906
223	44.80	0.00132	0.03214	0.32185
215	46.50	0.00118	0.02882	0.31706
192	52.00	0.00108	0.02685	0.34351
179	56.00	0.00138	0.03430	0.43008
161	62.00	0.00070	0.01774	0.29580
159	63.00	0.00065	0.01651	0.28382
120	83.00	0.00040	0.01052	0.23377
100	100.00	0.00063	0.01641	0.34081
85	117.00	0.00117	0.03026	0.50246
67	150.00	0.00061	0.01611	0.35764
66	152.00	0.00060	0.01585	0.35430

Table IV-17

<Cosθ> for Ice Spheres
after Irvine and Pollack, 1968

$\nu(cm^{-1})$	λ (μ) a =	1μ	3μ	10μ
2500	4.000	0.49289	0.85618	0.86536
2439	4.10	0.46636	0.86029	0.86794
2381	4.20	0.44171	0.86123	0.84994
2326	4.30	0.41919	0.86137	0.85426
2273	4.40	0.39788	0.86237	0.86025
2222	4.50	0.37828	0.86185	0.87054
2174	4.60	0.35833	0.85804	0.85706
2128	4.70	0.33925	0.85314	0.83741
2083	4.80	0.32198	0.84941	0.84100
2041	4.90	0.30654	0.84598	0.84530
2000	5.000	0.29252	0.84306	0.85839
1961	5.10	0.27950	0.84108	0.87491
1923	5.20	0.26753	0.83932	0.88588
1887	5.30	0.25654	0.83812	0.89882
1852	5.40	0.24636	0.83659	0.90941
1818	5.50	0.23718	0.83453	0.91617
1786	5.60	0.22857	0.83187	0.92057
1754	5.70	0.22073	0.82959	0.92664
1724	5.80	0.21369	0.82758	0.93308
1695	5.90	0.20716	0.82468	0.93557
1667	6.000	0.20068	0.82131	0.93801
1653	6.05	0.19733	0.81925	0.93906
1639	6.10	0.19379	0.81656	0.93936
1613	6.20	0.18688	0.81051	0.93925
1587	6.30	0.18020	0.80396	0.93982
1563	6.40	0.17401	0.79722	0.93969
1538	6.50	0.16833	0.79103	0.93984
1515	6.60	0.16293	0.78522	0.94053
1504	6.65	0.16033	0.78242	0.94084
1493	6.70	0.15778	0.77926	0.94040
1471	6.80	0.15283	0.77316	0.93993
1449	6.90	0.14813	0.76707	0.93902
1429	7.000	0.14369	0.76159	0.93849
1408	7.10	0.13945	0.75644	0.93797
1389	7.20	0.13540	0.75162	0.93729
1333	7.50	0.12426	0.73975	0.93745
1250	8.000	0.10873	0.72650	0.93222
1176	8.50	0.09598	0.71333	0.93023
1111	9.000	0.08527	0.69380	0.92922
1053	9.50	0.07592	0.66109	0.92809

Table IV-17 (Cont'd)

$\nu(cm^{-1})$	λ (μ) a =	1μ	3μ	10μ
1000	10.000	0.66761	0.61521	0.93346
952	10.50	0.06220	0.59007	0.92540
909	11.000	0.05868	0.58141	0.90959
870	11.50	0.05591	0.57132	0.88410
833	12.000	0.05328	0.55657	0.85405
800	12.50	0.05103	0.54248	0.81490
769	13.000	0.04824	0.51919	0.78153
741	13.50	0.04476	0.48110	0.76396
667	15.000	0.03525	0.35817	0.79414
571	17.50	0.02519	0.23585	0.78798
500	20.000	0.01905	0.17310	0.76789
400	25.000	0.01205	0.10781	0.71361
333	30.000	0.00838	0.07488	0.66878
286	35.000	0.00619	0.05540	0.64072
250	40.000	0.00476	0.04273	0.55369
230	43.40	0.00406	0.03640	0.48697
223	44.80	0.00364	0.03273	0.44565
215	46.50	0.00349	0.03137	0.42473
182	52.000	0.00290	0.02595	0.33726
179	56.000	0.00255	0.02271	0.27891
161	62.000	0.00208	0.01859	0.22733
159	63.000	0.00201	0.01798	0.21919
120	83.000	0.00121	0.01071	0.12092
100	100.000	0.00089	0.07552	0.08295
85	117.000	0.00069	0.00564	0.06163
67	150.000	0.00050	0.00349	0.03826
66	152.000	0.00055	0.00342	0.03742

Plots of the tabulated values of Q_{ext}, $\tilde{\omega}_o$, and $\langle\cos\theta\rangle$ are given in Figures IV-10, IV-11 and IV-12. These three parameters and their adaptation to this paper are discussed below:

a. Q_{ext}. Values of Q_{ext} over each of the 63 wave number intervals in Table IV-3 are needed for each particle size in Table IV-11.

Figures IV-13 and IV-14 are reproductions of figures 32 and 33 from van de Hulst (1957). From Figure IV-13 it is apparent that the variation of Q_{ext} with radius (actually with $2\pi a/\lambda=2\pi a\nu$) for real refractive indices, n_r, near 1 is monotonic and very roughly linear over much of the range from zero up to the first maximum of the extinction curve. Furthermore, this maximum becomes higher and shifts to smaller values of $2\pi a\nu$ as the real refractive index increases. Figure IV-14 shows that increasing the absorption steepens the initial portion of the curve and damps the Mie oscillations. The smoothness of Q_{abs} $(=(1-\tilde{\omega}_o)Q_{ext})$ is also shown, and will be used as an aid in computing $\tilde{\omega}_o$. Note that with strong absorption, ie. 45°, the linearity of Q_{ext} becomes much better for very small values of $2\pi a\nu$ but extends only about half as far (compare with 0°) into the larger values of $2\pi a\nu$. Assume that these effects of absorption apply qualitatively to cases with $1 < n_r < 1.6$, and the effects of absorption do not seriously affect the results in Figure IV-13 except as shown in Figure IV-14. It is then possible to explain most of the features shown in Figure IV-10 and thus locate regions where linear interpolation will give approximately valid results.

In Figure IV-10 the peaks at 160 and 220 cm^{-1} are due to absorption maxima. The 3μ and 10μ curves are in the quasi-linear part of the Mie curve, while the 1μ curve may be somewhat below it. In this region

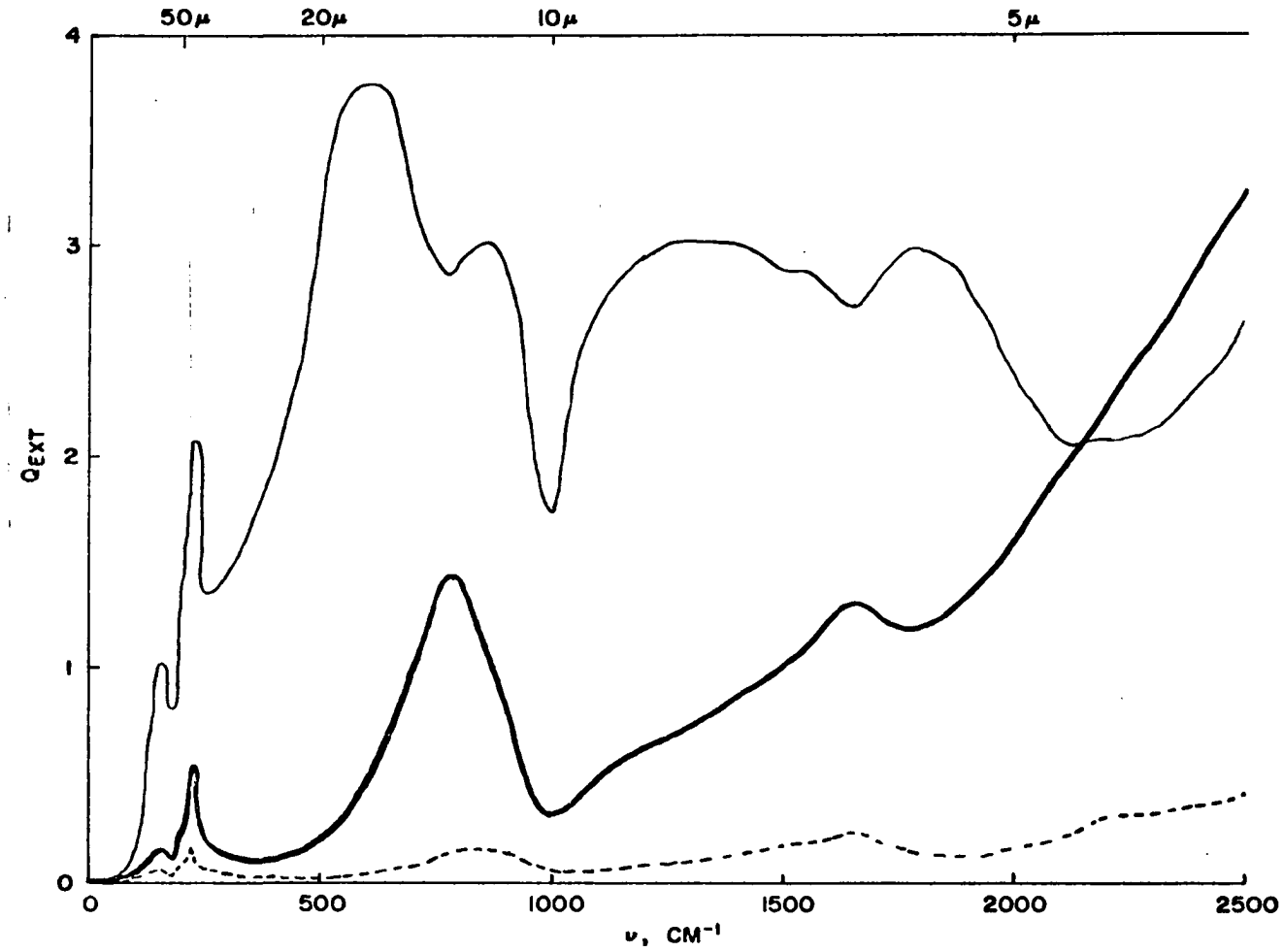

IV-10 Plot of the Mie efficiency factor for extinction, Q_{ext}, for ice spheres of radii 1, 3 and 10μ (values from Irvine and Pollack 1968). Dashed line for a = 1μ, heavy solid line a = 3μ, thin solid line for a = 10μ.

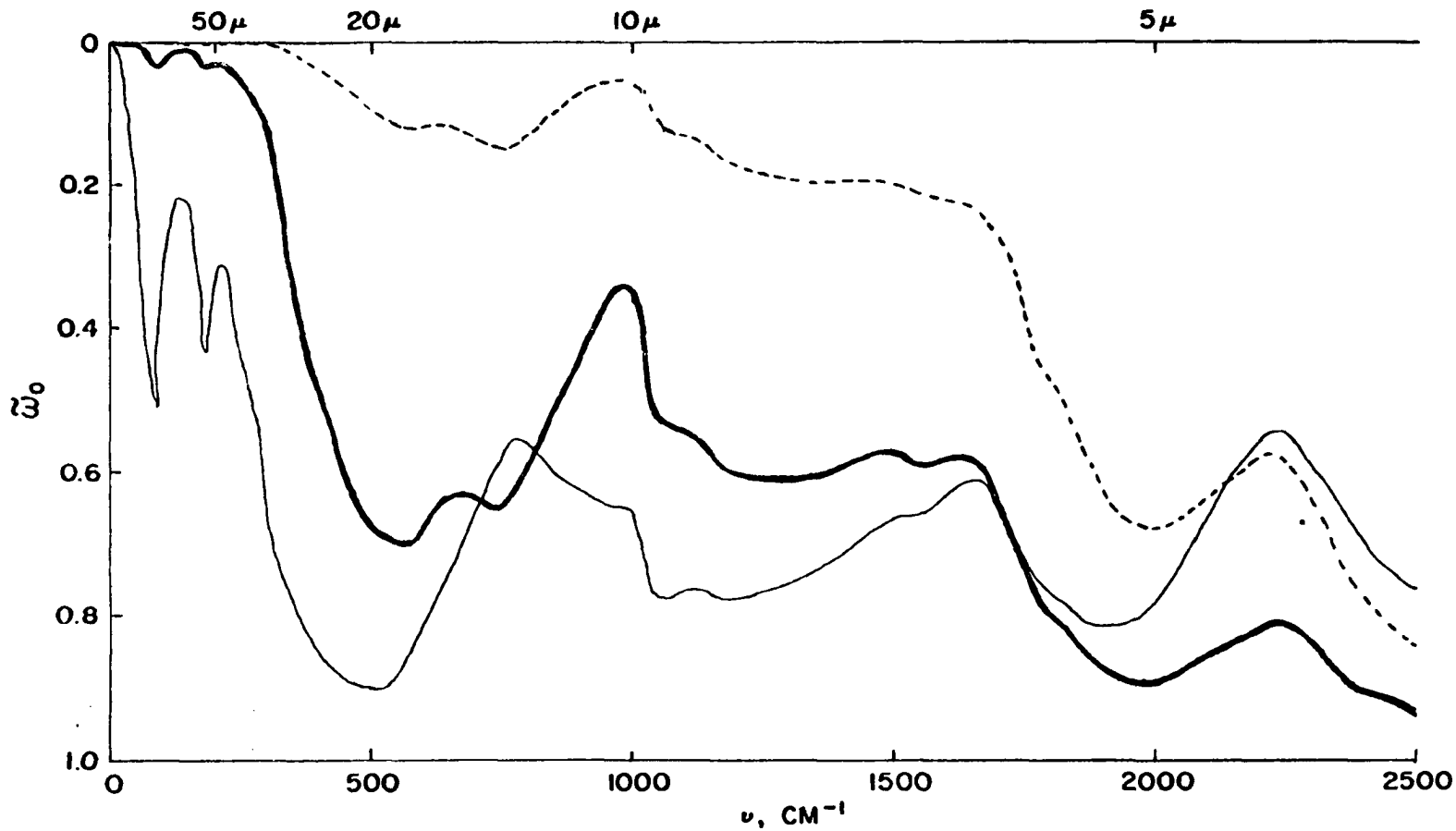

IV-11 Plot of the single scattering albedo, $\tilde{\omega}_o$, as absorption (zero at the top of the scale) for ice spheres of radii 1, 3 and 10μ (values from Irvine and Pollack, 1968). Dashed line for a = 1μ, heavy solid line a = 3μ, thin solid line for a = 10μ.

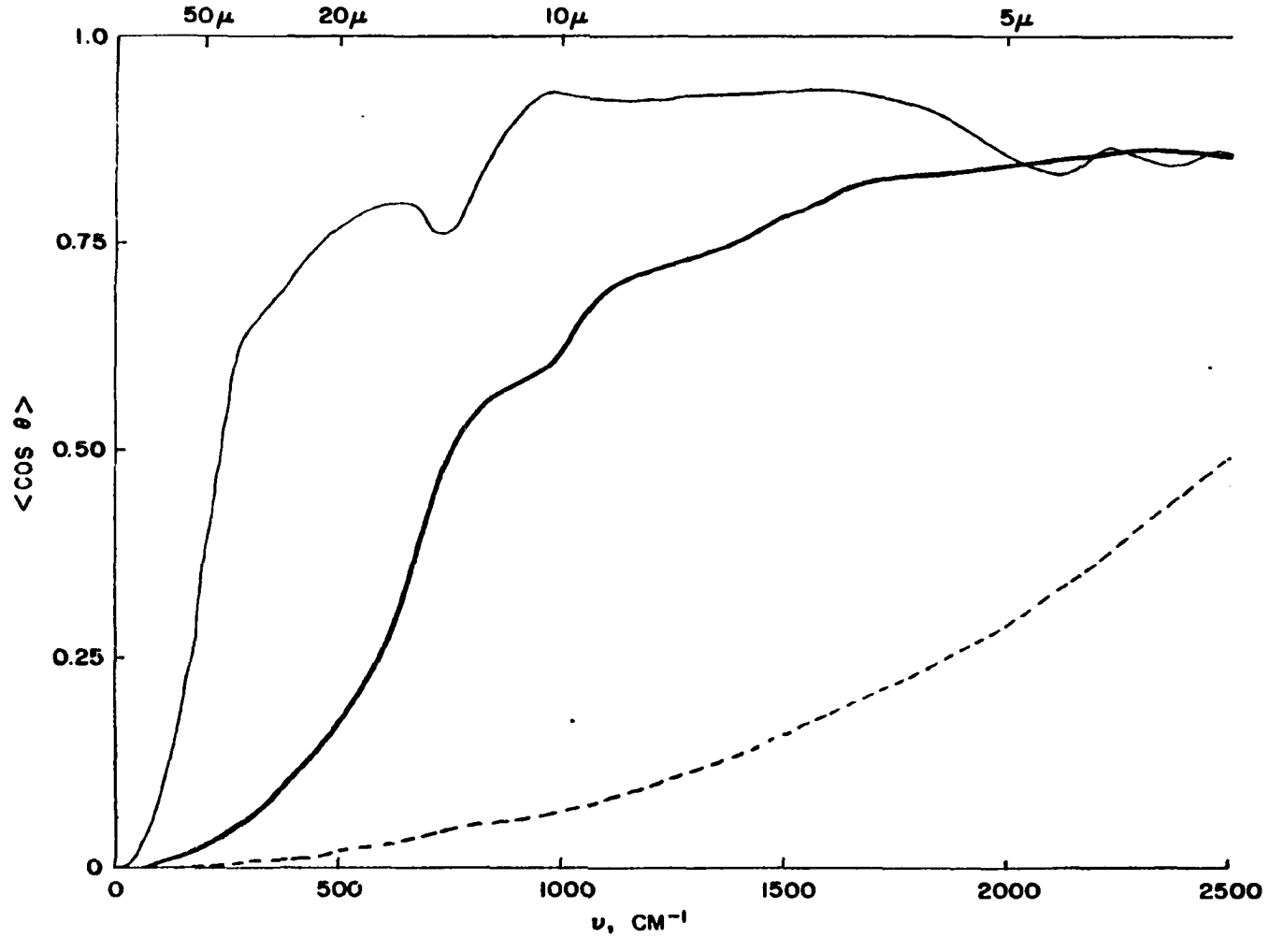

IV-12 Plot of the asymmetry factor, < cos θ >, for ice spheres of radii 1, 3 and 10μ (values from Irvine and Pollack, 1968). Dashed line for a = 1μ, heavy solid line a = 3μ, thin solid line for a = 10μ.

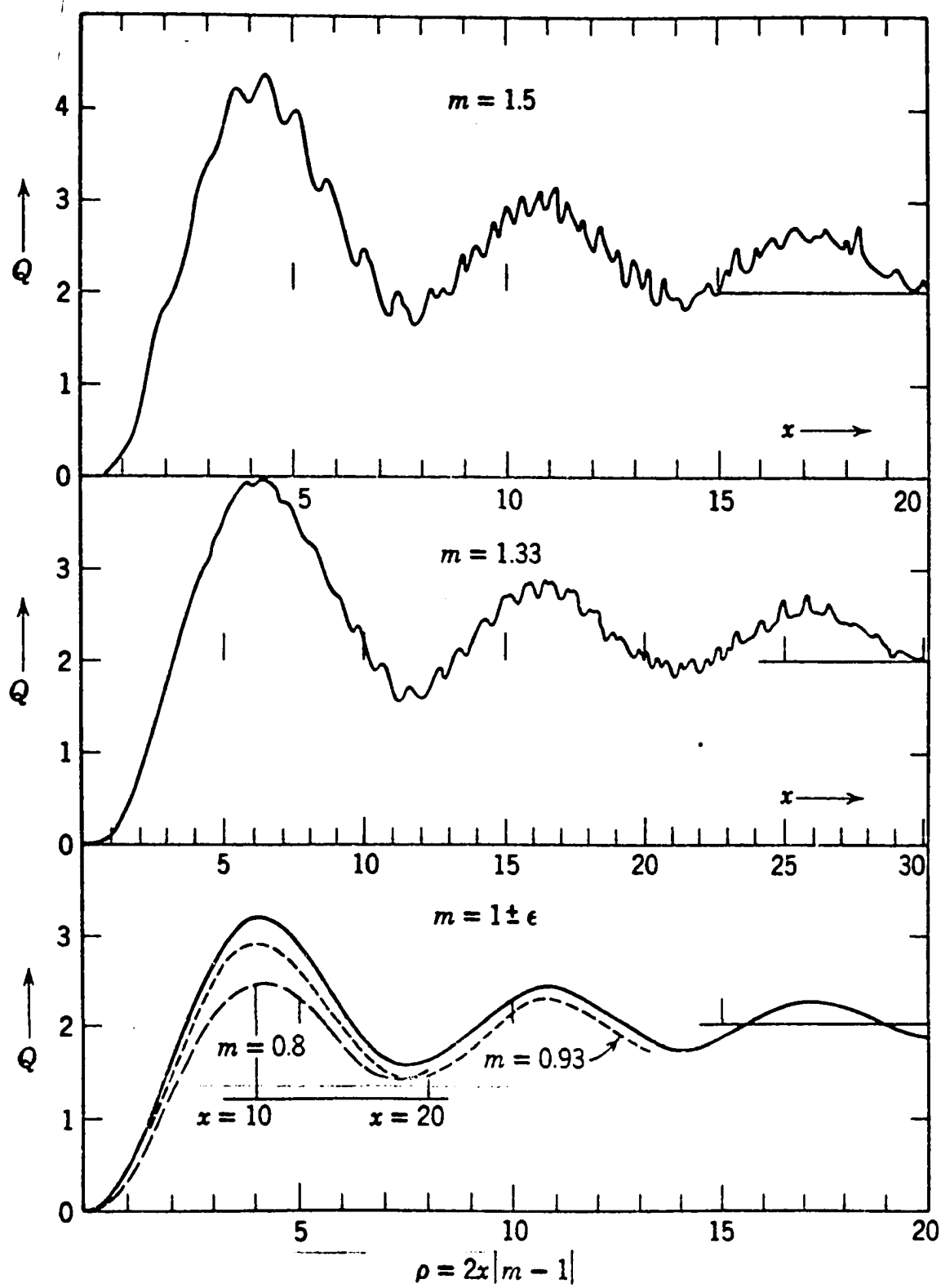

IV-13 Mie extinction curves for real refractive indices. From van de Hulst, 1957. Note that in this context $x = \frac{2\pi a}{\lambda}$ rather than optical distance.

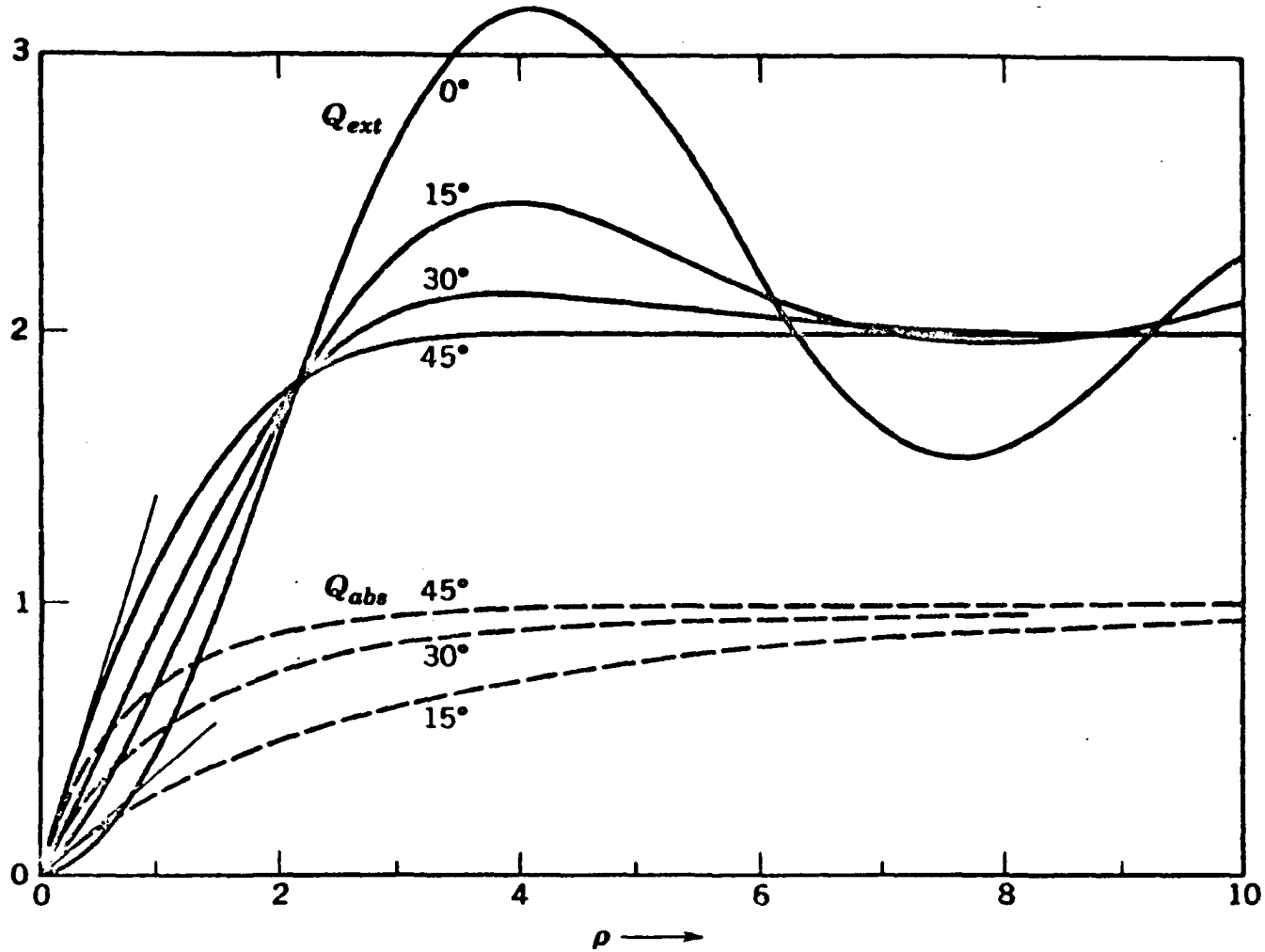

IV-14 Mie extinction and absorption curves for complex refractive indices near 1 from van de Hulst, 1957. $\rho = \frac{2\pi a}{\lambda} 2 (1-n_r)$.

we will interpolate between 1μ and 3μ and between 3μ and 10μ. At about 550 cm^{-1}, the 10μ curve begins to peak with simultaneous increases in $2\pi a\nu$ and n_r. Both n_r and the imaginary refractive index, n_i, peak at 740 cm^{-1} (13.5μ), giving peaks in the 1μ and 3μ curves and a minimum in the 10μ curve. At this point the 10μ curve is clearly beyond the first peak in the Mie extinction curve and interpolration between 3μ and 10μ is completely invalid. We obtain approximate values of Q_{ext} up to about 7.5μ by extrapolating from the 1μ and 3μ curves. Beyond 770 cm^{-1} n_r decreases rapidly and on the basis of values of $4\pi a\nu(1-n_r)$, which are decreasing with increasing $a\nu$ in this region, the small peak around 850 cm^{-1} in the 10μ curve actually represents a retracing of the first peak in the Mie extinction curve and a return to the quasi-linear part of the curve (Fig. IV-13). At 900 cm^{-1} we return to separate linear interpolations between the 1μ and 3μ and the 3μ and 10μ curves.

The minimum in n_r at 1000 cm^{-1} (Fig. IV-10) affects all three curves. From 1000 cm^{-1} to 2200 cm^{-1} n_r ranges from 1.22 to 1.24. At 1250 cm^{-1} the linear assumption again begins to break down and it is necessary to interpolate between 1μ and 3μ and extrapolate above 3μ. The difference between this extrapolation and that made in the range 550 cm^{-1} to 900 cm^{-1} is that we now assume an upper limit for $Q_{ext} = 3.5$. The form of the extinction curve is approximated for values of $\underline{a}$ which raise Q_{ext} to its limit of 3.5. Luckily this spectral region is of very little importance to us, having near-zero blackbody emission at low temperatures and being strongly absorbed by water vapor beyond 1400 cm^{-1}. Table IV-18 gives the resulting values of Q_{ext}.

TABLE IV - 18

Interpolated values of Q_{ext}

ν \ a	1	1.5	2	2.5	3	3.5	4	4.5	5	5.5	6	6.5	7	7.5	10
10	0	0	0	0	0	0	0	0	0	0	0	0	0	0	.005
40	0	0	0	0	.01	.01	.01	.01	.01	.01	.02	.02	.02	.02	.02
80	.01	.01	.015	.015	.02	.02	.02	.02	.03	.03	.03	.04	.04	.04	.06
120	.03	.045	.06	.08	.094	.12	.15	.18	.21	.24	.27	.30	.33	.36	.51
160	.06	.09	.12	.15	.18	.23	.29	.35	.41	.47	.53	.59	.65	.71	1.02
200	.08	.13	.18	.24	.30	.38	.46	.54	.62	.70	.78	.86	.94	1.02	1.40
240	.07	.11	.16	.21	.26	.34	.43	.52	.61	.70	.79	.88	.97	1.06	1.50
280	.05	.07	.10	.12	.15	.23	.32	.41	.50	.59	.68	.77	.86	.95	1.40
320	.03	.05	.07	.09	.11	.14	.18	.24	.30	.40	.50	.60	.70	.80	1.50
360	.02	.04	.06	.08	.10	.13	.17	.23	.29	.39	.50	.61	.72	.83	1.72
400	.017	.04	.06	.09	.12	.15	.21	.29	.39	.51	.65	.79	.93	1.07	1.98
440	.015	.04	.07	.10	.14	.20	.28	.38	.50	.64	.80	.96	1.12	1.28	2.32
480	.017	.06	.10	.14	.18	.26	.36	.48	.62	.78	.97	1.16	1.35	1.44	2.80
520	.02	.07	.12	.22	.24	.32	.42	.54	.69	.87	1.08	1.33	1.58	1.83	3.40
560	.03	.10	.18	.26	.34	.44	.56	.70	.86	1.04	1.25	1.50	1.77	2.06	3.65
570	.03	.11	.19	.27	.37	.49	.63	.79	.97	1.17	1.40	1.66	1.95	2.22	3.74
580	.04	.12	.21	.30	.39	.54	.69	.87	1.07	1.29	1.52	1.78	2.06	2.32	3.75
590	.04	.13	.23	.33	.43	.59	.75	.94	1.17	1.40	1.65	1.90	2.16	2.42	3.75
600	.04	.15	.26	.37	.48	.63	.81	1.02	1.27	1.52	1.77	2.02	2.27	2.52	3.76
610	.05	.16	.28	.40	.52	.69	.88	1.10	1.35	1.60	1.85	2.10	2.35	2.60	3.75
620	.05	.17	.30	.43	.56	.75	.95	1.18	1.43	1.68	1.93	2.18	2.43	2.68	3.73
630	.05	.19	.33	.47	.61	.80	1.02	1.26	1.51	1.76	2.01	2.26	2.51	2.76	3.71
640	.06	.20	.35	.50	.65	.85	1.09	1.33	1.58	1.83	2.08	2.33	2.58	2.83	3.69
650	.06	.22	.38	.54	.70	.90	1.15	1.40	1.65	1.90	2.15	2.40	2.65	2.90	3.66
660	.06	.23	.40	.57	.75	.97	1.22	1.47	1.72	1.97	2.22	2.47	2.72	2.96	3.63
670	.07	.24	.42	.61	.81	1.04	1.29	1.54	1.79	2.04	2.29	2.54	2.79	3.02	3.56
680	.07	.26	.46	.67	.88	1.11	1.36	1.61	1.86	2.11	2.36	2.61	2.86	3.08	3.48
690	.08	.28	.49	.70	.92	1.18	1.43	1.68	1.93	2.18	2.43	2.68	2.93	3.14	3.35
700	.08	.30	.53	.76	1.00	1.25	1.50	1.75	2.00	2.25	2.50	2.75	3.00	3.20	3.25
710	.09	.31	.55	.79	1.04	1.33	1.59	1.84	2.09	2.34	2.59	2.84	3.08	3.27	3.15
720	.09	.33	.58	.84	1.10	1.41	1.68	1.93	2.18	2.43	2.68	2.93	3.16	3.33	3.08
730	.10	.35	.61	.88	1.17	1.48	1.76	2.02	2.27	2.52	2.77	3.02	3.23	3.39	3.02
740	.11	.39	.68	.97	1.26	1.55	1.84	2.10	2.35	2.60	2.85	3.10	3.30	3.45	2.98
750	.12	.41	.71	1.02	1.33	1.63	1.93	2.22	2.51	2.79	3.05	3.30	3.45	3.50	2.92
760	.12	.43	.74	1.06	1.38	1.70	2.02	2.34	2.66	2.98	3.25	3.45	3.50	3.45	2.89
770	.13	.45	.78	1.11	1.44	1.75	2.07	2.39	2.71	3.03	3.30	3.47	3.47	3.30	2.86
780	.13	.46	.78	1.11	1.44	1.75	2.07	2.39	2.71	3.03	3.30	3.47	3.47	3.30	2,87
790	.14	.46	.78	1.10	1.43	1.75	2.07	2.39	2.71	3.03	3.30	3.47	3.47	3.30	2.88
800	.15	.47	.79	1.11	1.43	1.75	2.07	2.39	2.71	3.03	3.30	3.47	3.47	3.30	2.89
810	.16	.46	.76	1.07	1.38	1.69	2.00	2.31	2.61	2.91	3.25	3.45	3.50	3.45	2.92
840	.16	.42	.68	.94	1.20	1.46	1.71	1.95	2.17	2.37	2.55	2.71	2.83	2.90	3.00
880	.15	.35	.56	.77	.98	1.19	1.40	1.61	1.82	2.03	2.24	2.45	2.66	2.87	2.98
920	.13	.26	.39	.52	.66	.80	.94	1.08	1.22	1.36	1.50	1.64	1.78	1.92	2.64
960	.085	.16	.24	.33	.42	.53	.64	.75	.86	.97	1.08	1.19	1.30	1.41	2.00

TABLE IV - 18

Interpolated Values of Q_{ext}
(continued)

ν	1	1.5	2	2.5	3	3.5	4	4.5	5	5.5	6	6.5	7	7.5	10
1000	.072	.13	.19	.26	.33	.44	.55	.66	.77	.88	.99	1.10	1.21	1.32	1.76
1040	.059	.13	.21	.29	.37	.50	.63	.76	.89	1.03	1.17	1.31	1.45	1.59	2.30
1080	.065	.15	.24	.34	.44	.59	.74	.89	1.04	1.19	1.34	1.49	1.64	1.79	2.58
1120	.077	.18	.29	.40	.52	.68	.84	1.00	1.16	1.32	1.48	1.64	1.80	1.96	2.76
1160	.079	.205	.33	.45	.58	.75	.92	1.09	1.26	1.43	1.59	1.75	1.91	2.07	2.87
1200	.081	.215	.35	.48	.62	.79	.96	1.13	1.30	1.47	1.64	1.81	1.98	2.15	2.95
1240	.098	.24	.37	.51	.66	.83	1.00	1.17	1.34	1.51	1.68	1.85	2.02	2.19	3.00
1280	.10	.25	.40	.55	.71	.86	1.01	1.16	1.31	1.46	1.61	1.76	1.91	2.06	3.02
1320	.11	.27	.43	.59	.76	.92	1.08	1.24	1.40	1.56	1.72	1.88	2.04	2.20	3.03
1360	.12	.29	.46	.64	.82	1.00	1.18	1.36	1.54	1.72	1.90	2.08	2.26	2.44	3.02
1400	.14	.32	.50	.69	.88	1.07	1.26	1.45	1.64	1.83	2.02	2.21	2.40	2.59	2.99
1440	.15	.34	.54	.74	.94	1.14	1.34	1.54	1.74	1.94	2.14	2.34	2.54	2.74	2.95
1480	.17	.37	.58	.79	1.00	1.21	1.42	1.63	1.84	2.05	2.26	2.47	2.68	2.89	2.90
1520	.18	.40	.62	.84	1.06	1.28	1.50	1.72	1.94	2.16	2.38	2.60	2.82	3.04	2.89
1560	.19	.42	.65	.88	1.12	1.35	1.58	1.81	2.04	2.27	2.50	2.73	2.96	3.19	2.87
1600	.21	.46	.72	.98	1.24	1.44	1.70	1.96	2.22	2.48	2.74	3.00	3.26	3.50	2.79
1800	.13	.40	.67	.94	1.21	1.48	1.75	2.02	2.29	2.56	2.83	3.10	3.37	3.50	2.98
2000	.16	.51	.87	1.24	1.61	1.98	2.35	2.72	3.09	3.46	3.40	3.10	2.80	2.50	2.39
2200	.30	.78	1.27	1.76	2.25	2.74	3.23	3.45	3.50	3.45	3.25	3.00	2.75	2.50	2.09

b. $\tilde{\omega}_o$. Returning to Figure IV-14, it is clear that the variation of Q_{abs} (= $(1-\tilde{\omega}_o)\ Q_{ext}$) with $2\pi a\nu$ shows no trace of the major Mie oscillations and is monotonic at least for refractive indices near 1. If this relationship holds* for the refractive indices of Table IV-14, then the variation of $\tilde{\omega}_o$ with size must compensate for that of Q_{ext}; this would make direct interpolation of $\tilde{\omega}_o$ quite difficult. That a general relationship of this sort does exist can be seen by comparing Figures IV-10 and IV-11. On the other hand, the absorption efficiency factor Q_{abs} should be relatively easy to obtain by interpolation, and it is then easy to obtain the scattering efficiency factor Q_{sca} from the relationship $Q_{sca} = Q_{ext} - Q_{abs}$.

$Q_{ext}\ (1-\tilde{\omega}_o)$ for a = 1μ, 3μ, and 10μ is plotted from Irvine and Pollack's data in Figure IV-15. The curves are very similar in shape, and comparison with Table IV-14 indicates that the observed variation with wave number is almost entirely due to variation in the absorption coefficient. This increased regularity allows for more accurate interpolation than was possible for Q_{ext}. The interpolation for wave numbers which were multiples of 200 cm^{-1}, as well as for some near extreme values of Q_{abs}, was carried out graphically, using the known points for a = 0, 1μ, 3μ and 10μ to construct a smooth curve and then reading intermediate values off the curve. A sample interpolation diagram, for 600 cm^{-1}, is shown in Figure IV-16. Values of Q_{ext} for other wave numbers were interpolated both between these control values and between the points plotted from Figure IV-15. The resulting values for Q_{abs} are given in Table IV-19, and the values for Q_{sca} obtained from $Q_{sca} = Q_{ext} - Q_{abs}$ are given in Table IV-20.

*Except for rapid fluctuations which may be neglected in taking an integral over a range of sizes.

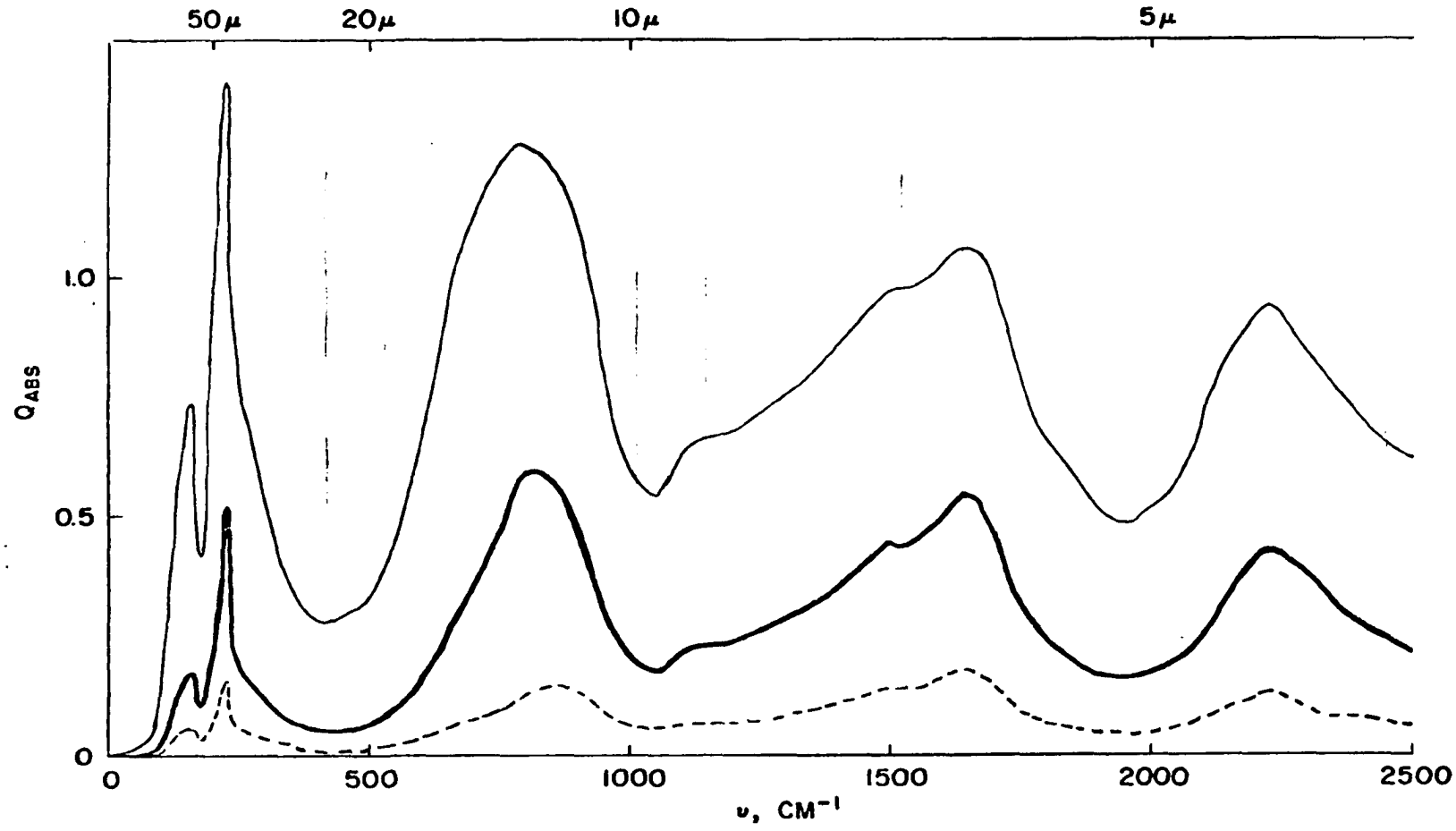

IV-15 Plot of the Mie absorption efficiency factor, Q_{abs}, for ice spheres of 1, 3 and 10μ radii. Dashed line for a = 1μ, heavy solid line a = 3μ, thin solid line for a = 10μ.

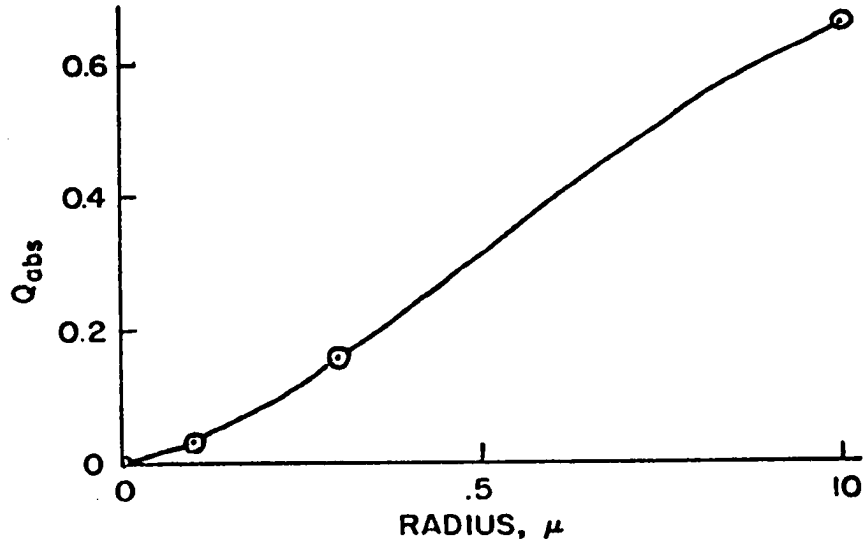

IV-16 Sample interpolation curve for Q_{abs}.

TABLE IV-19

Interpolated values of Q_{abs}

v/a	1	1.5	2	2.5	3	3.5	4	4.5	5	5.5	6	6.5	7	7.5	10
10	.000	0	0	0	0	0	0	0	0	0	0	0	0	0	.005
40	.002	.002	.003	.004	.004	.005	.006	.007	.008	.009	.010	.011	.012	.013	.019
80	.003	.004	.005	.006	.008	.009	.010	.012	.013	.015	.016	.018	.019	.021	.030
120	.030	.045	.062	.078	.094	.113	.130	.150	.170	.19	.21	.23	.25	.27	.392
160	.055	.083	.11	.14	.175	.21	.24	.28	.31	.35	.39	.43	.48	.54	.74
200	.08	.12	.16	.20	.24	.28	.33	.37	.41	.46	.51	.56	.62	.67	.95
240	.07	.11	.16	.20	.25	.29	.33	.37	.41	.46	.51	.56	.62	.67	.95
280	.045	.07	.09	.11	.14	.17	.20	.23	.26	.29	.32	.35	.38	.42	.64
320	.030	.04	.06	.08	.10	.12	.14	.16	.18	.20	.22	.24	.27	.30	.46
360	.020	.032	.044	.056	.069	.085	.10	.115	.13	.145	.16	.175	.19	.21	.34
400	.016	.026	.036	.047	.058	.069	.080	.091	.102	.113	.130	.148	.165	.180	.289
440	.010	.02	.03	.04	.052	.06	.07	.09	.10	.11	.12	.14	.16	.18	.285
480	.011	.023	.035	.047	.060	.07	.08	.10	.11	.13	.14	.16	.18	.20	.30
520	.019	.033	.048	.063	.078	.09	.10	.12	.14	.16	.18	.20	.22	.24	.35
560	.026	.044	.062	.08	.10	.12	.14	.16	.18	.21	.23	.26	.28	.31	.47
570	.027	.05	.07	.09	.109	.13	.16	.19	.22	.25	.28	.31	.34	.37	.508
580	.030	.05	.07	.10	.128	.16	.19	.22	.25	.28	.31	.34	.37	.40	.56
590	.033	.06	.08	.11	.14	.18	.21	.24	.28	.22	.35	.38	.42	.45	.61
600	.036	.060	.09	.12	.15	.20	.23	.27	.31	.35	.39	.43	.47	.50	.66
610	.040	.07	.10	.14	.18	.22	.26	.30	.34	.38	.42	.46	.50	.54	.71
620	.044	.08	.12	.16	.20	.24	.28	.32	.36	.40	.44	.48	.52	.56	.77
630	.049	.09	.13	.17	.22	.26	.30	.34	.38	.42	.46	.50	.54	.58	.82
640	.053	.10	.14	.19	.24	.28	.32	.37	.41	.46	.50	.54	.58	.62	.88
650	.058	.11	.16	.21	.26	.30	.35	.40	.45	.50	.55	.60	.65	.70	.93
660	.063	.11	.17	.22	.28	.33	.38	.43	.48	.53	.58	.63	.68	.73	1.00
670	.067	.12	.18	.24	.30	.35	.40	.45	.50	.55	.60	.65	.70	.75	1.02
680	.068	.13	.19	.25	.33	.38	.45	.51	.57	.62	.67	.72	.77	.81	1.05
690	.070	.13	.19	.27	.35	.43	.51	.58	.64	.70	.75	.80	.84	.86	1.09
700	.075	.14	.20	.28	.37	.47	.57	.65	.72	.78	.83	.88	.91	.94	1.11
710	.079	.15	.21	.29	.39	.49	.59	.67	.75	.81	.86	.91	.95	.98	1.14
720	.080	.15	.22	.31	.41	.51	.61	.70	.78	.84	.89	.94	.99	1.02	1.17
730	.085	.16	.23	.32	.43	.53	.63	.73	.81	.87	.92	.98	1.03	1.06	1.20
740	.0905	.17	.25	.34	.443	.56	.66	.76	.84	.90	.96	1.02	1.07	1.10	1.22
750	.095	.18	.26	.36	.47	.60	.70	.79	.88	.94	1.0	1.05	1.10	1.14	1.24
760	.10	.19	.27	.38	.50	.62	.72	.80	.89	.95	1.01	1.06	1.10	1.15	1.26
770	.109	.20	.29	.40	.537	.64	.74	.82	.91	.96	1.02	1.07	1.11	1.16	1.27
780	.115	.21	.31	.42	.56	.66	.76	.84	.92	.97	1.03	1.08	1.12	1.17	1.27
790	.12	.22	.32	.44	.58	.68	.78	.86	.93	.98	1.04	1.09	1.13	1.17	1.28
800	.130	.240	.340	.460	.591	.70	.80	.88	.94	1.0	1.05	1.10	1.14	1.18	1.275
810	.13	.24	.34	.45	.59	.70	.80	.88	.94	1.0	1.05	1.10	1.14	1.18	1.27
840	.15	.23	.33	.44	.58	.67	.76	.84	.90	.95	1.00	1.05	1.08	1.12	1.22
880	.15	.23	.32	.42	.53	.63	.72	.79	.85	.90	.95	1.0	1.03	1.05	1.14
920	.12	.19	.26	.34	.42	.50	.57	.63	.68	.72	.76	.80	.83	.85	.97
960	.09	.14	.20	.26	.28	.37	.43	.48	.52	.55	.57	.60	.63	.65	.74

TABLE IV-19

Interpolated Values of Q_{abs}
(continued)

ν/a	1	1.5	2	2.5	3	3.5	4	4.5	5	5.5	6	6.5	7	7.5	10
1000	.068	.10	.14	.18	.217	.25	.29	.33	.36	.39	.42	.45	.47	.50	.608
1040	.06	.09	.12	.15	.18	.21	.24	.27	.30	.33	.36	.39	.42	.45	.55
1080	.06	.10	.13	.16	.20	.23	.27	.30	.33	.36	.39	.42	.45	.48	.58
1120	.06	.11	.14	.18	.23	.25	.29	.32	.35	.39	.42	.45	.48	.51	.65
1160	.07	.11	.15	.19	.23	.26	.31	.34	.37	.41	.44	.47	.50	.53	.65
1200	.070	.11	.16	.20	.24	.28	.33	.36	.39	.43	.46	.49	.52	.55	.68
1240	.07	.12	.17	.22	.26	.30	.35	.38	.41	.46	.49	.52	.55	.58	.71
1280	.08	.13	.18	.23	.28	.32	.36	.40	.44	.49	.52	.55	.58	.61	.74
1320	.09	.14	.19	.24	.30	.34	.38	.42	.47	.52	.55	.58	.61	.64	.77
1360	.10	.15	.20	.26	.32	.37	.42	.46	.51	.56	.59	.62	.66	.69	.81
1400	.11	.17	.23	.29	.35	.41	.46	.51	.56	.60	.64	.67	.71	.74	.86
1440	.12	.18	.25	.32	.39	.45	.51	.56	.61	.65	.69	.72	.76	.79	.91
1480	.14	.21	.28	.35	.43	.49	.55	.60	.65	.69	.73	.77	.80	.83	.95
1520	.14	.21	.28	.36	.44	.52	.58	.63	.68	.72	.76	.80	.83	.86	.975
1560	.15	.225	.3	.375	.460	.54	.60	.65	.70	.74	.78	.82	.85	.88	.985
1600	.165	.25	.33	.41	.50	.57	.63	.68	.73	.77	.82	.86	.89	.92	1.03
1800	.07	.11	.15	.20	.25	.300	.34	.38	.42	.46	.49	.52	.55	.58	.67
2000	.049	.08	.11	.14	.173	.20	.22	.25	.28	.31	.33	.36	.38	.41	.506
2200	.125	.20	.27	.34	.420	.48	.54	.59	.64	.68	.72	.76	.79	.82	.920

TABLE IV - 20

Interpolated Values of Q_{sca}

ν \ a	1μ	1.5	2	2.5	3	3.5	4	4.5	5	5.5	6	6.5	7	7.5	10
10	0	0	0	0	0	0	0	0	0	0	0	0	0	0	0
40	0	0	0	0	.01	.01	.0	.0	0	.0	.01	.01	.01	.01	0
80	.01	.01	.01	.01	.01	.01	.01	.01	.02	.01	.01	.02	.02	.02	.03
120	0	0	0	0	0	.01	.02	.03	.04	.05	.06	.07	.08	.09	.12
160	0	.01	.01	.01	.01	.02	.05	.07	.10	.12	.14	.16	.17	.17	.28
200	0	.01	.02	.04	.06	.10	.13	.17	.21	.24	.27	.30	.32	.35	.45
240	0	0	0	.01	.01	.05	.10	.15	.20	.24	.28	.32	.35	.39	.55
280	0	0	.01	.01	.01	.06	.12	.18	.24	.30	.36	.42	.48	.53	.76
320	0	.01	.01	.01	.01	.02	.04	.08	.12	.20	.28	.36	.43	.50	1.04
360	0	.01	.02	.02	.03	.05	.07	.12	.16	.25	.34	.44	.53	.62	1.38
400	0	.01	.02	.04	.06	.08	.13	.20	.29	.40	.53	.64	.76	.89	1.69
440	.00	.02	.04	.06	.09	.14	.21	.29	.40	.53	.68	.82	.96	1.10	2.04
480	.01	.04	.07	.09	.12	.19	.28	.38	.51	.65	.83	1.00	1.17	1.24	2.50
520	.0	.04	.07	.12	.16	.23	.32	.42	.54	.71	.90	1.13	1.36	1.59	3.05
560	.0	.06	.12	.18	.24	.32	.42	.54	.68	.83	1.02	1.24	1.49	1.75	3.18
570	.0	.06	.12	.18	.26	.36	.47	.60	.75	.92	1.12	1.35	1.65	1.85	3.23
580	.01	.07	.14	.20	.26	.38	.50	.65	.82	1.01	1.21	1.44	1.69	1.92	3.20
590	.01	.07	.15	.22	.29	.41	.54	.70	.89	1.18	1.30	1.52	1.74	1.97	3.14
600	.0	.09	.17	.25	.32	.23	.58	.75	.96	1.17	1.38	1.59	1.80	2.02	3.10
610	.01	.09	.18	.26	.34	.47	.62	.80	1.01	1.22	1.43	1.64	1.85	2.06	3.04
620	.01	.09	.18	.27	.36	.51	.67	.86	1.07	1.28	1.49	1.70	1.91	2.12	2.96
630	0	.10	.20	.30	.39	.54	.72	.92	1.13	1.34	1.55	1.76	1.97	2.18	2.89
640	.01	.09	.19	.31	.41	.57	.77	.96	1.17	1.37	1.58	1.79	2.00	2.21	2.81
650	0	.11	.22	.33	.44	.60	.80	1.00	1.20	1.40	1.60	1.80	2.00	2.20	2.73
660	0	.12	.23	.35	.47	.64	.84	1.04	1.24	1.44	1.69	1.84	2.04	2.23	2.63
670	0	.12	.24	.37	.51	.69	.89	1.09	1.29	1.49	1.69	1.89	2.09	2.27	2.54
680	0	.13	.27	.42	.55	.73	.91	1.10	1.29	1.49	1.69	1.89	2.09	2.28	2.43
690	.01	.15	.30	.43	.57	.75	.92	1.10	1.29	1.48	1.68	1.88	2.09	2.28	2.26
700	.01	.16	.33	.48	.63	.78	.93	1.10	1.28	1.47	1.67	1.87	2.09	2.26	2.14
710	.01	.16	.34	.50	.65	.84	1.00	1.17	1.34	1.53	1.73	1.93	2.13	2.29	2.01
720	.01	.18	.36	.53	.69	.90	1.07	1.23	1.40	1.59	1.79	1.99	2.17	2.31	1.91
730	.01	.19	.38	.56	.74	.95	1.13	1.29	1.46	1.65	1.85	2.04	2.20	2.33	1.82
740	.02	.22	.43	.63	.82	.99	1.18	1.34	1.51	1.70	1.89	2.08	2.23	2.35	1.76

TABLE IV - 20

Interpolated Values of Q_{sca}
(continued)

ν/a	1	μ 1.5	2	2.5	3	3.5	4	4.5	5	5.5	6	6.5	7	7.5	10
750	.02	.23	.45	.66	.86	1.03	1.23	1.43	1.63	1.85	2.05	2.25	2.35	2.36	1.68
760	.02	.24	.47	.68	.88	1.08	1.30	1.54	1.77	2.03	2.24	2.39	2.40	2.30	1.63
770	.02	.25	.49	.71	.90	1.11	1.33	1.57	1.80	2.07	2.28	2.40	2.36	2.14	1.59
780	.02	.25	.47	.69	.88	1.09	1.31	1.55	1.79	2.06	2.27	2.39	2.35	2.13	1.60
790	.02	.24	.46	.66	.85	1.07	1.29	1.53	1.78	2.05	2.26	2.38	2.34	2.13	1.60
800	.02	.23	.45	.65	.84	1.05	1.27	1.51	1.77	2.03	2.25	2.37	2.33	2.12	1.62
810	.03	.22	.42	.62	.79	.99	1.20	1.43	1.67	1.91	2.20	2.35	2.36	2.27	1.65
840	.01	.19	.35	.50	.62	.79	.95	1.11	1.27	1.42	1.55	1.66	1.75	1.78	1.78
880	0	.12	.24	.35	.45	.56	.68	.82	.97	1.13	1.29	1.45	1.63	1.82	1.84
920	.01	.07	.13	.18	.24	.30	.37	.45	.54	.64	.74	.84	.95	1.07	1.67
960	0	.02	.04	.07	.14	.16	.21	.27	.34	.42	.51	.59	.67	.76	1.26
1000	0	.03	.05	.08	.11	.19	.26	.33	.41	.49	.57	.65	.74	.82	1.15
1040	0	.04	.09	.14	.19	.29	.39	.49	.59	.70	.81	.92	1.03	1.14	1.75
1080	0	.05	.11	.18	.24	.36	.47	.59	.71	.83	.95	1.07	1.19	1.31	2.00
1120	.02	.07	.15	.22	.29	.43	.55	.68	.81	.93	1.06	1.19	1.32	1.45	2.11
1160	.01	.09	.18	.26	.35	.49	.61	.75	.89	1.02	1.15	1.28	1.41	1.54	2.22
1200	.01	.10	.19	.28	.38	.51	.63	.77	.91	1.04	1.18	1.32	1.46	1.60	2.27
1240	.03	.12	.20	.29	.40	.53	.65	.79	.93	1.05	1.19	1.33	1.47	1.61	2.29
1280	.02	.12	.22	.32	.43	.54	.65	.76	.87	.97	1.09	1.21	1.33	1.45	2.28
1320	.02	.13	.24	.35	.46	.58	.70	.82	.93	1.04	1.17	1.30	1.43	1.56	2.26
1360	.02	.14	.26	.38	.50	.63	.76	.90	1.03	1.16	1.31	1.46	1.60	1.75	2.21
1400	.03	.15	.27	.40	.53	.66	.80	.94	1.08	1.23	1.38	1.54	1.69	1.85	2.13
1440	.03	.16	.29	.42	.55	.69	.83	.98	1.13	1.29	1.45	1.62	1.78	1.95	2.04
1480	.03	.16	.30	.44	.57	.72	.87	1.03	1.19	1.36	1.53	1.70	1.88	2.06	1.95
1520	.04	.19	.34	.48	.62	.76	.92	1.09	1.26	1.44	1.62	1.80	1.99	2.18	1.92
1560	.04	.20	.35	.50	.66	.81	.98	1.16	1.34	1.53	1.72	1.91	2.11	2.31	1.88
1600	.05	.21	.39	.57	.74	.87	1.07	1.28	1.49	1.71	1.92	2.14	2.37	2.58	1.76
1800	.06	.29	.52	.74	.96	1.18	1.41	1.64	1.87	2.10	2.34	2.58	2.82	2.92	2.31
2000	.11	.43	.76	1.10	1.44	1.78	2.13	2.47	2.81	3.15	3.07	2.86	2.42	2.09	1.88
2200	.18	.51	1.00	1.42	1.83	2.26	2.69	2.86	2.86	2.77	2.53	2.24	1.96	1.68	1.17

It is now possible to compute the ice transmissivity, $\tau_{ice}(z_2,z_1) = 2\,Ei_3\left(\int_{z_1}^{z_2} \Sigma P(a)Q_{abs}(a)\pi a^2 n dz\right)$. Let $P_a(a)$ be the size distribution and n_a the number density for distribution a and $P_b(a)$ and n_b be the corresponding quantities for distribution b. Define two functions, $k_a = \Sigma Q_{abs}(a)P_a(a)\pi a^2$ and $k_b = \Sigma Q_{abs}(a)\,P_b(a)\pi a^2$, such that

$$\tau_{ice} = 2Ei_3\left(\int_{z_1}^{z_2} (n_a k_a + n_b j_b)dz\ .\right)$$

Since we will be considering only cases in which neither n_a nor n_b changes with height (except to go to zero at the top of the scattering layer), $\tau_{ice} = 2Ei_3((n_a k_a + n_b k_b)\Delta z)$. Normally either n_a or n_b will equal zero throughout the sounding.

Columns 2 and 3 of Table IV-21 give values of k_a and k_b respectively for each wave number interval; Table IV-22 gives values of $2Ei_3(x)$. The values in IV-22 are in part taken from Elsasser (1942) and in part computed from the formula $2Ei_3(x) = \exp(-x) - x\exp(-x) + x^2Ei_1(x)$ (Dwight, 1961, 568.3) using values of $Ei_1(x)$ obtained from Jahnke and Emde (1945).

c. $\langle\cos\theta\rangle$. Irvine and Pollack (1968) give values for $\langle\cos\theta\rangle = 2\pi\int_0^{\pi} \Phi(\theta)\cos\theta\sin\theta d\theta$. From equation 2-26 we have $\beta(a) = 4\int_0^{\pi} \Phi(\theta)\,Q_{sca}(a)\pi a^2\theta\sin\theta d\theta = Q_{sca}(a)\pi a^2\, 2\pi\int_0^{\pi} \Phi(\theta)\,\frac{2\theta}{\pi}\sin\theta d\theta =$ $Q_{sca}(a)\pi a^2 \left\langle\frac{2\theta}{\pi}\right\rangle$. Sagan and Pollack (1967) use $\frac{\sqrt{3}}{2}(1-\langle\cos\theta\rangle)$ in

Table IV-21

Absorption and Backscatting Coefficients, in cm^3/m

I	ν	$k_a \times 10^6$	$k_b \times 10^6$	$\theta_a \times 10^6$	$\beta_b \times 10^6$
1	10	0	0	0	0
2	40	.069	.206	.036	.12
3	80	.118	.646	.168	.39
4	120	1.48	4.41	.106	.75
5	160	2.71	8.18	.355	1.81
6	200	3.76	10.95	.99	4.11
7	240	3.78	11.02	.53	3.19
8	280	2.21	6.68	.67	3.87
9	320	1.53	4.66	.32	2.35
10	360	1.09	3.33	.58	3.20
11	400	.886	2.71	.92	5.05
12	440	.779	2.51	1.45	6.74
13	480	.897	2.87	2.04	8.62
14	520	1.16	3.61	2.30	9.48
15	560	1.54	4.74	3.19	11.64
16	570	1.74	5.52	3.42	12.63
17	580	1.97	6.29	3.67	13.33
18	590	2.20	6.83	3.89	14.11
19	600	2.43	7.80	4.26	15.07
20	610	2.74	8.61	4.48	15.77
21	620	3.05	9.27	4.72	16.58
22	630	3.29	9.86	4.98	17.32
23	640	3.57	10.68	5.10	17.69
24	650	3.92	11.69	5.45	18.19
25	660	4.20	12.49	5.67	18.67
26	670	4.47	13.12	5.88	19.28
27	680	4.87	14.54	6.25	19.73
28	690	5.29	16.12	6.38	19.69
29	700	5.73	17.73	6.63	19.86
30	710	5.97	18.42	6.90	20.60
31	720	6.23	19.18	7.26	21.42
32	730	6.49	19.94	7.61	22.15
33	740	6.85	20.83	8.12	22.88
34	750	7.23	21.86	8.41	23.89
35	760	7.50	22.38	8.72	24.89
36	770	7.84	23.04	8.90	25.05
37	780	8.16	23.61	8.60	24.29
38	790	8.43	24.14	8.31	23.63
39	800	8.75	24.70	8.07	22.97
40	810	8.72	24.65	7.59	21.83
41	840	8.40	23.63	5.98	16.18
42	880	7.98	22.31	4.14	12.04

Table IV-21 (Cont'd)

Absorption and Backscattering Coefficients, in cm^3/m

I	ν	$k_a \times 10^6$	$k_b \times 10^6$	$\beta_a \times 10^6$	$\beta_b \times 10^6$
43	920	6.39	17.83	2.16	6.34
44	960	4.77	13.36	1.03	3.66
45	1000	3.32	9.43	1.17	4.03
46	1040	2.79	7.95	1.77	5.77
47	1080	3.07	8.72	2.14	6.83
48	1120	3.35	9.44	2.55	7.66
49	1160	3.52	9.90	2.83	8.14
50	1200	3.73	10.44	2.93	8.40
51	1240	3.99	11.13	3.02	8.39
52	1280	4.21	11.76	3.11	8.10
53	1320	4.45	12.45	3.31	8.63
54	1360	4.81	13.49	3.52	9.25
55	1400	5.36	14.81	3.69	9.59
56	1440	5.89	16.19	3.76	9.72
57	1480	6.47	17.46	3.77	9.80
58	1520	6.68	18.19	4.02	10.34
59	1560	6.99	18.84	4.06	10.44
60	1600	7.51	19.92	4.28	10.99
61	1800	3.78	10.94	5.44	13.70
62	2000	2.59	7.39	7.89	19.95
63	2200	6.30	17.13	9.27	20.87

Table IV-22

Transmission functions for flat (τ_f) and spherical (τ_s) black body aerosols. Not including radiation from the aerosol particles.

x	e^{-x}	$2Ei_3(x)$	x	e^{-x}	$2Ei_3(x)$
.001	.99900	.998007	.30	.74082	.600087
.002	.99800	.996027	.31	.73345	.590792
.003	.99700	.994056	.32	.72615	.581672
.004	.99601	.992105	.33	.71892	.572727
.005	.99501	.990153	.34	.71177	.563947
.006	.99402	.988226	.35	.70469	.555338
.007	.99302	.986284	.36	.69768	.546890
.008	.99203	.984367	.37	.69073	.538574
.009	.99104	.982457	.38	.68386	.530430
.010	.99005	.980553	.39	.67706	.522428
.02	.98020	.961758	.40	.67032	.514576
.03	.97045	.944000	.41	.66365	.506853
.04	.96079	.926649	.42	.65705	.499277
.05	.95123	.909838	.43	.65051	.491827
.06	.94176	.893517	.44	.64404	.484608
.07	.93239	.877662	.45	.63763	.477320
.08	.92312	.862242	.46	.63128	.470263
.09	.91393	.847217	.47	.62500	.463326
.10	.90484	.832585	.48	.61878	.456504
.11	.89583	.818308	.49	.61263	.449802
.12	.88692	.804387	.50	.60653	.443215
.13	.87810	.790799	.51	.60050	.436728
.14	.86936	.777522	.52	.59452	.430358
.15	.86071	.764554	.53	.58860	.424114
.16	.85214	.751874	.54	.58275	.417947
.17	.84366	.739478	.55	.57695	.411906
.18	.83527	.727359	.56	.57121	.405937
.19	.82696	.715501	.57	.56553	.400105
.20	.81873	.703892	.58	.55990	.394342
.21	.81058	.692474	.59	.55433	.388654
.22	.80252	.681403	.60	.54881	.383108
.23	.79453	.670502	.61	.54335	.377639
.24	.78663	.659828	.62	.53794	.372246
.25	.77880	.649369	.63	.53259	.366931
.26	.77105	.639117	.64	.52729	.361833
.27	.76338	.629066	.65	.52205	.356576
.28	.75578	.619214	.66	.51685	.351537
.29	.74826	.609554	.67	.51171	.346584

Table IV-22

(continued)

x	e^{-x}	$2\ Ei_3(x)$	x	e^{-x}	$2\ Ei_3(x)$
.68	.50662	.341668	1.6	.20190	.099814
.69	.50158	.336884	1.7	.18268	.087863
.70	.49659	.332139	1.8	.16530	.077420
.71	.49164	.327480	1.9	.14957	.068269
.72	.48675	.322862	2.0	.13534	.060260
.73	.48191	.318336	2.1	.12246	.053513
.74	.47711	.313902	2.2	.11080	.047040
.75	.47237	.309511	2.3	.10026	.041587
.76	.46767	.305217	2.4	.09072	.036806
.77	.46301	.300963	2.5	.08208	.032567
.78	.45841	.296816	2.6	.07427	.028874
.79	.45384	.292709	2.7	.06721	.025565
.80	.44933	.288650	2.8	.060809	.022726
.81	.44486	.284633	2.9	.055024	.020090
.82	.44043	.280728	3.0	.049786	.017788
.83	.43605	.276872	3.1	.045049	.015816
.84	.43171	.273063	3.2	.040761	.014057
.85	.42741	.269302	3.3	.036883	.012515
.86	.42316	.265590	3.4	.033373	.011113
.87	.41895	.262006	3.5	.030198	.008791
.88	.41478	.258397	3.6	.027324	.008791
.89	.41066	.254842	3.7	.024724	.007829
.90	.40657	.251419	3.8	.022371	.006962
.91	.40252	.247972	3.9	.020242	.006199
.92	.39852	.244582	4.0	.018316	.005517
.93	.39455	.241249	4.1	.016573	.004921
.94	.39063	.237964	4.2	.014995	.004387
.95	.38674	.234764	4.3	.013569	.003908
.96	.38289	.231615	4.4	.012277	.003482
.97	.37908	.228532	4.5	.011109	.003097
.98	.37531	.225421	4.6	.010052	.002769
.99	.37158	.222376	4.7	.009095	.0024655
1.00	.36788	.2194	4.8	.008230	.002204
1.1	.33287	.191773	4.9	.007447	.001955
1.2	.30119	.167858	5.0	.006738	.001748
1.3	.27253	.147236	6.	.002479	.000570
1.4	.24660	.129112	7.	.000912	.000188
1.5	.22313	.113435	8.	.000335	.0000627
			9.	.000123	.00002116
			10	.0000454	.0000071

a manner similar to our $\left\langle \frac{2\theta}{\pi} \right\rangle$. There are obvious similarities between $\left\langle \frac{2\theta}{\pi} \right\rangle = 2\pi \int_0^{\pi} \Phi(\theta) \frac{2\theta}{\pi} \sin\theta d\theta$ and $\left\langle 1-\cos\theta \right\rangle = 2\pi \int_0^{\pi} \Phi(\theta) \left[1-\cos\theta\right] \sin\theta d\theta =$ $(1-\langle\cos\theta\rangle)$. The last equality results from the normalization condition on $\Phi(\theta)$ defined on page 15. Both functions give a weight of 2 to the backward scattered light and 0 to forward scattering. $(1-\langle\cos\theta\rangle)$ gives somewhat more weight to light scattered at a small angle from 180° and less to light scattered nearly forward than does our $\left\langle \frac{2\theta}{\pi} \right\rangle$, and $\left\langle \frac{2\theta}{\pi} \right\rangle$ will thus have somewhat larger values than $\left\langle 1-\cos\theta \right\rangle$ for a forward peaked scattering diagram. However, if $\Phi(\theta)$ does not vary too much with refractive index it should be possible to obtain a relationship between $\left\langle \frac{2\theta}{\pi} \right\rangle$ and $\left\langle \cos\theta \right\rangle$ which will be valid to the accuracy we need. Samuelson (1969) has in fact demonstrated how little the form of $\Phi(\theta)$ depends on refractive index. We can thus make the assumption that a given value of $\left\langle \cos\theta \right\rangle$ corresponds to a given shape of $\Phi(\theta)$ and hence to a given value of $\left\langle \frac{2\theta}{\pi} \right\rangle$. On this assumption values of $\Phi(\theta)$ were scaled from van de Hulst's (1957) Figure 25 with a refractive index of 1.33 and used for numerical computation of both $\left\langle \frac{2\theta}{\pi} \right\rangle$ and $\left\langle \cos\theta \right\rangle$. Values for small $2\pi a\nu$ were obtained from the Rayleigh-Gans formula for spheres (van de Hulst, 1957, p. 89) while a point for $\langle\cos\theta\rangle = .96$ was obtained from the Henyey-Greenstein phase function $\Phi_{HG} = \frac{1 - \langle\cos\theta\rangle^2}{(1+\langle\cos\theta\rangle^2-2\langle\cos\theta\rangle\cos\theta)^{3/2}}$ (Irvine, 1968).

The resulting values of $\langle\cos\theta\rangle$ and $\left\langle \frac{2\theta}{\pi} \right\rangle$ are shown plotted against each other in Figure IV-17; the data are well approximated by the three straight line segments shown in Figure IV-17. As anticipated the

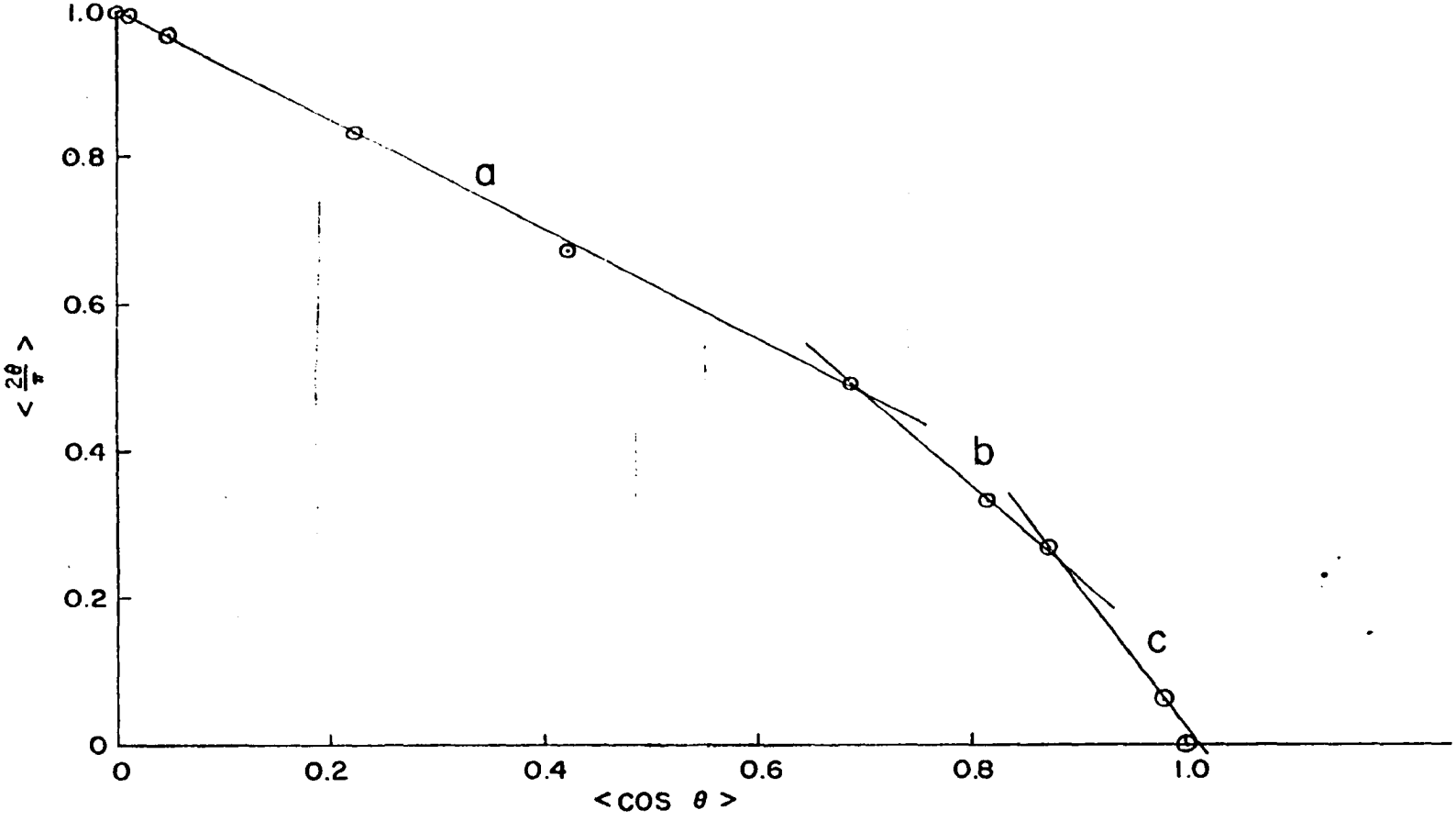

IV-17 Relationship between the flux backscatter factor, $\langle \frac{2\theta}{\pi} \rangle$, and the asymmetry factor, $\langle \cos \theta \rangle$.

resulting curve is convex upward, but fairly smooth, with the equations being:

$$\text{a. } \left\langle \frac{2\theta}{\pi} \right\rangle = 1-.74\langle\cos\theta\rangle,\ 0 < \langle\cos\theta\rangle < .7; \tag{4-17}$$

$$\text{b. } \left\langle \frac{2\theta}{\pi} \right\rangle = 1.29-1.11\ \langle\cos\theta\rangle,\ .7 < \langle\cos\theta\rangle < .87; \text{ and}$$

$$\text{c. } \left\langle \frac{2\theta}{\pi} \right\rangle = 1.47 - 1.33\ \langle\cos\theta\rangle,\ .87 < \langle\cos\theta\rangle\ .$$

The equations (Fig. 4.17) plus values of $\langle\cos\theta\rangle$ scaled from Figure IV-12, were used to obtain the values of $\left\langle \frac{2\theta}{\pi} \right\rangle$ given in Table IV-23 for a = 1μ, 3μ, and 10μ. Values of $\left\langle \frac{2\theta}{\pi} \right\rangle$ other than 1, 3 and 10μ were interpolated from these on the assumption that the major feature of the curve is upward concavity to about $\left\langle \frac{2\theta}{\pi} \right\rangle = 5$, followed by an assymptotic approach to $\left\langle \frac{2\theta}{\pi} \right\rangle = .95$. Minor variations in the assymptotic approach will again be neglected.

We can now define

$$\beta_a = \sum_a (P_a(a)\pi a^2 Q_{sca}(a) \left\langle \frac{2\theta}{\pi} \right\rangle (a) \quad \text{and} \quad \beta_b = \sum_a P_b(a)\pi a^2 Q_{sca}(a) \left\langle \frac{2\theta}{\pi} \right\rangle (a).$$

These values were computed from Tables IV-11, IV-20 and IV-23 to give columns 4 and 5 of Table IV-21.

Figure IV-18 shows the final values of k_a and β_a as functions of wave number, while Figure IV-19 gives similar results for k_b and β_b. Comparison of these curves with those in Figure IV-1 indicate that the region from 800-900 cm^{-1} will probably provide the greatest contribution from ice crystal effects. It is reassuring to note that the general shapes of the curves agree well with those of Deirmendjian (1960).

TABLE IV-23

Values of $\left\langle \frac{2\theta}{\pi} \right\rangle$ used in computations

v/a	1	1.5	2	2.5	3	3.5	4	4.5	5	5.5	6	6.5	7	7.5	10
10	1	1	1	1	1	1	1	1	1	1	1	1	1	1	1
40	1	1	1	1	1	1	1	1	1	1	1	1	1	1	.993
80	1	1	1	1	1	1	1	1	1	.999	.998	.996	.994	.990	.967
120	1	1	.999	.997	.993	.989	.984	.978	.972	.966	.960	.953	.947	.941	.913
160	.999	.998	.996	.993	.990	.979	.968	.957	.946	.935	.924	.913	.902	.891	.833
200	.998	.995	.991	.987	.982	.964	.946	.927	.908	.889	.870	.851	.832	.813	.719
240	.997	.991	.985	.978	.971	.946	.921	.896	.870	.844	.818	.792	.766	.740	.612
280	.996	.987	.978	.969	.960	.929	.898	.867	.836	.805	.774	.743	.712	.681	.526
320	.994	.983	.972	.961	.950	.919	.888	.857	.826	.795	.763	.731	.699	.667	.512
360	.993	.979	.965	.951	.937	.906	.875	.843	.811	.779	.747	.715	.683	.651	.493
400	.992	.974	.956	.938	.919	.887	.855	.822	.789	.756	.723	.690	.657	.624	.460
440	.990	.968	.946	.923	.900	.866	.832	.798	.764	.730	.696	.662	.628	.594	.423
480	.987	.961	.935	.909	.882	.848	.814	.780	.746	.711	.676	.641	.606	.571	.399
520	.984	.953	.922	.891	.859	.825	.791	.757	.723	.689	.655	.620	.586	.552	.380
560	.982	.955	.918	.871	.833	.799	.765	.732	.699	.666	.633	.600	.567	.534	.367
570	.981	.943	.905	.866	.827	.793	.760	.727	.694	.661	.628	.595	.562	.529	.363
580	.980	.941	.901	.861	.821	.788	.755	.722	.689	.656	.623	.590	.557	.524	.359
590	.980	.939	.898	.857	.815	.782	.749	.716	.683	.650	.618	.586	.554	.522	.356
600	.979	.937	.894	.851	.808	.775	.742	.709	.677	.645	.613	.581	.549	.517	.353
610	.978	.933	.888	.843	.798	.766	.734	.702	.670	.638	.606	.575	.544	.513	.352
620	.978	.931	.884	.836	.788	.756	.725	.694	.663	.632	.601	.570	.539	.508	.351
630	.977	.928	.878	.828	.778	.747	.716	.685	.654	.624	.594	.564	.534	.504	.350
640	.976	.925	.872	.820	.767	.737	.707	.677	.647	.617	.587	.558	.529	.500	.350
650	.975	.921	.866	.811	.756	.727	.698	.669	.640	.611	.582	.553	.524	.495	.350
660	.974	.917	.859	.801	.744	.715	.687	.659	.631	.603	.575	.547	.519	.491	.351
670	.973	.913	.852	.792	.732	.705	.678	.651	.624	.597	.571	.545	.519	.493	.358
680	.972	.909	.846	.783	.720	.694	.668	.643	.618	.593	.568	.543	.518	.493	.367
690	.971	.905	.839	.773	.707	.683	.659	.635	.611	.587	.563	.540	.517	.494	.374
700	.970	.901	.832	.763	.694	.671	.648	.625	.603	.581	.559	.537	.515	.493	.380
710	.970	.898	.826	.754	.681	.660	.639	.618	.597	.576	.555	.534	.513	.492	.388
720	.969	.894	.819	.744	.669	.649	.629	.609	.589	.569	.550	.531	.512	.493	.393
730	.969	.891	.813	.735	.657	.638	.619	.600	.581	.562	.543	.525	.507	.489	.393
740	.968	.888	.807	.726	.645	.627	.609	.591	.573	.555	.537	.519	.501	.482	.394
750	.967	.885	.802	.719	.636	.618	.600	.582	.564	.546	.529	.512	.495	.478	.393
760	.967	.883	.798	.713	.628	.610	.592	.574	.556	.538	.520	.502	.485	.468	.382
770	.966	.880	.794	.708	.621	.603	.585	.567	.549	.531	.513	.495	.477	.459	.373
780	.965	.878	.790	.702	.614	.595	.576	.557	.538	.519	.500	.481	.462	.443	.353
790	.964	.875	.786	.697	.607	.588	.569	.550	.531	.512	.493	.474	.455	.436	.343
800	.963	.873	.782	.691	.600	.580	.560	.541	.522	.503	.484	.465	.446	.427	.333
810	.963	.870	.777	.685	.595	.575	.555	.535	.515	.495	.475	.455	.435	.415	.320
840	.961	.867	.773	.679	.585	.563	.541	.519	.497	.475	.453	.431	.409	.387	.280
880	.959	.862	.766	.671	.575	.551	.527	.504	.481	.458	.435	.412	.389	.366	.251
920	.957	.858	.760	.663	.568	.541	.514	.487	.460	.433	.406	.379	.352	.325	.190
960	.953	.853	.754	.655	.560	.531	.502	.473	.444	.415	.386	.357	.328	.300	.160
1000	.950	.849	.748	.647	.545	.516	.487	.458	.429	.400	.371	.342	.314	.286	.147

TABLE IV-23

Values of $\langle \frac{2\theta}{\pi} \rangle$ used in computations (continued)

v/a	1	1.5	2	2.5	3	3.5	4	4.5	5	5.5	6	6.5	7	7.5	10
1040	.946	.842	.736	.632	.520	.484	.468	.442	.416	.390	.364	.338	.312	.286	.160
1080	.942	.834	.724	.617	.497	.473	.449	.425	.401	.377	.353	.329	.305	.281	.160
1120	.937	.826	.713	.602	.483	.460	.437	.414	.391	.368	.345	.322	.299	.276	.160
1160	.932	.818	.702	.587	.460	.438	.416	.394	.372	.350	.329	.308	.287	.266	.160
1200	.928	.810	.691	.572	.453	.432	.411	.390	.369	.348	.327	.306	.285	.264	.160
1240	.922	.803	.684	.563	.440	.419	.398	.377	.356	.335	.314	.293	.273	.253	.153
1280	.916	.796	.676	.555	.433	.412	.391	.370	.350	.330	.310	.290	.270	.250	.150
1320	.911	.790	.669	.547	.427	.406	.385	.364	.343	.323	.303	.283	.263	.243	.143
1360	.904	.783	.661	.539	.417	.397	.377	.357	.337	.317	.297	.277	.258	.239	.143
1400	.900	.777	.654	.531	.407	.388	.369	.350	.331	.312	.293	.274	.255	.236	.143
1440	.893	.768	.642	.518	.393	.375	.357	.339	.321	.303	.285	.267	.249	.231	.141
1480	.885	.759	.630	.505	.380	.362	.344	.326	.308	.290	.272	.254	.236	.218	.141
1520	.879	.750	.619	.492	.367	.350	.333	.316	.299	.282	.265	.269	.253	.237	.140
1560	.870	.741	.608	.478	.353	.337	.321	.305	.290	.275	.260	.245	.230	.215	.140
1600	.865	.731	.597	.464	.331	.317	.303	.289	.275	.261	.247	.233	.219	.205	.140
1800	.805	.702	.569	.436	.303	.294	.285	.276	.267	.258	.249	.241	.233	.225	.185
2000	.786	.663	.540	.417	.295	.293	.291	.289	.287	.285	.283	.282	.281	.280	.275
2200	.730	.615	.501	.387	.273	.272	.271	.271	.270	.270	.269	.269	.268	.268	.267

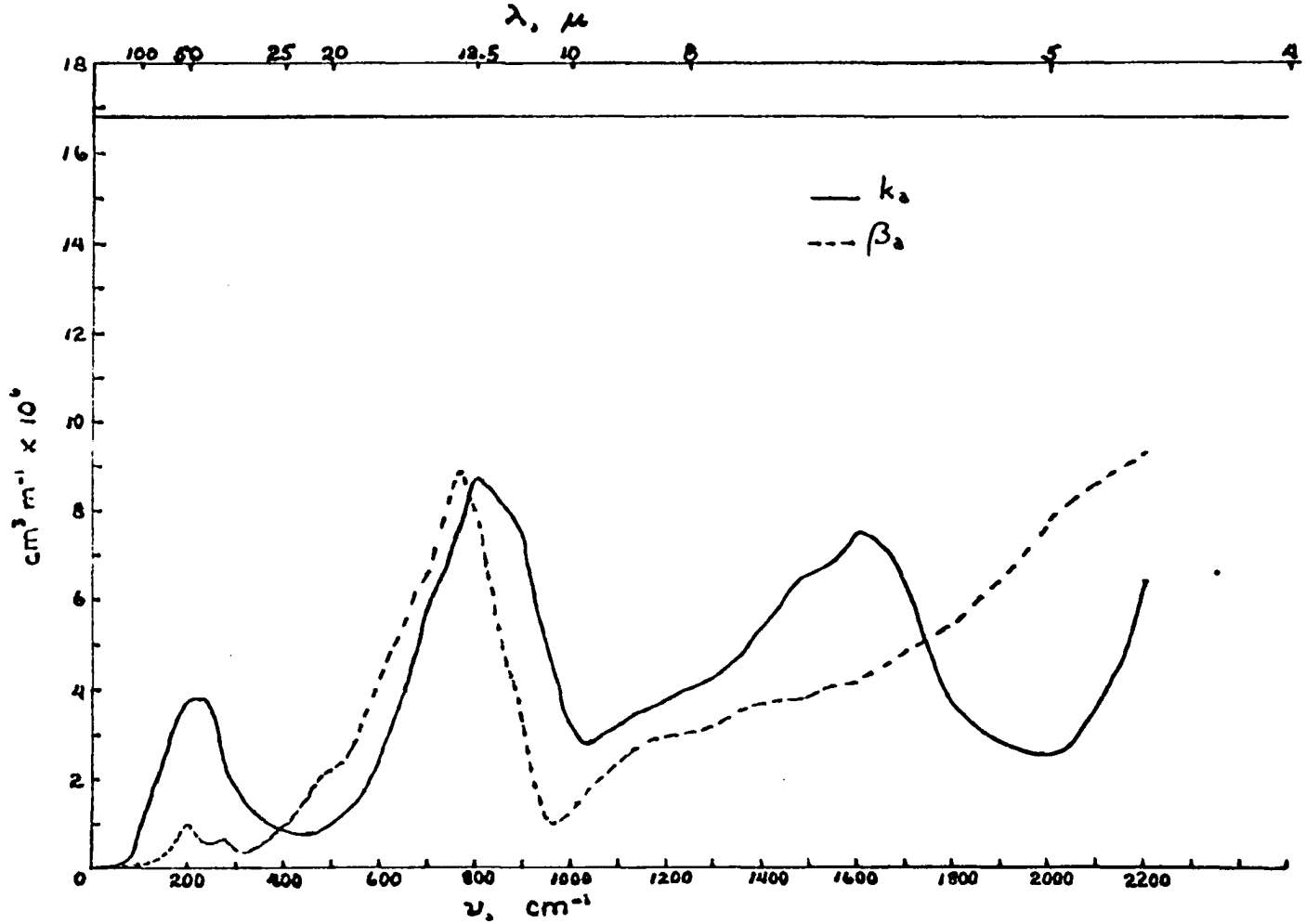

IV-18 Absorption and flux backscatter coefficients for ice crystal size distribution a, 1 crystal/cm^3.

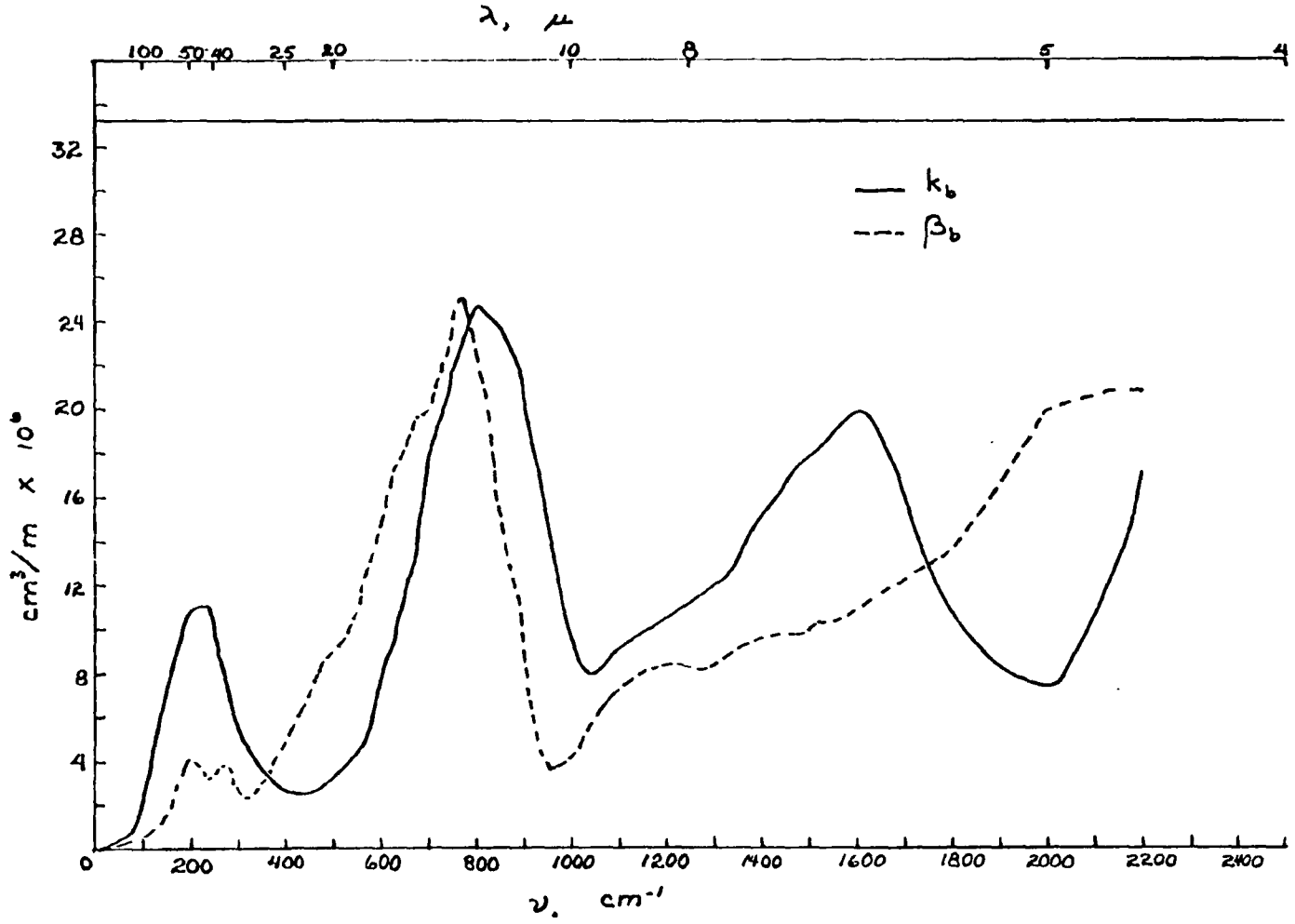

IV-19 Absorption and flux backscatter coefficients for ice crystal size distribution b, 1 crystal/cm^3. Note change in vertical scale from IV-18.

The value of $\left|\frac{d\ln\tau_{ice}}{dz}\right|_{z=z_o}$, for use in computing κ, may now readily be seen from Table IV-22 to be equal to $2(k_a n_a + k_b n_b)$, while β is equal to $n_a\beta_a + n_b\beta_b$.

6. Probable Errors in k and β

We fully realize that our values for Q_{ext}, Q_{abs} and $\left\langle\frac{2\theta}{\pi}\right\rangle$ are subject to considerable error, due both to the uncertainties in the optical constants used by Irvine and Pollack and to the interpolation procedures. In addition, the size distributions and number densities used are based on thoroughly inadequate data samples.

Random errors in the parameters mentioned above, which include interpolation errors in Q_{abs} and possibly some optical constant errors, will tend to be cancelled out by the initial integration over crystal size and the integration of the flux over wave number. Estimated errors of 2 to 5 percent in the interpolated values of Q_{abs} ($\pm$ 1 in the tabulated values) are probably reasonable enough, considering the method of interpolation. These would give errors of around $\pm$ .1 x 10^{-6} cm^3 m^{-1} in k_a and k_b. (Absolute errors for wave numbers 10, 40 and 80 cm^{-1} are smaller).

The interpolation errors in Q_{ext} and $\left\langle\frac{2\theta}{\pi}\right\rangle$ are not random, as the interpolations are roughly linear and the true curves are not. To some extent this will be compensated for by the fact that Q_{ext} is concave upward where $\left\langle\frac{2\theta}{\pi}\right\rangle$ is concave downward and vice versa. To gain some idea of the actual error in β, we used an interpolation procedure similar to that used for Q_{abs} (section 5b) which includes a visual estimate of curvature effects. Values of Q_{sca} and $\left\langle\frac{2\theta}{\pi}\right\rangle$ for one wave

number interval were obtained by this technique. β_a and β_b were computed from these, and the results were compared with those from Table IV-21. The interval centered at 840 cm^{-1} was chosen for the comparison because it is one of the intervals where the effects of ice fog were expected to be most prominent. Figure IV-20 shows the graphically interpolated values as lines, and the linearly interpolated values from Tables IV-20 and IV-23 as dots. The graphical values of β_a and β_b are 5.10×10^{-6} and 15.19×10^{-6} respectively, compared with linear-interpolation values of 5.98×10^{-6} and 16.18×10^{-6}. This suggests that errors in β_a and β_b are of the order of $\pm 1 \times 10^{-6}$, ie., $\pm$ 10 to 20%.

The effect of size distributions a and b on the absorption and backscatter coefficients is shown in Figures IV-21 and IV-22 respectively, again for ν = 840 cm^{-1}. As can readily be seen, the few large crystals contribute disproportionately large shares of both absorption and flux backscatter. A relatively small change in the upper end of either size distribution would result in considerable changes in the appropriate k and β. Such changes, together with changes in crystal number densities, produce effects which, while certainly not "errors", would completely swamp the errors contributed by the interpolation techniques. All available evidence indicates that size distributions a and/or b will occur in some ice fogs, and are as typical as any others available of widespread and city fogs respectively. Flux values obtained using these distributions and various number densities will give a good idea of the types of cooling rates to be expected for ice fogs in general, even though they will not be exact for any particular fog.

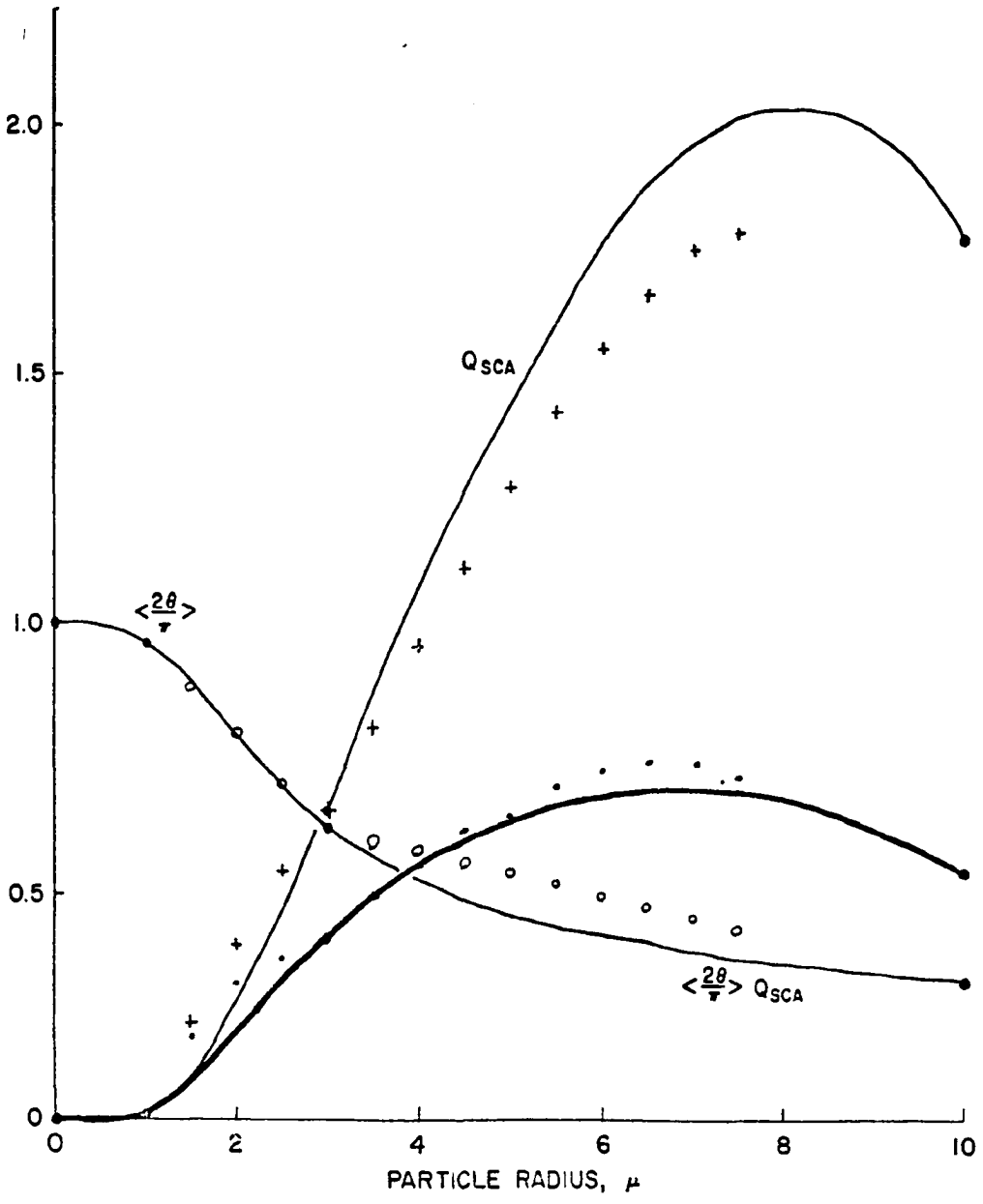

IV-20 Error estimate for β. Light lines are graphically interpolated vales for $\langle \frac{2\theta}{\pi} \rangle$ and Q_{sca}; heavy curves is resultant value of their product. 0's and +'s give linearly interpolated values of $\langle \frac{2\theta}{\pi} \rangle$ and Q_{sca} actually used in the computation; dots give the resultant values of $\langle \frac{2\theta}{\pi} \rangle Q_{sca}$.

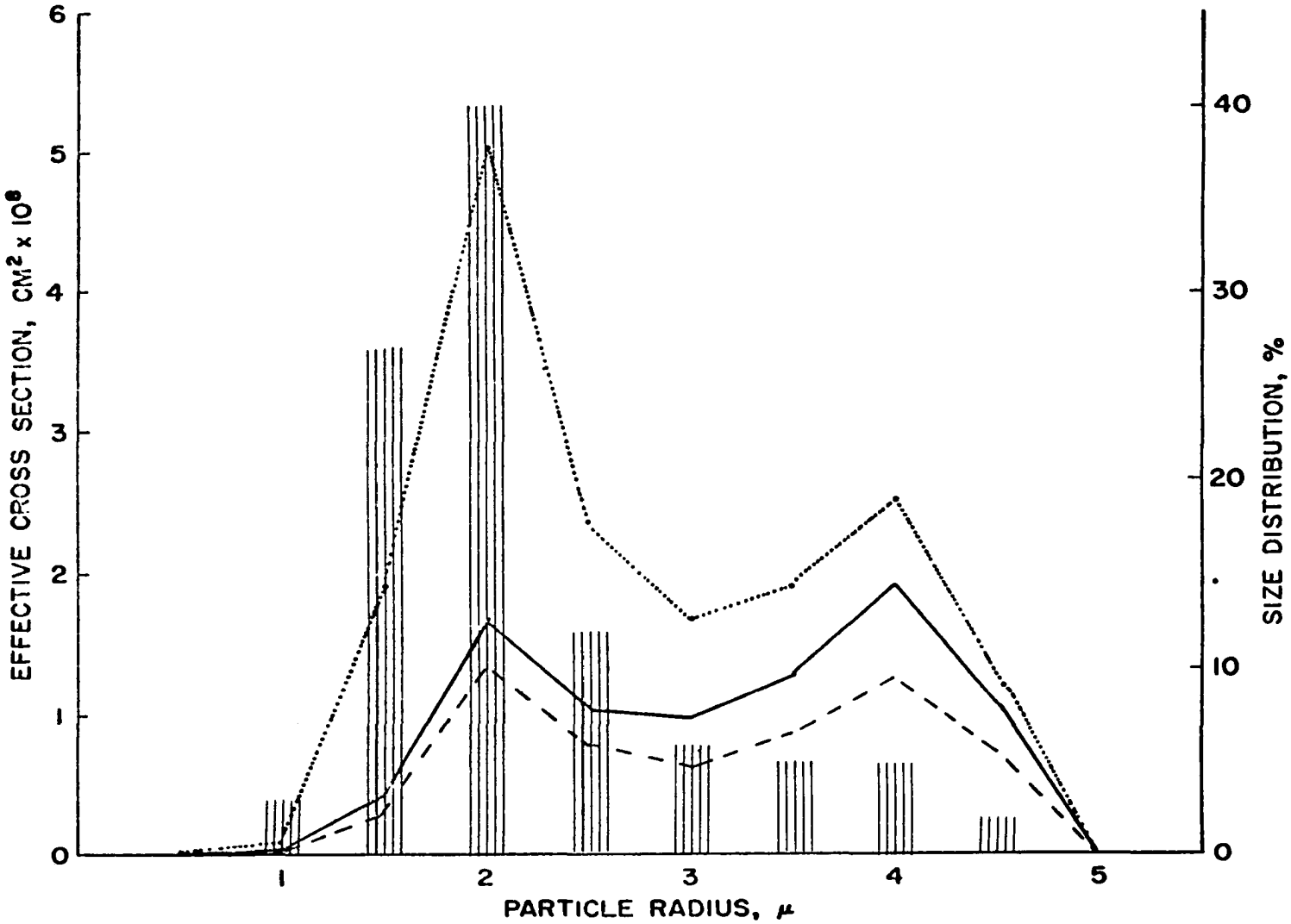

IV-21 Relative contributions of various particle sizes to total absorption and backscatter at 840 cm^{-1}, distribution a. Bar graph shows assumed size distribution, (right hand scale), dotted line shows size distribution weighted by geometrical cross sections, solid line, the Mie absorption, and dashed line, the flux backscatter.

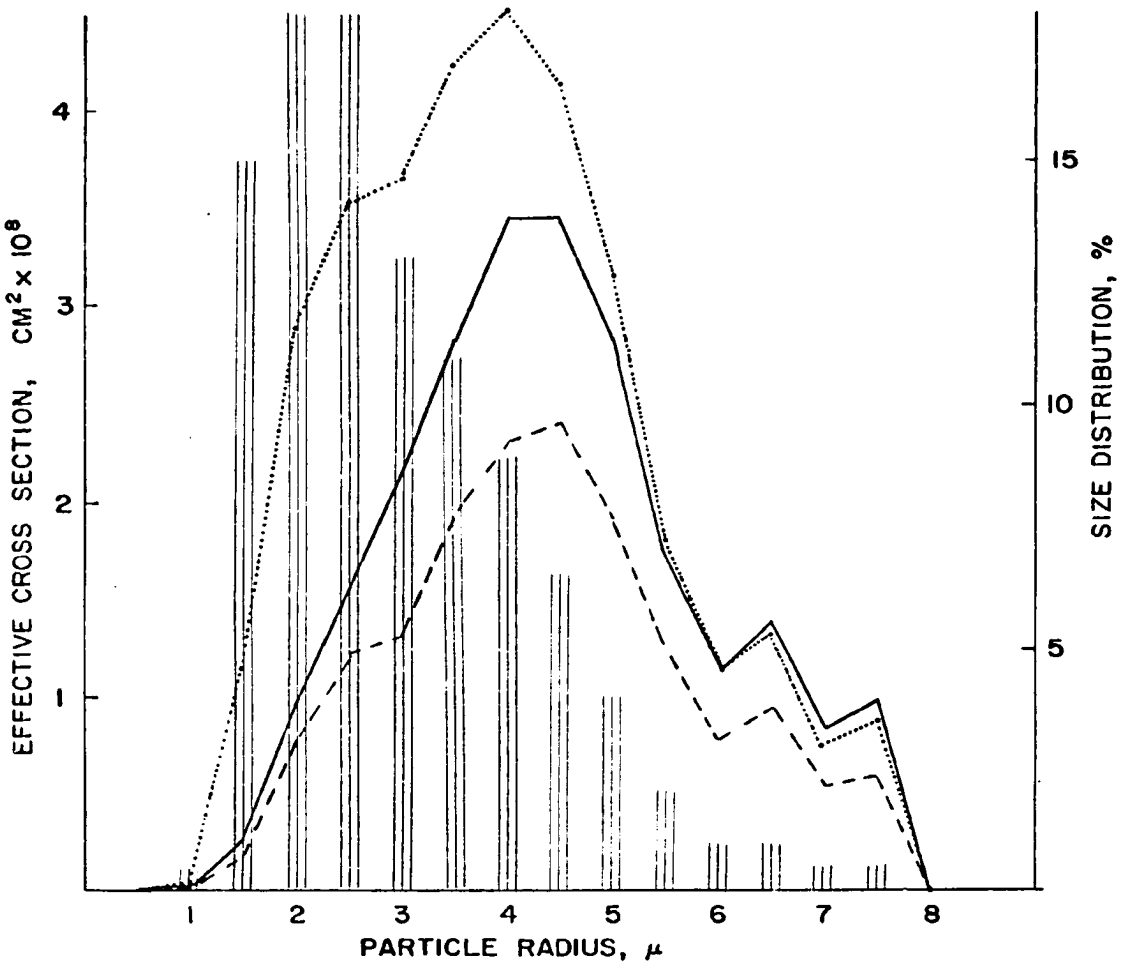

IV-22 Relative contributions of various particle sizes to total absorption and backscatter at 840 cm^{-1}, distribution b. Bar graph shows assumed size distribution, (right hand scale), dotted line shows size distribution weighted by geometrical cross sections, solid line, the Mie absorption, and dashed line, the flux backscatter.

One error which is not swamped by natural variability is that of the ratio of β to k. This will produce a similar proportional error in s.

E. Experimental Data

There are two types of data which might be used to check our theoretical results--temperature changes and radiometer records.

Rawinsonde data generally lack the low altitude resolution necessary to see the types of changes for which we are looking. Under extreme conditions (e.g., December 27-29, 1961), they can record temperature minima aloft within the first hundred meters of the ground. Temperature records are also available from several fifteen meter towers in the Fairbanks area at some times, but are not used in this thesis.

Radiometer records were taken at two heights at the Municipal Utilities System (MUS) generating plant during the winters of 1968-69 and 1969-70. Two ventilated Beckman-Whitley radiometers were used, supported and separated by a 20 meter utility pole. The site was near the bank of the Chena River just downstream of the point where MUS dumps their cooling water, and was thus in an area of dense fog whenever temperatures dropped below -30°C. The site was not an ideal one, having a chain-link fence about 2 m north of the radiometer with the river bank shortly beyond. However, it was the only available site with dense ice fog where neither traffic nor vandalism was a problem.

Considerable difficulty was encountered with the equipment, and as a result few good records were obtained. The air inlets for the ventilator fans on both radiometers were rapidly clogged with ice crystals, thus choking off the flow of air across the plates. This in

turn allowed both settling and growth of frost on the plates, as well as upsetting calibration. To combat this problem the radiometer bodies were inclosed in screen cages which provided a deposition area of around 700 cm^2/radiometer, and the upper cage was equipped with a weight and pully which allowed accumulated frost to be knocked off from the ground. This proved effective provided someone came by to knock the crystal deposit off the cages every three or four hours in dense fog (which was generally not possible) or daily in warmer weather. The ordinary window screening used proved surprisingly effective in removing ice crystals from foggy air forced through it.

Further difficulty was encountered in the different responses of the two instruments. When both radiometers were run side by side with a common chart zero, the 10% calibration difference was swamped by the effect of what appeared to be different time constants. It is evident that only a rather large difference in the readings of the two instruments may be relied on.

A final problem was that the crystal size distribution at the site, which was dominated by open-water fog, probably had larger crystals than either distributions a or b. The result of all these factors is that the radiometer records are of little quantitative value, although some of the qualitative results are interesting. For example, even relatively light large-crystal fog often produced radiative balance or incoming net radiation at the lower radiometer. Consequently, the original plan of comparing computed and measured flux divergences was dropped, and the project was confined to computing the height and density of typical fogs which would produce various cooling profiles.

F. The Transition from Flux to Cooling Rates

Thus far we have considered only one of the processes which may change the energy in a small volume of the atmosphere, and none of those that affect the storage of energy. The first group includes not only radiative but also conductive transfer of energy, plus any energy added by such artificial sources as cars and buildings. If any considerable gradient in water vapor content (mixing ratio) existed the possibility of latent heat transfer might also be significant, but under the extremely dry conditions common to ice fog and ice crystal displays this form of transfer may be neglected. The storage terms include adiabatic heating (which we will neglect), temperature changes in air and ice crystals and latent heat of sublimation of water vapor already in the air mass under consideration. In order to judge the significance of radiative processes, it is necessary to know at least the order of magnitude of all these terms in the energy balance of an air parcel. We will consider the storage terms first.

1. Storage Processes

a. Heating of the air. The power required to heat one gram of air at the rate dT/dt is given by $c_p\ dT/dt$, where c_p is the specific heat of air at constant pressure. The volume of air occupied by ice crystals is negligible (see discussion of mass of ice, below) so we can make use of the relationship for air density, $\rho_{air} = \frac{P}{1000}\frac{273}{T}\rho(P=1000\text{mb},\ T=273^\circ\text{K})$. Since ρ_{air} at a pressure of 1000mb and a temperature of 273°K is 1.275×10^{-3} g cm^{-3} (List, 1949), $\rho_{air} = 3.48(P/T) \times 10^{-4}$ gm cm^{-3}. It is convenient to introduce different units for density so as to be consistent

with the units of the other variables, namely: cm for horizontal and m for vertical lengths and a time unit of 12 hrs. Thus, the density is written as

$$\rho_{air} = 3.48(P/T) \times 10^{-2} \text{ gm cm}^{-2} \text{ m}^{-1}$$

From List (1949) $c_p = .24$ cal gm^{-1} $°K^{-1}$, so the energy storage rate from heating of the air is $c_p \rho_{air} (dT/dt) = 8.35 \times 10^{-3} (P/T)(dT/dt)$ in cal cm^{-2} m^{-1} $(12 \text{ hr})^{-1}$.

b. Heating of ice crystals. The greatest solid water content observed by Ohtake (1970) was .1g m^{-3}. Benson (1965) calculated values of 0.07 g m^{-3} for the outlying areas and 0.21 g m^{-3} for the core area of downtown Fairbanks. These calculations were based on observations of the rate of solution of the fog during warming. Our maximum value, obtained from distribution b and number density 1000, is .14 gm m^{-3}. Since the specific heat of ice is less than .5 for temperatures substantially below freezing, the maximum energy storage rate from heating suspended ice crystals is only about 10^{-5} (dT/dt) cal cm^{-2} m^{-1} $(12 \text{ hr})^{-1}$. As P/T is of the order of 3 in the foggy layer, this is three orders of magnitude less than the energy storage due to heating the air and may safely be neglected. Gotaas and Benson (1965) came to the same conclusion for ice crystal displays.

c. Latent heat of ice crystals. If the temperature of an ice-saturated 1 cm^3 parcel of air, initially at a temperature T, is increased by 1°C, an amount of ice $[d_{vi}(T+1°C) - d_{vi}(T)]$ must be evaporated to maintain ice saturation of the air. Here $d_{vi}(T)$ is the ice-saturation water vapor density, in g cm^{-3}, at temperature T and ambient pressure.

Since d_{vi} varies from ρ_i, the saturation vapor density over ice of pure water vapor in the absence of air, by less than 1% at the temperatures involved, ρ_i, (which is a function only of T) may be substituted for d_{vi} without serious error. The latent heat of sublimation of ice, L_s, is 678 cal gm^{-1} at -30 to -40°C, so the energy storage rate due to sublimation of ice is $6.78 \times 10^4 \frac{d\rho_i}{dT} \frac{dT}{dt}$ cal cm^{-2} m^{-1} $(12\ hr)^{-1}$. Values of $L_s \frac{d\rho_i}{dT}$ derived from Table 109 in List (1949) are given in Table IV-24. For T = -35°C, the energy storage rate is 1.45×10^{-3} dT/dt--about an order of magnitude less than the 8.35×10^{-3} (P/T) (dT/dt) accounted for by warming the air. The total energy storage rate (cal cm^{-2} $m^{-1}(12\ hr)^{-1}$ in air containing ice crystals is then $(8.35 \times 10^{-3}$ (P/T) + $L_s \frac{d\rho_i}{dT})$ (dT/dt), where P is pressure in millibars, T is temperature in degrees Kelvin, and $L_s \frac{d\rho_i}{dT}$ is tabulated in Table IV-24. All of the processes above are reversible and have the same algebraic form for decreasing temperatures.

2. Transfer Processes

These are processes which add energy to the air. Radiative transfer has already been discussed; the rate of energy addition in cal cm^{-2} m^{-1} $(12\ hr)^{-1}$ is -(dF/dz) if z is in meters throughout the calculation and F is in cal cm^{-2} $(12\ hours)^{-1}$. Conductive (including eddy transport) transfer and man-made heat sources will be considered here.

a. Conduction. Heat conduction is normally neglected in radiative transfer problems. However, we are looking at a situation in which the underlying surface, dry snow, is an extremely poor conductor, and conduction to the radiatively cooling snow surface from air, snow and the soil below occurs. Under ice fog conditions in Fairbanks, Wendler (1969)

Table IV-24

$L \frac{d\rho_i}{dT}$ in $cal°k^{-1}cm^{-2}m^{-1}$

T(°C)	$L \frac{d\rho_i}{dT}$	T(°C)	$L \frac{d\rho_i}{dT}$
-60	$9.75x10^{-5}$	-29	$2.52x10^{-3}$
-59	$1.10x10^{-4}$	-28	$2.76x10^{-3}$
-58	$1.24x10^{-4}$	-27	$3.02x10^{-3}$
-57	$1.39x10^{-4}$	-26	$3.29x10^{-3}$
-56	$1.56x10^{-4}$	-25	$3.59x10^{-3}$
-55	$1.75x10^{-4}$	-24	$3.92x10^{-3}$
-54	$1.97x10^{-4}$	-23	$4.28x10^{-3}$
-53	$2.21x10^{-4}$	-22	$4.67x10^{-3}$
-52	$2.47x10^{-4}$	-21	$5.12x10^{-3}$
-51	$2.76x10^{-4}$	-20	$5.55x10^{-3}$
-50	$3.08x10^{-4}$	-19	$6.04x10^{-3}$
-49	$3.59x10^{-4}$	-18	$6.52x10^{-3}$
-48	$3.84x10^{-4}$	-17	$7.12x10^{-3}$
-47	$4.28x10^{-4}$	-16	$7.74x10^{-3}$
-46	$4.85x10^{-4}$	-15	$8.30x10^{-3}$
-45	$5.28x10^{-4}$	-14	$8.96x10^{-3}$
-44	$5.87x10^{-4}$	-13	$9.71x10^{-2}$
-43	$6.52x10^{-4}$	-12	$1.05x10^{-2}$
-42	$7.19x10^{-4}$	-11	$1.14x10^{-2}$
-41	$7.94x10^{-4}$	-10	$1.23x10^{-2}$
-40	$8.81x10^{-4}$	- 9	$1.33x10^{-2}$
-39	$9.76x10^{-4}$	- 8	$1.44x10^{-2}$
-38	$1.07x10^{-3}$	- 7	$1.55x10^{-2}$
-37	$1.19x10^{-3}$	- 6	$1.67x10^{-2}$
-36	$1.31x10^{-3}$	- 5	$1.80x10^{-2}$
-35	$1.45x10^{-3}$	- 4	$1.94x10^{-2}$
-34	$1.58x10^{-3}$	- 3	$2.08x10^{-2}$
-33	$1.74x10^{-3}$	- 2	$2.24x10^{-2}$
-32	$1.91x10^{-3}$	- 1	$2.41x10^{-2}$
-31	$2.10x10^{-3}$	0	
-30	$2.30x10^{-3}$		

found sensible plus latent heat flux to the snow surface from the air of 20 cal cm^{-2} day^{-1}, and a flux to the surface from the snow pack of 25 cal cm^{-2} day^{-1}. Since the instrumentation for this study was located away from such sources of mechanical turbulence as moving automobiles, the actual flow of heat from the air to the snow surface in built-up areas would probably be somewhat higher, and a reasonable assumption is that under ice fog conditions the energy lost by radiation from the snow surface is supplied equally by the snow pack and the air.

The energy flow in cgs units into any given layer of air of unit thickness is $-\frac{dH'}{dz}$ where H' is the conductive heat flow upward; $H' = -k'\frac{dT'}{dz}$. k' is the thermal conductivity in cal cm^{-1} sec^{-1} $°C^{-1}$. Unfortunately the effective value of k' for air normally depends on turbulent transfer rather than on molecular conductivity, and thus varies in an irregular fashion with lapse rate, surface roughness, wind speed and height. Under conditions of high stability and very low wind speed k' will be small, but use of the molecular conductivity is still not justified. However, the assumption that half of the energy flux from the snow surface is supplied by the air allows computation of an effective conductivity for the air. The true variability of k' with height will be neglected, and we will simply define k' as

$$k' = \frac{\frac{1}{2}F(0)}{\left.\frac{dT}{dz}\right|_{z=0}} = \frac{1}{2}\frac{F(0)z_1}{(T(z_1)-T(0)},$$

where z_0 is the first value of z above the ground for which T is given. The rate of energy addition due to conduction is now

$$-\frac{dH'}{dz} = k' \frac{d^2T}{dz^2} = \frac{F(0)z_1}{T(z_1)-T(0)} \quad \frac{(z_n-z_{n-1})T_{n+1}+(z_{n+1}-z_n)T_{n-1}-(z_{n+1}-z_{n-1})T_n)}{(z_n-z_{n-1})(z_{n+1}-z_n)(z_{n+1}-z_{n-1})}$$

Technically, of course, the above equation applies to potential temperature. But in a layer < 100 m thick with temperature gradients of the order of 10 to 30°C/100m, the difference is negligible in an order of magnitude calculation such as the above.

In the simpler crystal display case, we retain the assumption that one half of the net flux from the snow surface is supplied by cooling of the air near the surface. However, we will not attempt to carry out conductive calculations. Instead, we will make the following assumption:

> If there exists within a foggy layer, or one which contains ice crystals, a level such that the mean cooling rate above the level exceeds that below the level (with one half the net flux from the surface assumed to be supplied by the air below the level), then that level will be called the neutral height, and the combination of radiative and conductive processes may lead to destabilization of the sounding at least at and above the neutral height.
>
> The closer to the ground this neutral height is, the more likelihood there is that a normal lapse rate will develop through all or most of the layer containing ice crystals.

b. Man-made heat sources. The same combustion processes which supply water vapor to the ice fog also supply heat to the air. This process may be direct, as in heating by car exhaust or chimney smoke; or may occur after use of the heat to warm buildings (after which it is conducted to the outside air through walls and particularly through

windows and doors) or to do mechanical work, after which it reappears as turbulence which ultimately degrades to heat. Given the rate at which various fuels are burned, it is at least theoretically possible to compute the artificial heat input to the air.

Benson (1965) gives the values listed in Table IV-25 for average daily fuel consumption in the Fairbanks area as of 1965. The heats of combustion were estimated from the Handbook of Chemistry and Physics, 1959. As a first approximation, we will assume that half of the total heat is generated in the core area and added uniformly to it. One third of the total is spread over the residential area and the remaining sixth is added to the outlying area. The thickness, areas and volumes for these regions are summarized in Table IV-26.

Table IV-25

Artificial Heat Sources

Fuel	Amount, kg day^{-1}	Heat of Combustion, cal kg^{-1}	Total Heat Input
Gasoline	90,000	10^7	4.5×10^{11} cal(12 hr)$^{-1}$
Fuel oil	152,000	10^7	7.6×10^{11} cal(12 hr)$^{-1}$
Coal, home	305,000	5×10^6	7.6×10^{11} cal(12 hr)$^{-1}$
Coal, power	1,118,000	5×10^6	2.8×10^{12} cal(12 hr)$^{-1}$
Total			4.8×10^{12} cal(12 hr)$^{-1}$
Latent Heat			$.3\times10^{12}$
			5.1×10^{12} cal(12 hr)$^{-1}$

Table IV-26

Artificial Heat Input

Region	Area (km^2)	Depth (m)	Volume (cm^2 m)	% Total Input	H	H_F
Core	5	20	10^{12}	50	2.5	51
Residential	50	5	2.5×10^{12}	33	.6	3
Outlying	200	5	10^{13}	17	.08	.4

Heats of combustion are computed with all products in the vapor phase. The latent heat released in the condensation and freezing of the water vapor created by combustion is in addition both to the heat of combustion, and to the latent heat of the natural water vapor content of the air which was discussed under heat storage. Water vapor resulting directly from power plant fuel consumption will be ignored on the assumption that these plumes often evaporate before blending with the fog (Benson, 1965). The heat used to evaporate cooling water is ultimately supplied by the heat of combustion of the power plant fuel, which was accounted for above. The evaporated water condenses into droplets within a few meters of the water surface, giving this latent heat of evaporation to the air. The two processes cancel as far as any net addition of heat to the system of air plus cooling water is concerned and the end result is simply a transfer of heat from the water to the air. Indeed, the whole process is merely the mechanism by which heat is transferred from the water to the air.

The latent heat of freezing of the droplets must be included and may be accounted for by using Benson's (1965) figures for the amount of water evaporated and multiplying by 80 cal/gm. There may also be some freezing of the water which does not evaporate, but probably most of the water which does not evaporate eventually goes to augment the winter flow of the Tanana rather than freezing. This contribution is probably small and virtually impossible to calculate. It will be neglected.

According to Benson (1965) the total water inputs (excluding that from power plant fuel combustion) are 533×10^6 gm day^{-1} from combustion

(vapor) and 2800 x 10^6 gm day^{-1} from cooling water.* Taking the latent heat of sublimation as 678 cal gm^{-1} and that of freezing as 80 cal gm^{-1}, the resulting energy inputs are 3.6 x 10^{11} cal day^{-1} and 2.2 x 10^{11} cal day^{-1}, or a total of 2.9 x 10^{11} cal $(12\ hr)^{-1}$. This amount must be added to the heat of combustion (Table IV-25). The resulting values are used to compute H, the artificial heat addition rate, and H_F, the equivalent flux (Table IV-26).

Although the calculations above look reasonable enough, they predict rather unreasonable-looking heating rates. For example, in the core area, the predicted heating rate due to man-made sources is 67°C $(12\ hr)^{-1}$. This derives from an energy input of 51 cal cm^{-2} $(12\ hr)^{-1}$, or .07 cal cm^{-2} min^{-1}. Much of this energy is being expended in an effort to keep buildings and vehicles warm at -40°C. Myrup (1969) estimated a man-made heat source of .05 cal cm^{-2} min^{-1} for a hypothetical city in central California and found that it would have only a minor effect on the intensity of the city heat island calculated. Therefore, it seems possible that even the Fairbanks heating rate may largely be compensated for by radiative effects, leaving the 5-6°C heat island actually observed for Fairbanks (Benson, 1965). This will be discussed in greater detail in Chapter VI, but two points deserve special mention here. First, the calculations above were for stagnant air. A net regional drift of the air over the city with speeds as low as 1 m sec^{-1}, which could not readily be detected, would limit the heat gain by the average parcel of air traversing the city core to about 10% of the nominal 12-hourly cooling rate, 6.5°C. This is sufficiently close to the observed magnitude of the Fairbanks heat island to be readily acceptable.

*Miscellaneous sources do not contribute much and are included as part of the cooling water.

Secondly, the large predicted heating rate near the ground indicates that vertical heat transfer within the fog is very likely. Convection reaching above the top of the fog layer would gradually thicken the fog over the city center (Benson 1965, Fig. 27).

With these reservations on the correct value of H, the cooling rate equation may be written by equating energy storage on the left hand sides of Eqs. 4-3 and 4-4 to net energy convergence on the right hand sides:

$$\frac{dT}{dt}\left(8.35 \times 10^{-3} P/T + L \frac{d\rho_i}{dT}\right) = \tag{4-3}$$

$$-\frac{dF_s}{dz} + \frac{F_s(0) z_1}{T(z_1)-T(0)} \frac{(z_n-z_{n-1})T_{n+1}+(z_{n+1}-z_n)T_{n-1}-(z_{n+1}-z_{n-1})T_n}{(z_n-z_{n-1})(z_{n+1}-z_n)(z_{n+1}-z_{n-1})}$$

$$+ H$$

in the ice fog layer, and

$$\frac{dT}{dt}\left(8.35 \times 10^{-3} P/T\right) = -\frac{dF_c}{dz} \tag{4-4}$$

$$+\frac{F_s(0) z_1}{T(z_1)-T(0)} \frac{(z_n-z_{n-1})T_{n+1}+(z_{n+1}-z_n)T_{n-1}-(z_{n+1}-z_{n-1})T_n}{(z_n-z_{n-1})(z_{n+1}-z_n)(z_{n+1}-z_{n-1})}$$

above it.

These equations are used in Chapter V to compute separately the radiative and conductive contributions to the heating rate.

CHAPTER V

PROGRAMMING AND NUMERICAL RESULTS

Two FORTRAN IV programs were were written to give fluxes and cooling rates in the presence of ice crystal displays and ice fogs. The first program was based on the numerical data for R presented by Elsasser and Culbertson (1960). Since in this case the integration over ν has already been carried out, only gray non-scattering crystals may be considered. However, this is what is needed for the ice crystal case, so the program was set up for plane ice crystals, with $\tau(\text{ice}) = \exp(-n\pi a^2 \Delta z)$. The second program was based directly on equations (3-17) and the parameters derived in Chapter IV. The first program was written by the author with some assistance from Mrs. Sharon Dean of the programming group. The second program was written by Mrs. Dean.

The remainder of this chapter will consist primarily of computer output. Section A gives both programs, plus the program used for recomputation of the Elsasser coefficients. The reasons behind this recomputation are discussed in Chapter VI, Section A. Section B gives the numerical results for ice crystal displays, and Section C gives results for ice fog. Note that the two programs frequently differ in notation.

A. Programs

1. Gray-Crystal Program

The program as given will print out a total of 21 tables in the format of Section B, one for each of 7 display heights and 3 ice

absorption coefficients. In addition, it prints working tables, not reproduced here, giving all values in an 8-digit exponential format. The program was run in this form only for the composite sounding. For the two soundings from Gotaas and Benson (1965) the statement DO 990 NA=1,3 between the initial READ and FORMAT statements was replaced by NA=1; ABICE(1) being the value of .00196m^{-1} which was obtained for the 25μradius crystals.

Each sounding was given an identification number. Sounding 1 is 1400 14 December 1961, sounding 2 is 1400 24 January 1962, and sounding 3 is the composite sounding.

In order to use the gray program for ice fog the sections marked in the program bracketed by the rows of letters are replaced by the similarly lettered sections presented under the heading "Modification of gray program to accept ice fog data."

```
C
C PROGRAM TO COMPUTE RADIATIVE COOLING RATES IN THE PRESENCE
C OF BLACK,HORIZONTAL PLANE ICE CRYSTALS.
C BASED ON THE ELSASSER CHART
C T PREFIXES ARE USED THROUGHOUT FOR TABULATED VALUES.
C ELSASSER'S R FOR WATER VAPOR IS RH2O.  THE NEGATIVE OF HIS CO2
C CORRECTION (=R FOR CO2 AT LOW WATER VAPOR CONTENTS) IS DRH2O.
C TLOGU AND TLOGV ARE THE VALUES OF LOG U AND LOG V FOR WHICH
C RH2O AND DRH2O ARE TABULATED.  U IS WATER IN LIQUID CM AND V I
C CO2 IN CM STP.  XLAHT IS THE DERIVATIVE OF THE WATER VAPOR
C DENSITY OVER ICE WITH RESPECT TO TEMPERATURE, MULTIPLIED BY TH
C LATENT HEAT OF SUBLIMATION OF ICE.  ID IDENTIFIES THE SOUNDING
C WHILE NZ GIVES THE VALUE OF J CORRESPONDING TO P(J)=50MB.
C Z IS HEIGHT IN M, P, PRESSURE IN MB, TEMPC, TEMPERATURE IN DEG
C C, DU(J)AND DV(J), WATER AND CO2 CONTENTS OF THE LAYERS
C FROM Z(J) TO Z(J+1).  TROT AND TRDTCO GIVE THE INTEGRALS OF R
C AND DR FROM T = -60. TO -273.
C
C
      DIMENSION TRH2O(16,6),TDRH2O(16,20),TLOGU(16),TLOGV(20)
      DIMENSION XLAHT(40)
      DIMENSION TROT(16),TRDTCO(16,20)
      DIMENSION Z(30),DU(30),DV(30),TEMPC(30),P(30),FLUXZ(30)
      DIMENSION COOL(30)
C     A     A     A     A     A     A     A     A     A     A
      DIMENSION NCA(11)
      DIMENSION ABICE(3)
C     A     A     A     A     A     A     A     A     A     A
      DIMENSION TEMPCO(20)
      READ(1,101)((TRH2O(IU,IT),IT=1,6),IU=1,16)
      READ(1,102)((TDRH2O(IU,IV),IV=1,20),IU=1,16)
      READ(1,103)TLOGU
      READ(1,104)TLOGV
      READ(1,107)XLAHT
      READ(1,109)TRDT
      READ (1,102)((TRDTCO(IU,IV),IV=1,20),IU=1,16)
      READ(1,106)ID,NZ
      NZPLUS=NZ+1
      DO 420 I=1,NZPLUS
  420 READ(1,105)J,Z(J),P(J),TEMPC(J),DU(J),DV(J)
      READ(1,108)ABICE
      READ(1,110)NCA
      DO 885 J=1,20
  885 TEMPCO(J)=TEMPC(J)
  101 FORMAT(6F10.3)
  102 FORMAT(10F7.0)
  103 FORMAT(16F5.0)
  104 FORMAT(20F4.0)
  105 FORMAT(I2,F7.0,F8.2,F7.1,E12.4,F8.2)
  106 FORMAT(2I5)
```

```
  107 FORMAT(10E7.3)
  108 FORMAT(F6.5)
  109 FORMAT(8F7.2)
  110 FORMAT(I2)
      DO 240 J=1,NZ
 2002 WRITE(3,2003)J,Z(J),P(J),TEMPC(J),DU(J),DV(J)
 2003 FORMAT(I3,F8.1,F8.2,F7.1,E12.4,F8.2)
      DU(J)=DU(J)*((P(J)+P(J+1))/2026.)*SQRT(586./(TEMPC(J)+
     1 TEMPC(J+1) + 546.))
      DV(J)=DV(J)*((P(J)+P(J+1))/2026.)*SQRT(586./(TEMPC(J)+
     1 TEMPC(J+1) + 546.))
  240 CONTINUE
C     B     B     B     B     B     B     B     B     B     B
      DO 990 N=1,7
      DO 990 NA=1,3
      ABSICE=ABICE(NA)
      NC=NCA(N)
C     B     B     B     B     B     B     B     B     B     B
      WRITE(3,2002)ABSICE,NC,Z(NC),ID
C
C K DO LOOP VARIES HEIGHT AT WHICH FLUX IS COMPUTED.
C
      DO 901 K=1,NZ
      FLUX=0
      KMINU1=K-1
C
C J DO LOOP COMPUTES INTEGRAL.  U AND V COMPUTED FROM Z(K) TO
C HALFWAY BETWEEN Z(J) AND Z(J+1).
C
      DO 902 J=1,NZ
      JPLUS1=J+1
      JMINU1=J-1
C
C COMPUTATION OF AMOUNT OF PATH IN CRYSTAL LAYER,
C COMPUTATION OF WATER VAPOR AND CO2 CONTENTS.
C
      IF(J-K)204,203,205
C
C EMERGENCY STOP IF A SUPPOSEDLY IMPOSSIBLE BRANCH OCCURS
C
  900 WRITE(3,999)
      STOP
  203 U=.5*DU(J)
      V=.5*DV(J)
      IF(K+J-2*NC)401,402,402
  401 DELZ=.5*(Z(J+1)-Z(J))
      GO TO 211
  402 DELZ=0
      GO TO 211
  204 IF(J+1-K)206,203,900
```

```
  206 U=.5*DU(J)
      V=.5*DV(J)
      DO 207 M=JPLUS1,KMINU1
      U=U+DU(M)
  207 V=V+DV(M)
      IF(K-NC)403,403,404
  403 DELZ=Z(K)-Z(J+1)+.5*(Z(J+1)-Z(J))
      GO TO 211
  404 IF(J+1-NC)407,407,408
  407 DELZ=Z(NC)-Z(J+1)+.5*(Z(J+1)-Z(J))
      GO TO 211
  408 DELZ=0
      GO TO 211
  205 U=.5*DU(J)
      V=.5*DV(J)
      DO 209 M=K,JMINU1
      U=U+DU(M)
  209 V=V+DV(M)
      IF(J-NC)405,406,406
  405 DELZ=Z(J)-Z(K)+.5*(Z(J+1)-Z(J))
      GO TO 211
  406 IF(K-NC)409,408,408
  409 DELZ=Z(NC)-Z(K)
      GO TO 211
C
C     READY TO INTERPOLATE
C FIRST TEST THAT U IS NOT BELOW THE TABULATED RANGE.  IF IT IS,
C RH2O IS ZERO, AND DRCO2 IS SIMPLY R FOR CO2, WHICH ANY SMALL
C VALUE OF U WILL GIVE.
C
  211 IU=1
      IV=1
      IT=1
      XLOGU=ALOG10(U)
      IF(XLOGU)611,611,600
  611 CONTINUE
      IF(TLOGU(1)-XLOGU)212,250,501
  250 IU=2
      GO TO 215
  501 XLOGV=ALOG10(V)
      IF(TLOGV(IV)-XLOGV)502,502,503
  502 RH2O=0
      IU=2
      GO TO 241
  503 RH2O=0
      DRH2O=0
      IU=2
      IV=2
      GO TO 504
C
```

```
C NOW LOCATE TLOGU.
C
  212 IF(TLOGU(IU)-XLOGU)213,215,215
  213 IU=IU+1
      GO TO 212
C
C NEXT LOCATE TTEMPC.
C
  215 XIT=IT
      TTEMPC=-70.+XIT*10.
      IF (60.+.5*(TEMPC(J+1)+TEMPC(J)))252,252,253
  252 IT=2
      GO TO 226
  253 CONTINUE
      IF(TTEMPC-(TEMPC(J+1)+TEMPC(J))/2.)224,226,226
  224 IT=IT+1
      GO TO 215
C
C PORU, PORT AND PORV ARE PORPORTIONAL PARTS FOR LOG U, T, AND
C LOG V.
C
  226 PORU=(TLOGU(IU)-XLOGU)/(TLOGU(IU)-TLOGU(IU-1))
      PORT=.1*TTEMPC-.05*(TEMPC(J+1)+TEMPC(J))
C
C INTERPOLATION FORMULA FOR RH2O
C
      RH2O=TRH2O(IU,IT)*(1.-PORU)*(1.-PORT)+TRH2O(IU,IT-1)*
     1 (PORT*(1.-PORU))
     2   +TRH2O(IU-1,IT)*(PORU*(1.-PORT))+TRH2O(IU-1,IT-1)*
     3 PORU*PORT
  241 XLOGV=ALOG10(V)
C
C  TEST THAT V IS IN THE TABULATED RANGE.
C
      IF(XLOGV-3)610,610,600
  600 WRITE(3,601)
      STOP
  610 CONTINUE
      IF(TLOGV(1)-XLOGV)231,251,505
  251 IV=2
      GO TO 234
C
C IF V IS BELOW RANGE, DRH2O =ZERO.
C
  505 DRH2O=0
      IV=2
      GO TO 504
C
C IF V IS IN RANGE, LOCATE TLOGV.
C
```

```
  231 IF(TLOGV(IV)-XLOGV)232,234,234
  232 IV=IV+1
      GO TO 231
  234 PORV=(TLOGV(IV)-XLOGV)/(TLOGV(IV)-TLOGV(IV-1))
      PORU=(TLOGU(IU)-XLOGU)/(TLOGU(IU)-TLOGU(IU-1))
C
C INTERPOLATION FORMULA FOR DRH2O
C
      DRH2O=TDRH2O(IU,IV)*(1.-PORU)*(1.-PORV)+TDRH2O(IU,IV-1)
     1 *PORV*(1.-PORU)
     2    +TDRH2O(IU-1,IV)*PORU*(1.-PORV)+TDRH2O(IU-1,IV-1)
     3  *PORU*PORV
  504 TEMPCJ=(TEMPC(J+1)+TEMPC(J))*.5
      DT=TEMPC(J+1)-TEMPC(J)
      TAUICE = EXP(-ABSICE*DELZ)
      TK = TEMPCJ + 273.
      TD40 = TEMPCJ + 40.
      IF (XLOGV) 5000,5000,5001
 5000 CCO2T = 1.+.011*TD40
      GO TO 5003
 5001 CCO2T = 1. + .012 * TD40 + .00001 * TD40*TD40
 5003 CONTINUE
      IF(RH2O)3000,3005,3005
 3000 RH2O=0
 3005 IF(DRH2O)3002,3003,3003
 3002 DRH2O=0
 3003 CONTINUE
C
C ONE ELEMENT OF INTEGRAL
C
      DFLUX = .5* (RH2O+CCO2T*DRH2O -4.6784E-7*TK*TK*TK)*DT*T
     1        TAUICE
C
C SUMMATION AND STORAGE OF THE INTEGRAL OVER Z.
C
  902 FLUX=FLUX+DFLUX
      PORU=(TLOGU(IU)-XLOGU)/(TLOGU(IU)-TLOGU(IU-1))
      PORV=(TLOGV(IV)-XLOGV)/(TLOGV(IV)-TLOGV(IV-1))
      IF(PORU-1.)701,701,700
  700 PORU=1.
  701 CONTINUE
      IF(PORV-1.)703,703,702
  702 PORV=1.
  703 CONTINUE
      X1 = TRDTCO(IU,IV)
      X2 = TRDTCO(IU-1,IV)
      X3 = TRDTCO(IU,IV-1)
      X4 = TRDTCO(IU-1,IV-1)
      RDTCO = X1*(1.-PORU)*(1.-PORV) +X2*PORU*(1.-PORV)+X3*PORV*
     1 (1.-PORU)+X4*PORU*PORV
```

```
      RDT = TRDT(IU)*(1.-PORU) +TRDT(IU-1)*PORU
      FLUX = FLUX - TAUICE*(RDT +RDTCO-240.7434)*.5
      FLUXZ(K)=FLUX
      IF(K-1)907,907,300
  907 WRITE(3,622)
      GO TO 901
  300 T=(TEMPC(K)+TEMPC(K-1))*.5+273.
      PR=(P(K)+P(K-1))*.5
C
C IF LAYER FOR WHICH COOLING RATE IS DESIRED IS IN THE
C CRYSTAL LAYER, WE MUST INCLUDE LATENT HEAT TERM.
C
      IF(K-NC)305,305,306
  306 XLH=0
      GO TO 905
  305 L=1
  301 XL=L
      TT=222.+XL
      IF(TT-T)302,304,304
  302 L=L+1
      GO TO 301
  304 XLH=XLAHT(L)-(TT-T)*(XLAHT(L)-XLAHT(L-1))
C
C COMPUTE COOLING RATE, STORE
C
  905 COOL(K-1)=-(FLUXZ(K)-FLUXZ(K-1))/((Z(K)-Z(K-1))*((8.35E-3)
     1 *(PR/T)+XLH))
      WRITE(3,621)COOL(K-1)
  901 WRITE(3,620)FLUX,Z(K)
      GO TO 910
C
C WRITE OUT RESULTS
C
  910 WRITE(3,1000)ID,ABSICE,Z(NC)
      WRITE(2,1000)ID,ABSICE,Z(NC)
      NZMIN=NZ-1
      DO 920 K=1,NZMIN
      WRITE(2,1001)Z(K),TEMPC(K),FLUXZ(K),COOL(K)
  920 WRITE(3,1001)Z(K),TEMPC(K),FLUXZ(K),COOL(K)
      WRITE(3,1001)Z(NZ),TEMPC(NZ),FLUXZ(NZ)
      WRITE(2,1001)Z(NZ),TEMPC(NZ),FLUXZ(NZ)
      K=2
 1104 IF((FLUXZ(K)-.5*FLUXZ(1))/(P(1)-P(K))-(FLUXZ(NC)-FLUXZ(K))
     1(P(K)-P(NC)))1100,1102,1101
 1101 K=K+1
      IF(K+1-NC)1105,1105,1106
 1105 GO TO 1104
 1106 WRITE(3,1112)
      WRITE(2,1112)
      GO TO 1125
```

```
 1100 WRITE(3,1110)Z(K),Z(K-1)
      WRITE(2,1110)Z(K),Z(K-1)
      GO TO 1125
 1102 WRITE(3,1111)Z(K)
      WRITE(2,1111)Z(K)
 1125 CONTINUE
  990 CONTINUE
  601 FORMAT('OU OR V ABOVE TABLE RANGE')
  620 FORMAT('0',E15.8,T25,F8.1)
  621 FORMAT(T40,E15.8)
  622 FORMAT(' NET FLUX',T25,'HEIGHT',T40,'HEATING RATE')
  999 FORMAT('0ERROR IN IF DIRECTING')
C     C     C     C     C     C     C     C     C     C
 1000 FORMAT('1'//////37X,'ICE CRYSTAL DISPLAY'//16X,'SOUNDING',
     1I2,',  ICE ABSORPTION ',F8.5,'/M,  DISPLAY DEPTH',F6.0,
     1' M',//16X,
     2'HEIGHT     TEMPERATURE        FLUX          ',
     2'MEAN HEATING RATE,'/
     318X,' (M)          (DEG C)   (CAL/SQ CM/12 HR)     ',
     3 'LAYER ABOVE Z',/
     462X,'(DEG C/12 HR)'/)
C     C     C     C     C     C     C     C     C     C
 1001 FORMAT(' ',15X,F7.1,8X,F5.1,T46,F6.1,T63,F8.3)
 1020 FORMAT(' ',6(E15.8,5X))
 1021 FORMAT(' END OF J LOOP',T20,2(E15.8,5X))
 1110 FORMAT(' ',T20,'NEUTRAL HEIGHT BETWEEN ',F5.0,' M AND ',
     1 F5.0,'M.  '   )
 1111 FORMAT(' ',T20,'NEUTRAL HEIGHT ABOUT ',F5.0,' M.')
C     D     D     D     D     D     D     D     D     D     D
 1112 FORMAT(' ',T20,'NEUTRAL HEIGHT AT OR ABOVE TOP OF DISPLAY.
     1)
C     D     D     D     D     D     D     D     D     D     D
 2004 FORMAT(F7.5,/,I3)
 2005 FORMAT('1',F10.5,/,I10,/,F11.5,/,I10)
      CALL EXIT
      END
```

```
C      2.  MODIFICATION OF GRAY-CRYSTAL PROGRAM TO ACCEPT
C                          ICE FOG DATA

C      A     A     A     A     A     A     A     A     A     A
       DIMENSION NCA(5),ABICE(10)
C      A     A     A     A     A     A     A     A     A     A

C      B     B     B     B     B     B     B     B     B     B
       IF(ID-4)855,855,856
  855  RH=.8
       GO TO 857
  856  RH=.5
  857  DO 990 N=1,5
       NC=NCA(N)
       IF(Z(NC)-100.)850,864,864
  850  NCP=NCA(N-1)-1
       DO 852 J=NC,NCP
       DU(J)=DU(J)*RH
  852  DV(J)=DV(J)*RH
       IF(Z(NC))863,863,864
  863  LIM1=1
       LIM2=1
       GO TO 865
  864  IF(Z(NC)-20.)860,861,862
  860  LIM1=1
       LIM2=4
       GO TO 865
  861  LIM1=1
       LIM2=10
       GO TO 865
  862  LIM1=5
       LIM2=10
  865  DO 990 NA=LIM1,LIM2
       ABSICE=1.6*ABICE(NA)
C      B     B     B     B     B     B     B     B     B     B

C      C     C     C     C     C     C     C     C     C     C
 1000  FORMAT('1',//////43X,'ICE FOG'//16X,'SOUNDING',I2,
      1',  ICE ABSORPTION ',F8.5,'/M,  FOG DEPTH',F6.0,' M',//16X
      2'HEIGHT     TEMPERATURE        FLUX              '
      2'MEAN HEATING RATE,'/
      318X,' (M)          (DEG C)   (CAL/SQ CM/12 HR)     LAYER AB
      318X,' (M)          (DEG C)   (CAL/SQ CM/12 HR)     '
      3 'LAYER ABOVE Z',/
      462X,'(DEG C/12 HR)'/)
C      C     C     C     C     C     C     C     C     C     C

C      D     D     D     D     D     D     D     D     D     D
 1112  FORMAT(' ',T20,'NEUTRAL HEIGHT AT OR ABOVE TOP OF FOG.')
C      D     D     D     D     D     D     D     D     D     D
```

```
C              3.SCATTERING PROGRAM
C
C      PROGRAM COOL   FORTRAN IV   IBM 360-40 64K
       COMMON TX(154),T2EI3(154),TAB42(11,8),
      1       TAB41(11,6),TLH20(63),TLCO2(63),
      2       Z(30),P(30),T(30),WV(30),V(30),
      3       ENA,ENB,NHT,AKA(63),AKB(63),
      4       BETAA(63),BETAB(63),SQP,NU,
      5              WAVENO(63),K,JMAX,BLAK(63,30)
C
       REAL DNU(63),WV100(30),STF(30)
C
       DO 33 I=1,30
       WV(I)=0.
   33  V(I)=0.
C
C      READ TABLES FOR X AND 2EI3(X)
C      TX(154),T2EI3(154)
       READ(1,301)(TX(I),T2EI3(I),I=1,154)
  301  FORMAT(5(F6.0,F10.0))
C
C
C      READ TABLE IV-2, TAUCO2 FOR CARBON DIOXIDE
C      TAB42(11,8)
C
       READ(1,303)((TAB42(I,J),J=1,8),I=1,11)
  303  FORMAT(2X,2P8F6.2)
C
C
C      READ TABLE IV-1, TAUM20 FOR WATER VAPOR
C      TAB41(11,6)
C
       READ(1,305)((TAB41(I,J),J=1,6),I=1,11)
  305  FORMAT(2X,2P6F6.2)
C
C
C      READ WAVENO DATA FOR 63 WAVE NUMBERS
C
       DO 30 I=1,63
   30  READ(1,307)NU,WAVENO(NU),DNU(NU),TLH20(NU),TLCO2(NU)
  307  FORMAT(I3,2F5.0,2F9.2)
C
C      READ ABSORPTION AND BACKSCATTERING COEFFICIENTS AND
C      REDUCE BY 10E6
       DO 32 I=1,63
   32  READ(1,309)NU,AKA(NU),AKB(NU),BETAA(NU),BETAB(NU)
  309  FORMAT(I3,6P4F7.3)
C
C
C      READ SOUNDING DATA
```

```
C          CC      FORMAT  VARIABLE  DESCRIPTION
C         1- 2     I2        J       INDEX
C         3- 8     F7.0      Z(J)    HEIGHT
C        10-17     F8.2      P(J)    PRESSURE
C        18-24     F7.1      T(J)    TEMPERATURE (CENTIGRADE)
C        25-36     E12.4     WV100(J) WATER VAPOR (100 PERCENT)
C        37-44     F8.2      V(J)    CARBON DIOXIDE
C        45-56     E12.4     WV(J)   WATER VAPOR (80 PERCENT)
C
   11 READ(1,101,END=10) J,Z(J),P(J),T(J),WV100(J),V(J),WV(J)
  101 FORMAT(I2,F7.0,F8.2,F7.1,E12.4,F8.2,E12.4)
      GO TO 11
C     READ NA AND NB AND INDEX OF LAST HT FOR WHICH THEY ARE
C     VALID (NHT)
   10 READ(1,102)ENA,ENB,NHT
  102 FORMAT(2F10.0,7X,I3)
      WRITE(2,902)ENA,ENB,NHT
  902 FORMAT(2F5.0,I3)
      JMAX1=J
      JMAX=J-1
C     JS IS TOP OF SCATTERING LAYER
      JS=NHT+1
C
      DO 45 I=1,JMAX1
      IF(WV(I) .EQ. 0.)WV(I)=WV100(I)
   45 CONTINUE
C     USE 100 PERCENT WATER VAPOR FOR HTS BELOW NHT
C     DO 13 I=1,NHT
C  13 WV(I)=WV100(I)
C     PRINT OUT SOUNDING DATA
      DO 49 I=1,JMAX1
   49 WRITE(3,103)I,Z(I),P(I),T(I),WV(I),V(I)
  103 FORMAT(I3,F7.0,F8.2,F7.1,E12.4,F8.2)
      WRITE(3,901)ENA,ENB,NHT
  901 FORMAT('ONA=',F5.0,'   NB=',F5.0,'   NHT=',I4)
C
      DO 31 I=1,JMAX
      PFACT=(P(I) + P(I+1))/2026.
      WV(I)=WV(I) * PFACT
   31 V(I)=V(I) * PFACT
C
C     COMPUTE BLACKBODY FUNCTION
      DO 46 NU=1,63
      T(JMAX1)=-273.
      IF(NU .EQ. 45 .OR. NU .EQ. 46)T(JMAX1)=-40.
      WAVNU=WAVENO(NU)
      DO 46 I=1,JMAX1
      TK=T(I)+273.
   46 BLAK(NU,I)=BLACKB(WAVNU,TK)
C
```

```
      DO 21 K=1,JMAX
C     WRITE COLUMN HEADING-- -- -- TEMPORARY
      WRITE(3,203)K
  203 FORMAT('1',16X,'PARTIAL VALUES FOR Z=Z(',I2,')'/
     A'0',1X,'I  WAVENO(I)',
     1  '       FLUX       FLUX DIVERGENCE  FLUX CONTRI-',
     B'  FLUX DIV. CONT.    DELFDZ(K-1)'/48X,'BUTION'//)
C
C     SET TOTALS AT ZERO
      TF=0.
      TDFDZ=0.
      TFDNU=0.
      TDFDN=0.
      TDEL=0.
C
      DO 12 NU=1,63
      T(JMAX1)=-273.
      IF(NU .EQ. 45 .OR. NU .EQ. 46)T(JMAX1)=-40.
C
C     COMPUTE S(NU)
C     SET SQP=SQRT((1.+S)/(1.-S)) = 1 FOR COMPUTING S
      SQP= 1.
C     IF ICODE=0 TAU IS OUTSIDE THE INTEGRAL
C     IF ICODE=1 TAU IS INSIDE THE INTEGRAL
      ICODE=0
C     COMPUTE TAU AT THE TOP OF SCATTERING LAYER  (TAUSS)
      IF(JS-K)36,37,36
   37 TAUSS=1.
      GO TO 38
   36 TAUSS=TAUM20(  JS,ICODE)*TAUCO2(  JS,ICODE)*
     1       TAUICE(JS,ICODE)
C     COMPUTE TAU AT GROUND LEVEL   (TAUSG)
   38 IF(K-1)39,34,39
   34 TAUSG=1.
      GO TO 35
   39 TAUSG=TAUM20(  1,ICODE)*TAUCO2(  1,ICODE)*
     1       TAUICE(1,ICODE)
   35 A=(BETAA(NU) * ENA + BETAB(NU) * ENB) * Z(JS)
C
      IF(TAUSG .NE. 0. .AND. TAUSS .NE. 0. .AND. JS .NE. 1)
     1 GO TO 50
      S=0.
      GO TO 44
   50 IF(K-JS)41,41,43
   41 S=A/(A - ALOG(TAUSG * TAUSS))
      GO TO 44
C
   43 S=A/(A - ALOG(TAUSG/TAUSS))
C
C     COMPUTE REOCCURING FACTORS CONTAINING S
```

```
C
   44 SQP=SQRT((1.+S)/(1.-S))
      SQN1=1.-SQP
      SQP1=1.+SQP
      SQN=SQRT((1.-S)/(1.+S))
      S1=1.-S
      S2=SQRT(1.-S*S)
      S3=1.-S2
      S4=1.+S2
      TG2=TAUSG * TAUSG
      TS2 = TAUSS * TAUSS
      TGTS2 = TG2 * TS2
C
C     COMPUTE TAU AT THE TOP OF SCATTERING LAYER
   16 IF(JS-K)136,137,136
  137 TAUSS=1.
      GO TO 138
  136 TAUSS=TAUM20(  JS,ICODE)*TAUCO2(  JS,ICODE)*
     1      TAUICE(JS,ICODE)
C     COMPUTE TAU AT GROUND LEVEL
  138 IF(K-1)133,134,133
  134 TAUSG=1.
      GO TO 135
  133 TAUSG=TAUM20(  1,ICODE)*TAUCO2(  1,ICODE)*TAUICE(  1,ICODE
  135 CONTINUE
C
C
C     CHECKING K - - IF K .GT. JS COMPUTE FC
C                  IF K .LT. JS COMPUTE FS
C
      IF(K .GE. JS ) GO TO 2
C
C     K IS LESS THAN JS.  COMPUTE FS
C
C
      CIE1=CI(K,JS,1)
      IF(TAUSG .EQ. 0.) GO TO 67
      CID1=CI(1,K,-1)
   67 CID2=CI(1,K,1)
      CID3=CI(JS,JMAX1,1)
      IF(TAUSS .EQ. 0.) GO TO 68
      CID4=CI(K,JS,-1)
C
   68 CONTINUE
C
C     COMPUTE FS
      SSQN=S*SQN
      S1SQN=S1 + SQN
      S1MSQN=S1 - SQN
      ADP=1. /(S4 - S3 * TGTS2)
```

```
C
      IF(TAUSG)61,61,62
   61 FS1=0.
      FZ1=0.
      GO TO 63
C
   62 FS1=TG2 *(SSQN - S1MSQN * TS2) * CID1
      FZ1=TG2*(S - S3 * TS2) * CID1
C
   63 FS2 = (S1SQN + SSQN * TS2) * CID2
      FZ2 = (S4 - S * TS2) * CID2
C
      IF(TAUSS)64,64,65
   64 FS3=0.
      FZ3=0.
      GO TO 66
C
   65 FS3=TS2 *(SSQN - S1MSQN * TG2) * CID4
      FZ3 = TS2 * (S - S3 * TG2) * CID4
C
   66 FS4 = (S1SQN + SSQN * TG2) * CIE1
      FZ4 = (S4 - S * TG2) * CIE1
C
      FS5 =(S1 + S2 -(S1 - S2) * TG2) * CID3
      FZ5=(S + S4 -(S + S3)*TG2) * CID3
      F=ADP *(-FS1-FS2-FS3-FS4-FS5)
      DFDZ=ADP * CAPA(JS) *S1*(FZ1 + FZ2 - FZ3 - FZ4 - FZ5)
C
      GO TO 3
C
C * * * * * * * * * * * * * * * * * * * * * * * * * * * * * * * * * * * *
C
C     COMPUTE FC AND DF/DZ
C
    2 IF(TAUSS .EQ. 0.) GO TO 70
      CIFC1=CI(JS,K,-1)
   70 CIFC2 = CI(K,JMAX1,1)
      CIFC4=CI(1,JS,1)
      IF(TAUSG .EQ.0.) GO TO 69
      CIFC3=CI(1,JS,-1)
   69 CIFC5=CI(JS,K,1)
      IF(TG2) 51,51,52
   51 APRIME= 1./S4
      GO TO 53
   52 APRIME= 1./(S4-(S3*TG2/TS2))
   53 C=APRIME*S*(TG2-TS2)
      IF(TAUSG) 54,54,55
   54 FC1=0.
      GO TO 56
   55 FC1=APRIME*TG2*S1*SQN1*CIFC3
```

```
   56 FC2=APRIME*S1*SQP1*CIFC4
      IF(TAUSS) 57,57,58
   57 FC3=0.
      GO TO 59
   58 FC3=C*CIFC1
   59 F=FC1-FC2-FC3-CIFC5-(C+1.)*CIFC2
      DFDZ=CAPA(JS)*(-FC1+FC2+FC3+CIFC5-(1.-C)*CIFC2)
C
C* * * * * * * * * * * * * * * * * * * * * * * * * * * * * * * * * * * *
C
    3 FDNU = F * DNU(NU)
      DFDZDN = DFDZ * DNU(NU)
      IF(K - 1)71,71,72
   71 DELFDZ=0.
      GO TO  73
   72 DELFDZ=(F-OLDF)/(Z(K) - Z(K-1))
   73 OLDF=F
C
      WRITE(3,201)NU,WAVENO(NU),F,DFDZ,FDNU,DFDZDN,DELFDZ
  201 FORMAT( 1X,I2,F8.0,4X,E14.7,2X,E14.7,3X,E14.7,2X,E14.7,2X,
     1        E14.7)
C
C     SUM ABOVE QUANTITIES FOR 63 WAVENUMBERS
C
      TF=F + TF
      TDFDZ= TDFDZ + DFDZ
      TFDNU= TFDNU + FDNU
   12 TDFDN = TDFDN + DFDZDN
C     ADD HEAT TERMS
      IF(K .GT. 1) GO TO 47
      FLUX1=TFDNU
      TDEL=0.
      OF=TFDNU
      HEATF=0.
      CONDH=0.
      GO TO 48
C
   47 TP=(T(K) + T(K-1)) *.5 + 273.
      PR=(P(K) + P(K-1)) * .5
      DTEMP=8.35E-3 * PR/TP
      HEATF=-TDFDZ/DTEMP
      DZKM1=Z(K)-Z(K-1)
      IF(K .LT. JMAX)GO TO 60
      CONDH=0.
      GO TO 48
   60 CONDH= FLUX1 * Z(2)/( T(2)-T(1) + 273.)
     1 *(DZKM1             * (T(K+1) + 273.) + (Z(K+1) - Z(K)) *
     2 (T(K-1) + 273.) - (Z(K+1) - Z(K-1)) * (T(K) + 273.)) /
     3 ((Z(K+1) - Z(K)) * DZKM1           * (Z(K+1) - Z(K-1)))
      TDEL=(TFDNU - OF)/DZKM1
```

```
      OF=TFDNU
C     PRINT TOTAL OF K FOR 63 WAVENO.
   48 WRITE(3,202) TF,TDFDZ,TFDNU,TDFDN,TDEL,HEATF,CONDH
  202 FORMAT('0',    'TOTAL',9X, E14.7,2X,   E14.7,3X,E14.7,2X,
     1 E14.7,2X,E14.7,2X,E14.7,2X,E14.7)
      WRITE(2,900)K,TF,TFDNU,TDFDN,TDEL
  900 FORMAT(I2,4E14.7)
   21 CONTINUE
C
      CALL EXIT
      END
```

```
      FUNCTION TAUICE(   JS,ICODE)
C
C     TAUICE= 2EI3(X) WHERE
C     X = SUM OF (NA(J)*KA(NU) + NB(J) * KB(NU)) * (Z(J+1)-Z(J))
C     AND 2EI3 IS PICKED FROM A TABLE WHICH HAS BEEN READ IN
C
      COMMON TX(154),T2EI3(154),TAB42(11,8),
     1       TAB41(11,6),TLH20(63),TLCO2(63),
     2       Z(30),P(30),T(30),WV(30),V(30),
     3       ENA,ENB,NHT,AKA(63),AKB(63),
     4       BETAA(63),BETAB(63),SQ ,NU,
     5                 WAVENO(63),K,JMAX
      REAL XS(30)
      DATA XS/30*0.0/
C
      DO 1 I=1,NHT
    1 XS(I)=(ENA    * AKA(NU) + ENB    * AKB(NU))
     1      * (Z(I+1) - Z(I))
C
      CALL SUM(XS,JS,K ,NHT,SQ,ICODE,X)
C
C     X HAS NOW BEEN COMPUTED.  LOOK FOR CLOSEST X IN TX TABLE
C
      IF(X .GT. 0.) GO TO 5
      TAUICE=1.
      RETURN
    5 DO 11 J=1,153
C
      IF(X .GE. .001) GO TO 2
C     EXTRAPOLATE VALUE OF 2EI3 IF X .LT. .001
      FACTOR=(TX(1)-X)/(TX(2)-TX(1))
      TAUICE=T2EI3(1) + FACTOR * (T2EI3(1)- T2EI3(2))
      RETURN
    2 IF(X .GE. TX(J) .AND. X .LT. TX(J+1)) GO TO 3
   11 CONTINUE
C
C     EXTRAPOLATE FOR VALUES OF X .GT. 10
      FACTOR=(X - TX(154))/(TX(154) - TX(153))
      TAUICE=T2EI3(154) -ABS(FACTOR *(T2EI3(154) - T2EI3(153)))
      IF(TAUICE .LT. 0.) TAUICE=0.
      RETURN
C
C     INTERPOLATE FOR EI3 VALUE
    3 FACTOR=(X - TX(J))/(TX(J+1) - TX(J))
      TAUICE=T2EI3(J) - (T2EI3(J) - T2EI3(J+1)) * FACTOR
    4 RETURN
      END
```

```
      FUNCTION BLACKB(WAVENO,T)
C
C     BLACKBODY FUNCTION
      IF(T .EQ. 0.) GO TO 1
C
      BLACKB= 3.86E-8 * WAVENO**3/(EXP(1.4389 * WAVENO/T)-1.)
      RETURN
    1 BLACKB=0.
      RETURN
      END
```

```
      SUBROUTINE SUM(ARRAY,J,K,NHT,SQ,ICODE,U)
C
      REAL ARRAY(30)
      U=0.
      IF(ICODE .EQ. 1) GO TO 5
C
      IF(J - K)2,12,3
    3 I1=K
      I2=J-1
      GO TO 4
C
    2 I1=J
      I2=K-1
C
    4 DO 1 J1=I1,I2
      SQP=1.
      IF(J1 .LE. NHT)SQP=SQ
    1 U=U + ARRAY(J1)* SQP
   12 RETURN
C
C
    5 IF(J - K)6,7,8
    8 I1=K
      I2=J - 1
      GO TO 9
C
    6 IF(J .EQ. K-1)GO TO 7
C
      I1= J + 1
      I2=K - 1
    9 U=0.
      DO 11 J1=I1,I2
      SQP=1.
      IF(J1 .LE. NHT)SQP=SQ
   11 U=U+ARRAY(J1) *SQP
    7 SQP=1.
      IF(J .LE. NHT)SQP=SQ
      U=U + .5*ARRAY(J) * SQP
      RETURN
      END
```

```
      FUNCTION TAUM20(   J,ICODE)
C
C     FUNCTION TAUM20 LOOKS UP VALUE IN TABLE 4-1
C     TAUM20=ALOG10(U) + TLH20(NU)  WHERE U IS THE WATER VAPOR S
C     AND TLH20 IS READ IN
C
      COMMON TX(154),T2EI3(154),TAB42(11,8),
     1       TAB41(11,6),TLH20(63),TLCO2(63),
     2       Z(30),P(30),T(30),WV(30),V(30),
     3       ENA,ENB,NHT,AKA(63),AKB(63),
     4       BETAA(63),BETAB(63),SQP,NU,
     5                  WAVENO(63),K,JMAX
      REAL X(30)
      DO 20 I=1,30
   20 X(I)=WV(I)
      SQ=SQP
      CALL SUM(X,J ,K,NHT,SQ,ICODE,U)
C
      TAUM20=ALOG10(U) + TLH20(NU)  -5.0
C
C     IF TAUM20 .LT. -3.7 - 5. EXTRAPOLATE FROM TABLE
C
      IF(TAUM20 + 8.7)6,6,7
    6 FACTOR=TAUM20 + 8.7
      TAUM20 = TAB41(4,1) +(TAB41(5,1)-TAB41(4,1)) * FACTOR
      IF(TAUM20 .GT. 1.)TAUM20=1.
      RETURN
C
    7 IF(TAUM20 .LT.-3.8) GO TO 5
      TAUM20=0.
      RETURN
C
C     SEPARATE CHARACTERISTIC AND MANTISSA OF
C     ALOG10(U) + TLH20(NU)
C
    5 ICHAR=IFIX(TAUM20)
      TMAN=ABS(TAUM20 - FLOAT(ICHAR))
C
C     TABLE 4-1 EXTENDS FROM -3.7 TO 1.2
      L=-8
C
C     FIND APPROPRIATE COLUMN IN TABLE
C
      DO 2 IC=1,6
C
      IF(ICHAR .EQ. L) GO TO 1
    2 L=L+1
C
C     FIND APPROPRIATE ROWS IN TABLE
    1 B =1.0
```

```
C
      DO 3 IM=1,10
      H=B-.1
      IF(TMAN .LE. B .AND. TMAN .GE. H) GO TO 4
C
    3 B=B-.1
C
C     INTERPOLATE BETWEEN TABLE VALUES
    4 FACTOR=(B-TMAN) * 10.
C
      TAUM20 = TAB41(IM,IC) - ABS((TAB41(IM+1,IC)
     1- TAB41(IM,IC)) * FACTOR)
C
    8 RETURN
      END
```

```
      FUNCTION TAUCO2(   J,ICODE)
C
C     FUNCTION TAUCO2 LOOKS UP VALUE FROM TABLE 4-2
C
      COMMON TX(154),T2EI3(154),TAB42(11,8),
     1       TAB41(11,6),TLH20(63),TLCO2(63),
     2       Z(30),P(30),T(30),WV(30),V(30),
     3       ENA,ENB,NHT,AKA(63),AKB(63),
     4       BETAA(63),BETAB(63),SQP,NU,
     5                 WAVENO(63),K,JMAX
      REAL X(30)
C
      DO 20 I=1,30
   20 X(I)=V(I)
      SQ=SQP
      CALL SUM(X,J ,K,NHT,SQ,ICODE,SUMV)
C
      TAUCO2=ALOG10(SUMV) + TLCO2(NU)   -5.0
C
C     IF TAUCO2 .LT. -5.2 - 5. EXTRAPOLATE FROM TABLE
      IF(TAUCO2 +10.2) 6,6,7
    6 FACTOR=TAUCO2 +10.2
      TAUCO2=TAB42(9,1) + (TAB42(10,1) - TAB42(9,1)) * FACTOR
      IF(TAUCO2 .GT. 1.) TAUCO2=1.
      RETURN
C
    7 IF(TAUCO2 .LE. -3.) GO TO 5
      TAUCO2=0.
      RETURN
C * * * * * * * * * * * * * * * * * * * * * * * * * * * * * * * * * * *
    5 ICHAR=IFIX(TAUCO2)
      TMAN=ABS(TAUCO2 - FLOAT(ICHAR))
C
C     TABLE 4-2 EXTENDS FROM -5.2 TO 2.0
      L=-10
C
C     FIND APPROPRIATE COLUMN IN TABLE
      DO 2 IC=1,8
      IF(ICHAR .EQ. L) GO TO 1
    2 L=L+1
C
C     FIND APPROPRIATE ROWS IN TABLE
    1 B=1.0
C
      DO 3 IM=1,10
      H=B-.1
      IF(TMAN .LE. B .AND. TMAN .GE. H)GO TO 4
    3 B=B-.1
C
C     INTERPOLATE BETWEEN TABLE VALUES
```

```
     4 FACTOR=(B - TMAN) * 10.
C
       TAUCO2 = TAB42(IM,IC) -ABS((TAB42(IM+1,IC) - TAB42(IM,IC))
      1 * FACTOR)
     8 RETURN
       END
```

```
      FUNCTION CAPA(JS)
      COMMON TX(154),T2EI3(154),TAB42(11,8),
     1       TAB41(11,6),TLH20(63),TLC02(63),
     2       Z(30),P(30),T(30),WV(30),V(30),
     3       ENA,ENB,NHT,AKA(63),AKB(63),
     4       BETAA(63),BETAB(63),SQ ,NU,
     5                  WAVENO(63),K,JMAX
C     SET KAPPA=0 WHEN Z=0
      IF(K .GT. 1) GO TO 2
      CAPA=0.
      RETURN
C
C     NA AND NB =0 WHEN K GE JS
    2 IF(K .GT. JS) GO TO 1
C
      CAPA=34. * 10.**TLH20(NU) * (WV(K-1) + WV(K))/
     1    (Z(K+1) - Z(K-1)) + 3.3
     A    * 10.**TLC02(NU) * P(K)/(T(K) + 273.)
     2     + 2. * (AKA(NU) * ENA + AKB(NU) * ENB)
     3     + BETAA(NU) * ENA + BETAB(NU) * ENB
C
      RETURN
    1 CAPA=34. * 10.**TLH20(NU) * (WV(K-1) + WV(K))/
     1      (Z(K+1)- Z(K-1)) + 3.3
     2      * 10.**TLC02(NU) * P(K)/(T(K) + 273.)
C
    3 RETURN
      END
```

```
      FUNCTION CI(J1,J2,L)
C
C     THIS FUNCTION COMPUTES AN INTEGRAL OF THE FORM F(Y)**L
C     WHERE L= +1 OR -1
C
      COMMON TX(154),T2EI3(154),TAB42(11,8),
     1       TAB41(11,6),TLH20(63),TLCO2(63),
     2       Z(30),P(30),T(30),WV(30),V(30),
     3       ENA,ENB,NHT,AKA(63),AKB(63),
     4       BETAA(63),BETAB(63),SQ ,NU,
     5                 WAVENO(63),K,JMAX,BLAK(63,30)
      CI=0.
      IF(J1 .EQ. J2) GO TO 6
      J3=J2-1
      I=J1
      IF(K-I)3,4,3
    3 TAU1= TAUM20(I,0)*TAUCO2(I,0)*TAUICE(I,0)
      GO TO 9
    4 TAU1=1.
C
    9 DO 1 I=J1,J3
      J4=I+1
      IF(J4-K)10,11,10
   10 TAU2=TAUM20(J4,0)*TAUCO2(J4,0)*TAUICE(J4,0)
      GO TO 12
   11 TAU2=1.
   12 TAU3=TAUM20(I,1)*TAUCO2(I,1)*TAUICE(I,1)
      TAU=(TAU1+TAU2+4.*TAU3)/6.
      TAU1=TAU2
    5 IF(L .LT. 1) GO TO 2
      CI= TAU *(BLAK(NU,I+1) - BLAK(NU,I)) + CI
      GO TO 1
C
    2 CI=(BLAK(NU,I+1) - BLAK(NU,I))/TAU + CI
C
    1 CONTINUE
C
    6 RETURN
      END
```

4. Recomputation of Elsasser Coefficients

The following program was used to recompute the Elsasser coefficients (see Chapter VI).

```
C      4 . RECOMPUTATION OF ELSASSER COEFFICIENTS
       COMMON TAB42(11,8),TAB41(11,6),TLH20(63),TLC02(63)
       REAL SUM1(8,3),US(16), SUM(16,8,3),WAVENO(63),DNU(63)
       REAL P(20),P1(11,20),VS(20)
       INTEGER TP(8)
C      READ TABLE IV-2,TAUCO2 FOR CARBON DIOXIDE
C
       READ(1,303)((TAB42(I,J),J=1,8),I=1,11)
  303  FORMAT(2X,2P8F6.2)
C
C
C      READ TABLE IV-1, TAUM20 FOR WATER VAPOR
C
       READ(1,305)((TAB41(I,J),J=1,6),I=1,11)
  305  FORMAT(2X,2P6F6.2)
C
C
C      READ WAVENO DATA FOR 63 WAVE NUMBERS
C
       DO 30 I=1,63
   30  READ(1,307)NU,WAVENO(NU),DNU(NU),TLH20(NU),TLC02(NU)
  307  FORMAT(I3,2F5.0,2F9.2)
       S=.3
       U=-5.3
       J3=1
       DO 1 J=1,16
       J3=J3+1
       U=U+S
       US(J)=U
C
       DO 2 I=1,8
C
       T=10 * I
       T=273.-T
       TP(I)=T
       SO=0.
       SO1=C.
C
       DO 3 NU=1,42
       WAVE=WAVENO(NU)
C
       SO=(1.-TAUM20(NU,U)) * BLACKB(WAVE,T) * DNU(NU) + SO
       SO1=SO1 +(1.-TAUM20(NU,U))* DBDT(WAVE,T) * DNU(NU)
C
C
       IF(NU .NE. 14) GO TO 3
       SUM(J,I,1)=2. * SO
       SUM1(I,1)=SO1
     3 CONTINUE
       SUM(J,I,2)=SO * 2.
```

```
      SUM1(I,2)=SO1
      SO=0.
      SO1=0.
      DO 4 NU=43,63
      WAVE=WAVENO(NU)
      SO=(1. - TAUM20(NU,U)) * BLACKB(WAVE,T) * DNU(NU) + SO
    4 SO1=SO1 +(1.-TAUM20(NU,U))* DBDT(WAVE,T) * DNU(NU)
      SUM1(I,3)=SO1
      IV=9 - I
      P(IV)=SUM1(I,1) + SUM1(I,3)
    2 SUM(J,I,3)=SO*2.
C
C     PRINT OUT 3 SETS OF SUMS OF ONE ROW
      IF(J .GT. 1)GO TO 9
      WRITE(3,204)(TP(I),I=1,8)
  204 FORMAT('1',3X,8(5X,I3))
C
    9 WRITE(3,201)U,(SUM1(I,1),I=1,8)
  201 FORMAT('0',F4.1,8F8.3)
C
      WRITE(3,202)((SUM1(I,K),I=1,8),K=2,3)
  202 FORMAT(5X,8F8.3)
C
      WRITE(2,207)(P(IV),IV=3,8)
  207 FORMAT(6F10.3)
C
      IF(J3 - 3)5,6,6
    6 J3=0
      S=.4
      GO TO 1
    5 S=.3
    1 CONTINUE
C
C     PRINT COMPLETE TABLE - - 2
      DO 11 J=1,16
      P(J)=SUM(J,8,1) + SUM(J,8,3)
      IF(J .GT. 1) GO TO 12
      WRITE(3,204)(TP(I),I=1,8)
C
   12 WRITE(3,201)US(J),(SUM(J,I,1),I=1,8)
   11 WRITE(3,202)((SUM(J,I,K),I=1,8),K=2,3)
      WRITE(2,208)(P(J),J=1,16)
  208 FORMAT(8F7.2)
C * * * * * * * * * * * * * * * * * * * * * * * * * * * * * * * * * * * * *
C
C
      J3=2
      U=-3.7
      DO 13 IU=1,11
      J3=J3 + 1
```

```
      IF(J3 - 3)14,15,15
   15 S=.4
      J3=0
      GO TO 16
C
   14 S=.3
   16 U=U + S
      US(IU)=U
      V=-3.7
      JV3=2
C
      DO 17 IV=1,20
      JV3=JV3 + 1
      IF(JV3 - 3)18,19,19
   19 S=.4
      JV3=0
      GO TO 20
   18 S=.3
   20 V=V + S
      VS(IV)=V
      SO=0.
      SO1=0.
C
      T=233.
      T1=213.
      DO 7 NU=15,42
      TH=TAUM20(NU,U)
      TC=TAUCO2(NU,V)
      THTC=TH * TC
C
      WAVE=WAVENO(NU)
      SO=(1.-THTC) * DBDT(WAVE,T) * DNU(NU) + SO
C
    7 SO1=(1.-THTC) * BLACKB(WAVE,T1)* DNU(NU) + SO1
      P(IV)=SO
      P1(IU,IV)=SO1 * 2.
   17 CONTINUE
      IF(IU .NE. 1) GO TO 10
      WRITE(3,203)T,(VS(IV),IV=1,20)
  203 FORMAT('1',44X,'T= ',F5.0/' ',T8,10F10.3/' ',T8,10F10.3/)
   10 WRITE(3,205)U,( P(IV),IV=1,20)
  205 FORMAT(F6.1,T8,10F10.3/' ',T8,10F10.3)
      WRITE(2,206)( P(IV),IV=1,20)
  206 FORMAT(10F7.3)
   13 CONTINUE
C
      DO 21 IU=1,11
      IF(IU .NE. 1) GO TO 22
      WRITE(3,203)T1,(VS(IV),IV=1,20)
   22 WRITE(3,205)US(IU),(P1(IU,IV),IV=1,20)
```

```
   21 WRITE(2,206)(P1(IU,IV),IV=1,20)
C
      CALL EXIT
      END
```

```
      FUNCTION DBDT(WAVE,T)
C
      C=1.4389 * WAVE
      E=EXP(C/T)
      EM1=E-1.
      DBDT=(2.5915E-8 * C**4)/(T*T) *E/(EM1 * EM1)
      RETURN
      END
```

```
      FUNCTION TAUM20(NU,U)
C
C     FUNCTION TAUM20 LOOKS UP VALUE IN TABLE 4-1
C     TAUM20=ALOG10(U) + TLH20(NU)  WHERE U IS THE WATER VAPOR S
C     AND TLH20 IS READ IN
C
      COMMON TAB42(11,8),TAB41(11,6),TLH20(63),TLCO2(63)
C
      TAUM20=U + TLH20(NU) - 5.0
C
C     IF TAUM20 .LT. -3.7 - 5. EXTRAPOLATE FROM TABLE
C
      IF(TAUM20 + 8.7)6,6,7
    6 FACTOR=TAUM20 + 8.7
      TAUM20 = TAB41(4,1) +(TAB41(5,1)-TAB41(4,1)) * FACTOR
      IF(TAUM20 .GT. 1.)TAUM20=1.
      RETURN
C
    7 IF(TAUM20 .LT.-3.8) GO TO 5
      TAUM20=0.
      RETURN
C
C     SEPARATE CHARACTERISTIC AND MANTISSA OF
C     ALOG10(U) + TLH20(NU)
C
    5 ICHAR=IFIX(TAUM20)
      TMAN=ABS(TAUM20 - FLOAT(ICHAR))
C
C     TABLE 4-1 EXTENDS FROM -3.7 TO 1.2
      L=-8
C
C     FIND APPROPRIATE COLUMN IN TABLE
C
      DO 2 IC=1,6
C
      IF(ICHAR .EQ. L) GO TO 1
    2 L=L+1
C
C     FIND APPROPRIATE ROWS IN TABLE
    1 B =1.0
C
      DO 3 IM=1,10
      H=B-.1
      IF(TMAN .LE. B .AND. TMAN .GE. H) GO TO 4
C
    3 B=B-.1
C
C     INTERPOLATE BETWEEN TABLE VALUES
    4 FACTOR=(B-TMAN) * 10.
C
```

```
      TAUM20 = TAB41(IM,IC) - ABS((TAB41(IM+1,IC)
     1- TAB41(IM,IC)) * FACTOR)
C
    8 RETURN
      END
```

```
      FUNCTION TAUCO2(NU,V)
C
C     FUNCTION TAUCO2 LOOKS UP VALUE FROM TABLE 4-2
C
      COMMON TAB42(11,8),TAB41(11,6),TLH20(63),TLCO2(63)
      TAUCO2=V + TLCO2(NU) - 5.0
C
C     IF TAUCO2 .LT. -5.2 - 5. EXTRAPOLATE FROM TABLE
      IF(TAUCO2 +10.2) 6,6,7
    6 FACTOR=TAUCO2 +10.2
      TAUCO2=TAB42(9,1) + (TAB42(10,1) - TAB42(9,1)) * FACTOR
      IF(TAUCO2 .GT. 1.) TAUCO2=1.
      RETURN
C
    7 IF(TAUCO2 .LE. -3.) GO TO 5
      TAUCO2=0.
      RETURN
C * * * * * * * * * * * * * * * * * * * * * * * * * * * * * * * * * * *
    5 ICHAR=IFIX(TAUCO2)
      TMAN=ABS(TAUCO2 - FLOAT(ICHAR))
C
C     TABLE 4-2 EXTENDS FROM -5.2 TO 2.0
      L=-10
C
C     FIND APPROPRIATE COLUMN IN TABLE
      DO 2 IC=1,8
      IF(ICHAR .EQ. L) GO TO 1
    2 L=L+1
C
C     FIND APPROPRIATE ROWS IN TABLE
    1 B=1.0
C
      DO 3 IM=1,10
      H=B-.1
      IF(TMAN .LE. B .AND. TMAN .GE. H)GO TO 4
    3 B=B-.1
C
C     INTERPOLATE BETWEEN TABLE VALUES
    4 FACTOR=(B - TMAN) * 10.
C
      TAUCO2 = TAB42(IM,IC) -ABS((TAB42(IM+1,IC) - TAB42(IM,IC))
     1 * FACTOR)
    8 RETURN
      END
```

B. Ice Crystal Display Results

1. 25 MICRON CRYSTALS, 1400 14 DECEMBER 1961.

ICE CRYSTAL DISPLAY

SOUNDING 1, ICE ABSORPTION 0.00196/M, DISPLAY DEPTH 0. M

HEIGHT (M)	TEMPERATURE (DEG C)	FLUX (CAL/SQ CM/12 HR)	MEAN HEATING RATE, LAYER ABOVE Z (DEG C/12 HR)
0.0	-18.2	103.5	-0.333
25.0	-18.4	103.8	-0.259
50.0	-18.6	104.0	-0.202
75.0	-18.8	104.2	-0.181
100.0	-18.9	104.3	-0.186
200.0	-19.6	104.9	-0.151
400.0	-21.0	105.8	-0.105
600.0	-22.4	106.5	-0.035
915.0	-24.5	106.8	-0.046
1910.0	-24.5	108.1	0.160
1920.0	-24.5	108.1	-0.002
2000.0	-23.4	108.1	-0.229
2080.0	-22.3	108.5	-0.484
2160.0	-21.2	109.5	-0.682
2170.0	-21.2	109.6	-0.451
2561.0	-21.7	113.9	-0.457
3106.0	-23.0	119.5	-0.537
3690.0	-25.2	126.0	-0.524
4310.0	-29.8	132.4	-0.542
4983.0	-33.7	139.0	-0.907
6509.0	-46.7	161.4	-0.615
7380.0	-54.0	168.9	-0.403
8363.0	-55.4	173.8	-0.397
19074.0	-50.0	202.0	

NEUTRAL HEIGHT AT OR ABOVE TOP OF DISPLAY.

ICE CRYSTAL DISPLAY

SOUNDING 1, ICE ABSORPTION 0.00196/M, DISPLAY DEPTH 100. M

HEIGHT (M)	TEMPERATURE (DEG C)	FLUX (CAL/SQ CM/12 HR)	MEAN HEATING RATE, LAYER ABOVE Z (DEG C/12 HR)
0.0	-18.2	85.3	-4.622
25.0	-18.4	89.8	-4.763
50.0	-18.6	94.4	-4.934
75.0	-18.8	99.1	-5.164
100.0	-18.9	104.1	-0.191
200.0	-19.6	104.7	-0.153
400.0	-21.0	105.7	-0.106
600.0	-22.4	106.3	-0.036
915.0	-24.5	106.7	-0.047
1910.0	-24.5	107.9	0.160
1920.0	-24.5	107.9	-0.002
2000.0	-23.4	107.9	-0.229
2080.0	-22.3	108.4	-0.484
2160.0	-21.2	109.3	-0.683
2170.0	-21.2	109.5	-0.452
2561.0	-21.7	113.7	-0.457
3106.0	-23.0	119.3	-0.537
3690.0	-25.2	125.9	-0.524
4310.0	-29.8	132.2	-0.542
4983.0	-33.7	138.9	-0.907
6509.0	-46.7	161.2	-0.615
7380.0	-54.0	168.7	-0.403
8363.0	-55.4	173.7	-0.397
19074.0	-50.0	201.9	

NEUTRAL HEIGHT AT OR ABOVE TOP OF DISPLAY.

ICE CRYSTAL DISPLAY

SOUNDING 1, ICE ABSORPTION 0.00196/M, DISPLAY DEPTH 600. M

HEIGHT (M)	TEMPERATURE (DEG C)	FLUX (CAL/SQ CM/12 HR)	MEAN HEATING RATE, LAYER ABOVE Z (DEG C/12 HR)
0.0	-18.2	35.0	-1.947
25.0	-18.4	36.9	-1.935
50.0	-18.6	38.8	-1.943
75.0	-18.8	40.7	-2.001
100.0	-18.9	42.6	-2.218
200.0	-19.6	51.0	-2.867
400.0	-21.0	72.2	-4.217
600.0	-22.4	102.3	-0.064
915.0	-24.5	102.9	-0.058
1910.0	-24.5	104.5	0.152
1920.0	-24.5	104.4	-0.010
2000.0	-23.4	104.4	-0.237
2080.0	-22.3	104.9	-0.492
2160.0	-21.2	105.9	-0.691
2170.0	-21.2	106.1	-0.459
2561.0	-21.7	110.3	-0.463
3106.0	-23.0	116.0	-0.541
3690.0	-25.2	122.6	-0.527
4310.0	-29.8	129.0	-0.544
4983.0	-33.7	135.7	-0.908
6509.0	-46.7	158.1	-0.615
7380.0	-54.0	165.6	-0.403
8363.0	-55.4	170.5	-0.397
19074.0	-50.0	198.7	

NEUTRAL HEIGHT BETWEEN 400. M AND 200.M.

ICE CRYSTAL DISPLAY

SOUNDING 1, ICE ABSORPTION 0.00196/M, DISPLAY DEPTH 915. M

HEIGHT (M)	TEMPERATURE (DEG C)	FLUX (CAL/SQ CM/12 HR)	MEAN HEATING RATE, LAYER ABOVE Z (DEG C/12 HR)
0.0	-18.2	22.1	-1.262
25.0	-18.4	23.3	-1.211
50.0	-18.6	24.5	-1.179
75.0	-18.8	25.6	-1.194
100.0	-18.9	26.8	-1.291
200.0	-19.6	31.7	-1.573
400.0	-21.0	43.3	-2.207
600.0	-22.4	59.0	-3.711
915.0	-24.5	98.9	-0.076
1910.0	-24.5	101.0	0.143
1920.0	-24.5	100.9	-0.020
2000.0	-23.4	101.0	-0.247
2080.0	-22.3	101.5	-0.502
2160.0	-21.2	102.5	-0.701
2170.0	-21.2	102.6	-0.467
2561.0	-21.7	107.0	-0.469
3106.0	-23.0	112.7	-0.546
3690.0	-25.2	119.4	-0.530
4310.0	-29.8	125.8	-0.546
4983.0	-33.7	132.5	-0.909
6509.0	-46.7	154.9	-0.616
7380.0	-54.0	162.5	-0.403
8363.0	-55.4	167.4	-0.397
19074.0	-50.0	195.6	

NEUTRAL HEIGHT BETWEEN 400. M AND 200.M.

ICE CRYSTAL DISPLAY

SOUNDING 1, ICE ABSORPTION 0.00196/M, DISPLAY DEPTH 1910. M

HEIGHT (M)	TEMPERATURE (DEG C)	FLUX (CAL/SQ CM/12 HR)	MEAN HEATING RATE, LAYER ABOVE Z (DEG C/12 HR)
0.0	-18.2	9.4	-0.594
25.0	-18.4	10.0	-0.507
50.0	-18.6	10.5	-0.434
75.0	-18.8	10.9	-0.408
100.0	-18.9	11.3	-0.389
200.0	-19.6	12.8	-0.316
400.0	-21.0	15.1	-0.264
600.0	-22.4	17.0	-0.277
915.0	-24.5	20.0	-2.434
1910.0	-24.5	95.9	0.128
1920.0	-24.5	95.8	-0.035
2000.0	-23.4	95.9	-0.262
2080.0	-22.3	96.4	-0.517
2160.0	-21.2	97.4	-0.716
2170.0	-21.2	97.6	-0.481
2561.0	-21.7	102.1	-0.479
3106.0	-23.0	108.0	-0.552
3690.0	-25.2	114.7	-0.534
4310.0	-29.8	121.2	-0.549
4983.0	-33.7	127.9	-0.911
6509.0	-46.7	150.4	-0.617
7380.0	-54.0	157.9	-0.404
8363.0	-55.4	162.9	-0.397
19074.0	-50.0	191.1	

NEUTRAL HEIGHT BETWEEN 200. M AND 100.M.

ICE CRYSTAL DISPLAY

SOUNDING 1, ICE ABSORPTION 0.00196/M, DISPLAY DEPTH 1920. M

HEIGHT (M)	TEMPERATURE (DEG C)	FLUX (CAL/SQ CM/12 HR)	MEAN HEATING RATE, LAYER ABOVE Z (DEG C/12 HR)
0.0	-18.2	9.4	-0.592
25.0	-18.4	10.0	-0.504
50.0	-18.6	10.5	-0.432
75.0	-18.8	10.9	-0.406
100.0	-18.9	11.3	-0.386
200.0	-19.6	12.7	-0.312
400.0	-21.0	15.0	-0.257
600.0	-22.4	16.9	-0.266
915.0	-24.5	19.7	-2.383
1910.0	-24.5	94.0	-6.095
1920.0	-24.5	95.8	-0.035
2000.0	-23.4	95.9	-0.262
2080.0	-22.3	96.4	-0.517
2160.0	-21.2	97.4	-0.716
2170.0	-21.2	97.6	-0.481
2561.0	-21.7	102.1	-0.479
3106.0	-23.0	108.0	-0.552
3690.0	-25.2	114.7	-0.534
4310.0	-29.8	121.2	-0.549
4983.0	-33.7	127.9	-0.911
6509.0	-46.7	150.4	-0.617
7380.0	-54.0	157.9	-0.404
8363.0	-55.4	162.8	-0.397
19074.0	-50.0	191.1	

NEUTRAL HEIGHT BETWEEN 200. M AND 100.M.

ICE CRYSTAL DISPLAY

SOUNDING 1; ICE ABSORPTION 0.00196/M, DISPLAY DEPTH 2080. M

HEIGHT (M)	TEMPERATURE (DEG C)	FLUX (CAL/SQ CM/12 HR)	MEAN HEATING RATE, LAYER ABOVE Z (DEG C/12 HR)
0.0	-18.2	8.8	-0.562
25.0	-18.4	9.4	-0.473
50.0	-18.6	9.8	-0.399
75.0	-18.8	10.2	-0.371
100.0	-18.9	10.6	-0.346
200.0	-19.6	11.9	-0.255
400.0	-21.0	13.8	-0.170
600.0	-22.4	15.0	-0.112
915.0	-24.5	16.2	-1.668
1910.0	-24.5	68.2	-4.347
1920.0	-24.5	69.5	-5.128
2000.0	-23.4	81.5	-6.585
2080.0	-22.3	97.0	-0.491
2160.0	-21.2	98.0	-0.699
2170.0	-21.2	98.2	-0.472
2561.0	-21.7	102.6	-0.476
3106.0	-23.0	108.4	-0.551
3690.0	-25.2	115.1	-0.533
4310.0	-29.8	121.6	-0.549
4983.0	-33.7	128.3	-0.911
6509.0	-46.7	150.7	-0.617
7380.0	-54.0	158.3	-0.404
8363.0	-55.4	163.2	-0.397
19074.0	-50.0	191.5	

NEUTRAL HEIGHT BETWEEN 200. M AND 100.M.

2. 25 MICRON CRYSTALS, 1400 24 JANUARY 1962

ICE CRYSTAL DISPLAY

SOUNDING 2, ICE ABSORPTION 0.00196/M, DISPLAY DEPTH 0. M

HEIGHT (M)	TEMPERATURE (DEG C)	FLUX (CAL/SQ CM/12 HR)	MEAN HEATING RATE, LAYER ABOVE Z (DEG C/12 HR)
0.0	-30.4	84.6	0.052
25.0	-30.2	84.5	0.003
50.0	-30.0	84.5	-0.035
75.0	-29.8	84.6	-0.045
100.0	-29.7	84.6	-0.006
200.0	-29.1	84.6	-0.044
250.0	-28.3	84.7	-0.208
350.0	-26.7	85.4	-0.463
450.0	-25.1	86.9	-0.756
460.0	-25.2	87.1	-0.563
500.0	-25.3	87.8	-0.399
600.0	-26.0	89.1	-0.271
800.0	-27.1	90.7	-0.207
900.0	-27.3	91.4	-0.299
1150.0	-26.4	93.6	-0.398
1208.0	-26.4	94.3	-0.306
2103.0	-30.8	101.7	-0.305
2592.0	-32.0	105.5	-0.335
3667.0	-36.9	113.7	-0.362
4911.0	-42.5	122.5	-0.385
6395.0	-49.1	132.0	-0.589
8262.0	-53.8	146.5	-1.006
8525.0	-54.4	149.5	-0.380
19832.0	-51.0	177.1	

NEUTRAL HEIGHT AT OR ABOVE TOP OF DISPLAY.

ICE CRYSTAL DISPLAY

SOUNDING 2, ICE ABSORPTION 0.00196/M, DISPLAY DEPTH 100. M

HEIGHT (M)	TEMPERATURE (DEG C)	FLUX (CAL/SQ CM/12 HR)	MEAN HEATING RATE, LAYER ABOVE Z (DEG C/12 HR)
0.0	-30.4	69.3	-3.772
25.0	-30.2	72.8	-4.077
50.0	-30.0	76.6	-4.381
75.0	-29.8	80.6	-4.654
100.0	-29.7	84.8	-0.002
200.0	-29.1	84.8	-0.042
250.0	-28.3	84.9	-0.206
350.0	-26.7	85.5	-0.461
450.0	-25.1	87.0	-0.755
460.0	-25.2	87.3	-0.562
500.0	-25.3	88.0	-0.398
600.0	-26.0	89.2	-0.270
800.0	-27.1	90.9	-0.206
900.0	-27.3	91.5	-0.299
1150.0	-26.4	93.7	-0.397
1208.0	-26.4	94.4	-0.306
2103.0	-30.8	101.9	-0.305
2592.0	-32.0	105.6	-0.335
3667.0	-36.9	113.8	-0.362
4911.0	-42.5	122.7	-0.385
6395.0	-49.1	132.1	-0.589
8262.0	-53.8	146.6	-1.005
8525.0	-54.4	149.6	-0.380
19832.0	-51.0	177.2	

NEUTRAL HEIGHT AT OR ABOVE TOP OF DISPLAY.

ICE CRYSTAL DISPLAY

SOUNDING 2, ICE ABSORPTION 0.00196/M, DISPLAY DEPTH 460. M

HEIGHT (M)	TEMPERATURE (DEG C)	FLUX (CAL/SQ CM/12 HR)	MEAN HEATING RATE, LAYER ABOVE Z (DEG C/12 HR)
0.0	-30.4	31.7	-1.681
25.0	-30.2	33.2	-1.876
50.0	-30.0	35.0	-2.064
75.0	-29.8	36.8	-2.217
100.0	-29.7	38.9	-2.563
200.0	-29.1	48.1	-3.182
250.0	-28.3	53.8	-4.137
350.0	-26.7	68.6	-5.603
450.0	-25.1	88.4	-6.604
460.0	-25.2	90.8	-0.505
500.0	-25.3	91.4	-0.361
600.0	-26.0	92.5	-0.246
800.0	-27.1	94.1	-0.189
900.0	-27.3	94.6	-0.285
1150.0	-26.4	96.7	-0.387
1208.0	-26.4	97.4	-0.299
2103.0	-30.8	104.7	-0.301
2592.0	-32.0	108.4	-0.332
3667.0	-36.9	116.5	-0.360
4911.0	-42.5	125.4	-0.384
6395.0	-49.1	134.8	-0.589
8262.0	-53.8	149.3	-1.005
8525.0	-54.4	152.3	-0.380
19832.0	-51.0	179.9	

NEUTRAL HEIGHT BETWEEN 200. M AND 100.M.

ICE CRYSTAL DISPLAY

SOUNDING 2, ICE ABSORPTION 0.00196/M, DISPLAY DEPTH 600. M

HEIGHT (M)	TEMPERATURE (DEG C)	FLUX (CAL/SQ CM/12 HR)	MEAN HEATING RATE, LAYER ABOVE Z (DEG C/12 HR)
0.0	-30.4	22.3	-1.156
25.0	-30.2	23.4	-1.322
50.0	-30.0	24.6	-1.479
75.0	-29.8	25.9	-1.600
100.0	-29.7	27.4	-1.858
200.0	-29.1	34.1	-2.356
250.0	-28.3	38.3	-3.166
350.0	-26.7	49.6	-4.395
450.0	-25.1	65.2	-5.235
460.0	-25.2	67.0	-5.262
500.0	-25.3	74.5	-5.706
600.0	-26.0	94.3	-0.234
800.0	-27.1	95.8	-0.179
900.0	-27.3	96.3	-0.278
1150.0	-26.4	98.4	-0.381
1208.0	-26.4	99.0	-0.296
2103.0	-30.8	106.2	-0.299
2592.0	-32.0	109.9	-0.331
3667.0	-36.9	118.0	-0.360
4911.0	-42.5	126.8	-0.384
6395.0	-49.1	136.2	-0.589
8262.0	-53.8	150.7	-1.005
8525.0	-54.4	153.7	-0.380
19832.0	-51.0	181.3	

NEUTRAL HEIGHT BETWEEN 200. M AND 100.M.

ICE CRYSTAL DISPLAY

SOUNDING 2, ICE ABSORPTION 0.00196/M, DISPLAY DEPTH 900. M

HEIGHT (M)	TEMPERATURE (DEG C)	FLUX (CAL/SQ CM/12 HR)	MEAN HEATING RATE, LAYER ABOVE Z (DEG C/12 HR)
0.0	-30.4	9.5	-0.436
25.0	-30.2	9.9	-0.563
50.0	-30.0	10.4	-0.679
75.0	-29.8	11.0	-0.757
100.0	-29.7	11.7	-0.895
200.0	-29.1	14.9	-1.227
250.0	-28.3	17.1	-1.839
350.0	-26.7	23.7	-2.753
450.0	-25.1	33.4	-3.381
460.0	-25.2	34.6	-3.308
500.0	-25.3	39.3	-3.428
600.0	-26.0	51.2	-4.142
800.0	-27.1	79.4	-5.376
900.0	-27.3	97.3	-0.280
1150.0	-26.4	99.4	-0.380
1208.0	-26.4	100.0	-0.295
2103.0	-30.8	107.2	-0.298
2592.0	-32.0	110.9	-0.330
3667.0	-36.9	118.9	-0.359
4911.0	-42.5	127.7	-0.384
6395.0	-49.1	137.2	-0.588
8262.0	-53.8	151.6	-1.005
8525.0	-54.4	154.6	-0.380
19832.0	-51.0	182.2	

NEUTRAL HEIGHT BETWEEN 75. M AND 50.M.

ICE CRYSTAL DISPLAY

SOUNDING 2, ICE ABSORPTION 0.00196/M, DISPLAY DEPTH 1150. M

HEIGHT (M)	TEMPERATURE (DEG C)	FLUX (CAL/SQ CM/12 HR)	MEAN HEATING RATE, LAYER ABOVE Z (DEG C/12 HR)
0.0	-30.4	3.3	-0.089
25.0	-30.2	3.3	-0.198
50.0	-30.0	3.5	-0.294
75.0	-29.8	3.8	-0.351
100.0	-29.7	4.1	-0.431
200.0	-29.1	5.7	-0.684
250.0	-28.3	6.9	-1.202
350.0	-26.7	11.2	-1.963
450.0	-25.1	18.1	-2.491
460.0	-25.2	19.0	-2.370
500.0	-25.3	22.4	-2.336
600.0	-26.0	30.5	-2.617
800.0	-27.1	48.3	-3.271
900.0	-27.3	59.2	-4.999
1150.0	-26.4	99.9	-0.374
1208.0	-26.4	100.6	-0.293
2103.0	-30.8	107.7	-0.298
2592.0	-32.0	111.4	-0.330
3667.0	-36.9	119.4	-0.359
4911.0	-42.5	128.2	-0.383
6395.0	-49.1	137.7	-0.588
8262.0	-53.8	152.1	-1.005
8525.0	-54.4	155.1	-0.380
19832.0	-51.0	182.7	

NEUTRAL HEIGHT BETWEEN 25. M AND 0.M.

ICE CRYSTAL DISPLAY

SOUNDING 2, ICE ABSORPTION 0.00196/M, DISPLAY DEPTH 1208. M

HEIGHT (M)	TEMPERATURE (DEG C)	FLUX (CAL/SQ CM/12 HR)	MEAN HEATING RATE, LAYER ABOVE Z (DEG C/12 HR)
0.0	-30.4	2.2	-0.030
25.0	-30.2	2.2	-0.135
50.0	-30.0	2.3	-0.228
75.0	-29.8	2.6	-0.281
100.0	-29.7	2.8	-0.352
200.0	-29.1	4.1	-0.591
250.0	-28.3	5.1	-1.092
350.0	-26.7	9.0	-1.827
450.0	-25.1	15.5	-2.337
460.0	-25.2	16.3	-2.209
500.0	-25.3	19.4	-2.148
600.0	-26.0	26.9	-2.354
800.0	-27.1	42.9	-2.907
900.0	-27.3	52.6	-4.461
1150.0	-26.4	89.0	-6.328
1208.0	-26.4	100.8	-0.292
2103.0	-30.8	107.9	-0.297
2592.0	-32.0	111.6	-0.330
3667.0	-36.9	119.6	-0.359
4911.0	-42.5	128.4	-0.383
6395.0	-49.1	137.8	-0.588
8262.0	-53.8	152.3	-1.005
8525.0	-54.4	155.3	-0.380
19832.0	-51.0	182.9	

NEUTRAL HEIGHT BETWEEN 25. M AND 0.M.

3. 25 MICRON CRYSTALS, COMPOSITE SOUNDING.

ICE CRYSTAL DISPLAY

SOUNDING 3, ICE ABSORPTION 0.00196/M, DISPLAY DEPTH 0. M

HEIGHT (M)	TEMPERATURE (DEG C)	FLUX (CAL/SQ CM/12 HR)	MEAN HEATING RATE, LAYER ABOVE Z (DEG C/12 HR)
0.0	-28.0	90.0	-0.127
25.0	-28.0	90.1	-0.128
50.0	-28.0	90.2	-0.130
75.0	-28.0	90.3	-0.131
100.0	-28.0	90.4	-0.124
200.0	-28.0	90.8	-0.145
400.0	-28.0	91.8	-0.157
600.0	-28.0	92.8	-0.176
1000.0	-28.0	94.9	-0.199
1167.0	-28.0	95.9	-0.231
1602.0	-28.0	98.8	-0.309
2065.0	-28.0	102.5	-0.428
2308.0	-28.0	105.1	-0.570
2358.0	-28.0	105.8	-0.509
2408.0	-28.6	106.5	-0.414
2560.0	-29.3	108.0	-0.440
3086.0	-32.0	113.4	-0.439
3649.0	-35.2	118.8	-0.447
4250.0	-38.3	124.2	-0.294
5402.0	-42.5	130.6	-0.511
6883.0	-51.2	143.2	-0.666
7478.0	-54.5	148.9	-0.416
7656.0	-55.0	149.9	-0.265
8731.0	-54.0	153.5	-0.394
20466.0	-47.0	183.9	

NEUTRAL HEIGHT AT OR ABOVE TOP OF DISPLAY.

ICE CRYSTAL DISPLAY

SOUNDING 3, ICE ABSORPTION 0.00196/M, DISPLAY DEPTH 100. M

HEIGHT (M)	TEMPERATURE (DEG C)	FLUX (CAL/SQ CM/12 HR)	MEAN HEATING RATE, LAYER ABOVE Z (DEG C/12 HR)
0.0	-28.0	74.0	-4.142
25.0	-28.0	77.8	-4.370
50.0	-28.0	81.8	-4.611
75.0	-28.0	86.0	-4.864
100.0	-28.0	90.4	-0.124
200.0	-28.0	90.8	-0.145
400.0	-28.0	91.8	-0.157
600.0	-28.0	92.8	-0.176
1000.0	-28.0	94.9	-0.199
1167.0	-28.0	95.9	-0.231
1602.0	-28.0	98.8	-0.309
2065.0	-28.0	102.5	-0.428
2308.0	-28.0	105.1	-0.570
2358.0	-28.0	105.8	-0.509
2408.0	-28.6	106.5	-0.414
2560.0	-29.3	108.0	-0.440
3086.0	-32.0	113.4	-0.439
3649.0	-35.2	118.8	-0.447
4250.0	-38.3	124.2	-0.294
5402.0	-42.5	130.6	-0.511
6883.0	-51.2	143.2	-0.666
7478.0	-54.5	148.9	-0.416
7656.0	-55.0	149.9	-0.265
8731.0	-54.0	153.5	-0.394
20466.0	-47.0	183.9	

NEUTRAL HEIGHT AT OR ABOVE TOP OF DISPLAY.

ICE CRYSTAL DISPLAY

SOUNDING 3, ICE ABSORPTION 0.00196/M, DISPLAY DEPTH 600. M

HEIGHT (M)	TEMPERATURE (DEG C)	FLUX (CAL/SQ CM/12 HR)	MEAN HEATING RATE, LAYER ABOVE Z (DEG C/12 HR)
0.0	-28.0	27.8	-1.554
25.0	-28.0	29.2	-1.640
50.0	-28.0	30.7	-1.730
75.0	-28.0	32.3	-1.826
100.0	-28.0	33.9	-2.087
200.0	-28.0	41.5	-2.898
400.0	-28.0	62.0	-4.451
600.0	-28.0	92.8	-0.176
1000.0	-28.0	94.9	-0.199
1167.0	-28.0	95.9	-0.231
1602.0	-28.0	98.8	-0.309
2065.0	-28.0	102.5	-0.428
2308.0	-28.0	105.1	-0.570
2358.0	-28.0	105.8	-0.509
2408.0	-28.6	106.5	-0.414
2560.0	-29.3	108.0	-0.440
3086.0	-32.0	113.4	-0.439
3649.0	-35.2	118.8	-0.447
4250.0	-38.3	124.2	-0.294
5402.0	-42.5	130.6	-0.511
6883.0	-51.2	143.2	-0.666
7478.0	-54.5	148.9	-0.416
7656.0	-55.0	149.9	-0.265
8731.0	-54.0	153.5	-0.394
20466.0	-47.0	183.9	

NEUTRAL HEIGHT BETWEEN 200. M AND 100.M.

ICE CRYSTAL DISPLAY

SOUNDING 3, ICE ABSORPTION 0.00196/M, DISPLAY DEPTH 1167. M

HEIGHT (M)	TEMPERATURE (DEG C)	FLUX (CAL/SQ CM/12 HR)	MEAN HEATING RATE, LAYER ABOVE Z (DEG C/12 HR)
0.0	-28.0	9.1	-0.512
25.0	-28.0	9.6	-0.540
50.0	-28.0	10.1	-0.570
75.0	-28.0	10.6	-0.601
100.0	-28.0	11.2	-0.687
200.0	-28.0	13.7	-0.954
400.0	-28.0	20.4	-1.465
600.0	-28.0	30.5	-2.849
1000.0	-28.0	68.4	-5.131
1167.0	-28.0	95.9	-0.231
1602.0	-28.0	98.8	-0.309
2065.0	-28.0	102.5	-0.428
2308.0	-28.0	105.1	-0.570
2358.0	-28.0	105.8	-0.509
2408.0	-28.6	106.5	-0.414
2560.0	-29.3	108.0	-0.440
3086.0	-32.0	113.4	-0.439
3649.0	-35.2	118.8	-0.447
4250.0	-38.3	124.2	-0.294
5402.0	-42.5	130.6	-0.511
6883.0	-51.2	143.2	-0.666
7478.0	-54.5	148.9	-0.416
7656.0	-55.0	149.9	-0.265
8731.0	-54.0	153.5	-0.394
20466.0	-47.0	183.9	

NEUTRAL HEIGHT BETWEEN 75. M AND 50. M.

ICE CRYSTAL DISPLAY

SOUNDING 3, ICE ABSORPTION 0.00196/M, DISPLAY DEPTH 2308. M

HEIGHT (M)	TEMPERATURE (DEG C)	FLUX (CAL/SQ CM/12 HR)	MEAN HEATING RATE, LAYER ABOVE Z (DEG C/12 HR)
0.0	-28.0	1.0	-0.055
25.0	-28.0	1.0	-0.058
50.0	-28.0	1.1	-0.061
75.0	-28.0	1.1	-0.064
100.0	-28.0	1.2	-0.073
200.0	-28.0	1.5	-0.102
400.0	-28.0	2.2	-0.157
600.0	-28.0	3.3	-0.304
1000.0	-28.0	7.3	-0.548
1167.0	-28.0	10.2	-1.080
1602.0	-28.0	24.8	-2.882
2065.0	-28.0	63.7	-6.117
2308.0	-28.0	105.1	-0.570
2358.0	-28.0	105.8	-0.509
2408.0	-28.6	106.5	-0.414
2560.0	-29.3	108.0	-0.440
3086.0	-32.0	113.4	-0.439
3649.0	-35.2	118.8	-0.447
4250.0	-38.3	124.2	-0.294
5402.0	-42.5	130.6	-0.511
6883.0	-51.2	143.2	-0.666
7478.0	-54.5	148.9	-0.416
7656.0	-55.0	149.9	-0.265
8731.0	-54.0	153.5	-0.394
20466.0	-47.0	183.9	

NEUTRAL HEIGHT BETWEEN 25. M AND 0.M.

ICE CRYSTAL DISPLAY

SOUNDING 3, ICE ABSORPTION 0.00196/M, DISPLAY DEPTH 2358. M

HEIGHT (M)	TEMPERATURE (DEG C)	FLUX (CAL/SQ CM/12 HR)	MEAN HEATING RATE, LAYER ABOVE Z (DEG C/12 HR)
0.0	-28.0	0.9	-0.050
25.0	-28.0	0.9	-0.052
50.0	-28.0	1.0	-0.055
75.0	-28.0	1.0	-0.058
100.0	-28.0	1.1	-0.067
200.0	-28.0	1.3	-0.092
400.0	-28.0	2.0	-0.142
600.0	-28.0	3.0	-0.276
1000.0	-28.0	6.6	-0.497
1167.0	-28.0	9.3	-0.979
1602.0	-28.0	22.4	-2.613
2065.0	-28.0	57.7	-5.546
2308.0	-28.0	95.3	-7.682
2358.0	-28.0	105.8	-0.509
2408.0	-28.6	106.5	-0.414
2560.0	-29.3	108.0	-0.440
3086.0	-32.0	113.4	-0.439
3649.0	-35.2	118.8	-0.447
4250.0	-38.3	124.2	-0.294
5402.0	-42.5	130.6	-0.511
6883.0	-51.2	143.2	-0.666
7478.0	-54.5	148.9	-0.416
7656.0	-55.0	149.9	-0.265
8731.0	-54.0	153.5	-0.394
20466.0	-47.0	183.9	

NEUTRAL HEIGHT BETWEEN 25. M AND 0.M.

ICE CRYSTAL DISPLAY

SOUNDING 3, ICE ABSORPTION 0.00196/M, DISPLAY DEPTH 2408. M

HEIGHT (M)	TEMPERATURE (DEG C)	FLUX (CAL/SQ CM/12 HR)	MEAN HEATING RATE, LAYER ABOVE Z (DEG C/12 HR)
0.0	-28.0	0.8	-0.045
25.0	-28.0	0.8	-0.047
50.0	-28.0	0.9	-0.050
75.0	-28.0	0.9	-0.053
100.0	-28.0	1.0	-0.060
200.0	-28.0	1.2	-0.084
400.0	-28.0	1.8	-0.129
600.0	-28.0	2.7	-0.250
1000.0	-28.0	6.0	-0.451
1167.0	-28.0	8.4	-0.888
1602.0	-28.0	20.4	-2.371
2065.0	-28.0	52.4	-5.033
2308.0	-28.0	86.5	-6.974
2358.0	-28.0	96.0	-7.614
2408.0	-28.6	106.4	-0.417
2560.0	-29.3	107.9	-0.441
3086.0	-32.0	113.3	-0.439
3649.0	-35.2	118.7	-0.447
4250.0	-38.3	124.2	-0.294
5402.0	-42.5	130.6	-0.511
6883.0	-51.2	143.1	-0.666
7478.0	-54.5	148.9	-0.416
7656.0	-55.0	149.9	-0.265
8731.0	-54.0	153.5	-0.394
20466.0	-47.0	183.8	

NEUTRAL HEIGHT BETWEEN 25. M AND 0.M.

4. LARGE CRYSTALS, COMPOSITE SOUNDING.

ICE CRYSTAL DISPLAY

SOUNDING 3, ICE ABSORPTION 0.00800/M, DISPLAY DEPTH 100. M

HEIGHT (M)	TEMPERATURE (DEG C)	FLUX (CAL/SQ CM/12 HR)	MEAN HEATING RATE, LAYER ABOVE Z (DEG C/12 HR)
0.0	-28.0	40.4	-9.801
25.0	-28.0	49.5	-12.025
50.0	-28.0	60.5	-14.754
75.0	-28.0	74.0	-18.102
100.0	-28.0	90.4	-0.124
200.0	-28.0	90.8	-0.145
400.0	-28.0	91.8	-0.157
600.0	-28.0	92.8	-0.176
1000.0	-28.0	94.9	-0.199
1167.0	-28.0	95.9	-0.231
1602.0	-28.0	98.8	-0.309
2065.0	-28.0	102.5	-0.428
2308.0	-28.0	105.1	-0.570
2358.0	-28.0	105.8	-0.509
2408.0	-28.6	106.5	-0.414
2560.0	-29.3	108.0	-0.440
3086.0	-32.0	113.4	-0.439
3649.0	-35.2	118.8	-0.447
4250.0	-38.3	124.2	-0.294
5402.0	-42.5	130.6	-0.511
6883.0	-51.2	143.2	-0.666
7478.0	-54.5	148.9	-0.416
7656.0	-55.0	149.9	-0.265
8731.0	-54.0	153.5	-0.394
20466.0	-47.0	183.9	

NEUTRAL HEIGHT AT OR ABOVE TOP OF DISPLAY.

ICE CRYSTAL DISPLAY

SOUNDING 3, ICE ABSORPTION 0.00800/M, DISPLAY DEPTH 600. M

HEIGHT (M)	TEMPERATURE (DEG C)	FLUX (CAL/SQ CM/12 HR)	MEAN HEATING RATE, LAYER ABOVE Z (DEG C/12 HR)
0.0	-28.0	0.7	-0.180
25.0	-28.0	0.9	-0.220
50.0	-28.0	1.1	-0.270
75.0	-28.0	1.4	-0.332
100.0	-28.0	1.7	-0.567
200.0	-28.0	3.7	-2.092
400.0	-28.0	18.5	-10.744
600.0	-28.0	92.8	-0.176
1000.0	-28.0	94.9	-0.199
1167.0	-28.0	95.9	-0.231
1602.0	-28.0	98.8	-0.309
2065.0	-28.0	102.5	-0.428
2308.0	-28.0	105.1	-0.570
2358.0	-28.0	105.8	-0.509
2408.0	-28.6	106.5	-0.414
2560.0	-29.3	108.0	-0.440
3086.0	-32.0	113.4	-0.439
3649.0	-35.2	118.8	-0.447
4250.0	-38.3	124.2	-0.294
5402.0	-42.5	130.6	-0.511
6883.0	-51.2	143.2	-0.666
7478.0	-54.5	148.9	-0.416
7656.0	-55.0	149.9	-0.265
8731.0	-54.0	153.5	-0.394
20466.0	-47.0	183.9	

NEUTRAL HEIGHT BETWEEN 25. M AND 0.M.

ICE CRYSTAL DISPLAY

SOUNDING 3, ICE ABSORPTION 0.00800/M, DISPLAY DEPTH 1167. M

HEIGHT (M)	TEMPERATURE (DEG C)	FLUX (CAL/SQ CM/12 HR)	MEAN HEATING RATE, LAYER ABOVE Z (DEG C/12 HR)
0.0	-28.0	0.0	-0.002
25.0	-28.0	0.0	-0.002
50.0	-28.0	0.0	-0.003
75.0	-28.0	0.0	-0.004
100.0	-28.0	0.0	-0.006
200.0	-28.0	0.0	-0.022
400.0	-28.0	0.2	-0.115
600.0	-28.0	1.0	-1.801
1000.0	-28.0	25.0	-13.250
1167.0	-28.0	95.9	-0.231
1602.0	-28.0	98.8	-0.309
2065.0	-28.0	102.5	-0.428
2308.0	-28.0	105.1	-0.570
2358.0	-28.0	105.8	-0.509
2408.0	-28.6	106.5	-0.414
2560.0	-29.3	108.0	-0.440
3086.0	-32.0	113.4	-0.439
3649.0	-35.2	118.8	-0.447
4250.0	-38.3	124.2	-0.294
5402.0	-42.5	130.6	-0.511
6883.0	-51.2	143.2	-0.666
7478.0	-54.5	148.9	-0.416
7656.0	-55.0	149.9	-0.265
8731.0	-54.0	153.5	-0.394
20466.0	-47.0	183.9	

NEUTRAL HEIGHT BETWEEN 25. M AND 0.M.

ICE CRYSTAL DISPLAY

SOUNDING 3, ICE ABSORPTION 0.00800/M, DISPLAY DEPTH 2308. M

HEIGHT (M)	TEMPERATURE (DEG C)	FLUX (CAL/SQ CM/12 HR)	MEAN HEATING RATE, LAYER ABOVE Z (DEG C/12 HR)
0.0	-28.0	0.0	-0.000
25.0	-28.0	0.0	-0.000
50.0	-28.0	0.0	-0.000
75.0	-28.0	0.0	-0.000
100.0	-28.0	0.0	-0.000
200.0	-28.0	0.0	-0.000
400.0	-28.0	0.0	-0.000
600.0	-28.0	0.0	-0.000
1000.0	-28.0	0.0	-0.001
1167.0	-28.0	0.0	-0.025
1602.0	-28.0	0.3	-1.061
2065.0	-28.0	14.7	-13.347
2308.0	-28.0	105.1	-0.570
2358.0	-28.0	105.8	-0.509
2408.0	-28.6	106.5	-0.414
2560.0	-29.3	108.0	-0.440
3086.0	-32.0	113.4	-0.439
3649.0	-35.2	118.8	-0.447
4250.0	-38.3	124.2	-0.294
5402.0	-42.5	130.6	-0.511
6883.0	-51.2	143.2	-0.666
7478.0	-54.5	148.9	-0.416
7656.0	-55.0	149.9	-0.265
8731.0	-54.0	153.5	-0.394
20466.0	-47.0	183.9	

NEUTRAL HEIGHT BETWEEN 25. M AND 0.M.

ICE CRYSTAL DISPLAY

SOUNDING 3, ICE ABSORPTION 0.00800/M, DISPLAY DEPTH 2358. M

HEIGHT (M)	TEMPERATURE (DEG C)	FLUX (CAL/SQ CM/12 HR)	MEAN HEATING RATE, LAYER ABOVE Z (DEG C/12 HR)
0.0	-28.0	0.0	-0.000
25.0	-28.0	0.0	-0.000
50.0	-28.0	0.0	-0.000
75.0	-28.0	0.0	-0.000
100.0	-28.0	0.0	-0.000
200.0	-28.0	0.0	-0.000
400.0	-28.0	0.0	-0.000
600.0	-28.0	0.0	-0.000
1000.0	-28.0	0.0	-0.001
1167.0	-28.0	0.0	-0.017
1602.0	-28.0	0.2	-0.711
2065.0	-28.0	9.8	-8.946
2308.0	-28.0	70.5	-25.830
2358.0	-28.0	105.8	-0.509
2408.0	-28.6	106.5	-0.414
2560.0	-29.3	108.0	-0.440
3086.0	-32.0	113.4	-0.439
3649.0	-35.2	118.8	-0.447
4250.0	-38.3	124.2	-0.294
5402.0	-42.5	130.6	-0.511
6883.0	-51.2	143.2	-0.666
7478.0	-54.5	148.9	-0.416
7656.0	-55.0	149.9	-0.265
8731.0	-54.0	153.5	-0.394
20466.0	-47.0	183.9	

NEUTRAL HEIGHT BETWEEN 25. M AND 0.M.

ICE CRYSTAL DISPLAY

SOUNDING 3, ICE ABSORPTION 0.00800/M, DISPLAY DEPTH 2408. M

HEIGHT (M)	TEMPERATURE (DEG C)	FLUX (CAL/SQ CM/12 HR)	MEAN HEATING RATE, LAYER ABOVE Z (DEG C/12 HR)
0.0	-28.0	0.0	-0.000
25.0	-28.0	0.0	-0.000
50.0	-28.0	0.0	-0.000
75.0	-28.0	0.0	-0.000
100.0	-28.0	0.0	-0.000
200.0	-28.0	0.0	-0.000
400.0	-28.0	0.0	-0.000
600.0	-28.0	0.0	-0.000
1000.0	-28.0	0.0	-0.001
1167.0	-28.0	0.0	-0.011
1602.0	-28.0	0.2	-0.478
2065.0	-28.0	6.6	-6.017
2308.0	-28.0	47.4	-17.385
2358.0	-28.0	71.2	-25.727
2408.0	-28.6	106.2	-0.425
2560.0	-29.3	107.7	-0.443
3086.0	-32.0	113.1	-0.440
3649.0	-35.2	118.5	-0.447
4250.0	-38.3	124.0	-0.294
5402.0	-42.5	130.4	-0.511
6883.0	-51.2	143.0	-0.666
7478.0	-54.5	148.7	-0.416
7656.0	-55.0	149.7	-0.265
8731.0	-54.0	153.3	-0.394
20466.0	-47.0	183.7	

NEUTRAL HEIGHT BETWEEN 25. M AND 0.M.

5. SNOW, COMPOSITE SOUNDING.

ICE CRYSTAL DISPLAY

SOUNDING 3, ICE ABSORPTION 0.08000/M, DISPLAY DEPTH 100. M

HEIGHT (M)	TEMPERATURE (DEG C)	FLUX (CAL/SQ CM/12 HR)	MEAN HEATING RATE, LAYER ABOVE Z (DEG C/12 HR)
0.0	-28.0	0.0	-0.210
25.0	-28.0	0.2	-1.559
50.0	-28.0	1.7	-11.572
75.0	-28.0	12.2	-85.889
100.0	-28.0	90.4	-0.124
200.0	-28.0	90.8	-0.145
400.0	-28.0	91.8	-0.157
600.0	-28.0	92.8	-0.176
1000.0	-28.0	94.9	-0.199
1167.0	-28.0	95.9	-0.231
1602.0	-28.0	98.8	-0.309
2065.0	-28.0	102.5	-0.428
2308.0	-28.0	105.1	-0.570
2358.0	-28.0	105.8	-0.509
2408.0	-28.6	106.5	-0.414
2560.0	-29.3	108.0	-0.440
3086.0	-32.0	113.4	-0.439
3649.0	-35.2	118.8	-0.447
4250.0	-38.3	124.2	-0.294
5402.0	-42.5	130.6	-0.511
6883.0	-51.2	143.2	-0.666
7478.0	-54.5	148.9	-0.416
7656.0	-55.0	149.9	-0.265
8731.0	-54.0	153.5	-0.394
20466.0	-47.0	183.9	

NEUTRAL HEIGHT BETWEEN 25. M AND 0.M.

ICE CRYSTAL DISPLAY

SOUNDING 3, ICE ABSORPTION 0.08000/M, DISPLAY DEPTH 600. M

HEIGHT (M)	TEMPERATURE (DEG C)	FLUX (CAL/SQ CM/12 HR)	MEAN HEATING RATE, LAYER ABOVE Z (DEG C/12 HR)
0.0	-28.0	0.0	-0.000
25.0	-28.0	0.0	-0.000
50.0	-28.0	0.0	-0.000
75.0	-28.0	0.0	-0.000
100.0	-28.0	0.0	-0.000
200.0	-28.0	0.0	-0.000
400.0	-28.0	0.0	-13.426
600.0	-28.0	92.8	-0.176
1000.0	-28.0	94.9	-0.199
1167.0	-28.0	95.9	-0.231
1602.0	-28.0	98.8	-0.309
2065.0	-28.0	102.5	-0.428
2308.0	-28.0	105.1	-0.570
2358.0	-28.0	105.8	-0.509
2408.0	-28.6	106.5	-0.414
2560.0	-29.3	108.0	-0.440
3086.0	-32.0	113.4	-0.439
3649.0	-35.2	118.8	-0.447
4250.0	-38.3	124.2	-0.294
5402.0	-42.5	130.6	-0.511
6883.0	-51.2	143.2	-0.666
7478.0	-54.5	148.9	-0.416
7656.0	-55.0	149.9	-0.265
8731.0	-54.0	153.5	-0.394
20466.0	-47.0	183.9	

NEUTRAL HEIGHT BETWEEN 25. M AND 0.M.

ICE CRYSTAL DISPLAY

SOUNDING 3, ICE ABSORPTION 0.08000/M, DISPLAY DEPTH 1167. M

HEIGHT (M)	TEMPERATURE (DEG C)	FLUX (CAL/SQ CM/12 HR)	MEAN HEATING RATE, LAYER ABOVE Z (DEG C/12 HR)
0.0	-28.0	0.0	-0.000
25.0	-28.0	0.0	-0.000
50.0	-28.0	0.0	-0.000
75.0	-28.0	0.0	-0.000
100.0	-28.0	0.0	-0.000
200.0	-28.0	0.0	-0.000
400.0	-28.0	0.0	-0.000
600.0	-28.0	0.0	-0.000
1000.0	-28.0	0.0	-17.910
1167.0	-28.0	95.9	-0.231
1602.0	-28.0	98.8	-0.309
2065.0	-28.0	102.5	-0.428
2308.0	-28.0	105.1	-0.570
2358.0	-28.0	105.8	-0.509
2408.0	-28.6	106.5	-0.414
2560.0	-29.3	108.0	-0.440
3086.0	-32.0	113.4	-0.439
3649.0	-35.2	118.8	-0.447
4250.0	-38.3	124.2	-0.294
5402.0	-42.5	130.6	-0.511
6883.0	-51.2	143.2	-0.666
7478.0	-54.5	148.9	-0.416
7656.0	-55.0	149.9	-0.265
8731.0	-54.0	153.5	-0.394
20466.0	-47.0	183.9	

NEUTRAL HEIGHT BETWEEN 25. M AND 0.M.

ICE CRYSTAL DISPLAY

SOUNDING 3, ICE ABSORPTION 0.08000/M, DISPLAY DEPTH 2308. M

HEIGHT (M)	TEMPERATURE (DEG C)	FLUX (CAL/SQ CM/12 HR)	MEAN HEATING RATE, LAYER ABOVE Z (DEG C/12 HR)
0.0	-28.0	-0.0	-0.0
25.0	-28.0	-0.0	-0.0
50.0	-28.0	-0.0	-0.000
75.0	-28.0	0.0	-0.000
100.0	-28.0	0.0	-0.000
200.0	-28.0	0.0	-0.000
400.0	-28.0	0.0	-0.000
600.0	-28.0	0.0	-0.000
1000.0	-28.0	0.0	-0.000
1167.0	-28.0	0.0	-0.000
1602.0	-28.0	0.0	-0.000
2065.0	-28.0	0.0	-15.511
2308.0	-28.0	105.1	-0.570
2358.0	-28.0	105.8	-0.509
2408.0	-28.6	106.5	-0.414
2560.0	-29.3	108.0	-0.440
3086.0	-32.0	113.4	-0.439
3649.0	-35.2	118.8	-0.447
4250.0	-38.3	124.2	-0.294
5402.0	-42.5	130.6	-0.511
6883.0	-51.2	143.2	-0.666
7478.0	-54.5	148.9	-0.416
7656.0	-55.0	149.9	-0.265
8731.0	-54.0	153.5	-0.394
20466.0	-47.0	183.9	

NEUTRAL HEIGHT BETWEEN 25. M AND 0.M.

ICE CRYSTAL DISPLAY

SOUNDING 3, ICE ABSORPTION 0.08000/M, DISPLAY DEPTH 2358. M

HEIGHT (M)	TEMPERATURE (DEG C)	FLUX (CAL/SQ CM/12 HR)	MEAN HEATING RATE, LAYER ABOVE Z (DEG C/12 HR)
0.0	-28.0	-0.0	-0.0
25.0	-28.0	-0.0	-0.0
50.0	-28.0	-0.0	-0.0
75.0	-28.0	-0.0	-0.0
100.0	-28.0	-0.0	-0.000
200.0	-28.0	0.0	-0.000
400.0	-28.0	0.0	-0.000
600.0	-28.0	0.0	-0.000
1000.0	-28.0	0.0	-0.000
1167.0	-28.0	0.0	-0.000
1602.0	-28.0	0.0	-0.000
2065.0	-28.0	0.0	-0.284
2308.0	-28.0	1.9	-75.900
2358.0	-28.0	105.8	-0.509
2408.0	-28.6	106.5	-0.414
2560.0	-29.3	108.0	-0.440
3086.0	-32.0	113.4	-0.439
3649.0	-35.2	118.8	-0.447
4250.0	-38.3	124.2	-0.294
5402.0	-42.5	130.6	-0.511
6883.0	-51.2	143.2	-0.666
7478.0	-54.5	148.9	-0.416
7656.0	-55.0	149.9	-0.265
8731.0	-54.0	153.5	-0.394
20466.0	-47.0	183.9	

NEUTRAL HEIGHT BETWEEN 25. M AND 0.M.

ICE CRYSTAL DISPLAY

SOUNDING 3, ICE ABSORPTION 0.08000/M, DISPLAY DEPTH 2408. M

HEIGHT (M)	TEMPERATURE (DEG C)	FLUX (CAL/SQ CM/12 HR)	MEAN HEATING RATE, LAYER ABOVE Z (DEG C/12 HR)
0.0	-28.0	-0.0	-0.0
25.0	-28.0	-0.0	-0.0
50.0	-28.0	-0.0	-0.0
75.0	-28.0	-0.0	-0.0
100.0	-28.0	-0.0	-0.000
200.0	-28.0	0.0	-0.000
400.0	-28.0	0.0	-0.000
600.0	-28.0	0.0	-0.000
1000.0	-28.0	0.0	-0.000
1167.0	-28.0	0.0	-0.000
1602.0	-28.0	0.0	-0.000
2065.0	-28.0	0.0	-0.006
2308.0	-28.0	0.0	-1.535
2358.0	-28.0	2.1	-75.701
2408.0	-28.6	105.0	-0.469
2560.0	-29.3	106.7	-0.452
3086.0	-32.0	112.2	-0.443
3649.0	-35.2	117.7	-0.449
4250.0	-38.3	123.2	-0.295
5402.0	-42.5	129.6	-0.512
6883.0	-51.2	142.2	-0.666
7478.0	-54.5	147.9	-0.416
7656.0	-55.0	148.9	-0.265
8731.0	-54.0	152.5	-0.394
20466.0	-47.0	182.9	

NEUTRAL HEIGHT BETWEEN 25. M AND 0.M.

C. Ice Fog Results

The ice fog program with scattering included proved to be very time-consuming, requiring around two hours on the IBM 360 computer for a single complete sounding. (In contrast, the gray program required less than a minute per sounding, taking slightly over 14 minutes to compute the cooling rates for all heights for 27 combinations of fog height, number density, size distribution and degree of blackness.) Furthermore, the formula for $\frac{dF}{dz}$ proved to be computationally unstable at the intervals of z used. It is probable that a modified (and stable) program can be written for dF/dz at some time in the future. At the present time, $\frac{dF}{dz}$ is being approximated by $\frac{\Delta F}{\Delta z}$.

It is clearly not practical to attempt to run all of the eleven cases in Table IV-12 for both soundings. Consequently, the scattering program was run for five cases near the diagonal of Table IV-12: $n_a = 100$, $z = 10$ m; $n_a = 200$, $z = 20$ m; $n_b = 200$, $z = 20$ m; $n_b = 500$, $z = 50$ m; and $n_b = 1000$, $z = 100$ m. The composite sounding for terminal ice fog was used in all cases. The complete set of ice fog cases was run using the gray program. All soundings which showed any tendency toward destabilization (neutral height in the fog layer) were then rerun with the initial lapse rate in the fog replaced by an adiabatic lapse rate, maintaining the same temperature at the top of the fog. If the neutral height (page IV-34) remained inside the fog layer, that particular case was considered to be convectively unstable.

In order to obtain a series of absorption coefficients for use in the gray formula, the possible black coefficients were taken from

Table IV-13. They are .00168 and .00336 for distribution a, and .00666, .01665 and.0333 for distribution b. Assume that the lowest probable effective absorption coefficient is .25 times the lowest value for each distribution, and the highest probable value is the black value for the highest number density. Then we can select values to cover the range between. The resulting values of k are .0004, .0008, .0016 and .0032 for distribution a, and .001, .002, .004, .008, .016 and .032 for distribution b. In practice the transmissivity was obtained from $\tau(\text{ice}) = \exp(-1.6\ k\Delta z)$, and the transmissivity actually listed on the computer printout is 1.6 k.

Once an approximate value of k was established by comparing the results from the values above with those from the scattering formula, a final set of values was calculated with the k's spaced more closely.

The first of the following tables gives the clear-air cooling rates as obtained from the gray formula. Note that the values below 2 m are questionable, as will be discussed in Chapter VI. The next five sets of tables give the results from the scattering theory, followed by those from the gray formula which give the best agreement with the scattering results. In the thicker fog layers, the shape of the cooling curve was sometimes best approximated by a different absorption coefficient then the magnitude and both curves are included. In those cases where there appeared to be a possibility of destabilization of the lapse rate,the non-scattering computations for adiabatic lapse rates in the fog layer are presented. The section on terminal ice fog concludes with the non-scattering results for absorption coefficients which did not closely correspond to any of the five cases for which scattering computations were made.

Finally, the results for the initial ice fog sounding using the gray absorption coefficients are presented.

1. TERMINAL ICE FOG.

A. COOLING RATES WITHOUT ICE FOG.

ICE FOG

SOUNDING 5, ICE ABSORPTION 0.00064/M, FOG DEPTH 0. M

HEIGHT (M)	TEMPERATURE (DEG C)	FLUX (CAL/SQ CM/12 HR)	MEAN HEATING RATE, LAYER ABOVE Z (DEG C/12 HR)
0.0	-50.0	31.5	5.343
0.5	-47.0	31.4	-1.783
1.0	-45.0	31.5	-2.857
2.0	-44.0	31.6	-3.273
5.0	-43.5	31.9	-0.777
10.0	-43.0	32.1	-0.217
15.0	-42.0	32.1	-0.415
20.0	-41.0	32.2	-0.268
30.0	-40.0	32.3	-0.245
40.0	-38.0	32.4	-0.859
50.0	-36.0	32.7	-1.616
60.0	-34.0	33.2	-1.719
80.0	-33.0	34.4	-1.341
100.0	-32.0	35.4	-1.326
139.0	-30.6	37.2	-1.072
213.0	-28.0	39.8	-0.904
287.0	-27.6	42.0	-0.605
438.0	-27.0	45.0	-0.399
829.0	-25.3	49.9	-0.375
1246.0	-23.6	54.5	-0.445
1690.0	-22.0	59.9	-0.504
2164.0	-23.3	66.1	-0.408
2667.0	-26.6	71.1	-0.472
3783.0	-28.0	82.8	-0.580
5071.0	-36.0	97.0	-0.554
6588.0	-45.7	110.6	-0.514
8047.0	-55.0	120.7	-0.641
8459.0	-55.0	123.9	-0.337
19908.0	-55.0	149.7	

NEUTRAL HEIGHT AT OR ABOVE TOP OF FOG.

B. COMPARISON OF SCATTERING AND GRAY RESULTS.

ATMOSPHERIC HEATING RATES

ATMOSPHERE TERMINAL ICE FOG

CRYSTAL DENSITY 100/CC

SIZE DISTRIBUTION A

FOG DEPTH 10.

HEIGHT METERS	FLUX (CAL/SQ CM/12 HR)	RADIATIVE HEATING (DEG/12 HR)	CONDUCTIVE HEATING (DEG/12 HR)
0.0	26.9	7.106	0.0
0.5	26.8	-4.808	-2.572
1.0	26.9	-7.163	-2.592
2.0	27.2	-4.064	-0.271
5.0	27.6	-1.621	-0.011
10.0	27.9	-0.089	0.013
15.0	27.9	-0.508	0.0
20.0	28.0	-0.148	-0.009
30.0	28.1	-0.125	0.007
40.0	28.1	-0.790	0.0
50.0	28.4	-1.690	0.0
60.0	29.0	-1.698	-0.007
80.0	30.2	-1.214	0.0
100.0	31.0	-0.945	-0.000
139.0	32.3	-1.018	-0.000
213.0	34.8	-0.939	-0.000
287.0	37.1	-0.558	-0.000
438.0	39.9	-0.383	0.000
829.0	44.6	-0.378	-0.000
1246.0	49.2	-0.486	-0.000
1690.0	55.1	-0.569	-0.000
2164.0	62.1	-0.413	-0.000
2667.0	67.2	-0.508	0.000
3783.0	79.7	-0.624	-0.000
5071.0	95.0	-0.550	-0.000
6588.0	108.5	-0.464	0.000
8047.0	117.6	-0.479	0.000
8459.0	120.0	-0.367	0.0
19908.0	148.2		0.0

ICE FOG

SOUNDING 5, ICE ABSORPTION 0.00064/M, FOG DEPTH 10. M

HEIGHT (M)	TEMPERATURE (DEG C)	FLUX (CAL/SQ CM/12 HR)	MEAN HEATING RATE, LAYER ABOVE Z (DEG C/12 HR)
0.0	-50.0	31.8	5.982
0.5	-47.0	31.6	-2.817
1.0	-45.0	31.7	-6.568
2.0	-44.0	31.9	-4.200
5.0	-43.5	32.4	-1.057
10.0	-43.0	32.6	0.420
15.0	-42.0	32.5	-0.114
20.0	-41.0	32.6	-0.037
30.0	-40.0	32.6	-0.161
40.0	-38.0	32.6	-0.716
50.0	-36.0	32.9	-1.577
60.0	-34.0	33.4	-1.684
80.0	-33.0	34.6	-1.317
100.0	-32.0	35.5	-1.305
139.0	-30.6	37.3	-1.064
213.0	-28.0	39.9	-0.901
287.0	-27.6	42.1	-0.603
438.0	-27.0	45.1	-0.398
829.0	-25.3	50.0	-0.375
1246.0	-23.6	54.6	-0.445
1690.0	-22.0	60.0	-0.504
2164.0	-23.3	66.2	-0.408
2667.0	-26.6	71.2	-0.472
3783.0	-28.0	82.8	-0.579
5071.0	-36.0	97.1	-0.554
6588.0	-45.7	110.7	-0.514
8047.0	-55.0	120.8	-0.641
8459.0	-55.0	123.9	-0.337
19908.0	-55.0	149.8	

NEUTRAL HEIGHT AT OR ABOVE TOP OF FOG.
EFFECTIVE ABSORPTION .25 OF BLACK.

ATMOSPHERIC HEATING RATES

ATMOSPHERE TERMINAL ICE FOG

CRYSTAL DENSITY 200/CC

SIZE DISTRIBUTION A

FOG DEPTH 20.

HEIGHT METERS	FLUX (CAL/SQ CM/12 HR)	RADIATIVE HEATING (DEG/12 HR)	CONDUCTIVE HEATING (DEG/12 HR)
0.0	25.4	6.124	0.0
0.5	25.3	-5.810	-2.426
1.0	25.4	-8.355	-2.445
2.0	25.7	-5.357	-0.256
5.0	26.3	-3.003	-0.010
10.0	26.9	-3.119	0.012
15.0	27.4	-3.677	0.0
20.0	28.1	-0.182	-0.008
30.0	28.2	-0.118	0.006
40.0	28.2	-0.778	0.0
50.0	28.5	-1.682	0.0
60.0	29.1	-1.688	-0.007
80.0	30.3	-1.206	0.0
100.0	31.1	-0.939	-0.000
139.0	32.4	-1.014	-0.000
213.0	34.9	-0.936	-0.000
287.0	37.2	-0.556	-0.000
438.0	39.9	-0.382	0.000
829.0	44.6	-0.378	-0.000
1246.0	49.2	-0.486	-0.000
1690.0	55.2	-0.569	-0.000
2164.0	62.1	-0.412	-0.000
2667.0	67.2	-0.507	0.000
3783.0	79.7	-0.623	-0.000
5071.0	95.0	-0.549	-0.000
6588.0	108.5	-0.464	0.000
8047.0	117.6	-0.479	0.000
8459.0	120.0	-0.367	0.0
19908.0	148.2		0.0

ICE FOG

SOUNDING 5, ICE ABSORPTION 0.00128/M, FOG DEPTH 20. M

HEIGHT (M)	TEMPERATURE (DEG C)	FLUX (CAL/SQ CM/12 HR)	MEAN HEATING RATE, LAYER ABOVE Z (DEG C/12 HR)
0.0	-50.0	31.1	5.133
0.5	-47.0	31.0	-3.880
1.0	-45.0	31.0	-7.866
2.0	-44.0	31.3	-5.600
5.0	-43.5	32.0	-2.756
10.0	-43.0	32.5	-2.098
15.0	-42.0	32.9	-2.132
20.0	-41.0	33.3	0.246
30.0	-40.0	33.2	0.067
40.0	-38.0	33.1	-0.614
50.0	-36.0	33.4	-1.489
60.0	-34.0	33.9	-1.626
80.0	-33.0	35.0	-1.278
100.0	-32.0	35.9	-1.273
139.0	-30.6	37.6	-1.050
213.0	-28.0	40.2	-0.893
287.0	-27.6	42.4	-0.599
438.0	-27.0	45.4	-0.396
829.0	-25.3	50.2	-0.374
1246.0	-23.6	54.8	-0.444
1690.0	-22.0	60.2	-0.504
2164.0	-23.3	66.4	-0.407
2667.0	-26.6	71.4	-0.472
3783.0	-28.0	83.0	-0.579
5071.0	-36.0	97.2	-0.554
6588.0	-45.7	110.9	-0.514
8047.0	-55.0	121.0	-0.641
8459.0	-55.0	124.1	-0.337
19908.0	-55.0	150.0	

NEUTRAL HEIGHT AT OR ABOVE TOP OF FOG.
EFFECTIVE ABSORPTION .25 OF BLACK.

ATMOSPHERIC HEATING RATES

ATMOSPHERE TERMINAL ICE FOG

CRYSTAL DENSITY 200/CC

SIZE DISTRIBUTION B

FOG DEPTH 20.

HEIGHT METERS	FLUX (CAL/SQ CM/12 HR)	RADIATIVE HEATING (DEG/12 HR)	CONDUCTIVE HEATING (DEG/12 HR)
0.0	22.0	3.194	0.0
0.5	21.9	-9.185	-2.097
1.0	22.1	-12.328	-2.113
2.0	22.5	-9.680	-0.221
5.0	23.6	-7.647	-0.009
10.0	25.0	-8.321	0.011
15.0	26.6	-9.632	0.0
20.0	28.4	-0.153	-0.007
30.0	28.4	-0.083	0.006
40.0	28.5	-0.751	0.0
50.0	28.7	-1.660	0.0
60.0	29.3	-1.663	-0.006
80.0	30.5	-1.188	0.0
100.0	31.3	-0.926	-0.000
139.0	32.5	-1.006	-0.000
213.0	35.0	-0.930	-0.000
287.0	37.3	-0.552	-0.000
438.0	40.0	-0.380	0.000
829.0	44.7	-0.377	-0.000
1246.0	49.3	-0.485	-0.000
1690.0	55.2	-0.568	-0.000
2164.0	62.2	-0.411	-0.000
2667.0	67.2	-0.506	0.000
3783.0	79.7	-0.622	-0.000
5071.0	95.0	-0.548	-0.000
6588.0	108.4	-0.463	0.000
8047.0	117.6	-0.479	0.000
8459.0	119.9	-0.367	0.0
19908.0	148.1		0.0

ICE FOG

SOUNDING 5, ICE ABSORPTION 0.00512/M, FOG DEPTH 20. M

HEIGHT (M)	TEMPERATURE (DEG C)	FLUX (CAL/SQ CM/12 HR)	MEAN HEATING RATE, LAYER ABOVE Z (DEG C/12 HR)
0.0	-50.0	27.4	1.604
0.5	-47.0	27.4	-8.739
1.0	-45.0	27.6	-13.545
2.0	-44.0	28.1	-11.657
5.0	-43.5	29.4	-9.069
10.0	-43.0	31.1	-8.817
15.0	-42.0	32.7	-9.407
20.0	-41.0	34.4	0.296
30.0	-40.0	34.3	0.109
40.0	-38.0	34.3	-0.573
50.0	-36.0	34.5	-1.450
60.0	-34.0	35.0	-1.587
80.0	-33.0	36.1	-1.247
100.0	-32.0	37.0	-1.244
139.0	-30.6	38.6	-1.029
213.0	-28.0	41.2	-0.879
287.0	-27.6	43.4	-0.589
438.0	-27.0	46.3	-0.391
829.0	-25.3	51.1	-0.370
1246.0	-23.6	55.6	-0.442
1690.0	-22.0	61.0	-0.502
2164.0	-23.3	67.1	-0.406
2667.0	-26.6	72.1	-0.471
3783.0	-28.0	83.7	-0.579
5071.0	-36.0	98.0	-0.554
6588.0	-45.7	111.6	-0.514
8047.0	-55.0	121.7	-0.641
8459.0	-55.0	124.8	-0.337
19908.0	-55.0	150.7	

NEUTRAL HEIGHT AT OR ABOVE TOP OF FOG.
EFFECTIVE ABSORPTION .50 OF BLACK.

ATMOSPHERIC HEATING RATES

ATMOSPHERE TERMINAL ICE FOG

CRYSTAL DENSITY 500/CC

SIZE DISTRIBUTION B

FOG DEPTH 50.

HEIGHT METERS	FLUX (CAL/SQ CM/12 HR)	RADIATIVE HEATING (DEG/12 HR)	CONDUCTIVE HEATING (DEG/12 HR)
0.0	4.4	3.412	0.0
0.5	4.3	9.354	-0.418
1.0	4.5	-13.916	-0.421
2.0	5.0	-11.895	-0.044
5.0	6.3	-10.208	-0.002
10.0	8.2	-10.546	0.002
15.0	10.2	-12.323	0.0
20.0	12.5	-13.978	-0.001
30.0	17.7	-17.672	0.001
40.0	24.2	-24.716	0.0
50.0	33.2	-1.264	0.0
60.0	33.7	-1.278	-0.001
80.0	34.6	-0.923	0.0
100.0	35.2	-0.759	-0.000
139.0	36.2	-0.900	-0.000
213.0	38.5	-0.864	-0.000
287.0	40.6	-0.511	-0.000
438.0	43.1	-0.360	0.000
829.0	47.5	-0.366	-0.000
1246.0	52.0	-0.477	-0.000
1690.0	57.8	-0.559	-0.000
2164.0	64.7	-0.402	-0.000
2667.0	69.6	-0.499	0.000
3783.0	81.9	-0.615	-0.000
5071.0	97.0	-0.542	-0.000
6588.0	110.3	-0.459	0.000
8047.0	119.4	-0.476	0.000
8459.0	121.7	-0.366	0.0
19908.0	149.8		0.0

ICE FOG

SOUNDING 5, ICE ABSORPTION 0.00640/M, FOG DEPTH 50. M

HEIGHT (M)	TEMPERATURE (DEG C)	FLUX (CAL/SQ CM/12 HR)	MEAN HEATING RATE, LAYER ABOVE Z (DEG C/12 HR)
0.0	-50.0	17.3	1.886
0.5	-47.0	17.3	-8.888
1.0	-45.0	17.4	-14.015
2.0	-44.0	18.0	-12.279
5.0	-43.5	19.3	-9.876
10.0	-43.0	21.2	-9.912
15.0	-42.0	23.0	-11.009
20.0	-41.0	25.1	-11.787
30.0	-40.0	29.4	-13.141
40.0	-38.0	34.3	-15.496
50.0	-36.0	39.9	-0.715
60.0	-34.0	40.2	-1.143
80.0	-33.0	41.0	-0.981
100.0	-32.0	41.7	-1.024
139.0	-30.6	43.0	-0.909
213.0	-28.0	45.3	-0.807
287.0	-27.6	47.3	-0.544
438.0	-27.0	50.0	-0.367
829.0	-25.3	54.5	-0.356
1246.0	-23.6	58.8	-0.432
1690.0	-22.0	64.1	-0.495
2164.0	-23.3	70.2	-0.401
2667.0	-26.6	75.1	-0.468
3783.0	-28.0	86.6	-0.577
5071.0	-36.0	100.8	-0.553
6588.0	-45.7	114.4	-0.514
8047.0	-55.0	124.5	-0.641
8459.0	-55.0	127.6	-0.337
19908.0	-55.0	153.5	

NEUTRAL HEIGHT AT OR ABOVE TOP OF FOG.
EFFECTIVE ABSORPTION .25 OF BLACK.

ICE FOG

SOUNDING 5, ICE ABSORPTION 0.01600/M, FOG DEPTH 50. M

HEIGHT (M)	TEMPERATURE (DEG C)	FLUX (CAL/SQ CM/12 HR)	MEAN HEATING RATE, LAYER ABOVE Z (DEG C/12 HR)
0.0	-50.0	2.1	1.744
0.5	-47.0	2.1	-12.265
1.0	-45.0	2.3	-19.388
2.0	-44.0	3.0	-18.523
5.0	-43.5	5.1	-16.687
10.0	-43.0	8.2	-17.746
15.0	-42.0	11.5	-20.354
20.0	-41.0	15.3	-22.965
30.0	-40.0	23.8	-27.495
40.0	-38.0	33.9	-34.354
50.0	-36.0	46.5	-0.499
60.0	-34.0	46.7	-0.950
80.0	-33.0	47.3	-0.815
100.0	-32.0	47.9	-0.872
139.0	-30.6	49.1	-0.795
213.0	-28.0	51.1	-0.729
287.0	-27.6	52.8	-0.489
438.0	-27.0	55.3	-0.336
829.0	-25.3	59.4	-0.337
1246.0	-23.6	63.5	-0.418
1690.0	-22.0	68.6	-0.484
2164.0	-23.3	74.5	-0.394
2667.0	-26.6	79.4	-0.463
3783.0	-28.0	90.8	-0.575
5071.0	-36.0	104.9	-0.552
6588.0	-45.7	118.5	-0.513
8047.0	-55.0	128.6	-0.640
8459.0	-55.0	131.7	-0.337
19908.0	-55.0	157.5	

NEUTRAL HEIGHT BETWEEN 5. M AND 2.M.
EFFECTIVE ABSORPTION .75 OF BLACK,
ALBEDO ABOUT .3.

ICE FOG

SOUNDING 5, ICE ABSORPTION 0.01280/M, FOG DEPTH 50. M

HEIGHT (M)	TEMPERATURE (DEG C)	FLUX (CAL/SQ CM/12 HR)	MEAN HEATING RATE, LAYER ABOVE Z (DEG C/12 HR)
0.0	-35.5	37.1	-12.844
0.5	-35.5	37.3	-12.904
1.0	-35.5	37.5	-12.976
2.0	-35.5	38.0	-13.238
5.0	-35.5	39.5	-13.820
10.0	-35.6	42.0	-14.587
15.0	-35.6	44.7	-15.418
20.0	-35.7	47.5	-16.765
30.0	-35.8	53.7	-18.618
40.0	-35.9	60.5	-20.159
50.0	-36.0	67.9	0.555
60.0	-34.0	67.7	-0.135
80.0	-33.0	67.8	-0.180
100.0	-32.0	68.0	-0.312
139.0	-30.6	68.4	-0.409
213.0	-28.0	69.4	-0.472
287.0	-27.6	70.5	-0.312
438.0	-27.0	72.1	-0.238
829.0	-25.3	75.0	-0.276
1246.0	-23.6	78.4	-0.374
1690.0	-22.0	83.0	-0.452
2164.0	-23.3	88.5	-0.372
2667.0	-26.6	93.1	-0.448
3783.0	-28.0	104.1	-0.567
5071.0	-36.0	118.0	-0.548
6588.0	-45.7	131.5	-0.511
8047.0	-55.0	141.6	-0.639
8459.0	-55.0	144.7	-0.336
19908.0	-55.0	170.5	

NEUTRAL HEIGHT AT OR ABOVE TOP OF FOG.

ICE FOG

SOUNDING 5, ICE ABSORPTION 0.02560/M, FOG DEPTH 50. M

HEIGHT (M)	TEMPERATURE (DEG C)	FLUX (CAL/SQ CM/12 HR)	MEAN HEATING RATE, LAYER ABOVE Z (DEG C/12 HR)
0.0	-35.5	19.8	-13.808
0.5	-35.5	20.0	-13.950
1.0	-35.5	20.3	-14.170
2.0	-35.5	20.8	-14.813
5.0	-35.5	22.4	-16.243
10.0	-35.6	25.4	-18.259
15.0	-35.6	28.8	-20.572
20.0	-35.7	32.6	-24.708
30.0	-35.8	41.7	-31.433
40.0	-35.9	53.2	-39.513
50.0	-36.0	67.7	0.546
60.0	-34.0	67.5	-0.143
80.0	-33.0	67.6	-0.187
100.0	-32.0	67.7	-0.318
139.0	-30.6	68.2	-0.413
213.0	-28.0	69.2	-0.474
287.0	-27.6	70.4	-0.314
438.0	-27.0	71.9	-0.239
829.0	-25.3	74.8	-0.276
1246.0	-23.6	78.2	-0.375
1690.0	-22.0	82.8	-0.452
2164.0	-23.3	88.3	-0.372
2667.0	-26.6	92.9	-0.449
3783.0	-28.0	104.0	-0.567
5071.0	-36.0	117.9	-0.548
6588.0	-45.7	131.3	-0.511
8047.0	-55.0	141.4	-0.639
8459.0	-55.0	144.5	-0.336
19908.0	-55.0	170.4	

NEUTRAL HEIGHT BETWEEN 20. M AND 15.M.

ATMOSPHERIC HEATING RATES

ATMOSPHERE TERMINAL ICE FOG

CRYSTAL DENSITY 1000/CC

SIZE DISTRIBUTION B

FOG DEPTH 100.

HEIGHT METERS	FLUX (CAL/SQ CM/12 HR)	RADIATIVE HEATING (DEG/12 HR)	CONDUCTIVE HEATING (DEG/12 HR)
0.0	-14.6	9.578	********
0.5	-14.7	-4.471	********
1.0	-14.7	-10.654	********
2.0	-14.3	-8.593	********
5.0	-13.3	-5.330	********
10.0	-12.3	-4.642	********
15.0	-11.4	-6.110	********
20.0	-10.3	-5.802	********
30.0	-8.2	-6.999	********
40.0	-5.6	-10.540	********
50.0	-1.7	-15.402	********
60.0	3.9	-20.902	********
80.0	19.2	-38.030	********
100.0	46.9	-0.594	********
139.0	47.7	-0.715	********
213.0	49.5	-0.732	********
287.0	51.3	-0.422	********
438.0	53.4	-0.312	********
829.0	57.2	-0.338	********
1246.0	61.3	-0.456	********
1690.0	66.9	-0.539	********
2164.0	73.5	-0.385	********
2667.0	78.2	-0.485	********
3783.0	90.2	-0.603	********
5071.0	105.0	-0.534	********
6588.0	118.1	-0.454	********
8047.0	127.1	-0.472	********
8459.0	129.4	-0.364	********
19908.0	157.3		********

* CONDUCTIVITY EQUATION INAPPLICABLE

ICE FOG

SOUNDING 5, ICE ABSORPTION 0.01280/M, FOG DEPTH 100. M

HEIGHT (M)	TEMPERATURE (DEG C)	FLUX (CAL/SQ CM/12 HR)	MEAN HEATING RATE, LAYER ABOVE Z (DEG C/12 HR)
0.0	-50.0	-12.2	7.418
0.5	-47.0	-12.3	-5.426
1.0	-45.0	-12.2	-11.824
2.0	-44.0	-11.8	-10.516
5.0	-43.5	-10.6	-8.179
10.0	-43.0	-9.1	-8.473
15.0	-42.0	-7.5	-10.104
20.0	-41.0	-5.6	-11.303
30.0	-40.0	-1.4	-13.605
40.0	-38.0	3.6	-17.776
50.0	-36.0	10.1	-22.586
60.0	-34.0	18.4	-26.450
80.0	-33.0	37.7	-30.829
100.0	-32.0	60.2	-0.274
139.0	-30.6	60.5	-0.488
213.0	-28.0	61.7	-0.546
287.0	-27.6	63.1	-0.373
438.0	-27.0	64.9	-0.276
829.0	-25.3	68.3	-0.301
1246.0	-23.6	72.0	-0.393
1690.0	-22.0	76.8	-0.465
2164.0	-23.3	82.5	-0.381
2667.0	-26.6	87.2	-0.455
3783.0	-28.0	98.4	-0.570
5071.0	-36.0	112.4	-0.550
6588.0	-45.7	125.9	-0.512
8047.0	-55.0	136.0	-0.639
8459.0	-55.0	139.1	-0.336
19908.0	-55.0	164.9	

NEUTRAL HEIGHT BETWEEN 1. M AND 0.M.
EFFECTIVE ABSORPTION .25 OF BLACK.

ICE FOG

SOUNDING 5, ICE ABSORPTION 0.01280/M, FOG DEPTH 100. M

HEIGHT (M)	TEMPERATURE (DEG C)	FLUX (CAL/SQ CM/12 HR)	MEAN HEATING RATE, LAYER ABOVE Z (DEG C/12 HR)
0.0	-31.0	23.4	-8.219
0.5	-31.0	23.6	-8.244
1.0	-31.0	23.7	-8.308
2.0	-31.0	24.0	-8.465
5.0	-31.0	25.0	-8.821
10.0	-31.1	26.6	-9.301
15.0	-31.1	28.3	-9.821
20.0	-31.2	30.1	-10.689
30.0	-31.3	34.1	-12.002
40.0	-31.4	38.5	-13.509
50.0	-31.5	43.4	-15.216
60.0	-31.6	49.0	-18.279
80.0	-31.8	62.4	-23.247
100.0	-32.0	79.3	0.271
139.0	-30.6	79.0	-0.138
213.0	-28.0	79.3	-0.310
287.0	-27.6	80.1	-0.210
438.0	-27.0	81.1	-0.184
829.0	-25.3	83.3	-0.243
1246.0	-23.6	86.3	-0.351
1690.0	-22.0	90.6	-0.435
2164.0	-23.3	95.9	-0.360
2667.0	-26.6	100.4	-0.441
3783.0	-28.0	111.2	-0.563
5071.0	-36.0	125.0	-0.547
6588.0	-45.7	138.5	-0.510
8047.0	-55.0	148.5	-0.638
8459.0	-55.0	151.6	-0.336
19908.0	-55.0	177.4	

NEUTRAL HEIGHT BETWEEN 40. M AND 30.M.

ICE FOG

SOUNDING 5, ICE ABSORPTION 0.03840/M, FOG DEPTH 100. M

HEIGHT (M)	TEMPERATURE (DEG C)	FLUX (CAL/SQ CM/12 HR)	MEAN HEATING RATE, LAYER ABOVE Z (DEG C/12 HR)
0.0	-50.0	-22.4	20.633
0.5	-47.0	-22.8	-0.350
1.0	-45.0	-22.8	-11.333
2.0	-44.0	-22.4	-10.689
5.0	-43.5	-21.2	-6.639
10.0	-43.0	-20.0	-5.570
15.0	-42.0	-18.9	-7.020
20.0	-41.0	-17.6	-6.605
30.0	-40.0	-15.2	-8.095
40.0	-38.0	-12.2	-14.387
50.0	-36.0	-6.9	-23.371
60.0	-34.0	1.6	-34.741
80.0	-33.0	27.0	-62.617
100.0	-32.0	72.7	0.024
139.0	-30.6	72.6	-0.276
213.0	-28.0	73.3	-0.398
287.0	-27.6	74.3	-0.268
438.0	-27.0	75.6	-0.216
829.0	-25.3	78.2	-0.262
1246.0	-23.6	81.5	-0.365
1690.0	-22.0	85.9	-0.445
2164.0	-23.3	91.4	-0.367
2667.0	-26.6	95.9	-0.445
3783.0	-28.0	106.9	-0.566
5071.0	-36.0	120.7	-0.548
6588.0	-45.7	134.2	-0.511
8047.0	-55.0	144.3	-0.639
8459.0	-55.0	147.4	-0.336
19908.0	-55.0	173.2	

NEUTRAL HEIGHT BETWEEN 1. M AND 0.M.
EFFECTIVE ABSORPTION .75 OF BLACK,
ALBEDO ABOUT .4.

ICE FOG

SOUNDING 5, ICE ABSORPTION 0.02560/M, FOG DEPTH 100. M

HEIGHT (M)	TEMPERATURE (DEG C)	FLUX (CAL/SQ CM/12 HR)	MEAN HEATING RATE, LAYER ABOVE Z (DEG C/12 HR)
0.0	-31.0	7.1	-5.012
0.5	-31.0	7.2	-5.040
1.0	-31.0	7.3	-5.104
2.0	-31.0	7.5	-5.275
5.0	-31.0	8.0	-5.685
10.0	-31.1	9.1	-6.284
15.0	-31.1	10.3	-6.989
20.0	-31.2	11.5	-8.293
30.0	-31.3	14.6	-10.511
40.0	-31.4	18.5	-13.425
50.0	-31.5	23.4	-17.212
60.0	-31.6	29.7	-25.319
80.0	-31.8	48.2	-41.930
100.0	-32.0	78.8	0.257
139.0	-30.6	78.4	-0.148
213.0	-28.0	78.8	-0.317
287.0	-27.6	79.6	-0.214
438.0	-27.0	80.6	-0.186
829.0	-25.3	82.9	-0.244
1246.0	-23.6	85.9	-0.352
1690.0	-22.0	90.2	-0.435
2164.0	-23.3	95.6	-0.360
2667.0	-26.6	100.0	-0.441
3783.0	-28.0	110.9	-0.563
5071.0	-36.0	124.7	-0.547
6588.0	-45.7	138.1	-0.510
8047.0	-55.0	148.2	-0.638
8459.0	-55.0	151.3	-0.336
19908.0	-55.0	177.1	

NEUTRAL HEIGHT BETWEEN 10. M AND 5. M.

ICE FOG

SOUNDING 5, ICE ABSORPTION 0.00128/M, FOG DEPTH 10. M

HEIGHT (M)	TEMPERATURE (DEG C)	FLUX (CAL/SQ CM/12 HR)	MEAN HEATING RATE, LAYER ABOVE Z (DEG C/12 HR)
0.0	-50.0	31.5	5.312
0.5	-47.0	31.4	-3.706
1.0	-45.0	31.4	-7.590
2.0	-44.0	31.7	-5.279
5.0	-43.5	32.3	-2.167
10.0	-43.0	32.7	0.425
15.0	-42.0	32.6	-0.109
20.0	-41.0	32.6	-0.033
30.0	-40.0	32.7	-0.157
40.0	-38.0	32.7	-0.712
50.0	-36.0	33.0	-1.574
60.0	-34.0	33.5	-1.681
80.0	-33.0	34.7	-1.315
100.0	-32.0	35.6	-1.303
139.0	-30.6	37.3	-1.063
213.0	-28.0	40.0	-0.899
287.0	-27.6	42.2	-0.602
438.0	-27.0	45.2	-0.398
829.0	-25.3	50.0	-0.375
1246.0	-23.6	54.6	-0.445
1690.0	-22.0	60.1	-0.504
2164.0	-23.3	66.2	-0.407
2667.0	-26.6	71.2	-0.472
3783.0	-28.0	82.9	-0.579
5071.0	-36.0	97.1	-0.554
6588.0	-45.7	110.7	-0.514
8047.0	-55.0	120.8	-0.641
8459.0	-55.0	124.0	-0.337
19908.0	-55.0	149.8	

NEUTRAL HEIGHT AT OR ABOVE TOP OF FOG.

ICE FOG

SOUNDING 5, ICE ABSORPTION 0.00256/M, FOG DEPTH 10. M

HEIGHT (M)	TEMPERATURE (DEG C)	FLUX (CAL/SQ CM/12 HR)	MEAN HEATING RATE, LAYER ABOVE Z (DEG C/12 HR)
0.0	-50.0	30.9	4.010
0.5	-47.0	30.8	-5.451
1.0	-45.0	30.9	-9.608
2.0	-44.0	31.2	-7.414
5.0	-43.5	32.1	-4.370
10.0	-43.0	32.9	0.437
15.0	-42.0	32.8	-0.099
20.0	-41.0	32.8	-0.025
30.0	-40.0	32.8	-0.149
40.0	-38.0	32.9	-0.706
50.0	-36.0	33.1	-1.568
60.0	-34.0	33.7	-1.675
80.0	-33.0	34.9	-1.310
100.0	-32.0	35.8	-1.298
139.0	-30.6	37.5	-1.059
213.0	-28.0	40.1	-0.897
287.0	-27.6	42.4	-0.601
438.0	-27.0	45.3	-0.397
829.0	-25.3	50.2	-0.374
1246.0	-23.6	54.7	-0.444
1690.0	-22.0	60.2	-0.504
2164.0	-23.3	66.4	-0.407
2667.0	-26.6	71.4	-0.472
3783.0	-28.0	83.0	-0.579
5071.0	-36.0	97.2	-0.554
6588.0	-45.7	110.8	-0.514
8047.0	-55.0	120.9	-0.641
8459.0	-55.0	124.1	-0.337
19908.0	-55.0	150.0	

NEUTRAL HEIGHT AT OR ABOVE TOP OF FOG.

ICE FOG

SOUNDING 5, ICE ABSORPTION 0.00512/M, FOG DEPTH 10. M

HEIGHT (M)	TEMPERATURE (DEG C)	FLUX (CAL/SQ CM/12 HR)	MEAN HEATING RATE, LAYER ABOVE Z (DEG C/12 HR)
0.0	-50.0	29.7	1.524
0.5	-47.0	29.6	-8.829
1.0	-45.0	29.8	-13.534
2.0	-44.0	30.3	-11.592
5.0	-43.5	31.6	-8.718
10.0	-43.0	33.2	0.459
15.0	-42.0	33.2	-0.080
20.0	-41.0	33.2	-0.010
30.0	-40.0	33.2	-0.134
40.0	-38.0	33.2	-0.693
50.0	-36.0	33.5	-1.556
60.0	-34.0	34.0	-1.663
80.0	-33.0	35.2	-1.300
100.0	-32.0	36.1	-1.289
139.0	-30.6	37.8	-1.053
213.0	-28.0	40.4	-0.893
287.0	-27.6	42.6	-0.598
438.0	-27.0	45.6	-0.395
829.0	-25.3	50.4	-0.373
1246.0	-23.6	55.0	-0.444
1690.0	-22.0	60.4	-0.503
2164.0	-23.3	66.6	-0.407
2667.0	-26.6	71.6	-0.472
3783.0	-28.0	83.2	-0.579
5071.0	-36.0	97.4	-0.554
6588.0	-45.7	111.0	-0.514
8047.0	-55.0	121.2	-0.641
8459.0	-55.0	124.3	-0.337
19908.0	-55.0	150.2	

NEUTRAL HEIGHT AT OR ABOVE TOP OF FOG.

ICE FOG

SOUNDING 5, ICE ABSORPTION 0.00064/M, FOG DEPTH 20. M

HEIGHT (M)	TEMPERATURE (DEG C)	FLUX (CAL/SQ CM/12 HR)	MEAN HEATING RATE, LAYER ABOVE Z (DEG C/12 HR)
0.0	-50.0	31.7	5.791
0.5	-47.0	31.6	-2.998
1.0	-45.0	31.6	-6.849
2.0	-44.0	31.9	-4.526
5.0	-43.5	32.4	-1.648
10.0	-43.0	32.7	-0.934
15.0	-42.0	32.9	-0.889
20.0	-41.0	33.0	0.238
30.0	-40.0	33.0	0.060
40.0	-38.0	32.9	-0.621
50.0	-36.0	33.2	-1.496
60.0	-34.0	33.7	-1.632
80.0	-33.0	34.8	-1.283
100.0	-32.0	35.7	-1.278
139.0	-30.6	37.4	-1.053
213.0	-28.0	40.1	-0.895
287.0	-27.6	42.3	-0.600
438.0	-27.0	45.2	-0.397
829.0	-25.3	50.1	-0.374
1246.0	-23.6	54.7	-0.445
1690.0	-22.0	60.1	-0.504
2164.0	-23.3	66.3	-0.407
2667.0	-26.6	71.3	-0.472
3783.0	-28.0	82.9	-0.579
5071.0	-36.0	97.1	-0.554
6588.0	-45.7	110.7	-0.514
8047.0	-55.0	120.9	-0.641
8459.0	-55.0	124.0	-0.337
19908.0	-55.0	149.9	

NEUTRAL HEIGHT AT OR ABOVE TOP OF FOG.

ICE FOG

SOUNDING 5, ICE ABSORPTION 0.00160/M, FOG DEPTH 20. M

HEIGHT (M)	TEMPERATURE (DEG C)	FLUX (CAL/SQ CM/12 HR)	MEAN HEATING RATE, LAYER ABOVE Z (DEG C/12 HR)
0.0	-50.0	30.7	4.812
0.5	-47.0	30.7	-4.310
1.0	-45.0	30.7	-8.365
2.0	-44.0	31.0	-6.131
5.0	-43.5	31.7	-3.304
10.0	-43.0	32.3	-2.674
15.0	-42.0	32.8	-2.750
20.0	-41.0	33.4	0.251
30.0	-40.0	33.3	0.071
40.0	-38.0	33.2	-0.611
50.0	-36.0	33.5	-1.486
60.0	-34.0	34.0	-1.623
80.0	-33.0	35.1	-1.275
100.0	-32.0	36.0	-1.270
139.0	-30.6	37.7	-1.048
213.0	-28.0	40.3	-0.892
287.0	-27.6	42.5	-0.598
438.0	-27.0	45.4	-0.396
829.0	-25.3	50.3	-0.373
1246.0	-23.6	54.9	-0.444
1690.0	-22.0	60.3	-0.503
2164.0	-23.3	66.5	-0.407
2667.0	-26.6	71.5	-0.472
3783.0	-28.0	83.1	-0.579
5071.0	-36.0	97.3	-0.554
6588.0	-45.7	110.9	-0.514
8047.0	-55.0	121.0	-0.641
8459.0	-55.0	124.2	-0.337
19908.0	-55.0	150.0	

NEUTRAL HEIGHT AT OR ABOVE TOP OF FOG.

ICE FOG

SOUNDING 5, ICE ABSORPTION 0.00256/M, FOG DEPTH 20. M

HEIGHT (M)	TEMPERATURE (DEG C)	FLUX (CAL/SQ CM/12 HR)	MEAN HEATING RATE, LAYER ABOVE Z (DEG C/12 HR)
0.0	-50.0	29.8	3.878
0.5	-47.0	29.7	-5.579
1.0	-45.0	29.8	-9.836
2.0	-44.0	30.2	-7.693
5.0	-43.5	31.1	-4.923
10.0	-43.0	32.0	-4.387
15.0	-42.0	32.8	-4.591
20.0	-41.0	33.7	0.263
30.0	-40.0	33.6	0.082
40.0	-38.0	33.5	-0.600
50.0	-36.0	33.7	-1.476
60.0	-34.0	34.3	-1.613
80.0	-33.0	35.4	-1.267
100.0	-32.0	36.3	-1.263
139.0	-30.6	38.0	-1.043
213.0	-28.0	40.6	-0.888
287.0	-27.6	42.7	-0.595
438.0	-27.0	45.7	-0.394
829.0	-25.3	50.5	-0.373
1246.0	-23.6	55.1	-0.443
1690.0	-22.0	60.5	-0.503
2164.0	-23.3	66.7	-0.407
2667.0	-26.6	71.6	-0.472
3783.0	-28.0	83.3	-0.579
5071.0	-36.0	97.5	-0.554
6588.0	-45.7	111.1	-0.514
8047.0	-55.0	121.2	-0.641
8459.0	-55.0	124.4	-0.337
19908.0	-55.0	150.2	

NEUTRAL HEIGHT AT OR ABOVE TOP OF FOG.

ICE FOG

SOUNDING 5, ICE ABSORPTION 0.00320/M, FOG DEPTH 20. M

HEIGHT (M)	TEMPERATURE (DEG C)	FLUX (CAL/SQ CM/12 HR)	MEAN HEATING RATE, LAYER ABOVE Z (DEG C/12 HR)
0.0	-50.0	29.2	3.278
0.5	-47.0	29.1	-6.393
1.0	-45.0	29.3	-10.792
2.0	-44.0	29.7	-8.711
5.0	-43.5	30.6	-5.983
10.0	-43.0	31.8	-5.513
15.0	-42.0	32.8	-5.808
20.0	-41.0	33.9	0.272
30.0	-40.0	33.8	0.089
40.0	-38.0	33.7	-0.593
50.0	-36.0	33.9	-1.469
60.0	-34.0	34.5	-1.606
80.0	-33.0	35.6	-1.262
100.0	-32.0	36.5	-1.258
139.0	-30.6	38.1	-1.039
213.0	-28.0	40.7	-0.886
287.0	-27.6	42.9	-0.594
438.0	-27.0	45.8	-0.393
829.0	-25.3	50.6	-0.372
1246.0	-23.6	55.2	-0.443
1690.0	-22.0	60.6	-0.503
2164.0	-23.3	66.8	-0.407
2667.0	-26.6	71.8	-0.472
3783.0	-28.0	83.4	-0.579
5071.0	-36.0	97.6	-0.554
6588.0	-45.7	111.2	-0.514
8047.0	-55.0	121.3	-0.641
8459.0	-55.0	124.5	-0.337
19908.0	-55.0	150.3	

NEUTRAL HEIGHT AT OR ABOVE TOP OF FOG.

ICE FOG

SOUNDING 5, ICE ABSORPTION 0.00640/M, FOG DEPTH 20. M

HEIGHT (M)	TEMPERATURE (DEG C)	FLUX (CAL/SQ CM/12 HR)	MEAN HEATING RATE, LAYER ABOVE Z (DEG C/12 HR)
0.0	-50.0	26.3	0.586
0.5	-47.0	26.3	-10.206
1.0	-45.0	26.5	-15.288
2.0	-44.0	27.0	-13.533
5.0	-43.5	28.5	-11.050
10.0	-43.0	30.6	-10.960
15.0	-42.0	32.6	-11.766
20.0	-41.0	34.8	0.312
30.0	-40.0	34.7	0.123
40.0	-38.0	34.7	-0.560
50.0	-36.0	34.9	-1.438
60.0	-34.0	35.4	-1.575
80.0	-33.0	36.5	-1.238
100.0	-32.0	37.3	-1.235
139.0	-30.6	39.0	-1.023
213.0	-28.0	41.5	-0.875
287.0	-27.6	43.7	-0.586
438.0	-27.0	46.6	-0.389
829.0	-25.3	51.3	-0.369
1246.0	-23.6	55.9	-0.441
1690.0	-22.0	61.2	-0.501
2164.0	-23.3	67.4	-0.406
2667.0	-26.6	72.4	-0.471
3783.0	-28.0	84.0	-0.579
5071.0	-36.0	98.2	-0.554
6588.0	-45.7	111.8	-0.514
8047.0	-55.0	121.9	-0.641
8459.0	-55.0	125.0	-0.337
19908.0	-55.0	150.9	

NEUTRAL HEIGHT AT OR ABOVE TOP OF FOG.

ICE FOG

SOUNDING 5, ICE ABSORPTION 0.01280/M, FOG DEPTH 20. M

HEIGHT (M)	TEMPERATURE (DEG C)	FLUX (CAL/SQ CM/12 HR)	MEAN HEATING RATE, LAYER ABOVE Z (DEG C/12 HR)
0.0	-50.0	21.0	-3.508
0.5	-47.0	21.0	-16.517
1.0	-45.0	21.3	-22.994
2.0	-44.0	22.2	-21.947
5.0	-43.5	24.7	-20.093
10.0	-43.0	28.4	-20.988
15.0	-42.0	32.3	-23.090
20.0	-41.0	36.6	0.386
30.0	-40.0	36.5	0.186
40.0	-38.0	36.4	-0.500
50.0	-36.0	36.6	-1.380
60.0	-34.0	37.1	-1.518
80.0	-33.0	38.1	-1.192
100.0	-32.0	38.9	-1.192
139.0	-30.6	40.5	-0.992
213.0	-28.0	43.0	-0.854
287.0	-27.6	45.1	-0.572
438.0	-27.0	47.9	-0.381
829.0	-25.3	52.6	-0.364
1246.0	-23.6	57.1	-0.437
1690.0	-22.0	62.4	-0.499
2164.0	-23.3	68.5	-0.404
2667.0	-26.6	73.5	-0.470
3783.0	-28.0	85.0	-0.578
5071.0	-36.0	99.2	-0.554
6588.0	-45.7	112.8	-0.514
8047.0	-55.0	123.0	-0.641
8459.0	-55.0	126.1	-0.337
19908.0	-55.0	151.9	

NEUTRAL HEIGHT AT OR ABOVE TOP OF FOG.

ICE FOG

SOUNDING 5, ICE ABSORPTION 0.02560/M, FOG DEPTH 20. M

HEIGHT (M)	TEMPERATURE (DEG C)	FLUX (CAL/SQ CM/12 HR)	MEAN HEATING RATE, LAYER ABOVE Z (DEG C/12 HR)
0.0	-50.0	12.3	-7.569
0.5	-47.0	12.4	-25.001
1.0	-45.0	12.9	-34.237
2.0	-44.0	14.2	-34.668
5.0	-43.5	18.0	-34.369
10.0	-43.0	24.5	-37.904
15.0	-42.0	31.5	-43.651
20.0	-41.0	39.6	0.513
30.0	-40.0	39.4	0.293
40.0	-38.0	39.3	-0.396
50.0	-36.0	39.5	-1.281
60.0	-34.0	39.9	-1.422
80.0	-33.0	40.9	-1.115
100.0	-32.0	41.7	-1.120
139.0	-30.6	43.2	-0.940
213.0	-28.0	45.5	-0.819
287.0	-27.6	47.5	-0.547
438.0	-27.0	50.2	-0.367
829.0	-25.3	54.7	-0.356
1246.0	-23.6	59.1	-0.431
1690.0	-22.0	64.3	-0.494
2164.0	-23.3	70.4	-0.401
2667.0	-26.6	75.3	-0.468
3783.0	-28.0	86.9	-0.577
5071.0	-36.0	101.0	-0.553
6588.0	-45.7	114.6	-0.514
8047.0	-55.0	124.7	-0.641
8459.0	-55.0	127.9	-0.337
19908.0	-55.0	153.7	

NEUTRAL HEIGHT AT OR ABOVE TOP OF FOG.

ICE FOG

SOUNDING 5, ICE ABSORPTION 0.05120/M, FOG DEPTH 20. M

HEIGHT (M)	TEMPERATURE (DEG C)	FLUX (CAL/SQ CM/12 HR)	MEAN HEATING RATE, LAYER ABOVE Z (DEG C/12 HR)
0.0	-50.0	0.5	-5.519
0.5	-47.0	0.6	-31.520
1.0	-45.0	1.2	-45.928
2.0	-44.0	2.9	-48.766
5.0	-43.5	8.4	-51.332
10.0	-43.0	18.0	-61.481
15.0	-42.0	29.4	-78.187
20.0	-41.0	43.9	0.700
30.0	-40.0	43.7	0.451
40.0	-38.0	43.5	-0.245
50.0	-36.0	43.6	-1.138
60.0	-34.0	44.0	-1.282
80.0	-33.0	44.9	-1.003
100.0	-32.0	45.6	-1.015
139.0	-30.6	46.9	-0.865
213.0	-28.0	49.1	-0.768
287.0	-27.6	51.0	-0.513
438.0	-27.0	53.5	-0.348
829.0	-25.3	57.8	-0.344
1246.0	-23.6	62.0	-0.423
1690.0	-22.0	67.2	-0.488
2164.0	-23.3	73.1	-0.396
2667.0	-26.6	78.0	-0.465
3783.0	-28.0	89.5	-0.576
5071.0	-36.0	103.6	-0.552
6588.0	-45.7	117.1	-0.513
8047.0	-55.0	127.3	-0.640
8459.0	-55.0	130.4	-0.337
19908.0	-55.0	156.2	

NEUTRAL HEIGHT BETWEEN 1. M AND 0.M.

ICE FOG

SOUNDING 5, ICE ABSORPTION 0.05120/M, FOG DEPTH 20. M

HEIGHT (M)	TEMPERATURE (DEG C)	FLUX (CAL/SQ CM/12 HR)	MEAN HEATING RATE, LAYER ABOVE Z (DEG C/12 HR)
0.0	-40.8	20.2	-27.882
0.5	-40.8	20.7	-28.554
1.0	-40.8	21.2	-29.495
2.0	-40.8	22.3	-32.456
5.0	-40.8	25.9	-39.364
10.0	-40.9	33.2	-49.846
15.0	-40.9	42.5	-62.410
20.0	-41.0	54.0	0.421
30.0	-35.8	53.9	-1.040
40.0	-35.9	54.3	0.065
50.0	-36.0	54.2	-0.254
60.0	-34.0	54.3	-0.740
80.0	-33.0	54.8	-0.637
100.0	-32.0	55.3	-0.710
139.0	-30.6	56.2	-0.667
213.0	-28.0	57.9	-0.639
287.0	-27.6	59.5	-0.425
438.0	-27.0	61.6	-0.300
829.0	-25.3	65.2	-0.314
1246.0	-23.6	69.1	-0.402
1690.0	-22.0	74.0	-0.472
2164.0	-23.3	79.8	-0.385
2667.0	-26.6	84.5	-0.458
3783.0	-28.0	95.8	-0.572
5071.0	-36.0	109.8	-0.551
6588.0	-45.7	123.4	-0.513
8047.0	-55.0	133.4	-0.640
8459.0	-55.0	136.6	-0.337
19908.0	-55.0	162.4	

ICE FOG

SOUNDING 5, ICE ABSORPTION 0.00160/M, FOG DEPTH 50. M

HEIGHT (M)	TEMPERATURE (DEG C)	FLUX (CAL/SQ CM/12 HR)	MEAN HEATING RATE, LAYER ABOVE Z (DEG C/12 HR)
0.0	-50.0	28.4	4.729
0.5	-47.0	28.3	-4.394
1.0	-45.0	28.4	-8.491
2.0	-44.0	28.7	-6.290
5.0	-43.5	29.4	-3.569
10.0	-43.0	30.1	-3.085
15.0	-42.0	30.7	-3.460
20.0	-41.0	31.3	-3.480
30.0	-40.0	32.6	-3.648
40.0	-38.0	34.0	-4.434
50.0	-36.0	35.6	-0.853
60.0	-34.0	35.9	-1.268
80.0	-33.0	36.8	-1.090
100.0	-32.0	37.5	-1.125
139.0	-30.6	39.0	-0.985
213.0	-28.0	41.5	-0.858
287.0	-27.6	43.6	-0.580
438.0	-27.0	46.5	-0.387
829.0	-25.3	51.2	-0.369
1246.0	-23.6	55.7	-0.441
1690.0	-22.0	61.1	-0.501
2164.0	-23.3	67.3	-0.406
2667.0	-26.6	72.2	-0.471
3783.0	-28.0	83.8	-0.579
5071.0	-36.0	98.0	-0.554
6588.0	-45.7	111.6	-0.514
8047.0	-55.0	121.8	-0.641
8459.0	-55.0	124.9	-0.337
19908.0	-55.0	150.8	

NEUTRAL HEIGHT AT OR ABOVE TOP OF FOG.

ICE FOG

SOUNDING 5, ICE ABSORPTION 0.00320/M, FOG DEPTH 50. M

HEIGHT (M)	TEMPERATURE (DEG C)	FLUX (CAL/SQ CM/12 HR)	MEAN HEATING RATE, LAYER ABOVE Z (DEG C/12 HR)
0.0	-50.0	24.4	3.491
0.5	-47.0	24.3	-6.180
1.0	-45.0	24.4	-10.622
2.0	-44.0	24.8	-8.576
5.0	-43.5	25.8	-5.954
10.0	-43.0	26.9	-5.633
15.0	-42.0	28.0	-6.236
20.0	-41.0	29.1	-6.485
30.0	-40.0	31.5	-7.009
40.0	-38.0	34.1	-8.266
50.0	-36.0	37.1	-0.804
60.0	-34.0	37.4	-1.224
80.0	-33.0	38.3	-1.052
100.0	-32.0	39.0	-1.089
139.0	-30.6	40.5	-0.958
213.0	-28.0	42.8	-0.840
287.0	-27.6	44.9	-0.567
438.0	-27.0	47.7	-0.380
829.0	-25.3	52.4	-0.365
1246.0	-23.6	56.8	-0.438
1690.0	-22.0	62.2	-0.499
2164.0	-23.3	68.3	-0.404
2667.0	-26.6	73.2	-0.470
3783.0	-28.0	84.8	-0.578
5071.0	-36.0	99.0	-0.554
6588.0	-45.7	112.6	-0.514
8047.0	-55.0	122.7	-0.641
8459.0	-55.0	125.9	-0.337
19908.0	-55.0	151.7	

NEUTRAL HEIGHT AT OR ABOVE TOP OF FOG.

ICE FOG

SOUNDING 5, ICE ABSORPTION 0.01280/M, FOG DEPTH 50. M

HEIGHT (M)	TEMPERATURE (DEG C)	FLUX (CAL/SQ CM/12 HR)	MEAN HEATING RATE, LAYER ABOVE Z (DEG C/12 HR)
0.0	-50.0	6.3	1.213
0.5	-47.0	6.3	-11.727
1.0	-45.0	6.5	-18.198
2.0	-44.0	7.2	-17.064
5.0	-43.5	9.1	-15.073
10.0	-43.0	11.9	-15.822
15.0	-42.0	14.8	-17.943
20.0	-41.0	18.2	-19.931
30.0	-40.0	25.5	-23.316
40.0	-38.0	34.1	-28.480
50.0	-36.0	44.6	-0.563
60.0	-34.0	44.8	-1.007
80.0	-33.0	45.5	-0.864
100.0	-32.0	46.1	-0.916
139.0	-30.6	47.3	-0.829
213.0	-28.0	49.4	-0.752
287.0	-27.6	51.2	-0.505
438.0	-27.0	53.7	-0.345
829.0	-25.3	57.9	-0.343
1246.0	-23.6	62.1	-0.422
1690.0	-22.0	67.3	-0.487
2164.0	-23.3	73.3	-0.396
2667.0	-26.6	78.1	-0.465
3783.0	-28.0	89.6	-0.576
5071.0	-36.0	103.7	-0.552
6588.0	-45.7	117.3	-0.513
8047.0	-55.0	127.4	-0.640
8459.0	-55.0	130.5	-0.337
19908.0	-55.0	156.4	

NEUTRAL HEIGHT BETWEEN 15. M AND 10.M.

ICE FOG

SOUNDING 5, ICE ABSORPTION 0.01920/M, FOG DEPTH 50. M

HEIGHT (M)	TEMPERATURE (DEG C)	FLUX (CAL/SQ CM/12 HR)	MEAN HEATING RATE, LAYER ABOVE Z (DEG C/12 HR)
0.0	-50.0	-1.5	2.651
0.5	-47.0	-1.5	-12.416
1.0	-45.0	-1.3	-20.179
2.0	-44.0	-0.5	-19.553
5.0	-43.5	1.7	-17.823
10.0	-43.0	5.0	-19.141
15.0	-42.0	8.6	-22.201
20.0	-41.0	12.7	-25.418
30.0	-40.0	22.1	-31.146
40.0	-38.0	33.6	-39.880
50.0	-36.0	48.2	-0.442
60.0	-34.0	48.3	-0.900
80.0	-33.0	49.0	-0.771
100.0	-32.0	49.5	-0.832
139.0	-30.6	50.6	-0.766
213.0	-28.0	52.5	-0.709
287.0	-27.6	54.3	-0.475
438.0	-27.0	56.6	-0.329
829.0	-25.3	60.6	-0.332
1246.0	-23.6	64.7	-0.415
1690.0	-22.0	69.8	-0.482
2164.0	-23.3	75.7	-0.392
2667.0	-26.6	80.5	-0.462
3783.0	-28.0	91.9	-0.574
5071.0	-36.0	106.0	-0.552
6588.0	-45.7	119.5	-0.513
8047.0	-55.0	129.6	-0.640
8459.0	-55.0	132.7	-0.337
19908.0	-55.0	158.6	

NEUTRAL HEIGHT BETWEEN 1. M AND 0.M.

ICE FOG

SOUNDING 5, ICE ABSORPTION 0.02240/M, FOG DEPTH 50. M

HEIGHT (M)	TEMPERATURE (DEG C)	FLUX (CAL/SQ CM/12 HR)	MEAN HEATING RATE, LAYER ABOVE Z (DEG C/12 HR)
0.0	-50.0	-4.4	3.826
0.5	-47.0	-4.5	-12.291
1.0	-45.0	-4.3	-20.680
2.0	-44.0	-3.5	-20.262
5.0	-43.5	-1.2	-18.584
10.0	-43.0	2.3	-20.105
15.0	-42.0	6.0	-23.570
20.0	-41.0	10.4	-27.362
30.0	-40.0	20.5	-34.323
40.0	-38.0	33.1	-45.098
50.0	-36.0	49.7	-0.390
60.0	-34.0	49.8	-0.854
80.0	-33.0	50.4	-0.733
100.0	-32.0	50.9	-0.796
139.0	-30.6	52.0	-0.740
213.0	-28.0	53.8	-0.691
287.0	-27.6	55.5	-0.463
438.0	-27.0	57.8	-0.322
829.0	-25.3	61.7	-0.328
1246.0	-23.6	65.8	-0.411
1690.0	-22.0	70.8	-0.479
2164.0	-23.3	76.7	-0.391
2667.0	-26.6	81.5	-0.461
3783.0	-28.0	92.8	-0.574
5071.0	-36.0	106.9	-0.551
6588.0	-45.7	120.4	-0.513
8047.0	-55.0	130.5	-0.640
8459.0	-55.0	133.7	-0.337
19908.0	-55.0	159.5	

NEUTRAL HEIGHT BETWEEN 1. M AND 0.M.

ICE FOG

SOUNDING 5, ICE ABSORPTION 0.02560/M, FOG DEPTH 50. M

HEIGHT (M)	TEMPERATURE (DEG C)	FLUX (CAL/SQ CM/12 HR)	MEAN HEATING RATE, LAYER ABOVE Z (DEG C/12 HR)
0.0	-50.0	-6.9	5.180
0.5	-47.0	-7.0	-11.982
1.0	-45.0	-6.8	-20.977
2.0	-44.0	-6.0	-20.737
5.0	-43.5	-3.6	-19.055
10.0	-43.0	-0.1	-20.716
15.0	-42.0	3.8	-24.537
20.0	-41.0	8.3	-28.862
30.0	-40.0	19.0	-37.071
40.0	-38.0	32.6	-50.040
50.0	-36.0	51.0	-0.344
60.0	-34.0	51.1	-0.813
80.0	-33.0	51.7	-0.698
100.0	-32.0	52.2	-0.765
139.0	-30.6	53.2	-0.717
213.0	-28.0	55.0	-0.675
287.0	-27.6	56.6	-0.452
438.0	-27.0	58.9	-0.315
829.0	-25.3	62.7	-0.324
1246.0	-23.6	66.7	-0.409
1690.0	-22.0	71.7	-0.477
2164.0	-23.3	77.5	-0.389
2667.0	-26.6	82.3	-0.460
3783.0	-28.0	93.7	-0.573
5071.0	-36.0	107.7	-0.551
6588.0	-45.7	121.3	-0.513
8047.0	-55.0	131.4	-0.640
8459.0	-55.0	134.5	-0.337
19908.0	-55.0	160.3	

NEUTRAL HEIGHT BETWEEN 1. M AND 0.M.

ICE FOG

SOUNDING 5, ICE ABSORPTION 0.05120/M, FOG DEPTH 50. M

HEIGHT (M)	TEMPERATURE (DEG C)	FLUX (CAL/SQ CM/12 HR)	MEAN HEATING RATE, LAYER ABOVE Z (DEG C/12 HR)
0.0	-50.0	-16.1	17.045
0.5	-47.0	-16.4	-8.182
1.0	-45.0	-16.3	-21.630
2.0	-44.0	-15.5	-21.830
5.0	-43.5	-13.0	-18.340
10.0	-43.0	-9.6	-19.116
15.0	-42.0	-6.1	-23.987
20.0	-41.0	-1.6	-30.571
30.0	-40.0	9.7	-47.933
40.0	-38.0	27.3	-82.340
50.0	-36.0	57.6	-0.092
60.0	-34.0	57.6	-0.600
80.0	-33.0	58.0	-0.522
100.0	-32.0	58.4	-0.604
139.0	-30.6	59.2	-0.601
213.0	-28.0	60.7	-0.597
287.0	-27.6	62.1	-0.397
438.0	-27.0	64.1	-0.285
829.0	-25.3	67.6	-0.305
1246.0	-23.6	71.3	-0.395
1690.0	-22.0	76.2	-0.467
2164.0	-23.3	81.9	-0.382
2667.0	-26.6	86.6	-0.455
3783.0	-28.0	97.8	-0.571
5071.0	-36.0	111.8	-0.550
6588.0	-45.7	125.3	-0.512
8047.0	-55.0	135.4	-0.639
8459.0	-55.0	138.5	-0.337
19908.0	-55.0	164.4	

NEUTRAL HEIGHT BETWEEN 1. M AND 0.M.

ICE FOG

SOUNDING 5, ICE ABSORPTION 0.05120/M, FOG DEPTH 50. M

HEIGHT (M)	TEMPERATURE (DEG C)	FLUX (CAL/SQ CM/12 HR)	MEAN HEATING RATE, LAYER ABOVE Z (DEG C/12 HR)
0.0	-35.5	5.8	-8.149
0.5	-35.5	5.9	-8.304
1.0	-35.5	6.1	-8.561
2.0	-35.5	6.4	-9.323
5.0	-35.5	7.4	-11.180
10.0	-35.6	9.5	-14.154
15.0	-35.6	12.1	-18.055
20.0	-35.7	15.4	-26.430
30.0	-35.8	25.1	-43.643
40.0	-35.9	41.2	-71.662
50.0	-36.0	67.4	0.535
60.0	-34.0	67.2	-0.153
80.0	-33.0	67.3	-0.194
100.0	-32.0	67.5	-0.324
139.0	-30.6	67.9	-0.417
213.0	-28.0	69.0	-0.478
287.0	-27.6	70.1	-0.316
438.0	-27.0	71.7	-0.240
829.0	-25.3	74.6	-0.277
1246.0	-23.6	78.0	-0.375
1690.0	-22.0	82.6	-0.453
2164.0	-23.3	88.2	-0.372
2667.0	-26.6	92.7	-0.449
3783.0	-28.0	103.8	-0.567
5071.0	-36.0	117.7	-0.549
6588.0	-45.7	131.2	-0.511
8047.0	-55.0	141.3	-0.639
8459.0	-55.0	144.4	-0.336
19908.0	-55.0	170.2	

NEUTRAL HEIGHT BETWEEN 5. M AND 2.M.

ICE FOG

SOUNDING 5, ICE ABSORPTION 0.00160/M, FOG DEPTH 100. M

HEIGHT (M)	TEMPERATURE (DEG C)	FLUX (CAL/SQ CM/12 HR)	MEAN HEATING RATE, LAYER ABOVE Z (DEG C/12 HR)
0.0	-50.0	23.3	4.898
0.5	-47.0	23.3	-4.217
1.0	-45.0	23.3	-8.331
2.0	-44.0	23.6	-6.133
5.0	-43.5	24.3	-3.418
10.0	-43.0	25.0	-2.947
15.0	-42.0	25.5	-3.336
20.0	-41.0	26.1	-3.368
30.0	-40.0	27.4	-3.637
40.0	-38.0	28.7	-4.709
50.0	-36.0	30.5	-6.059
60.0	-34.0	32.7	-6.344
80.0	-33.0	37.3	-5.993
100.0	-32.0	41.7	-0.672
139.0	-30.6	42.6	-0.787
213.0	-28.0	44.5	-0.760
287.0	-27.6	46.4	-0.527
438.0	-27.0	49.0	-0.365
829.0	-25.3	53.5	-0.357
1246.0	-23.6	57.8	-0.434
1690.0	-22.0	63.1	-0.496
2164.0	-23.3	69.2	-0.402
2667.0	-26.6	74.2	-0.469
3783.0	-28.0	85.7	-0.578
5071.0	-36.0	99.9	-0.553
6588.0	-45.7	113.5	-0.514
8047.0	-55.0	123.6	-0.641
8459.0	-55.0	126.7	-0.337
19908.0	-55.0	152.6	

NEUTRAL HEIGHT AT OR ABOVE TOP OF FOG.

ICE FOG

SOUNDING 5, ICE ABSORPTION 0.00320/M, FOG DEPTH 100. M

HEIGHT (M)	TEMPERATURE (DEG C)	FLUX (CAL/SQ CM/12 HR)	MEAN HEATING RATE, LAYER ABOVE Z (DEG C/12 HR)
0.0	-50.0	15.2	4.224
0.5	-47.0	15.1	-5.438
1.0	-45.0	15.2	-9.892
2.0	-44.0	15.6	-7.842
5.0	-43.5	16.4	-5.218
10.0	-43.0	17.4	-4.900
15.0	-42.0	18.3	-5.505
20.0	-41.0	19.4	-5.750
30.0	-40.0	21.5	-6.355
40.0	-38.0	23.8	-7.886
50.0	-36.0	26.7	-9.709
60.0	-34.0	30.3	-10.379
80.0	-33.0	37.8	-10.357
100.0	-32.0	45.4	-0.593
139.0	-30.6	46.2	-0.727
213.0	-28.0	48.0	-0.718
287.0	-27.6	49.8	-0.496
438.0	-27.0	52.2	-0.347
829.0	-25.3	56.5	-0.346
1246.0	-23.6	60.7	-0.425
1690.0	-22.0	65.9	-0.490
2164.0	-23.3	71.9	-0.398
2667.0	-26.6	76.8	-0.466
3783.0	-28.0	88.3	-0.576
5071.0	-36.0	102.4	-0.553
6588.0	-45.7	116.0	-0.514
8047.0	-55.0	126.1	-0.640
8459.0	-55.0	129.2	-0.337
19908.0	-55.0	155.1	

NEUTRAL HEIGHT BETWEEN 50. M AND 40.M.

ICE FOG

SOUNDING 5, ICE ABSORPTION 0.00320/M, FOG DEPTH 100. M

HEIGHT (M)	TEMPERATURE (DEG C)	FLUX (CAL/SQ CM/12 HR)	MEAN HEATING RATE, LAYER ABOVE Z (DEG C/12 HR)
0.0	-31.0	59.4	-5.231
0.5	-31.0	59.5	-5.219
1.0	-31.0	59.6	-5.226
2.0	-31.0	59.8	-5.228
5.0	-31.0	60.4	-5.260
10.0	-31.1	61.4	-5.301
15.0	-31.1	62.3	-5.346
20.0	-31.2	63.3	-5.420
30.0	-31.3	65.3	-5.524
40.0	-31.4	67.3	-5.625
50.0	-31.5	69.4	-5.705
60.0	-31.6	71.5	-5.826
80.0	-31.8	75.8	-5.901
100.0	-32.0	80.1	0.291
139.0	-30.6	79.7	-0.125
213.0	-28.0	80.0	-0.302
287.0	-27.6	80.7	-0.203
438.0	-27.0	81.7	-0.180
829.0	-25.3	83.9	-0.240
1246.0	-23.6	86.9	-0.349
1690.0	-22.0	91.2	-0.433
2164.0	-23.3	96.5	-0.359
2667.0	-26.6	100.9	-0.440
3783.0	-28.0	111.7	-0.563
5071.0	-36.0	125.5	-0.546
6588.0	-45.7	139.0	-0.510
8047.0	-55.0	149.0	-0.638
8459.0	-55.0	152.1	-0.336
19908.0	-55.0	177.9	

NEUTRAL HEIGHT AT OR ABOVE TOP OF FOG.

ICE FOG

SOUNDING 5, ICE ABSORPTION 0.00640/M, FOG DEPTH 100. M

HEIGHT (M)	TEMPERATURE (DEG C)	FLUX (CAL/SQ CM/12 HR)	MEAN HEATING RATE, LAYER ABOVE Z (DEG C/12 HR)
0.0	-50.0	2.6	4.320
0.5	-47.0	2.5	-6.419
1.0	-45.0	2.6	-11.541
2.0	-44.0	3.1	-9.775
5.0	-43.5	4.2	-7.312
10.0	-43.0	5.5	-7.275
15.0	-42.0	6.9	-8.295
20.0	-41.0	8.4	-8.952
30.0	-40.0	11.7	-10.224
40.0	-38.0	15.5	-12.698
50.0	-36.0	20.2	-15.525
60.0	-34.0	25.8	-17.132
80.0	-33.0	38.4	-18.131
100.0	-32.0	51.6	-0.462
139.0	-30.6	52.2	-0.628
213.0	-28.0	53.8	-0.646
287.0	-27.6	55.3	-0.445
438.0	-27.0	57.5	-0.317
829.0	-25.3	61.4	-0.327
1246.0	-23.6	65.4	-0.412
1690.0	-22.0	70.5	-0.480
2164.0	-23.3	76.3	-0.391
2667.0	-26.6	81.1	-0.461
3783.0	-28.0	92.5	-0.574
5071.0	-36.0	106.6	-0.551
6588.0	-45.7	120.1	-0.513
8047.0	-55.0	130.2	-0.640
8459.0	-55.0	133.4	-0.337
19908.0	-55.0	159.2	

NEUTRAL HEIGHT BETWEEN 10. M AND 5.M.

ICE FOG

SOUNDING 5, ICE ABSORPTION 0.00640/M, FOG DEPTH 100. M

HEIGHT (M)	TEMPERATURE (DEG C)	FLUX (CAL/SQ CM/12 HR)	MEAN HEATING RATE, LAYER ABOVE Z (DEG C/12 HR)
0.0	-31.0	43.5	-7.625
0.5	-31.0	43.6	-7.627
1.0	-31.0	43.8	-7.656
2.0	-31.0	44.0	-7.714
5.0	-31.0	44.9	-7.861
10.0	-31.1	46.3	-8.054
15.0	-31.1	47.8	-8.256
20.0	-31.2	49.4	-8.582
30.0	-31.3	52.5	-9.048
40.0	-31.4	55.8	-9.545
50.0	-31.5	59.3	-10.056
60.0	-31.6	63.0	-10.891
80.0	-31.8	71.0	-12.033
100.0	-32.0	79.8	0.283
139.0	-30.6	79.4	-0.131
213.0	-28.0	79.7	-0.305
287.0	-27.6	80.5	-0.206
438.0	-27.0	81.5	-0.182
829.0	-25.3	83.7	-0.241
1246.0	-23.6	86.7	-0.350
1690.0	-22.0	90.9	-0.434
2164.0	-23.3	96.3	-0.359
2667.0	-26.6	100.7	-0.440
3783.0	-28.0	111.5	-0.563
5071.0	-36.0	125.3	-0.546
6588.0	-45.7	138.8	-0.510
8047.0	-55.0	148.8	-0.638
8459.0	-55.0	151.9	-0.336
19908.0	-55.0	177.7	

NEUTRAL HEIGHT AT OR ABOVE TOP OF FOG.

ICE FOG

SOUNDING 5, ICE ABSORPTION 0.02560/M, FOG DEPTH 100. M

HEIGHT (M)	TEMPERATURE (DEG C)	FLUX (CAL/SQ CM/12 HR)	MEAN HEATING RATE, LAYER ABOVE Z (DEG C/12 HR)
0.0	-50.0	-21.7	15.215
0.5	-47.0	-22.0	-1.736
1.0	-45.0	-22.0	-10.492
2.0	-44.0	-21.6	-9.681
5.0	-43.5	-20.5	-6.791
10.0	-43.0	-19.2	-6.761
15.0	-42.0	-18.0	-8.651
20.0	-41.0	-16.4	-9.558
30.0	-40.0	-12.8	-12.200
40.0	-38.0	-8.3	-18.266
50.0	-36.0	-1.6	-25.986
60.0	-34.0	7.9	-34.339
80.0	-33.0	33.0	-49.318
100.0	-32.0	68.9	-0.072
139.0	-30.6	69.0	-0.342
213.0	-28.0	69.9	-0.443
287.0	-27.6	70.9	-0.300
438.0	-27.0	72.4	-0.234
829.0	-25.3	75.3	-0.274
1246.0	-23.6	78.6	-0.373
1690.0	-22.0	83.2	-0.451
2164.0	-23.3	88.7	-0.371
2667.0	-26.6	93.3	-0.448
3783.0	-28.0	104.3	-0.567
5071.0	-36.0	118.3	-0.548
6588.0	-45.7	131.7	-0.511
8047.0	-55.0	141.8	-0.639
8459.0	-55.0	144.9	-0.336
19908.0	-55.0	170.7	

NEUTRAL HEIGHT BETWEEN 1. M AND 0.M.

ICE FOG

SOUNDING 5, ICE ABSORPTION 0.03200/M, FOG DEPTH 100. M

HEIGHT (M)	TEMPERATURE (DEG C)	FLUX (CAL/SQ CM/12 HR)	MEAN HEATING RATE, LAYER ABOVE Z (DEG C/12 HR)
0.0	-50.0	-22.5	18.236
0.5	-47.0	-22.9	-0.736
1.0	-45.0	-22.9	-10.617
2.0	-44.0	-22.5	-9.917
5.0	-43.5	-21.3	-6.492
10.0	-43.0	-20.1	-5.990
15.0	-42.0	-19.0	-7.703
20.0	-41.0	-17.6	-8.009
30.0	-40.0	-14.6	-10.180
40.0	-38.0	-10.9	-16.509
50.0	-36.0	-4.8	-25.041
60.0	-34.0	4.3	-35.133
80.0	-33.0	30.0	-56.450
100.0	-32.0	71.1	-0.016
139.0	-30.6	71.2	-0.303
213.0	-28.0	71.9	-0.416
287.0	-27.6	72.9	-0.281
438.0	-27.0	74.3	-0.223
829.0	-25.3	77.1	-0.267
1246.0	-23.6	80.3	-0.368
1690.0	-22.0	84.8	-0.447
2164.0	-23.3	90.3	-0.369
2667.0	-26.6	94.8	-0.446
3783.0	-28.0	105.8	-0.566
5071.0	-36.0	119.7	-0.548
6588.0	-45.7	133.2	-0.511
8047.0	-55.0	143.3	-0.639
8459.0	-55.0	146.4	-0.336
19908.0	-55.0	172.2	

NEUTRAL HEIGHT BETWEEN 1. M AND 0.M.

ICE FOG

SOUNDING 5, ICE ABSORPTION 0.04480/M, FOG DEPTH 100. M

HEIGHT (M)	TEMPERATURE (DEG C)	FLUX (CAL/SQ CM/12 HR)	MEAN HEATING RATE, LAYER ABOVE Z (DEG C/12 HR)
0.0	-50.0	-22.0	22.560
0.5	-47.0	-22.4	-0.431
1.0	-45.0	-22.4	-12.492
2.0	-44.0	-21.9	-11.865
5.0	-43.5	-20.6	-7.130
10.0	-43.0	-19.2	-5.452
15.0	-42.0	-18.2	-6.611
20.0	-41.0	-17.0	-5.446
30.0	-40.0	-15.0	-6.173
40.0	-38.0	-12.7	-12.242
50.0	-36.0	-8.2	-21.399
60.0	-34.0	-0.4	-33.586
80.0	-33.0	24.1	-67.997
100.0	-32.0	73.7	0.053
139.0	-30.6	73.6	-0.267
213.0	-28.0	74.3	-0.385
287.0	-27.6	75.2	-0.259
438.0	-27.0	76.5	-0.211
829.0	-25.3	79.1	-0.259
1246.0	-23.6	82.2	-0.363
1690.0	-22.0	86.7	-0.443
2164.0	-23.3	92.1	-0.366
2667.0	-26.6	96.6	-0.445
3783.0	-28.0	107.6	-0.565
5071.0	-36.0	121.4	-0.548
6588.0	-45.7	134.9	-0.511
8047.0	-55.0	144.9	-0.638
8459.0	-55.0	148.1	-0.336
19908.0	-55.0	173.9	

NEUTRAL HEIGHT BETWEEN 1. M AND 0.M.

ICE FOG

SOUNDING 5, ICE ABSORPTION 0.05120/M, FOG DEPTH 100. M

HEIGHT (M)	TEMPERATURE (DEG C)	FLUX (CAL/SQ CM/12 HR)	MEAN HEATING RATE, LAYER ABOVE Z (DEG C/12 HR)
0.0	-50.0	-21.3	24.157
0.5	-47.0	-21.8	-0.826
1.0	-45.0	-21.8	-13.956
2.0	-44.0	-21.3	-13.304
5.0	-43.5	-19.8	-7.846
10.0	-43.0	-18.3	-5.541
15.0	-42.0	-17.3	-6.416
20.0	-41.0	-16.1	-4.533
30.0	-40.0	-14.4	-4.502
40.0	-38.0	-12.7	-10.251
50.0	-36.0	-9.0	-19.377
60.0	-34.0	-1.9	-31.961
80.0	-33.0	21.5	-72.715
100.0	-32.0	74.5	0.075
139.0	-30.6	74.4	-0.242
213.0	-28.0	75.0	-0.375
287.0	-27.6	75.9	-0.253
438.0	-27.0	77.1	-0.207
829.0	-25.3	79.7	-0.257
1246.0	-23.6	82.8	-0.361
1690.0	-22.0	87.2	-0.442
2164.0	-23.3	92.6	-0.365
2667.0	-26.6	97.1	-0.444
3783.0	-28.0	108.1	-0.565
5071.0	-36.0	121.9	-0.547
6588.0	-45.7	135.4	-0.511
8047.0	-55.0	145.4	-0.638
8459.0	-55.0	148.6	-0.336
19908.0	-55.0	174.4	

NEUTRAL HEIGHT BETWEEN 1. M AND 0.M.

ICE FOG

SOUNDING 5, ICE ABSORPTION 0.05120/M, FOG DEPTH 100. M

HEIGHT (M)	TEMPERATURE (DEG C)	FLUX (CAL/SQ CM/12 HR)	MEAN HEATING RATE, LAYER ABOVE Z (DEG C/12 HR)
0.0	-31.0	1.0	-1.488
0.5	-31.0	1.1	-1.467
1.0	-31.0	1.1	-1.458
2.0	-31.0	1.1	-1.442
5.0	-31.0	1.3	-1.484
10.0	-31.1	1.6	-1.630
15.0	-31.1	1.9	-1.885
20.0	-31.2	2.2	-2.546
30.0	-31.3	3.2	-4.037
40.0	-31.4	4.6	-6.618
50.0	-31.5	7.1	-10.970
60.0	-31.6	11.1	-24.398
80.0	-31.8	28.9	-67.750
100.0	-32.0	78.3	0.242
139.0	-30.6	78.0	-0.157
213.0	-28.0	78.4	-0.323
287.0	-27.6	79.2	-0.218
438.0	-27.0	80.3	-0.188
829.0	-25.3	82.6	-0.246
1246.0	-23.6	85.6	-0.353
1690.0	-22.0	89.9	-0.436
2164.0	-23.3	95.2	-0.361
2667.0	-26.6	99.7	-0.441
3783.0	-28.0	110.6	-0.563
5071.0	-36.0	124.4	-0.547
6588.0	-45.7	137.8	-0.510
8047.0	-55.0	147.9	-0.638
8459.0	-55.0	151.0	-0.336
19908.0	-55.0	176.8	

NEUTRAL HEIGHT BETWEEN 1. M AND 1.M.

2. INITIAL STAGES OF ICE FOG.

ICE FOG

SOUNDING 4, ICE ABSORPTION 0.00064/M, FOG DEPTH 0. M

HEIGHT (M)	TEMPERATURE (DEG C)	FLUX (CAL/SQ CM/12 HR)	MEAN HEATING RATE, LAYER ABOVE Z (DEG C/12 HR)
0.0	-44.0	52.9	3.453
0.5	-43.0	52.8	0.162
1.0	-42.5	52.8	-1.601
2.0	-42.0	52.9	-0.657
5.0	-41.5	52.9	-0.195
10.0	-41.0	53.0	-0.059
15.0	-40.5	53.0	-0.183
20.0	-40.0	53.0	-0.142
30.0	-39.5	53.1	0.116
40.0	-39.0	53.0	0.003
50.0	-38.0	53.0	-0.299
75.0	-36.0	53.3	-0.659
100.0	-34.0	53.9	-0.949
138.0	-32.0	55.1	-0.782
210.0	-31.3	57.0	-0.563
283.0	-30.7	58.4	-0.445
433.0	-30.0	60.6	-0.333
818.0	-30.0	64.7	-0.266
1225.0	-30.0	67.9	-0.269
1657.0	-30.0	71.2	-0.314
2117.0	-30.0	75.1	-0.404
2608.0	-30.0	80.0	-0.404
3692.0	-35.3	89.9	-0.429
4948.0	-41.4	100.4	-0.444
6439.0	-49.0	111.4	-0.520
7310.0	-52.0	117.7	-0.805
8302.0	-55.0	127.6	-0.340
19751.0	-55.0	153.7	

NEUTRAL HEIGHT AT OR ABOVE TOP OF FOG.

ICE FOG

SOUNDING 4, ICE ABSORPTION 0.00064/M, FOG DEPTH 10. M

HEIGHT (M)	TEMPERATURE (DEG C)	FLUX (CAL/SQ CM/12 HR)	MEAN HEATING RATE, LAYER ABOVE Z (DEG C/12 HR)
0.0	-44.0	52.6	2.017
0.5	-43.0	52.5	-0.061
1.0	-42.5	52.6	-2.735
2.0	-42.0	52.7	-1.716
5.0	-41.5	52.8	-1.223
10.0	-41.0	53.1	0.058
15.0	-40.5	53.1	-0.117
20.0	-40.0	53.1	-0.112
30.0	-39.5	53.1	0.135
40.0	-39.0	53.1	0.010
50.0	-38.0	53.1	-0.291
75.0	-36.0	53.3	-0.656
100.0	-34.0	53.9	-0.947
138.0	-32.0	55.1	-0.780
210.0	-31.3	57.1	-0.562
283.0	-30.7	58.4	-0.445
433.0	-30.0	60.6	-0.333
818.0	-30.0	64.7	-0.266
1225.0	-30.0	68.0	-0.269
1657.0	-30.0	71.3	-0.314
2117.0	-30.0	75.1	-0.404
2608.0	-30.0	80.0	-0.404
3692.0	-35.3	89.9	-0.429
4948.0	-41.4	100.5	-0.444
6439.0	-49.0	111.4	-0.520
7310.0	-52.0	117.8	-0.805
8302.0	-55.0	127.6	-0.340
19751.0	-55.0	153.7	

NEUTRAL HEIGHT AT OR ABOVE TOP OF FOG.

ICE FOG

SOUNDING 4, ICE ABSORPTION 0.00128/M, FOG DEPTH 10. M

HEIGHT (M)	TEMPERATURE (DEG C)	FLUX (CAL/SQ CM/12 HR)	MEAN HEATING RATE, LAYER ABOVE Z (DEG C/12 HR)
0.0	-44.0	52.2	1.073
0.5	-43.0	52.2	-1.074
1.0	-42.5	52.2	-3.794
2.0	-42.0	52.4	-2.821
5.0	-41.5	52.7	-2.373
10.0	-41.0	53.1	0.062
15.0	-40.5	53.1	-0.115
20.0	-40.0	53.1	-0.110
30.0	-39.5	53.2	0.136
40.0	-39.0	53.1	0.012
50.0	-38.0	53.1	-0.290
75.0	-36.0	53.4	-0.655
100.0	-34.0	53.9	-0.946
138.0	-32.0	55.2	-0.780
210.0	-31.3	57.1	-0.561
283.0	-30.7	58.5	-0.444
433.0	-30.0	60.7	-0.332
818.0	-30.0	64.7	-0.266
1225.0	-30.0	68.0	-0.269
1657.0	-30.0	71.3	-0.314
2117.0	-30.0	75.1	-0.404
2608.0	-30.0	80.1	-0.404
3692.0	-35.3	90.0	-0.429
4948.0	-41.4	100.5	-0.444
6439.0	-49.0	111.4	-0.520
7310.0	-52.0	117.8	-0.805
8302.0	-55.0	127.7	-0.340
19751.0	-55.0	153.8	

NEUTRAL HEIGHT AT OR ABOVE TOP OF FOG.

ICE FOG

SOUNDING 4, ICE ABSORPTION 0.00256/M, FOG DEPTH 10. M

HEIGHT (M)	TEMPERATURE (DEG C)	FLUX (CAL/SQ CM/12 HR)	MEAN HEATING RATE, LAYER ABOVE Z (DEG C/12 HR)
0.0	-44.0	51.5	-0.772
0.5	-43.0	51.5	-3.063
1.0	-42.5	51.5	-5.880
2.0	-42.0	51.8	-5.003
5.0	-41.5	52.3	-4.660
10.0	-41.0	53.2	0.069
15.0	-40.5	53.2	-0.109
20.0	-40.0	53.2	-0.105
30.0	-39.5	53.2	0.140
40.0	-39.0	53.2	0.014
50.0	-38.0	53.2	-0.287
75.0	-36.0	53.4	-0.652
100.0	-34.0	54.0	-0.944
138.0	-32.0	55.2	-0.778
210.0	-31.3	57.1	-0.561
283.0	-30.7	58.5	-0.444
433.0	-30.0	60.7	-0.332
818.0	-30.0	64.8	-0.266
1225.0	-30.0	68.0	-0.269
1657.0	-30.0	71.3	-0.314
2117.0	-30.0	75.2	-0.404
2608.0	-30.0	80.1	-0.404
3692.0	-35.3	90.0	-0.429
4948.0	-41.4	100.5	-0.444
6439.0	-49.0	111.4	-0.520
7310.0	-52.0	117.8	-0.805
8302.0	-55.0	127.7	-0.340
19751.0	-55.0	153.8	

NEUTRAL HEIGHT AT OR ABOVE TOP OF FOG.

ICE FOG

SOUNDING 4, ICE ABSORPTION 0.00512/M, FOG DEPTH 10. M

HEIGHT (M)	TEMPERATURE (DEG C)	FLUX (CAL/SQ CM/12 HR)	MEAN HEATING RATE, LAYER ABOVE Z (DEG C/12 HR)
0.0	-44.0	50.0	+4.317
0.5	-43.0	50.1	-6.907
1.0	-42.5	50.2	-9.920
2.0	-42.0	50.6	-9.265
5.0	-41.5	51.6	-9.183
10.0	-41.0	53.3	0.084
15.0	-40.5	53.3	-0.099
20.0	-40.0	53.3	-0.096
30.0	-39.5	53.4	0.147
40.0	-39.0	53.3	0.020
50.0	-38.0	53.3	-0.283
75.0	-36.0	53.6	-0.648
100.0	-34.0	54.1	-0.941
138.0	-32.0	55.4	-0.776
210.0	-31.3	57.3	-0.559
283.0	-30.7	58.6	-0.443
433.0	-30.0	60.8	-0.332
818.0	-30.0	64.9	-0.265
1225.0	-30.0	68.1	-0.268
1657.0	-30.0	71.4	-0.314
2117.0	-30.0	75.3	-0.403
2608.0	-30.0	80.2	-0.404
3692.0	-35.3	90.1	-0.429
4948.0	-41.4	100.6	-0.444
6439.0	-49.0	111.5	-0.520
7310.0	-52.0	117.9	-0.805
8302.0	-55.0	127.8	-0.340
19751.0	-55.0	153.9	

NEUTRAL HEIGHT AT OR ABOVE TOP OF FOG.

ICE FOG

SOUNDING 4, ICE ABSORPTION 0.00064/M, FOG DEPTH 20. M

HEIGHT (M)	TEMPERATURE (DEG C)	FLUX (CAL/SQ CM/12 HR)	MEAN HEATING RATE, LAYER ABOVE Z (DEG C/12 HR)
0.0	-44.0	52.2	1.993
0.5	-43.0	52.2	-0.089
1.0	-42.5	52.2	-2.781
2.0	-42.0	52.3	-1.762
5.0	-41.5	52.5	-1.301
10.0	-41.0	52.7	-1.177
15.0	-40.5	53.0	-1.296
20.0	-40.0	53.2	-0.033
30.0	-39.5	53.2	0.168
40.0	-39.0	53.2	0.025
50.0	-38.0	53.1	-0.278
75.0	-36.0	53.4	-0.649
100.0	-34.0	54.0	-0.943
138.0	-32.0	55.2	-0.778
210.0	-31.3	57.1	-0.561
283.0	-30.7	58.5	-0.444
433.0	-30.0	60.7	-0.332
818.0	-30.0	64.8	-0.266
1225.0	-30.0	68.0	-0.269
1657.0	-30.0	71.3	-0.314
2117.0	-30.0	75.1	-0.404
2608.0	-30.0	80.1	-0.404
3692.0	-35.3	90.0	-0.429
4948.0	-41.4	100.5	-0.444
6439.0	-49.0	111.4	-0.520
7310.0	-52.0	117.8	-0.805
8302.0	-55.0	127.7	-0.340
19751.0	-55.0	153.8	

NEUTRAL HEIGHT AT OR ABOVE TOP OF FOG.

ICE FOG

SOUNDING 4, ICE ABSORPTION 0.00128/M, FOG DEPTH 20. M

HEIGHT (M)	TEMPERATURE (DEG C)	FLUX (CAL/SQ CM/12 HR)	MEAN HEATING RATE, LAYER ABOVE Z (DEG C/12 HR)
0.0	-44.0	51.5	1.067
0.5	-43.0	51.5	-1.088
1.0	-42.5	51.5	-3.823
2.0	-42.0	51.6	-2.852
5.0	-41.5	51.9	-2.436
10.0	-41.0	52.4	-2.359
15.0	-40.5	52.8	-2.525
20.0	-40.0	53.3	-0.027
30.0	-39.5	53.3	0.172
40.0	-39.0	53.2	0.028
50.0	-38.0	53.2	-0.275
75.0	-36.0	53.5	-0.647
100.0	-34.0	54.0	-0.941
138.0	-32.0	55.3	-0.776
210.0	-31.3	57.2	-0.560
283.0	-30.7	58.6	-0.443
433.0	-30.0	60.8	-0.332
818.0	-30.0	64.8	-0.266
1225.0	-30.0	68.1	-0.268
1657.0	-30.0	71.4	-0.314
2117.0	-30.0	75.2	-0.403
2608.0	-30.0	80.1	-0.404
3692.0	-35.3	90.0	-0.429
4948.0	-41.4	100.6	-0.444
6439.0	-49.0	111.5	-0.520
7310.0	-52.0	117.8	-0.805
8302.0	-55.0	127.7	-0.340
19751.0	-55.0	153.8	

NEUTRAL HEIGHT AT OR ABOVE TOP OF FOG.

ICE FOG

SOUNDING 4, ICE ABSORPTION 0.00256/M, FOG DEPTH 20. M

HEIGHT (M)	TEMPERATURE (DEG C)	FLUX (CAL/SQ CM/12 HR)	MEAN HEATING RATE, LAYER ABOVE Z (DEG C/12 HR)
0.0	-44.0	50.0	-0.712
0.5	-43.0	50.0	-3.006
1.0	-42.5	50.0	-5.840
2.0	-42.0	50.3	-4.964
5.0	-41.5	50.8	-4.654
10.0	-41.0	51.7	-4.688
15.0	-40.5	52.6	-4.967
20.0	-40.0	53.5	-0.016
30.0	-39.5	53.5	0.181
40.0	-39.0	53.4	0.035
50.0	-38.0	53.4	-0.269
75.0	-36.0	53.6	-0.641
100.0	-34.0	54.2	-0.937
138.0	-32.0	55.4	-0.774
210.0	-31.3	57.3	-0.558
283.0	-30.7	58.7	-0.442
433.0	-30.0	60.9	-0.331
818.0	-30.0	64.9	-0.265
1225.0	-30.0	68.2	-0.268
1657.0	-30.0	71.5	-0.314
2117.0	-30.0	75.3	-0.403
2608.0	-30.0	80.2	-0.404
3692.0	-35.3	90.1	-0.429
4948.0	-41.4	100.7	-0.444
6439.0	-49.0	111.6	-0.520
7310.0	-52.0	118.0	-0.805
8302.0	-55.0	127.8	-0.340
19751.0	-55.0	153.9	

NEUTRAL HEIGHT AT OR ABOVE TOP OF FOG.

ICE FOG

SOUNDING 4, ICE ABSORPTION 0.00512/M, FOG DEPTH 20. M

HEIGHT (M)	TEMPERATURE (DEG C)	FLUX (CAL/SQ CM/12 HR)	MEAN HEATING RATE, LAYER ABOVE Z (DEG C/12 HR)
0.0	-44.0	47.1	-3.970
0.5	-43.0	47.2	-6.563
1.0	-42.5	47.3	-9.592
2.0	-42.0	47.7	-8.937
5.0	-41.5	48.6	-8.886
10.0	-41.0	50.3	-9.206
15.0	-40.5	52.0	-9.779
20.0	-40.0	53.8	0.007
30.0	-39.5	53.8	0.197
40.0	-39.0	53.7	0.048
50.0	-38.0	53.7	-0.258
75.0	-36.0	54.0	-0.631
100.0	-34.0	54.5	-0.929
138.0	-32.0	55.7	-0.768
210.0	-31.3	57.6	-0.554
283.0	-30.7	59.0	-0.440
433.0	-30.0	61.1	-0.330
818.0	-30.0	65.2	-0.264
1225.0	-30.0	68.4	-0.268
1657.0	-30.0	71.7	-0.314
2117.0	-30.0	75.5	-0.403
2608.0	-30.0	80.5	-0.403
3692.0	-35.3	90.3	-0.428
4948.0	-41.4	100.9	-0.444
6439.0	-49.0	111.8	-0.520
7310.0	-52.0	118.2	-0.805
8302.0	-55.0	128.0	-0.340
19751.0	-55.0	154.1	

NEUTRAL HEIGHT AT OR ABOVE TOP OF FOG.

ICE FOG

SOUNDING 4, ICE ABSORPTION 0.00160/M, FOG DEPTH 20. M

HEIGHT (M)	TEMPERATURE (DEG C)	FLUX (CAL/SQ CM/12 HR)	MEAN HEATING RATE, LAYER ABOVE Z (DEG C/12 HR)
0.0	-44.0	51.1	0.612
0.5	-43.0	51.1	-1.573
1.0	-42.5	51.1	-4.338
2.0	-42.0	51.3	-3.388
5.0	-41.5	51.7	-2.997
10.0	-41.0	52.2	-2.946
15.0	-40.5	52.8	-3.138
20.0	-40.0	53.3	-0.024
30.0	-39.5	53.3	0.174
40.0	-39.0	53.3	0.030
50.0	-38.0	53.3	-0.274
75.0	-36.0	53.5	-0.645
100.0	-34.0	54.1	-0.940
138.0	-32.0	55.3	-0.776
210.0	-31.3	57.2	-0.559
283.0	-30.7	58.6	-0.443
433.0	-30.0	60.8	-0.332
818.0	-30.0	64.8	-0.265
1225.0	-30.0	68.1	-0.268
1657.0	-30.0	71.4	-0.314
2117.0	-30.0	75.2	-0.403
2608.0	-30.0	80.2	-0.404
3692.0	-35.3	90.0	-0.429
4948.0	-41.4	100.6	-0.444
6439.0	-49.0	111.5	-0.520
7310.0	-52.0	117.9	-0.805
8302.0	-55.0	127.8	-0.340
19751.0	-55.0	153.8	

NEUTRAL HEIGHT AT OR ABOVE TOP OF FOG.

ICE FOG

SOUNDING 4, ICE ABSORPTION 0.00320/M, FOG DEPTH 20. M

HEIGHT (M)	TEMPERATURE (DEG C)	FLUX (CAL/SQ CM/12 HR)	MEAN HEATING RATE, LAYER ABOVE Z (DEG C/12 HR)
0.0	-44.0	49.2	-1.562
0.5	-43.0	49.3	-3.931
1.0	-42.5	49.3	-6.812
2.0	-42.0	49.6	-5.989
5.0	-41.5	50.3	-5.737
10.0	-41.0	51.3	-5.835
15.0	-40.5	52.4	-6.179
20.0	-40.0	53.6	-0.010
30.0	-39.5	53.6	0.185
40.0	-39.0	53.5	0.038
50.0	-38.0	53.5	-0.267
75.0	-36.0	53.7	-0.639
100.0	-34.0	54.3	-0.935
138.0	-32.0	55.5	-0.772
210.0	-31.3	57.4	-0.557
283.0	-30.7	58.8	-0.441
433.0	-30.0	61.0	-0.331
818.0	-30.0	65.0	-0.265
1225.0	-30.0	68.2	-0.268
1657.0	-30.0	71.5	-0.314
2117.0	-30.0	75.4	-0.403
2608.0	-30.0	80.3	-0.404
3692.0	-35.3	90.2	-0.429
4948.0	-41.4	100.7	-0.444
6439.0	-49.0	111.6	-0.520
7310.0	-52.0	118.0	-0.805
8302.0	-55.0	127.9	-0.340
19751.0	-55.0	154.0	

NEUTRAL HEIGHT AT OR ABOVE TOP OF FOG.

ICE FOG

SOUNDING 4, ICE ABSORPTION 0.00640/M, FOG DEPTH 20. M

HEIGHT (M)	TEMPERATURE (DEG C)	FLUX (CAL/SQ CM/12 HR)	MEAN HEATING RATE, LAYER ABOVE Z (DEG C/12 HR)
0.0	-44.0	45.7	-5.463
0.5	-43.0	45.8	-8.205
1.0	-42.5	46.0	-11.338
2.0	-42.0	46.4	-10.802
5.0	-41.5	47.6	-10.903
10.0	-41.0	49.6	-11.397
15.0	-40.5	51.7	-12.151
20.0	-40.0	54.0	0.018
30.0	-39.5	54.0	0.205
40.0	-39.0	53.9	0.054
50.0	-38.0	53.9	-0.252
75.0	-36.0	54.1	-0.627
100.0	-34.0	54.7	-0.925
138.0	-32.0	55.9	-0.765
210.0	-31.3	57.7	-0.552
283.0	-30.7	59.1	-0.438
433.0	-30.0	61.3	-0.329
818.0	-30.0	65.3	-0.264
1225.0	-30.0	68.5	-0.267
1657.0	-30.0	71.8	-0.313
2117.0	-30.0	75.6	-0.403
2608.0	-30.0	80.6	-0.403
3692.0	-35.3	90.4	-0.428
4948.0	-41.4	101.0	-0.444
6439.0	-49.0	111.9	-0.520
7310.0	-52.0	118.3	-0.805
8302.0	-55.0	128.1	-0.340
19751.0	-55.0	154.2	

NEUTRAL HEIGHT AT OR ABOVE TOP OF FOG.

ICE FOG

SOUNDING 4, ICE ABSORPTION 0.01280/M, FOG DEPTH 20. M

HEIGHT (M)	TEMPERATURE (DEG C)	FLUX (CAL/SQ CM/12 HR)	MEAN HEATING RATE, LAYER ABOVE Z (DEG C/12 HR)
0.0	-44.0	39.3	-11.686
0.5	-43.0	39.5	-15.190
1.0	-42.5	39.8	-18.867
2.0	-42.0	40.5	-19.012
5.0	-41.5	42.6	-20.062
10.0	-41.0	46.4	-21.700
15.0	-40.5	50.4	-23.681
20.0	-40.0	54.8	0.069
30.0	-39.5	54.7	0.243
40.0	-39.0	54.6	0.084
50.0	-38.0	54.6	-0.226
75.0	-36.0	54.8	-0.604
100.0	-34.0	55.3	-0.907
138.0	-32.0	56.5	-0.753
210.0	-31.3	58.4	-0.544
283.0	-30.7	59.7	-0.433
433.0	-30.0	61.9	-0.326
818.0	-30.0	65.8	-0.262
1225.0	-30.0	69.1	-0.266
1657.0	-30.0	72.3	-0.312
2117.0	-30.0	76.1	-0.402
2608.0	-30.0	81.1	-0.403
3692.0	-35.3	90.9	-0.428
4948.0	-41.4	101.4	-0.444
6439.0	-49.0	112.4	-0.520
7310.0	-52.0	118.7	-0.805
8302.0	-55.0	128.6	-0.340
19751.0	-55.0	154.7	

NEUTRAL HEIGHT AT OR ABOVE TOP OF FOG.

ICE FOG

SOUNDING 4, ICE ABSORPTION 0.02560/M, FOG DEPTH 20. M

HEIGHT (M)	TEMPERATURE (DEG C)	FLUX (CAL/SQ CM/12 HR)	MEAN HEATING RATE, LAYER ABOVE Z (DEG C/12 HR)
0.0	-44.0	28.8	-19.097
0.5	-43.0	29.1	-24.164
1.0	-42.5	29.6	-28.993
2.0	-42.0	30.6	-30.737
5.0	-41.5	34.1	-34.304
10.0	-41.0	40.4	-39.305
15.0	-40.5	47.7	-45.218
20.0	-40.0	56.1	0.157
30.0	-39.5	56.0	0.308
40.0	-39.0	55.9	0.134
50.0	-38.0	55.9	-0.181
75.0	-36.0	56.0	-0.565
100.0	-34.0	56.5	-0.877
138.0	-32.0	57.7	-0.732
210.0	-31.3	59.5	-0.529
283.0	-30.7	60.8	-0.423
433.0	-30.0	62.9	-0.320
818.0	-30.0	66.8	-0.259
1225.0	-30.0	70.0	-0.264
1657.0	-30.0	73.2	-0.311
2117.0	-30.0	77.0	-0.401
2608.0	-30.0	81.9	-0.402
3692.0	-35.3	91.7	-0.428
4948.0	-41.4	102.2	-0.443
6439.0	-49.0	113.1	-0.520
7310.0	-52.0	119.5	-0.805
8302.0	-55.0	129.4	-0.340
19751.0	-55.0	155.5	

NEUTRAL HEIGHT AT OR ABOVE TOP OF FOG.

ICE FOG

SOUNDING 4, ICE ABSORPTION 0.05120/M, FOG DEPTH 20. M

HEIGHT (M)	TEMPERATURE (DEG C)	FLUX (CAL/SQ CM/12 HR)	MEAN HEATING RATE, LAYER ABOVE Z (DEG C/12 HR)
0.0	-44.0	14.4	-21.367
0.5	-43.0	14.8	-29.479
1.0	-42.5	15.3	-36.508
2.0	-42.0	16.7	-41.366
5.0	-41.5	21.3	-50.513
10.0	-41.0	30.7	-64.543
15.0	-40.5	42.7	-83.118
20.0	-40.0	58.0	0.289
30.0	-39.5	57.9	0.405
40.0	-39.0	57.8	0.209
50.0	-38.0	57.7	-0.115
75.0	-36.0	57.8	-0.508
100.0	-34.0	58.3	-0.832
138.0	-32.0	59.4	-0.701
210.0	-31.3	61.1	-0.507
283.0	-30.7	62.3	-0.409
433.0	-30.0	64.3	-0.312
818.0	-30.0	68.2	-0.254
1225.0	-30.0	71.3	-0.260
1657.0	-30.0	74.5	-0.308
2117.0	-30.0	78.2	-0.399
2608.0	-30.0	83.1	-0.401
3692.0	-35.3	92.9	-0.427
4948.0	-41.4	103.4	-0.443
6439.0	-49.0	114.3	-0.519
7310.0	-52.0	120.7	-0.805
8302.0	-55.0	130.6	-0.340
19751.0	-55.0	156.6	

NEUTRAL HEIGHT BETWEEN 10. M AND 5.M.

ICE FOG

SOUNDING 4, ICE ABSORPTION 0.05120/M, FOG DEPTH 20. M

HEIGHT (M)	TEMPERATURE (DEG C)	FLUX (CAL/SQ CM/12 HR)	MEAN HEATING RATE, LAYER ABOVE Z (DEG C/12 HR)
0.0	-39.8	23.1	-32.224
0.5	-39.8	23.7	-33.015
1.0	-39.8	24.4	-34.194
2.0	-39.8	25.6	-37.728
5.0	-39.8	29.8	-46.016
10.0	-39.9	38.3	-58.913
15.0	-39.9	49.2	-75.360
20.0	-40.0	63.2	0.376
30.0	-37.8	63.0	-0.258
40.0	-37.9	63.1	0.312
50.0	-38.0	63.0	0.252
75.0	-36.0	62.8	-0.301
100.0	-34.0	63.1	-0.687
138.0	-32.0	64.0	-0.608
210.0	-31.3	65.4	-0.446
283.0	-30.7	66.5	-0.369
433.0	-30.0	68.4	-0.289
818.0	-30.0	71.9	-0.241
1225.0	-30.0	74.9	-0.251
1657.0	-30.0	77.9	-0.301
2117.0	-30.0	81.6	-0.393
2608.0	-30.0	86.4	-0.397
3692.0	-35.3	96.2	-0.425
4948.0	-41.4	106.6	-0.442
6439.0	-49.0	117.5	-0.519
7310.0	-52.0	123.9	-0.804
8302.0	-55.0	133.7	-0.340
19751.0	-55.0	159.8	

NEUTRAL HEIGHT BETWEEN 15. M AND 10.M.

ICE FOG

SOUNDING 4, ICE ABSORPTION 0.00160/M, FOG DEPTH 50. M

HEIGHT (M)	TEMPERATURE (DEG C)	FLUX (CAL/SQ CM/12 HR)	MEAN HEATING RATE, LAYER ABOVE Z (DEG C/12 HR)
0.0	-44.0	48.2	0.680
0.5	-43.0	48.2	-1.507
1.0	-42.5	48.2	-4.265
2.0	-42.0	48.4	-3.321
5.0	-41.5	48.8	-2.944
10.0	-41.0	49.3	-2.929
15.0	-40.5	49.8	-3.136
20.0	-40.0	50.4	-3.199
30.0	-39.5	51.6	-3.039
40.0	-39.0	52.7	-3.308
50.0	-38.0	53.9	-0.181
75.0	-36.0	54.1	-0.603
100.0	-34.0	54.6	-0.913
138.0	-32.0	55.8	-0.760
210.0	-31.3	57.7	-0.551
283.0	-30.7	59.0	-0.438
433.0	-30.0	61.2	-0.329
818.0	-30.0	65.2	-0.264
1225.0	-30.0	68.5	-0.267
1657.0	-30.0	71.7	-0.313
2117.0	-30.0	75.6	-0.403
2608.0	-30.0	80.5	-0.403
3692.0	-35.3	90.4	-0.428
4948.0	-41.4	100.9	-0.444
6439.0	-49.0	111.8	-0.520
7310.0	-52.0	118.2	-0.805
8302.0	-55.0	128.1	-0.340
19751.0	-55.0	154.2	

NEUTRAL HEIGHT AT OR ABOVE TOP OF FOG.

ICE FOG

SOUNDING 4, ICE ABSORPTION 0.00320/M, FOG DEPTH 50. M

HEIGHT (M)	TEMPERATURE (DEG C)	FLUX (CAL/SQ CM/12 HR)	MEAN HEATING RATE, LAYER ABOVE Z (DEG C/12 HR)
0.0	-44.0	43.7	-1.155
0.5	-43.0	43.7	-3.522
1.0	-42.5	43.8	-6.400
2.0	-42.0	44.0	-5.579
5.0	-41.5	44.6	-5.339
10.0	-41.0	45.6	-5.469
15.0	-40.5	46.6	-5.825
20.0	-40.0	47.7	-6.056
30.0	-39.5	50.0	-6.087
40.0	-39.0	52.2	-6.611
50.0	-38.0	54.6	-0.156
75.0	-36.0	54.8	-0.581
100.0	-34.0	55.3	-0.897
138.0	-32.0	56.5	-0.749
210.0	-31.3	58.3	-0.543
283.0	-30.7	59.6	-0.433
433.0	-30.0	61.8	-0.326
818.0	-30.0	65.8	-0.262
1225.0	-30.0	69.0	-0.266
1657.0	-30.0	72.2	-0.312
2117.0	-30.0	76.1	-0.402
2608.0	-30.0	81.0	-0.403
3692.0	-35.3	90.8	-0.428
4948.0	-41.4	101.4	-0.444
6439.0	-49.0	112.3	-0.520
7310.0	-52.0	118.6	-0.805
8302.0	-55.0	128.5	-0.340
19751.0	-55.0	154.6	

NEUTRAL HEIGHT AT OR ABOVE TOP OF FOG.

ICE FOG

SOUNDING 4, ICE ABSORPTION 0.00640/M, FOG DEPTH 50. M

HEIGHT (M)	TEMPERATURE (DEG C)	FLUX (CAL/SQ CM/12 HR)	MEAN HEATING RATE, LAYER ABOVE Z (DEG C/12 HR)
0.0	-44.0	35.7	-3.839
0.5	-43.0	35.8	-6.568
1.0	-42.5	35.9	-9.694
2.0	-42.0	36.3	-9.140
5.0	-41.5	37.3	-9.216
10.0	-41.0	39.0	-9.701
15.0	-40.5	40.8	-10.423
20.0	-40.0	42.7	-11.108
30.0	-39.5	46.8	-11.703
40.0	-39.0	51.1	-12.946
50.0	-38.0	55.9	-0.110
75.0	-36.0	56.0	-0.542
100.0	-34.0	56.5	-0.866
138.0	-32.0	57.6	-0.728
210.0	-31.3	59.4	-0.528
283.0	-30.7	60.7	-0.423
433.0	-30.0	62.8	-0.320
818.0	-30.0	66.7	-0.259
1225.0	-30.0	69.9	-0.264
1657.0	-30.0	73.1	-0.311
2117.0	-30.0	76.9	-0.401
2608.0	-30.0	81.8	-0.402
3692.0	-35.3	91.6	-0.428
4948.0	-41.4	102.2	-0.443
6439.0	-49.0	113.1	-0.520
7310.0	-52.0	119.4	-0.805
8302.0	-55.0	129.3	-0.340
19751.0	-55.0	155.4	

NEUTRAL HEIGHT AT OR ABOVE TOP OF FOG.

ICE FOG

SOUNDING 4, ICE ABSORPTION 0.01280/M, FOG DEPTH 50. M

HEIGHT (M)	TEMPERATURE (DEG C)	FLUX (CAL/SQ CM/12 HR)	MEAN HEATING RATE, LAYER ABOVE Z (DEG C/12 HR)
0.0	-44.0	23.2	-6.265
0.5	-43.0	23.3	-9.723
1.0	-42.5	23.5	-13.346
2.0	-42.0	24.0	-13.348
5.0	-41.5	25.5	-14.119
10.0	-41.0	28.1	-15.417
15.0	-40.5	30.9	-17.017
20.0	-40.0	34.1	-18.913
30.0	-39.5	41.1	-21.199
40.0	-39.0	48.9	-24.662
50.0	-38.0	58.0	-0.032
75.0	-36.0	58.0	-0.477
100.0	-34.0	58.4	-0.816
138.0	-32.0	59.5	-0.693
210.0	-31.3	61.2	-0.504
283.0	-30.7	62.4	-0.407
433.0	-30.0	64.4	-0.311
818.0	-30.0	68.2	-0.254
1225.0	-30.0	71.3	-0.260
1657.0	-30.0	74.5	-0.308
2117.0	-30.0	78.3	-0.399
2608.0	-30.0	83.2	-0.401
3692.0	-35.3	93.0	-0.427
4948.0	-41.4	103.5	-0.443
6439.0	-49.0	114.4	-0.519
7310.0	-52.0	120.7	-0.805
8302.0	-55.0	130.6	-0.340
19751.0	-55.0	156.7	

NEUTRAL HEIGHT BETWEEN 40. M AND 30.M.

ICE FOG

SOUNDING 4, ICE ABSORPTION 0.01280/M, FOG DEPTH 50. M

HEIGHT (M)	TEMPERATURE (DEG C)	FLUX (CAL/SQ CM/12 HR)	MEAN HEATING RATE, LAYER ABOVE Z (DEG C/12 HR)
0.0	-37.5	37.2	-12.885
0.5	-37.5	37.4	-12.957
1.0	-37.5	37.6	-13.027
2.0	-37.5	38.1	-13.309
5.0	-37.5	39.6	-13.906
10.0	-37.6	42.2	-14.693
15.0	-37.6	44.9	-15.552
20.0	-37.7	47.7	-16.931
30.0	-37.8	54.0	-18.954
40.0	-37.9	60.9	-21.137
50.0	-38.0	68.7	0.532
75.0	-36.0	68.2	-0.091
100.0	-34.0	68.3	-0.533
138.0	-32.0	69.0	-0.506
210.0	-31.3	70.3	-0.379
283.0	-30.7	71.2	-0.325
433.0	-30.0	72.8	-0.264
818.0	-30.0	76.0	-0.227
1225.0	-30.0	78.8	-0.242
1657.0	-30.0	81.8	-0.294
2117.0	-30.0	85.4	-0.388
2608.0	-30.0	90.1	-0.394
3692.0	-35.3	99.7	-0.423
4948.0	-41.4	110.1	-0.441
6439.0	-49.0	121.0	-0.518
7310.0	-52.0	127.3	-0.804
8302.0	-55.0	137.2	-0.340
19751.0	-55.0	163.3	

NEUTRAL HEIGHT AT OR ABOVE TOP OF FOG.

ICE FOG

SOUNDING 4, ICE ABSORPTION 0.02560/M, FOG DEPTH 50. M

HEIGHT (M)	TEMPERATURE (DEG C)	FLUX (CAL/SQ CM/12 HR)	MEAN HEATING RATE, LAYER ABOVE Z (DEG C/12 HR)
0.0	-44.0	7.8	-4.773
0.5	-43.0	7.9	-9.628
1.0	-42.5	8.0	-14.170
2.0	-42.0	8.6	-15.122
5.0	-41.5	10.3	-17.012
10.0	-41.0	13.4	-19.712
15.0	-40.5	17.1	-23.001
20.0	-40.0	21.3	-27.622
30.0	-39.5	31.5	-34.545
40.0	-39.0	44.3	-45.030
50.0	-38.0	60.8	0.079
75.0	-36.0	60.7	-0.386
100.0	-34.0	61.1	-0.745
138.0	-32.0	62.1	-0.645
210.0	-31.3	63.6	-0.471
283.0	-30.7	64.8	-0.385
433.0	-30.0	66.7	-0.298
818.0	-30.0	70.3	-0.247
1225.0	-30.0	73.4	-0.255
1657.0	-30.0	76.5	-0.304
2117.0	-30.0	80.2	-0.396
2608.0	-30.0	85.1	-0.399
3692.0	-35.3	94.8	-0.426
4948.0	-41.4	105.3	-0.443
6439.0	-49.0	116.2	-0.519
7310.0	-52.0	122.5	-0.805
8302.0	-55.0	132.4	-0.340
19751.0	-55.0	158.5	

NEUTRAL HEIGHT BETWEEN 10. M AND 5.M.

ICE FOG

SOUNDING 4, ICE ABSORPTION 0.02560/M, FOG DEPTH 50. M

HEIGHT (M)	TEMPERATURE (DEG C)	FLUX (CAL/SQ CM/12 HR)	MEAN HEATING RATE, LAYER ABOVE Z (DEG C/12 HR)
0.0	-37.5	19.8	-13.840
0.5	-37.5	20.1	-13.997
1.0	-37.5	20.3	-14.206
2.0	-37.5	20.9	-14.863
5.0	-37.5	22.5	-16.309
10.0	-37.6	25.5	-18.348
15.0	-37.6	28.9	-20.692
20.0	-37.7	32.7	-24.876
30.0	-37.8	41.9	-31.794
40.0	-37.9	53.6	-40.602
50.0	-38.0	68.5	0.522
75.0	-36.0	68.0	-0.099
100.0	-34.0	68.1	-0.539
138.0	-32.0	68.8	-0.510
210.0	-31.3	70.1	-0.381
283.0	-30.7	71.0	-0.327
433.0	-30.0	72.6	-0.265
818.0	-30.0	75.9	-0.228
1225.0	-30.0	78.6	-0.242
1657.0	-30.0	81.6	-0.294
2117.0	-30.0	85.2	-0.388
2608.0	-30.0	90.0	-0.394
3692.0	-35.3	99.6	-0.423
4948.0	-41.4	110.0	-0.441
6439.0	-49.0	120.9	-0.518
7310.0	-52.0	127.2	-0.804
8302.0	-55.0	137.1	-0.340
19751.0	-55.0	163.1	

NEUTRAL HEIGHT BETWEEN 20. M AND 15.M.

ICE FOG

SOUNDING 4, ICE ABSORPTION 0.05120/M, FOG DEPTH 50. M

HEIGHT (M)	TEMPERATURE (DEG C)	FLUX (CAL/SQ CM/12 HR)	MEAN HEATING RATE, LAYER ABOVE Z (DEG C/12 HR)
0.0	-44.0	-3.9	3.968
0.5	-43.0	-4.0	-3.435
1.0	-42.5	-4.0	-9.425
2.0	-42.0	-3.6	-11.312
5.0	-41.5	-2.3	-13.568
10.0	-41.0	0.2	-16.881
15.0	-40.5	3.3	-21.628
20.0	-40.0	7.3	-29.774
30.0	-39.5	18.3	-46.193
40.0	-39.0	35.3	-77.189
50.0	-38.0	63.7	0.202
75.0	-36.0	63.5	-0.290
100.0	-34.0	63.8	-0.673
138.0	-32.0	64.7	-0.596
210.0	-31.3	66.1	-0.437
283.0	-30.7	67.2	-0.363
433.0	-30.0	69.0	-0.285
818.0	-30.0	72.5	-0.239
1225.0	-30.0	75.4	-0.250
1657.0	-30.0	78.5	-0.300
2117.0	-30.0	82.1	-0.393
2608.0	-30.0	86.9	-0.397
3692.0	-35.3	96.7	-0.425
4948.0	-41.4	107.1	-0.442
6439.0	-49.0	118.0	-0.519
7310.0	-52.0	124.3	-0.804
8302.0	-55.0	134.2	-0.340
19751.0	-55.0	160.3	

NEUTRAL HEIGHT BETWEEN 1. M AND 0.M.

ICE FOG

SOUNDING 4, ICE ABSORPTION 0.05120/M, FOG DEPTH 50. M

HEIGHT (M)	TEMPERATURE (DEG C)	FLUX (CAL/SQ CM/12 HR)	MEAN HEATING RATE, LAYER ABOVE Z (DEG C/12 HR)
0.0	-37.5	5.8	-8.157
0.5	-37.5	5.9	-8.327
1.0	-37.5	6.1	-8.567
2.0	-37.5	6.4	-9.338
5.0	-37.5	7.4	-11.208
10.0	-37.6	9.5	-14.204
15.0	-37.6	12.1	-18.133
20.0	-37.7	15.5	-26.570
30.0	-37.8	25.3	-44.005
40.0	-37.9	41.4	-72.933
50.0	-38.0	68.2	0.509
75.0	-36.0	67.8	-0.108
100.0	-34.0	67.9	-0.546
138.0	-32.0	68.6	-0.515
210.0	-31.3	69.8	-0.384
283.0	-30.7	70.8	-0.329
433.0	-30.0	72.4	-0.266
818.0	-30.0	75.7	-0.228
1225.0	-30.0	78.5	-0.242
1657.0	-30.0	81.4	-0.295
2117.0	-30.0	85.0	-0.388
2608.0	-30.0	89.8	-0.394
3692.0	-35.3	99.4	-0.423
4948.0	-41.4	109.8	-0.441
6439.0	-49.0	120.7	-0.518
7310.0	-52.0	127.0	-0.804
8302.0	-55.0	136.9	-0.340
19751.0	-55.0	163.0	

NEUTRAL HEIGHT BETWEEN 5. M AND 2.M.

ICE FOG

SOUNDING 4, ICE ABSORPTION 0.00160/M, FOG DEPTH 100. M

HEIGHT (M)	TEMPERATURE (DEG C)	FLUX (CAL/SQ CM/12 HR)	MEAN HEATING RATE, LAYER ABOVE Z (DEG C/12 HR)
0.0	-44.0	43.1	0.875
0.5	-43.0	43.1	-1.309
1.0	-42.5	43.1	-4.071
2.0	-42.0	43.2	-3.126
5.0	-41.5	43.6	-2.752
10.0	-41.0	44.1	-2.744
15.0	-40.5	44.6	-2.955
20.0	-40.0	45.1	-3.018
30.0	-39.5	46.3	-2.891
40.0	-39.0	47.3	-3.219
50.0	-38.0	48.5	-3.848
75.0	-36.0	52.0	-4.667
100.0	-34.0	56.3	-0.775
138.0	-32.0	57.3	-0.706
210.0	-31.3	59.0	-0.523
283.0	-30.7	60.3	-0.422
433.0	-30.0	62.4	-0.321
818.0	-30.0	66.3	-0.260
1225.0	-30.0	69.5	-0.265
1657.0	-30.0	72.8	-0.311
2117.0	-30.0	76.6	-0.401
2608.0	-30.0	81.5	-0.402
3692.0	-35.3	91.3	-0.428
4948.0	-41.4	101.8	-0.444
6439.0	-49.0	112.7	-0.520
7310.0	-52.0	119.1	-0.805
8302.0	-55.0	129.0	-0.340
19751.0	-55.0	155.1	

NEUTRAL HEIGHT AT OR ABOVE TOP OF FOG.

ICE FOG

SOUNDING 4, ICE ABSORPTION 0.00320/M, FOG DEPTH 100. M

HEIGHT (M)	TEMPERATURE (DEG C)	FLUX (CAL/SQ CM/12 HR)	MEAN HEATING RATE, LAYER ABOVE Z (DEG C/12 HR)
0.0	-44.0	34.5	-0.397
0.5	-43.0	34.5	-2.761
1.0	-42.5	34.6	-5.642
2.0	-42.0	34.8	-4.815
5.0	-41.5	35.3	-4.568
10.0	-41.0	36.2	-4.694
15.0	-40.5	37.0	-5.043
20.0	-40.0	38.0	-5.260
30.0	-39.5	39.9	-5.304
40.0	-39.0	41.9	-5.868
50.0	-38.0	44.0	-6.968
75.0	-36.0	50.4	-8.456
100.0	-34.0	58.1	-0.723
138.0	-32.0	59.0	-0.673
210.0	-31.3	60.7	-0.500
283.0	-30.7	61.9	-0.407
433.0	-30.0	63.9	-0.312
818.0	-30.0	67.8	-0.255
1225.0	-30.0	70.9	-0.261
1657.0	-30.0	74.1	-0.309
2117.0	-30.0	77.9	-0.399
2608.0	-30.0	82.7	-0.401
3692.0	-35.3	92.6	-0.427
4948.0	-41.4	103.1	-0.443
6439.0	-49.0	114.0	-0.520
7310.0	-52.0	120.3	-0.805
8302.0	-55.0	130.2	-0.340
19751.0	-55.0	156.3	

NEUTRAL HEIGHT AT OR ABOVE TOP OF FOG.

ICE FOG

SOUNDING 4, ICE ABSORPTION 0.00320/M, FOG DEPTH 100. M

HEIGHT (M)	TEMPERATURE (DEG C)	FLUX (CAL/SQ CM/12 HR)	MEAN HEATING RATE, LAYER ABOVE Z (DEG C/12 HR)
0.0	-33.0	59.2	-5.251
0.5	-33.0	59.3	-5.256
1.0	-33.0	59.4	-5.240
2.0	-33.0	59.6	-5.242
5.0	-33.0	60.1	-5.274
10.0	-33.1	61.1	-5.320
15.0	-33.1	62.1	-5.370
20.0	-33.2	63.1	-5.448
30.0	-33.3	65.1	-5.562
40.0	-33.4	67.1	-5.674
50.0	-33.5	69.2	-5.869
75.0	-33.8	74.6	-6.048
100.0	-34.0	80.1	0.100
138.0	-32.0	79.9	-0.221
210.0	-31.3	80.5	-0.212
283.0	-30.7	81.0	-0.223
433.0	-30.0	82.1	-0.208
818.0	-30.0	84.7	-0.197
1225.0	-30.0	87.1	-0.221
1657.0	-30.0	89.8	-0.278
2117.0	-30.0	93.2	-0.376
2608.0	-30.0	97.8	-0.386
3692.0	-35.3	107.2	-0.419
4948.0	-41.4	117.5	-0.439
6439.0	-49.0	128.3	-0.517
7310.0	-52.0	134.7	-0.803
8302.0	-55.0	144.5	-0.339
19751.0	-55.0	170.6	

NEUTRAL HEIGHT AT OR ABOVE TOP OF FOG.

ICE FOG

SOUNDING 4, ICE ABSORPTION 0.00640/M, FOG DEPTH 100. M

HEIGHT (M)	TEMPERATURE (DEG C)	FLUX (CAL/SQ CM/12 HR)	MEAN HEATING RATE, LAYER ABOVE Z (DEG C/12 HR)
0.0	-44.0	21.2	-1.387
0.5	-43.0	21.2	-4.102
1.0	-42.5	21.3	-7.219
2.0	-42.0	21.6	-6.630
5.0	-41.5	22.3	-6.643
10.0	-41.0	23.5	-7.050
15.0	-40.5	24.8	-7.690
20.0	-40.0	26.3	-8.248
30.0	-39.5	29.3	-8.696
40.0	-39.0	32.5	-9.814
50.0	-38.0	36.1	-12.070
75.0	-36.0	47.2	-15.363
100.0	-34.0	61.2	-0.634
138.0	-32.0	62.0	-0.616
210.0	-31.3	63.5	-0.462
283.0	-30.7	64.6	-0.382
433.0	-30.0	66.5	-0.298
818.0	-30.0	70.2	-0.247
1225.0	-30.0	73.2	-0.255
1657.0	-30.0	76.3	-0.304
2117.0	-30.0	80.0	-0.396
2608.0	-30.0	84.9	-0.399
3692.0	-35.3	94.7	-0.426
4948.0	-41.4	105.1	-0.443
6439.0	-49.0	116.0	-0.519
7310.0	-52.0	122.4	-0.805
8302.0	-55.0	132.2	-0.340
19751.0	-55.0	158.3	

NEUTRAL HEIGHT BETWEEN 75. M AND 50.M.

ICE FOG

SOUNDING 4, ICE ABSORPTION 0.00640/M, FOG DEPTH 100. M

HEIGHT (M)	TEMPERATURE (DEG C)	FLUX (CAL/SQ CM/12 HR)	MEAN HEATING RATE, LAYER ABOVE Z (DEG C/12 HR)
0.0	-33.0	43.3	-7.633
0.5	-33.0	43.4	-7.654
1.0	-33.0	43.6	-7.657
2.0	-33.0	43.9	-7.716
5.0	-33.0	44.7	-7.863
10.0	-33.1	46.2	-8.060
15.0	-33.1	47.6	-8.266
20.0	-33.2	49.2	-8.598
30.0	-33.3	52.3	-9.074
40.0	-33.4	55.7	-9.582
50.0	-33.5	59.2	-10.561
75.0	-33.8	68.8	-12.047
100.0	-34.0	79.8	0.091
138.0	-32.0	79.7	-0.226
210.0	-31.3	80.2	-0.216
283.0	-30.7	80.7	-0.225
433.0	-30.0	81.9	-0.210
818.0	-30.0	84.4	-0.198
1225.0	-30.0	86.8	-0.221
1657.0	-30.0	89.6	-0.279
2117.0	-30.0	93.0	-0.376
2608.0	-30.0	97.6	-0.386
3692.0	-35.3	107.0	-0.419
4948.0	-41.4	117.3	-0.439
6439.0	-49.0	128.1	-0.517
7310.0	-52.0	134.5	-0.803
8302.0	-55.0	144.3	-0.339
19751.0	-55.0	170.4	

NEUTRAL HEIGHT AT OR ABOVE TOP OF FOG.

ICE FOG

SOUNDING 4, ICE ABSORPTION 0.01280/M, FOG DEPTH 100. M

HEIGHT (M)	TEMPERATURE (DEG C)	FLUX (CAL/SQ CM/12 HR)	MEAN HEATING RATE, LAYER ABOVE Z (DEG C/12 HR)
0.0	-44.0	5.0	-0.071
0.5	-43.0	5.0	-3.475
1.0	-42.5	5.1	-7.037
2.0	-42.0	5.4	-6.865
5.0	-41.5	6.1	-7.292
10.0	-41.0	7.5	-8.140
15.0	-40.5	9.0	-9.257
20.0	-40.0	10.7	-10.375
30.0	-39.5	14.5	-11.540
40.0	-39.0	18.8	-13.767
50.0	-38.0	23.8	-18.675
75.0	-36.0	40.9	-27.011
100.0	-34.0	65.5	-0.501
138.0	-32.0	66.2	-0.534
210.0	-31.3	67.5	-0.407
283.0	-30.7	68.5	-0.346
433.0	-30.0	70.2	-0.277
818.0	-30.0	73.6	-0.235
1225.0	-30.0	76.5	-0.247
1657.0	-30.0	79.5	-0.298
2117.0	-30.0	83.2	-0.391
2608.0	-30.0	87.9	-0.396
3692.0	-35.3	97.6	-0.424
4948.0	-41.4	108.1	-0.442
6439.0	-49.0	118.9	-0.519
7310.0	-52.0	125.3	-0.804
8302.0	-55.0	135.2	-0.340
19751.0	-55.0	161.2	

NEUTRAL HEIGHT BETWEEN 10. M AND 5.M.

ICE FOG

SOUNDING 4, ICE ABSORPTION 0.01280/M, FOG DEPTH 100. M

HEIGHT (M)	TEMPERATURE (DEG C)	FLUX (CAL/SQ CM/12 HR)	MEAN HEATING RATE, LAYER ABOVE Z (DEG C/12 HR)
0.0	-33.0	23.3	-8.216
0.5	-33.0	23.5	-8.258
1.0	-33.0	23.6	-8.297
2.0	-33.0	23.9	-8.454
5.0	-33.0	24.8	-8.810
10.0	-33.1	26.5	-9.293
15.0	-33.1	28.2	-9.816
20.0	-33.2	30.0	-10.691
30.0	-33.3	33.9	-12.013
40.0	-33.4	38.3	-13.527
50.0	-33.5	43.3	-16.787
75.0	-33.8	58.6	-22.754
100.0	-34.0	79.3	0.077
138.0	-32.0	79.2	-0.235
210.0	-31.3	79.8	-0.221
283.0	-30.7	80.4	-0.229
433.0	-30.0	81.5	-0.212
818.0	-30.0	84.1	-0.199
1225.0	-30.0	86.5	-0.222
1657.0	-30.0	89.2	-0.279
2117.0	-30.0	92.7	-0.376
2608.0	-30.0	97.3	-0.387
3692.0	-35.3	106.7	-0.419
4948.0	-41.4	117.0	-0.439
6439.0	-49.0	127.8	-0.517
7310.0	-52.0	134.2	-0.803
8302.0	-55.0	144.0	-0.339
19751.0	-55.0	170.1	

NEUTRAL HEIGHT BETWEEN 40. M AND 30.M.

ICE FOG

SOUNDING 4, ICE ABSORPTION 0.02560/M, FOG DEPTH 100. M

HEIGHT (M)	TEMPERATURE (DEG C)	FLUX (CAL/SQ CM/12 HR)	MEAN HEATING RATE, LAYER ABOVE Z (DEG C/12 HR)
0.0	-44.0	-6.7	5.203
0.5	-43.0	-6.8	0.495
1.0	-42.5	-6.8	-3.840
2.0	-42.0	-6.7	-4.233
5.0	-41.5	-6.2	-4.933
10.0	-41.0	-5.3	-5.976
15.0	-40.5	-4.2	-7.379
20.0	-40.0	-2.8	-8.657
30.0	-39.5	0.4	-10.089
40.0	-39.0	4.1	-13.535
50.0	-38.0	9.0	-22.922
75.0	-36.0	30.0	-44.261
100.0	-34.0	70.3	-0.342
138.0	-32.0	70.8	-0.439
210.0	-31.3	71.9	-0.345
283.0	-30.7	72.7	-0.306
433.0	-30.0	74.2	-0.254
818.0	-30.0	77.3	-0.222
1225.0	-30.0	80.1	-0.238
1657.0	-30.0	83.0	-0.291
2117.0	-30.0	86.5	-0.386
2608.0	-30.0	91.3	-0.393
3692.0	-35.3	100.9	-0.423
4948.0	-41.4	111.3	-0.441
6439.0	-49.0	122.1	-0.518
7310.0	-52.0	128.5	-0.804
8302.0	-55.0	138.3	-0.340
19751.0	-55.0	164.4	

NEUTRAL HEIGHT BETWEEN 1. M AND 0.M.

ICE FOG

SOUNDING 4, ICE ABSORPTION 0.02560/M, FOG DEPTH 100. M

HEIGHT (M)	TEMPERATURE (DEG C)	FLUX (CAL/SQ CM/12 HR)	MEAN HEATING RATE, LAYER ABOVE Z (DEG C/12 HR)
0.0	-33.0	7.0	-5.003
0.5	-33.0	7.1	-5.045
1.0	-33.0	7.2	-5.086
2.0	-33.0	7.4	-5.257
5.0	-33.0	8.0	-5.667
10.0	-33.1	9.0	-6.268
15.0	-33.1	10.2	-6.975
20.0	-33.2	11.5	-8.284
30.0	-33.3	14.5	-10.509
40.0	-33.4	18.4	-13.423
50.0	-33.5	23.3	-21.125
75.0	-33.8	42.6	-39.775
100.0	-34.0	78.8	0.058
138.0	-32.0	78.7	-0.246
210.0	-31.3	79.3	-0.228
283.0	-30.7	79.9	-0.233
433.0	-30.0	81.1	-0.214
818.0	-30.0	83.7	-0.200
1225.0	-30.0	86.1	-0.223
1657.0	-30.0	88.9	-0.280
2117.0	-30.0	92.3	-0.377
2608.0	-30.0	96.9	-0.387
3692.0	-35.3	106.4	-0.419
4948.0	-41.4	116.7	-0.439
6439.0	-49.0	127.5	-0.517
7310.0	-52.0	133.8	-0.803
8302.0	-55.0	143.7	-0.339
19751.0	-55.0	169.7	

NEUTRAL HEIGHT BETWEEN 10. M AND 5.M.

ICE FOG

SOUNDING 4, ICE ABSORPTION 0.05120/M, FOG DEPTH 100. M

HEIGHT (M)	TEMPERATURE (DEG C)	FLUX (CAL/SQ CM/12 HR)	MEAN HEATING RATE, LAYER ABOVE Z (DEG C/12 HR)
0.0	-44.0	-9.0	11.020
0.5	-43.0	-9.2	3.814
1.0	-42.5	-9.3	-1.884
2.0	-42.0	-9.2	-2.940
5.0	-41.5	-8.9	-3.265
10.0	-41.0	-8.3	-3.562
15.0	-40.5	-7.6	-4.409
20.0	-40.0	-6.8	-4.285
30.0	-39.5	-5.2	-3.697
40.0	-39.0	-3.9	-6.401
50.0	-38.0	-1.5	-18.128
75.0	-36.0	15.1	-64.752
100.0	-34.0	74.0	-0.195
138.0	-32.0	74.3	-0.361
210.0	-31.3	75.2	-0.296
283.0	-30.7	75.9	-0.275
433.0	-30.0	77.3	-0.237
818.0	-30.0	80.2	-0.212
1225.0	-30.0	82.8	-0.232
1657.0	-30.0	85.6	-0.286
2117.0	-30.0	89.1	-0.382
2608.0	-30.0	93.8	-0.390
3692.0	-35.3	103.3	-0.421
4948.0	-41.4	113.7	-0.440
6439.0	-49.0	124.5	-0.518
7310.0	-52.0	130.8	-0.803
8302.0	-55.0	140.7	-0.340
19751.0	-55.0	166.8	

NEUTRAL HEIGHT BETWEEN 1. M AND 0. M.

ICE FOG

SOUNDING 4, ICE ABSORPTION 0.05120/M, FOG DEPTH 100. M

HEIGHT (M)	TEMPERATURE (DEG C)	FLUX (CAL/SQ CM/12 HR)	MEAN HEATING RATE, LAYER ABOVE Z (DEG C/12 HR)
0.0	-33.0	1.0	-1.475
0.5	-33.0	1.0	-1.470
1.0	-33.0	1.1	-1.438
2.0	-33.0	1.1	-1.425
5.0	-33.0	1.3	-1.468
10.0	-33.1	1.5	-1.616
15.0	-33.1	1.8	-1.872
20.0	-33.2	2.2	-2.534
30.0	-33.3	3.1	-4.026
40.0	-33.4	4.6	-6.591
50.0	-33.5	7.0	-17.045
75.0	-33.8	22.6	-61.260
100.0	-34.0	78.4	0.040
138.0	-32.0	78.3	-0.255
210.0	-31.3	78.9	-0.234
283.0	-30.7	79.5	-0.237
433.0	-30.0	80.7	-0.216
818.0	-30.0	83.3	-0.201
1225.0	-30.0	85.8	-0.224
1657.0	-30.0	88.5	-0.280
2117.0	-30.0	92.0	-0.377
2608.0	-30.0	96.6	-0.387
3692.0	-35.3	106.1	-0.420
4948.0	-41.4	116.4	-0.439
6439.0	-49.0	127.2	-0.517
7310.0	-52.0	133.5	-0.803
8302.0	-55.0	143.4	-0.339
19751.0	-55.0	169.4	

NEUTRAL HEIGHT BETWEEN 1. M AND 1.M.

CHAPTER VI

DISCUSSION AND CONCLUSIONS

In the course of the computations, it became apparent that the values of the net fluxes even without fog computed by the two programs differed more than could be accounted for by the different order of integration in the computations. This led to a reexamination of the Elsasser tables, described in Section A. Section B deals with the results for ice crystals, and includes a reexamination of the temperature gradient between crystal and air, first examined by Gotaas and Benson (1965). The cooling rates for ice fog as computed for scattering and non-scattering gray crystals are considered in Section C. Section D discusses some of the possible effects on the local climate and air pollution potential of the type of cooling rates observed.

A. The Elsasser Chart

If both the gray-crystal program and the scattering program are run on the same sounding for the case in which there are no ice crystals or fog, the results should be nearly the same for both programs. The flux at ground level was computed in this way for the composite terminal ice fog sounding. The calculated fluxes were 94.3 cal $cm^{-2}(12\ hr)^{-1}$ using the gray formula and 27.2 cal $cm^{-2}\ (12\ hr)^{-1}$ using the scattering formula. Results in the black case were confirmed by hand calculation using Elsasser's values of R. (Note that the reference throughout this section is Elsasser and Culbertson, 1960.)

Physically, a net flux of 90 cal $cm^{-2}(12\ hr)^{-1}$ at a ground temperature of -50°C is extremely unrealistic. Measured net flux values

during ice fog but above the fog layer indicate that the incoming and outgoing fluxes should nearly balance at this temperature; the rarity of temperatures lower than -50°C in the Fairbanks area leads to the same conclusion. Furthermore, examination of fluxes for individual wave numbers in the scattering formula confirms that the net flux is essentially outgoing blackbody radiation in the window regions and incoming radiation in the centers of the water vapor and carbon dioxide bands, as would be expected.

There are only three differences between the two formulas for this particular case. One results from using generalized transmissivities for -40°C in the scattering formula; Elsasser allowed for the temperature variation in the generalized absorption coefficient by setting $\log L = \log L_0 - a' \frac{T_0-T}{T} (\nu-\nu_0)^2 + \log \frac{T_0}{T}$. a is a constant. Since the temperature variation in our soundings was only about $\pm$ 15°C, our neglect of this factor should not cause serious error, except possibly in the strong inversions near the ground. A second difference results from neglecting Elsasser's band area correction, which is especially important at small path lengths. This would be very difficult to do in the scattering formula.

The third point of difference is that Elsasser only computed the ΔR's for the CO_2-H_2O overlap region for a T of +20°C. Our application of these results to soundings with temperatures of the order of -40°C is a very crude approximation. This is especially true since in an ice fog sounding CO_2 may contribute a sizeable fraction of the total downward flux.

The Elsasser formulation should give better results than the scattering formula for the no-ice case, except possibly in the CO_2 band.

The ideal solution would probably include both the bandwidth correction and the temperature correction for the generalized absorption coefficient in the scattering formula, together with a recomputation of R (page 70) for the CO_2 region in the gray formula. We hope to carry out these computations in the near future. For the present discussion, the Elsasser R's were recomputed using the same optical constants for water vapor and carbon dioxide as were used in the scattering formula. The CO_2 band was handled by omitting the wave numbers from 540 to 900 cm^{-1} in computing $R(H_2O)$, and calculating $R(CO_2)$ = $\int_{540}^{900} (1-\tau(CO_2)\tau(H_2O)) \frac{dB}{dT} d\nu$. The temperature variation of $R_{(CO_2)}$ was handled by fitting a second order Taylor series to Elsasser's $R(CO_2)$ over a 20°C range both above and below -40°C. This gave $R_{CO_2}(T) = R_{CO_2}[1 + .011(T+40)]$ for $\log \nu < 0$, and $R_{CO_2}(T) = R_{CO_2}[1+.012(T+40) + .00001(T+40)^2]$ for $\log \nu > 0$. Table VI-1 shows the values of $R(H_2O)$ actually used in the program. Table VI-2 gives our recomputed $R(CO_2)$'s, which, for small values of u, may be compared with Elsasser's $R(CO_2)$'s for T = -40°C. The values of

$$\int_{-273}^{-60} R(H_2O)\, dT \quad \text{and} \quad \int_{-273}^{-60} R(CO_2)\, dT,$$

given in Tables VI-3 and VI-4, are not directly comparable with any of Elsasser's tabulated functions. The program used for the recomputation was given in Chapter V, Section A.

Flux and cooling rate values from the gray formula with the original and recomputed R's are given for the terminal ice fog sounding with

TABLE VI-1

R(H2O)

T	-60	-50	-40	-30	-20	-10
LOG U						
-5.0	0.050	0.054	0.058	0.063	0.069	0.076
-4.7	0.076	0.082	0.089	0.097	0.107	0.118
-4.3	0.127	0.137	0.149	0.164	0.181	0.201
-4.0	0.181	0.196	0.213	0.234	0.259	0.288
-3.7	0.251	0.271	0.296	0.326	0.360	0.401
-3.3	0.373	0.405	0.443	0.488	0.541	0.602
-3.0	0.487	0.530	0.581	0.641	0.712	0.794
-2.7	0.618	0.674	0.740	0.818	0.910	1.017
-2.3	0.809	0.885	0.975	1.081	1.206	1.351
-2.0	0.956	1.048	1.158	1.287	1.437	1.612
-1.7	1.101	1.210	1.339	1.490	1.667	1.872
-1.3	1.287	1.418	1.572	1.751	1.960	2.202
-1.0	1.417	1.563	1.734	1.932	2.163	2.428
-0.7	1.536	1.696	1.882	2.097	2.347	2.633
-0.3	1.672	1.849	2.053	2.289	2.562	2.873
0.0	1.755	1.943	2.160	2.410	2.697	3.026

TABLE VI-2

R(CO2)

LOG V	-3.3	-3.0	-2.7	-2.3	-2.0	-1.7	-1.3
	-1.0	-0.7	-0.3	0.0	0.3	0.7	1.0
	1.3	1.7	2.0	2.3	2.7	3.0	
LOG U							
-5.0	0.052	0.069	0.090	0.126	0.161	0.204	0.275
	0.340	0.412	0.518	0.600	0.681	0.784	0.857
	0.927	1.017	1.081	1.144	1.229	1.290	
-4.7	0.052	0.069	0.090	0.126	0.161	0.204	0.275
	0.340	0.412	0.518	0.600	0.681	0.784	0.857
	0.927	1.017	1.081	1.144	1.229	1.290	
-4.3	0.052	0.069	0.090	0.126	0.161	0.204	0.275
	0.340	0.412	0.518	0.600	0.681	0.784	0.857
	0.927	1.017	1.081	1.144	1.229	1.290	
-4.0	0.052	0.069	0.090	0.126	0.161	0.204	0.275
	0.340	0.412	0.518	0.600	0.681	0.784	0.857
	0.927	1.017	1.081	1.144	1.229	1.290	
-3.7	0.052	0.069	0.090	0.126	0.161	0.204	0.275
	0.340	0.412	0.518	0.600	0.681	0.784	0.857
	0.927	1.017	1.081	1.144	1.229	1.290	
-3.3	0.052	0.069	0.090	0.126	0.161	0.204	0.275
	0.340	0.412	0.518	0.600	0.681	0.784	0.857
	0.927	1.017	1.081	1.144	1.229	1.290	
-3.0	0.053	0.070	0.090	0.127	0.162	0.205	0.276
	0.340	0.413	0.519	0.601	0.682	0.785	0.858
	0.928	1.018	1.081	1.144	1.230	1.290	
-2.7	0.055	0.072	0.092	0.129	0.164	0.207	0.278
	0.342	0.415	0.521	0.602	0.683	0.786	0.859
	0.929	1.019	1.083	1.145	1.231	1.291	

TABLE VI-2 (CONT)

LOG V	-3.3	-3.0	-2.7	-2.3	-2.0	-1.7	-1.3
	-1.0	-0.7	-0.3	0.0	0.3	0.7	1.0
	1.3	1.7	2.0	2.3	2.7	3.0	
LOG U							
-2.3	0.063	0.080	0.100	0.137	0.171	0.214	0.286
	0.350	0.422	0.528	0.610	0.690	0.793	0.866
	0.936	1.025	1.089	1.151	1.236	1.296	
-2.0	0.074	0.090	0.111	0.147	0.182	0.225	0.296
	0.360	0.432	0.538	0.619	0.700	0.802	0.875
	0.944	1.033	1.096	1.158	1.242	1.302	
-1.7	0.089	0.105	0.126	0.162	0.197	0.240	0.311
	0.374	0.446	0.551	0.632	0.713	0.814	0.886
	0.955	1.043	1.106	1.167	1.250	1.309	
-1.3	0.120	0.136	0.156	0.192	0.227	0.269	0.339
	0.402	0.474	0.578	0.658	0.737	0.837	0.908
	0.976	1.063	1.124	1.184	1.265	1.323	
-1.0	0.152	0.168	0.189	0.224	0.258	0.300	0.369
	0.432	0.502	0.604	0.683	0.761	0.860	0.930
	0.997	1.082	1.142	1.201	1.281	1.337	
-0.7	0.196	0.212	0.232	0.267	0.300	0.341	0.409
	0.470	0.539	0.640	0.717	0.794	0.890	0.959
	1.024	1.107	1.166	1.223	1.301	1.355	
-0.3	0.277	0.292	0.311	0.345	0.377	0.416	0.482
	0.540	0.607	0.703	0.778	0.851	0.944	1.010
	1.072	1.151	1.207	1.262	1.336	1.387	
0.0	0.357	0.371	0.390	0.421	0.452	0.490	0.553
	0.609	0.673	0.765	0.837	0.907	0.996	1.058
	1.117	1.193	1.246	1.297	1.367	1.416	

TABLE VI-3

INTEGRAL R(H2O) DT

LOG U	INTEGRAL R DT
-5.0	5.000
-4.7	7.404
-4.3	12.058
-4.0	16.911
-3.7	23.122
-3.3	33.675
-3.0	43.195
-2.7	53.682
-2.3	68.144
-2.0	78.579
-1.7	88.356
-1.3	100.260
-1.0	108.233
-0.7	115.279
-0.3	124.022
0.0	127.517

TABLE VI-4

INTEGRAL R(CO2) DT

LOG V	-3.3	-3.0	-2.7	-2.3	-2.0	-1.7	-1.3
	-1.0	-0.7	-0.3	0.0	0.3	0.7	1.0
	1.3	1.7	2.0	2.3	2.7	3.0	
LOG U							
-5.0	1.975	2.600	3.379	4.740	6.056	7.671	10.352
	12.762	15.487	19.453	22.514	25.542	29.402	32.136
	34.762	38.124	40.506	42.869	46.046	48.311	
-4.7	1.975	2.600	3.379	4.740	6.056	7.671	10.352
	12.762	15.487	19.453	22.514	25.542	29.402	32.136
	34.762	38.124	40.506	42.869	46.046	48.311	
-4.3	1.975	2.600	3.379	4.740	6.056	7.671	10.352
	12.762	15.487	19.453	22.514	25.542	29.402	32.136
	34.762	38.124	40.506	42.869	46.046	48.311	
-4.0	1.975	2.600	3.379	4.740	6.056	7.671	10.352
	12.762	15.487	19.453	22.514	25.542	29.402	32.136
	34.762	38.124	40.506	42.869	46.046	48.311	
-3.7	1.975	2.600	3.379	4.740	6.056	7.671	10.352
	12.762	15.487	19.453	22.514	25.542	29.402	32.136
	34.762	38.124	40.506	42.869	46.046	48.311	
-3.3	1.975	2.600	3.379	4.740	6.056	7.671	10.352
	12.762	15.487	19.453	22.514	25.542	29.402	32.136
	34.762	38.124	40.506	42.869	46.046	48.311	
-3.0	2.015	2.639	3.418	4.778	6.093	7.707	10.386
	12.795	15.518	19.481	22.540	25.566	29.424	32.157
	34.782	38.142	40.523	42.884	46.059	48.323	
-2.7	2.101	2.725	3.503	4.862	6.175	7.788	10.465
	12.872	15.593	19.553	22.609	25.634	29.489	32.219
	34.842	38.200	40.578	42.938	46.109	48.370	

TABLE VI-4 (CONT)

LOG V	-3.3	-3.0	-2.7	-2.3	-2.0	-1.7	-1.3
	-1.0	-0.7	-0.3	0.0	0.3	0.7	1.0
	1.3	1.7	2.0	2.3	2.7	3.0	
LOG U							
-2.3	2.461	3.084	3.861	5.219	6.530	8.141	10.814
	13.217	15.935	19.889	22.941	25.960	29.807	32.530
	35.146	38.492	40.861	43.208	46.362	48.607	
-2.0	2.935	3.557	4.333	5.689	6.998	8.606	11.275
	13.674	16.386	20.331	23.376	26.386	30.219	32.930
	35.530	38.854	41.204	43.531	46.654	48.875	
-1.7	3.607	4.228	5.001	6.353	7.658	9.261	11.921
	14.311	17.013	20.941	23.971	26.963	30.768	33.455
	36.031	39.318	41.640	43.936	47.019	49.208	
-1.3	4.934	5.548	6.315	7.654	8.947	10.534	13.168
	15.534	18.207	22.091	25.083	28.034	31.779	34.419
	36.946	40.168	42.440	44.683	47.694	49.827	
-1.0	6.345	6.952	7.708	9.029	10.304	11.869	14.467
	16.800	19.435	23.264	26.212	29.119	32.803	35.396
	37.876	41.032	43.255	45.444	48.383	50.461	
-0.7	8.238	8.832	9.573	10.867	12.116	13.649	16.194
	18.479	21.060	24.810	27.697	30.542	34.143	36.675
	39.092	42.163	44.322	46.441	49.285	51.289	
-0.3	11.696	12.268	12.980	14.222	15.422	16.895	19.338
	21.532	24.009	27.607	30.375	33.098	36.537	38.950
	41.248	44.158	46.199	48.190	50.863	52.734	
0.0	15.074	15.622	16.304	17.494	18.643	20.054	22.393
	24.494	26.864	30.303	32.946	35.542	38.811	41.099
	43.272	46.017	47.936	49.802	52.308	54.051	

zero fog in Table VI-5. It is immediately apparent that the cooling rates near the ground are drastically changed by slight change in the coefficients. This is also true in the presence of fog. The equation utilizing Elsasser's values of R shows strong cooling in the lowest half meter of the sounding with a lesser cooling rate or even some heating higher up in all cases. Our modified values of R give heating rates very near the ground in most cases. It is not clear whether the difference obtained by using the two sets of R's is due to the neglect of corrections for temperature and band area or to the improved CO_2 correction in the modified coefficients. In the former case, the original Elsasser values are a better approximation and the rates near the ground are probably real. In the latter case the heating rates imply that the assumed surface inversion was too strong for radiative equilibrium, especially with the CO_2. Further investigation of this problem is planned.

Whatever may be the effects of the change in R on the cooling rate near the ground, there are two reasons for choosing the modified values in the present context. First, the net fluxes obtained are considerably more realistic than those obtained by the use of the unmodified Elsasser coefficients. Second, the modified coefficients for water vapor and carbon dioxide are compatible with those used in the scattering formula. Therefore, different results obtained by using the two formulas may be attributed, with confidence, to the way in which the ice crystals are treated. Consequently, all of the values from the gray formula in Chapter V were computed using the modified coefficients.

Table VI-5

Comparison of Results from Original and Modified

Sounding 5, no fog Height (M)	Temperature (°C)	Elsassar Coefficients Flux cal $cm^{-2}(12\ hr)^{-1}$	Mean Heating Rate Layer above Z °C $(12\ hr)^{-1}$
0.0	-50.0	94.3	-10.954
0.5	-47.0	94.5	4.205
1.0	-45.0	94.5	9.205
2.0	-44.0	94.1	2.875
5.0	-43.5	93.8	2.058
10.0	-43.0	93.4	1.490
15.0	-42.0	93.1	1.501
20.0	-41.0	92.9	0.909
30.0	-40.0	92.5	0.712
40.0	-38.0	92.3	1.051
50.0	-36.0	91.9	1.361
60.0	-34.0	91.4	1.078
80.0	-33.0	90.7	0.790
100.0	-32.0	90.1	1.397
139.0	-30.6	88.3	0.349
213.0	-28.0	87.4	0.119
287.0	-27.6	87.1	-0.016
438.0	-27.0	87.2	-0.091
829.0	-25.3	88.3	-0.199
1246.0	-23.6	90.7	-0.279
1690.0	-22.0	94.1	-0.342
2164.0	-23.3	98.3	-0.294
2667.0	-26.6	102.0	-0.326
3783.0	-28.0	110.0	-0.334
5071.0	-36.0	118.2	-0.345
6588.0	-45.7	126.7	-0.551
8047.0	-55.0	137.5	-0.846
8459.0	-55.0	141.7	-0.231
19908.0	-55.0	159.4	

Elsasser Coefficients

Modified Coefficients	
Flux cal $cm^{-2}(12\ hr)^{-1}$	Mean Heating Rate Layer above Z $°C\ (12\ hr)^{-1}$
31.5	5.343
31.4	-1.783
31.5	-2.857
31.6	-3.273
31.9	-0.777
32.1	-0.217
32.1	-0.415
32.2	-0.268
32.3	-0.245
32.4	-0.859
32.7	-1.616
33.2	-1.719
34.4	-1.341
35.4	-1.326
37.2	-1.072
39.8	-0.904
42.0	-0.605
45.0	-0.399
49.9	-0.375
54.5	-0.445
59.9	-0.504
66.1	-0.408
71.1	-0.472
82.8	-0.580
97.0	-0.554
110.6	-0.514
120.7	-0.641
123.9	-0.337
149.7	

For Comparison, the scattering formula gives 27.2 at z=0 and 149.2 at 19908 m.

B. Ice Crystal Display Results

1. Cooling Rates at a Given Height

It is immediately apparent from the tabulated data of Chapter V that atmospheric radiative cooling due even to the most tenuous crystal display considered is an order of magnitude greater than that due to radiation from atmospheric gases alone. However, the total outward energy loss, from the atmosphere and the underlying snow surface, as measured by the net flux at a level above the crystal display, varies by only about 10%. The increased radiative cooling rate in the atmosphere therefore implies a decreased cooling rate at the snow surface. Qualitatively, an increase in cooling aloft coupled with a relative decrease in cooling at ground level will lead, after a time, to a lapse rate which is less stable than it would have been after the same time interval with the original cooling rates*. Any tendency toward destabilization of the lapse rate near the ground will tend to increase the fraction of the energy loss from the surface which is balanced by eddy conduction from the air. One effect of a crystal display will then be to decrease sharply the energy loss from the snow pack and the ground.

The maximum cooling rate in the soundings considered is at the top of the crystal layer even when this is at a temperature minimum. Inside the crystal layer, the cooling rate increases roughly exponentially with height. This fact, together with the observed strong dominance of suspended ice crystals in the cooling process, suggests an approximate means of obtaining the cooling rate at a given height in the display.

*Note that in many cases this may mean that the near-ground air continues to increase in stability, but less rapidly than otherwise.

Let the crystal-containing layer be isothermal and at the same temperature, T, as the snow surface, as is the case in composite sounding 3. The upward flux will be constant with height in the isothermal layer, while the downward flux will vary with height primarily due to the change in number of ice crystals above a variable reference point as it moves vertically through the layer. If the variation of the downward flux with atmospheric gases is neglected within the crystal display and if k is the ice absorption coefficient and $\bar{z}_s$ is the height of the top of the display,

$$\dot{F} \tilde{=} F_+ - F_-(\bar{z}_s) - (1 - e^{-k(\bar{z}_1 - z)})\,(\sigma T^4 - F_-(\bar{z}_s)) \qquad (6\text{-}1)$$

and

$$\frac{dF}{dz} \tilde{=} k e^{-k(\bar{z}_s - z)}\,(\sigma T^4 - F_-(\bar{z}_s)) \qquad (6\text{-}2)$$

Also,

$$\bar{C}(z_1, z_2) = \left[\frac{D(\sigma T^4 - F_-(\bar{z}_1))}{z_2 - z_1}\right] = \frac{D}{z_2 - z_1} \int_{z_1}^{z_2} \frac{dF}{dz}\, dz, \qquad (6\text{-}3)$$

where $\bar{C}$ is the mean cooling rate for the layer from z_1 to z_2, taken from the tables in Chapter V. D is a constant, equal to $\left[8.35 \times 10^{-3}(P/T) + L_s \frac{d\rho_i}{dT}\right]^{-1}$ (see section IV-F). Substituting (6-2) in (6-3) gives:

$$\bar{C}(z_1, z_2) = \frac{D(\sigma T^4 - F_-(z_s))}{z_2 - z_1} \int_{z_1}^{z_2} k e^{-k(\bar{z}_s - z)}\, dz = \frac{D(\sigma T - F_-(\bar{z}_s))}{z_2 - z_1}\left[e^{-k(\bar{z}_s - z_2)} - e^{-k(z_2 - z_1)}\right]$$

and if c(z) is the cooling rate at a specific height z, $z_2 > z > z_1$,

$$c(z) = D \frac{dF}{dz} = D\, k e^{-k(\bar{z}_s - z)} (\sigma T^4 - F(\bar{z}_s)) \text{ and } \frac{c(z)}{\bar{C}(z_1, z_2)} = \frac{k e^{-k(\bar{z}_s - z)}(z_2 - z_1)}{e^{-k(\bar{z}_s - z_2)} - e^{-k(\bar{z}_s - z_1)}}$$ from which

$$c(z) = \bar{C}(z_1, z_2) \frac{k e^{-k(\bar{z}_s - z)}(z_2 - z_1)}{e^{-k(\bar{z}_s - z_2)} - e^{-k(\bar{z}_s - z_1)}} \qquad (6\text{-}4)$$

This expression should be accurate to within a few percent if the entire depth of the ice crystal display is isothermal. If there is a normal lapse rate within the layer, crystals near the top of the layer will radiate less and receive more radiation from below, while those near the bottom will radiate more but receive less from above. The magnitude of the cooling rate will be less than given by (6-4) near the top of the layer z_1 to z_2, and greater near the bottom. If the lapse rate is inverted, the situation is reversed. (6-4) now underestimates the cooling rate near z_2, and overestimates it near z_1.

2. Comparison with Results from Gotaas and Benson

Gotaas and Benson (1965) give cooling rates at 915 m for sounding 1 and 1025 m for sounding 2, neglecting interaction between crystals. Since they included the effects of radiation from water vapor and carbon dioxide incident on the crystals, their rates should be similar to those we obtain for the top of the crystal layer.

According to Table V-4, the cooling rate for the layer from 600 to 915 m, with 915 m as the top of the crystal display, is 3.7°C $(12\ hr)^{-1}$. The lapse rate to 915 m is normal. From (6-4) we have

$$_c(915) = 3.7\left(\frac{.618}{1-e^{-.618}}\right) = 5°C(12\ hr)^{-1}$$

The true cooling rate should be slightly less, but still greater than 3.7°C $(12\ hr)^{-1}$.

For sounding 2 we neglected to include a display height of 1025 m, but for a display with top at 1150 m the cooling rate at 1025 m is

$$_c(1025) = 5\ \frac{498\ e^{-.249}}{1-e^{.498}} = 5°C\ (12\ hr)^{-1}$$

and that at 1150 m is

$$_c(1150) = 6.5°C(12\ hr)^{-1}$$

As the temperature at 1150 m is slightly greater than that at 1025 m, the true cooling rate at 1025 m should be somewhere between these values.

The values for ice crystal cooling given by Gotaas and Benson (1965) are 3.1°C $(12\ hr)^{-1}$ at 915 m in sounding 1 and 2.5°C $(12\ hr)^{-1}$ at 1025 m for sounding 2. An attempt will be made to explain the difference between the two sets of calculated cooling rates. The Elsasser chart (1942 version) was used by Gotaas and Benson to obtain the upward and downward fluxes due to the snow surface and atmospheric gases without ice crystals, and the net radiative loss from the crystal was then computed by subtracting these incoming fluxes from twice the black body flux and multiplying the whole by the area of one face of the crystal. A repetition of this procedure, using the 1942 edition of the

Elsasser chart, led to the same results as were reported by Gotaas and Benson for the 14 December sounding, but to twice their results for the 24 January sounding. Accepting the 14 December cooling rate and doubling the one for 24 January gives values which are still low compared to ours. If the 1960 Elsasser coefficients rather than our modified values (above) are used the difference is even more pronounced. Comparison of the values given on the auxiliary table on the 1942 chart with those given by Elsasser and Culbertson (1960) indicate that the remaining discrepancy in cooling rates is due to differences in the two sets of unmodified Elsasser coefficients.

3. The Heat Flow between the Crystals and the Surrounding Air

Gotaas and Benson (1965) pointed out that the crystals would be colder than the ambient air and suggested this as the reason behind the measured humidities in the crystal layer being less than ice saturation. Although the computational method used here does not give the energy budget at the crystal surface directly, it is possible to obtain some approximate values.

Let the cooling rate at the top of the crystal layer be c, and the cooling rate at the same height in the absence of ice crystals be c'. We will assume that at all heights within the display the ratio of energy loss from the crystals to the total energy loss is given by

$$N = \frac{c-c'}{c} = 1 - \frac{c'}{c} = 1 - \left[\frac{(1-e^{-k(\bar{z}_s-z_1)})\,c'}{\bar{C}\,(\bar{z}_s,z_1)k(\bar{z}_s-z_1)}\right] \qquad (6\text{-}5)$$

At any given height, the net energy loss from a column 1 m deep by 1 cm^2 in area due to crystals will be approximately

$$E_F = M \frac{F(z_2)-F(z_1)}{z_2-z_1}$$

This much energy must be conducted to the crystals from the air. At the same time, an amount of energy $L_s \frac{d\rho_i}{dT} \bar{C} = E_L$ is being generated by the crystals from sublimation onto their surfaces. Using the formula

$$\frac{F(z_2) - F(z_1)}{(z_2-z_1)} = \bar{C} \left[8.35 \times 10^{-3} P/T + L_s \frac{d\rho_i}{dT} \right]$$

(see Eq. 4-3)

we have for the net energy flow to the crystal from the air

$$E = E_F - E_L = \left[M(8.35 \times 10^{-3} (P/T) + L_s \frac{d\rho_i}{dT}) - L_s \frac{d\rho_i}{dT} \right] \bar{C} ,$$

$$\text{or } E = \left[M(8.35 \times 10^{-3} (P/T)) - (1-M) L_s \frac{d\rho_i}{dT} \right] \bar{C} . \qquad (6\text{-}6)$$

Since 1 - M is of the order of .1 or less, and $L_s \frac{d\rho_i}{dT}$ is an order of magnitude less than 8.35×10^{-3} (P/T), the term (1-M) $L_s \frac{d\rho_i}{dT}$ is negligible, and to a good approximation

$$E = 8.35 \times 10^{-3} (P/T) M\bar{C} \qquad (6\text{-}6')$$

By definition k is the total area of the upper surfaces of the crystals in a m cm^2 volume, so the total conductive surface for plane crystals in this volume is 2k. The energy flow per cm^2 to the crystals is then

$$H' = \frac{8.35 \times 10^{-3} (P/T) M\bar{C}}{2k}$$

From Chapter IV, section F2a, the energy flow, H', is given by $-k'\vec{\nabla}T$. In the immediate vicinity of the crystal, then,

we will have

$$\vec{\nabla}T = - \frac{8.35 \times 10^{-3}(P/T)\ M\bar{C}}{2kk'} \qquad (6\text{-}7)$$

If we assume that our crystal is an infinitely thin circular plate of uniform temperature and zero heat capacity, it is also true that

$$\nabla^2 T = 0$$

Mathematically this is identical to the problem of the voltage distribution around a thin flat metal plate, charged to such a degree that $\vec{\nabla}V$ is numerically equal to $\vec{\nabla}T$, where V is the voltage. Since the electric field, $\vec{E}$, is equal to $-\vec{\nabla}V$, and the field at the surface of a flat plate will be that of an infinite charged plane,

$$\vec{\nabla}V = - \frac{g'}{2\epsilon_o} \approx - \frac{8.35 \times 10^{-3}(P/T)M\bar{C}}{2kk'} \qquad (6\text{-}8)$$

The $2\epsilon_o$ comes from the rationalized MKS system of electromagnetic units. The total "charge" on a single plate crystal will be $.01\ k\sigma'/n$, where σ', which is analogous to charge per unit area, is taken from equation (6-8) and n is the number of crystals per cm^3, so 100 n is the number of particles per cm^2m. The ratio of this "charge" to the difference between the "potentials" (actually temperatures) at the crystal surface and at a large distance is simply the capacity, which from Fletcher (1962, p.267) is equal to $8\epsilon_o$ a for a circular disc of radius a. So we have

$$\Delta T = \frac{.01k\sigma'}{8\epsilon_o an} = 1.04 \times 10^{-1}\ (P/T)\ M\bar{C}\ /\ nk'a\ .$$

k' is expressed in cal cm^{-2} $(12\ hr)^{-1}$ $°K^{-1}$, and a in μ. This equation gives the temperature difference between the crystal and the air at a distance large compared to a. As in the electrostatic analogue, the temperature difference will vary linearly with distance near the plane surfaces of the crystal and as one over the distance at a distance. In practice this equation will overestimate the temperature difference, since much of the heat transfer will actually take place at the edges of the crystal, making the temperature gradient adjacent to the plane surfaces less than that assumed above.

In order to put numbers into this equation, we shall use sounding 3 with 25 μ crystals and a display height of 600 m, to compute ΔT for the upper 200 m and the lowest 25 m. $N = .99$, $\bar{C} = 4.5$ and 1.6, and $a = 25$. If we assume that the molecular conductivity of the air is involved in the transfer process, the value of k' is 2.35 cal $°K^{-1}$ cm^{-2} $(12\ hr)^{-1}$. Values of P are 933 mb and 998.75 mb, while $T = 245$. In the interval of 400 to 600 m, this gives $\Delta T = 3 \times 10^{-2}$ °C, while from 0 to 25 m the temperature difference is $\Delta T = 1.1 \times 10^{-2}$ °C.

From the assumption $\vec{\nabla} T \tilde{=} \frac{\Delta T}{|\Delta \vec{r}|}$, where r is the distance normal to the crystal surface, we can also say that to a first approximation $\Delta r \tilde{=} 8.5\mu$.

In contrast to the treatment above, Gotaas and Benson (1965) started by assuming that the air in contact with the crystal surface was saturated. Next, they assumed that measured values of humidity less than ice saturation were due to the temperature difference between the ice crystals and the air. A temperature difference of 2°C is necessary to

account for relative humidities over ice of about 80%. The blackbody radiation to space was used to compute the energy loss from the ice crystals, which in turn was used to estimate a Δr of about 200μ. Our temperature gradient is of the same order of magnitude as theirs, but our calculations of the temperature difference from purely thermal considerations gives a ΔT which is so much smaller that it cannot possibly account for more than a fraction of a percent of any variation of the relative humidity from ice saturation. If the crystals are stable or growing, as appears to be the case, these calculations prove what most people suspect, namely that the humidity measurements at low temperatures are very unreliable.

4. General Conclusions for Ice Crystals and Snow

Several general conclusions can be drawn by comparing all soundings with crystal display absorption coefficients equal to .00196. Cooling rates near the ground decrease considerably as the total thickness of the layer containing crystals increases, but even for display depths around 600 m the cooling rates near the ground average an order of magnitude greater than in the absence of crystals. The radiative cooling in the upper part of the crystal layer exceeds the combined radiative and conductive cooling in the lower portion for all displays with tops above 600 m. If a lowering of the neutral height may be taken to indicate an increasing tendency toward destabilization of that portion of the airmass containing suspended crystals, then the tendency toward destabilization increases steadily with increasing thickness of the crystal display. Inside of a deep crystal layer a considerable amount of radiative cooling may take place while a normal

lapse rate is maintained. If the display has a sharp upper boundary, a strong inversion will form at the top of the crystal layer, but if the top of the display is diffuse (as may well be the actual case) the inversion will be weaker or an isothermal layer may develop.

In sharp contrast to this is the snowflake model. Even a 100 m layer of snowflakes is enough to cut the net flux at the snow surface to less than a tenth of a percent of its undisturbed value, although cooling rates in the air near the snow surface still show some enhancement. For all practical purposes, however, any thicker layer may be considered as a black cloud. Once an adiabatic lapse rate develops in such a cloud, the radiative heat loss from above will be spread over the depth of the cloud by convection.

The display composed of large crystals gives intermediate results, with near-ground cooling rates dropping below their undisturbed values for display thicknesses between 600 and 1000 m. It is evident that ice crystal fallout must be taken into account, regardless of crystal size, in considering radiative cooling, as first pointed out by Wexler (1936) and later emphasized by Gotaas and Benson (1965). Furthermore, the destabilizing influence of ice crystals on the air mass containing them must be considered, as well as the probable formation of an inversion at the top of the layer containing crystals.

One final statement should be made about ice crystal displays These displays frequently go unreported, and even if they are noted in the weather record there is no indication as to their height and density. Gotaas and Benson (1965) attributed the cooling at the start of ice fog events to ice crystal displays, but Bowling et al. (1968) pointed out

that advection of cold air was generally more than sufficient to account for the observed cooling rates at this time. Ohtake (1970) attributed some of the ice crystal displays in the Fairbanks area to fallout from power plant plumes. Taking a more general view, however, ice crystal displays occur generally over the uninhabited Arctic. It is clear that a considerable amount of water vapor must be removed from air as it cools from sea surface temperatures to -30°C or -40°C. Much of this moisture removal will take place conventionally, with precipitation from dense clouds. But by the time the air reaches temperatures of -25°C to -30°C, and especially if radiation is the primary cooling mechanism, the formation of scattered ice crystals with a clear sky is normal during the final stages of the cooling process. Many more data are needed on the prevalence, density and depth of crystal displays, particularly over the large continental masses of Canada and Siberia and over the Arctic Ocean. This may necessitate some special education for weather observers.

C. Ice Fog

1. Comparison of Scattering and Gray Results

There are two major differences between the gray and scattering formulas. Firstly, the gray formula neglects the variation of absorption due to ice crystals with wave number. This makes the effective ice absorption per crystal a function of the density of the fog.* Secondly

*Strictly speaking, the effective absorption coefficient depends on the ratio between ice crystal density and the densities of water vapor and CO_2. Since the two latter densities are essentially constant with constant temperature and pressure, only the fog density variation is significant.

the gray formula neglects scattering. The effects of scattering are (1) to reduce the effective emissivity of the fog top, thus reducing the amount of energy lost from the fog layer as a whole, and (2) to reduce the transmissivity without changing the emissivity, thus making it proportionately harder for radiation to escape from the lower layers of the fog.

The five sets of scattering and gray soundings in Chapter V give evidence that both effects occur but that scattering is the more important, especially as the optical depth of the entire fog layer becomes significant (in this case, of the order of unity). Thus the cooling rates for the two distribution a soundings can be approximated fairly well by assuming that the ice crystals absorb 25% of the radiation geometrically incident on them and transmit the remainder.

For a 20 m fog layer, distribution b, and 200 crystals cm^{-3}, fairly good agreement with both magnitude and shape of the cooling curve can be obtained from the gray formula with 50% of the black absorption by the crystals. For the 50 m fog depth with $n_b = 500$, and for the 100 m fog depth with $n_b = 1000$, the gray absorption coefficients which give the best mean cooling rates through the entire sounding are again 25% black, but the shape of the cooling rate curve is not correctly reproduced. The gray formula cooling rates are too low near the top of the fog and too high in the fog interior. If the absorption coefficients in the last two soundings are increased to 75% black, the shapes of the curves (as measured by the ratios of the cooling rates at various heights) match fairly well but the magnitude of the cooling rates are too high. Finally, if the 75% black cooling rates are multiplied by

the ratio of the outgoing fluxes for the scattering and gray cases, a curve is obtained which is quite close to the cooling rate from the scattering formula. As will be discussed in part 3 of this section, the ratio of scattering to non-scattering fluxes may be considered an albedo of sorts, and it is listed as such on the tables in Chapter V. Table VI-5 shows the cooling rates derived from the various procedures for the 100 m fog depth. The same procedure may be used to obtain the cooling rates for the 20 m fog, although in this case the improvement over the simple 50% black formula is not marked.

It appears that, at least for this sounding, a relatively simple means of calculating the cooling rates in a thick ice fog with a mixed-source type of size distribution and a strong ground inversion would be the following:

1. Calculate the flux-difference cooling rates for a gray fog with 75% of the black absorption.
2. Estimate the albedo from $n_b\Delta z$ and the known correlations $n_b\Delta z = 10^5$, albedo = .36; $n_b\Delta z = 25 \times 10^3$, albedo = .32; $n_b\Delta z = 4 \times 10^3$, albedo = .2. Δz is the thickness of the fog layer, and $n_b\Delta z$ has units of crystals per cm^2.
3. Multiply the cooling rates obtained in (1) by one minus the albedo found in (2).

This procedure appears to give results which agree with those from the scattering formula to approximately 10% for relative cooling rates (i.e., the shape of the cooling curve) and about 30% for the actual cooling rates above 5 m. Further investigation is needed to determine whether this procedure is workable for other temperature soundings.

Table VI-6

Comparison of Gray and Scattering Cooling Rates
for 100 m of 1000 crystal per cm^3 Ice Fog

height	Scattering	25% black	75% black	75% black x .64
0-.5	9.6	7.4	20.6	13.2
.5-1	-4.5	-5.4	-.35	-.22
1-2	-10.7	-11.8	-11.3	-7.2
2-5	-8.6	-10.5	-10.7	-6.9
5-10	-5.3	-8.2	-6.6	-4.2
10-15	-4.6	-8.5	-5.6	-3.6
15-20	-6.1	-10.1	-7.0	-4.5
20-30	-5.8	-11.3	-6.6	-4.2
30-40	-7.0	-13.6	-8.1	-5.2
40-50	-10.5	-17.8	-14.4	-9.2
50-60	-15.4	-22.6	-23.4	-15.0
60-80	-20.9	-26.5	-34.7	-22.2
80-100	-38.0	-30.8	-62.6	-40.0
100-139	-.594	-.274	.024	.015
Flux at 100 m	46.9	60.2	72.7	

Since our major interest is in whether a particular fog is likely to develop an adiabatic lapse rate, only the shape of the cooling curve is important here and the correction for magnitude of the cooling rate will not be discussed. For the purpose of determining the shape of the cooling curve, the equivalences in Table VI-7 will be assumed. The italic values are those most often observed in real ice fogs.

2. Stability of Lapse Rates in Ice Fog

As long as the cooling rate at the top of the fog layer exceeds that at the bottom, the lapse rate will destabilize towards the adiabatic.* If the cooling rate at the top is still greater than that near the bottom of the fog after the lapse rate becomes adiabatic, convection will begin in the fog. We will refer to an adiabatic lapse rate maintained by convection, which in turn is driven by differential cooling rates, as a convective lapse rate. Convective lapse rates are of considerable importance in considering the probable effects of air pollution, as will be discussed in Section D. Here we are concerned with the conditions under which convective lapse rates develop.

The strongest destabilizing influence in the core and residential areas will be the man-made heat term. This gives heating rates of about $65°C(12\ hr)^{-1}$ in the lowest 20 m of the core area and $16°C(12\ hr)^{-1}$ in the lowest 5 m of the residential area--enough to destabilize any fog considered in this paper. Even the $2°C(12\ hr)^{-1}$ heating rate calculated for the outlying area would have a noticable effect on the stability of borderline cases. It is probably a safe assumption that a

*Technically this entire discussion refers to a moist-adiabatic lapse rate. The numerical difference between dry and moist-adiabatic lapse rates at -40°C is unmeasurable in a 100 m layer.

TABLE VI-7

Equivalence between absorption coefficients (as given in tables) and number densities. Based on 25% absorption for distribution a and 75% absorption for distribution b.

Distribution a

1.6k (m^{-1})	n_a (cm^{-3})
.00064	100
.00128	200
.00256	400
.00512	800

Distribution b

1.6k (m^{-1})	n_b (cm^{-3})
.00160	42
.00320	83
.00640	166
.01280	330
.02560	665
.05120	1330

convective lapse rate develops downtown any time the fog depth exceeds 20 m, and the same may be true for the residential area.

Whether or not a convective lapse rate continues to exist in a fog which has drifted away from the city center will depend on radiative and conductive processes. According to the conductive heating calculations, tabulated with the scattering formula results in Chapter V, cooling due to conduction from the air to the snow occurs with a maximum value of $2.5°C(12\ hr)^{-1}$ in the lowest meter of the sounding, and values of about $0.1°C(12\ hr)^{-1}$ at greater heights. Since the cooling rates in the lowest meter of the sounding already have an uncertainty (Table VI-5) of the order of $5°C(12\ hr)^{-1}$, conduction may be neglected. If the shapes of the 75% black cooling rates can be trusted for normal lapse rates, it appears that radiative processes alone will produce a convective lapse rate any time $n_b \Delta z$ exceeds 10^6 crystals cm^{-2}. From the solid water content figures in Table IV-12, this corresponds to a total solid water content of 1.4×10^{-4} gm cm^{-2}. On the basis of commonly observed number densities, it is probable that many Fairbanks ice fogs are just at the point of transition from enhanced cooling rates through the fog depth to radiative cooling concentrated at the top of the fog. Thus a relatively small shift in the amount of fog in areas away from the main heat sources could produce a considerable change in the dynamics of the fog. An inversion will form just above the fog in all cases, as the cooling rate at the top of the fog invariably exceeds that in the clear air above.

3. The Fairbanks Heat Island

It is of some interest to calculate an equilibrium heat island temperature for Fairbanks under the following simplifying assumptions:

1. The air in Fairbanks is stagnant to the extent that it receives the full man-made heat contribution calculated in Chapter IV, Section F 2b. This does not exclude the possibility of air circulation within the city area.

2. The lapse rate in the ice fog layer is essentially isothermal (or adiabatic).

3. The net outgoing flux from the top of the fog layer equals the rate of heat addition by human activity.

4. The heat island is due entirely to the man-made heating and the fog. Differences in evapotranspiration and substrate thermal properties, which appear to be the major factors in heat island production in middle latitudes, are neglected. Evapotranspiration is negligible at -40°C with a fairly complete snow cover on the ground outside of town and on the roofs in town.

5. The downward flux at the top of the fog layer is the same as that at the undisturbed ground surface.

Let the ground temperature away from any ice fog be T_o, and the undisturbed net flux at the ground be F_o. The incoming flux will be $\sigma T_o^4 - F_o = F_-$. The foggy case is more complicated, but if the fog temperature is $T = T_o + \Delta T$ and the integrated reflectivity is r, then the net flux F at the fog top will be given by

$$F = (1-r)\sigma T^4 + rF_- - F_- = (1-r)(\sigma T^4 - F_-) \ . \qquad (6\text{-}9)$$

A value for r may be estimated by comparing the net fluxes at the fog top calculated from the black and scattering formulas; we assume that the difference between the calculated incoming fluxes is the same as at the ground without fog. (This difference was neglected in comparing the gray and scattering cooling rates.) Net fluxes without fog for the terminal ice fog sounding are 27.19 for the scattering formula and 31.54 for the black formula.* $F_{\downarrow}$ for the scattering formula is thus 4.35 cal cm^{-2} $(12\ hr)^{-1}$ more than that from the black formula. To obtain an accurate value for r, the soundings used should have isothermal fog layers. In that case (6-9) could be solved for $F_{\downarrow}$ in the black and scattering cases and the known difference between the two values of $F_{\downarrow}$ used to obtain r. The resulting equation is

$$r = 1 - \frac{F_{sca}}{F_{bla} - 4.35}$$

Application of this formula to a fog with a finite lapse rate is not strictly correct, as the effective temperature in (6-9) may differ for the scattering and non-scattering cases. As a first approximation, however, using the adiabatic gray case for $n_b = 500$ and a fog height of 50 m gives a value of r of

$$1 - \frac{55.8}{67.4 - 4.35} \approx .1$$

Returning to an isothermal fog layer and the initial assumptions, H_F is the man-made heating rate in flux units. Then

$$F_{\text{fog top}} = H_F, \text{ or}$$

$$(1-r)\ (\sigma T^4 - F_{\downarrow}) = H_F.$$

*This difference is probably accounted for by the neglect of ozone in the gray formula.

Applying the equation for F_-, we get

$$\sigma(T^4-T_o^4) = \frac{H_F}{(1-r)} - F_o \qquad (6\text{-}10)$$

Using the gray formula values for the area remote from the ice fog, ie, $F_o = 31.54$ and $T_o = 223°K = -50°C$, this may be written as

$$T^4 = 2.47 \times 10^9 + \frac{H_F}{(1-r)\sigma} - \frac{31.54}{\sigma}$$

or

$$T^4 = \left[1.93 + \frac{H_F}{5.848(1-r)} \times 10^{-1} \right] \times 10^9$$

For the core area, $H_F = 51$, the gray case (r=0) gives

$$T = 230°K = -43°C$$

while the scattering case (r=.1) gives

$$T = 232°K = -41°C$$

These values do not include the effects of cold air coming into the city from the surrounding areas. Nevertheless, they are in striking agreement with the coldest temperatures actually observed in downtown Fairbanks during ordinary ice fog events, and with the magnitude of the observed heat island (Benson, 1965). Note that the temperature at 2 m in our sounding, which would be measured as the undisturbed air temperature, is -44°C, not the -50°C surface value.

If the outlying area is in radiative equilibrium, the last term in (6-10) vanishes and the equilibrium temperatures in the core area are

$T = 240°K = -33°C$ for the black case

and

$T = 242°K = -31°C$ for the scattering case.

These should be near the maximum possible values for the 1965 heat addition figures.

The heat island actually observed will be controlled by the incoming flux, by the amount of air interchange with the surrounding area, and by the optical depth of the fog layer (which determines r).

As discussed in Chapter IV section F, any transport of cold air into the city from the outlying areas, either by net air motion or by mixing at the boundaries will have the effect of reducing the effective value of the man-made heat addition term. It is interesting to observe that the apparently unrealistic man-made heating rate of 65°C $(12\ hr)^{-1}$ can be balanced solely by the net flux at the fog top with a heat island which corresponds well with observed values. This indicates that the net air drainage through the city may be negligible.

D. Air Pollution Implications: A Natural Limitation on Industrialization

It should by now be evident that the effects of ice fogs observed in Fairbanks cover the range from a general enhancement of the cooling rate inside the fog layer (with the major cooling continuing to be by conduction and radiation to the snow surface) to the development, even without considering the effects of artificial heat sources, of an active convective layer in the fog and a steep inversion at the fog top. In all cases the lapse rate inside the fog will be less stable than in clear air in surrounding areas with similar topography. It is of

considerable interest to know what feedback effects these changes in the lapse rate will produce on further development of the fog.

A full elucidation of the feedback mechanisms would require observational data not currently available. In particular, there is very little quantitative data on mean wind vectors during an ice fog event in and around the area affected by ice fog, and virtually none on the temperature-height relationship in the foggy area. Also, there is no data on distribution of gaseous pollutants with height. Some wind data were collected during the winter of 1969-70. But most of these observations were made away from the core area, and there were no severe ice fog events during 1969-70. Plans are being made to obtain the necessary data, but at the present time only a very general discussion of probable effects is possible.

The lapse rate in the fog may affect the development of ice fog in the following ways: 1) it determines which pollution sources contribute to the ice fog, 2) it determines the depth of the layer of air available to dilute the pollutants, 3) it controls the amount of turbulence, which in turn affects both the rate at which small particulates such as ice fog crystals are removed and the upward growth of the fog layer, and 4) it creates boundaries which affect the interchange of air between the foggy and clear areas. Separate discussions of these factors follow.

1. Pollution Sources

As is well established in air pollution literature, the height of an inversion is as important a factor in determining the potential severity of an air pollution episode as is the inversion strength

(Strom, 1962). An inversion located several kilometers above the surface will have a negligible effect on local air pollution. A surface inversion, as is observed in light ice fog, will result in strong trapping of pollutants (including ice crystals) emitted at low levels, but will at the same time prevent pollutants released at higher levels from mixing downward. An inversion beginning slightly above the effective sources of most of the pollutants being released in an area will maximize the total amount of polluting material trapped, and will in most cases produce the maximum pollutant concentrations.

Benson (1965) observed that power plant plumes generally dissipated before blending with the fog layer. He also gave a maximum fog height of 50 m. As of 1965, the steepest part of the inversion was often below the effective stack height of most of the power plants in the area. More recently, however, the plumes have increasingly been observed to blend with the fog, and during the severe cold spell in December 1968-January 1969 individual plumes could not be distinguished in a fog layer 100 m deep. In this case there seems little room for doubt that the inversion had changed from a surface inversion to the type most significant for air pollution.

2. Dilution

If air movement through the Fairbanks area is unaffected by the presence of ice fog (see section VI-D-4 below) the volume of air available for dilution of pollutants is directly proportional to the depth of the layer through which they are mixed. If a strong inversion is established above the fog layer, this depth will correspond to the depth of the fog layer. In practice an increase in fog depth should lead to

decreased concentration of such pollutants as lead from automobiles, and an increase in any substances such as sulfur which are emitted primarily from stacks.

At the present time, the interaction of increased sources and increased dilution through any increase in the inversion height probably results in a greater ratio of air volume to pollutant input for higher inversions. However, any increased industrialization of the area, with the resultant increase in the emission of pollutants at height, would undoubtedly reverse this situation.

3. Convection

Benson (1965) pointed out that updrafts due to the city heat island would result in particles which would normally settle out having a net upward velocity. Even random turbulence will greatly enhance the residence time of small particles. According to List, Table 115 (1949) particles smaller than 1μ in diameter may be considered to be in permanent suspension in a calm atmosphere. In a disturbed atmosphere, however, the upper size limit for particles in suspension is 10μ. Since most ice fog crystals are in the diameter range 2 to 10μ, it is apparent that a convective lapse rate within the fog layer, with the accompanying thermal turbulence, may considerably reduce the crystal fallout and thus enhance the density of the fog. Such a density increase will in turn increase the difference in cooling rates at the top and bottom of the fog layer which drives the convection. Convective turbulence thus provides a positive feedback mechanism for fog densification once the threshold optical depth ($k \Delta z$) necessary to maintain a convective lapse rate is exceeded.

Once initiated, convection may also have a feedback effect on the height of an ice fog layer. A convective lapse rate is fundamentally one in which a parcel of air displaced vertically is accelerated in the same direction as the initial displacement. The acceleration stops at the top of the fog where the inversion begins, but the momentum of individual parcels of rising foggy air will carry them above the top of the fog layer. As a result, the fog layer will tend to grow vertically until growth upward is balanced by erosion from the top of the fog.

The effect of convection in any case is clearly to worsen the pollution, both by increasing the equilibrium concentration of ice crystals and by inhibiting any tendency the crystal fallout may have toward removing adsorbed pollutants.

4. Boundary Exchange

The exchange of air between Fairbanks and the surrounding area is very poorly understood, with or without ice fog. The basic air movement seems to be katabatic flow controlled almost entirely by topography, but a good deal of local eddying or back and forth motion with little net air motion appears also to be involved. The volume of air containing dense ice fog will be warmer near the ground and colder near the top of the fog than is the surrounding air at the same heights. The entire fog volume will be bounded by a domed inversion layer (Figure VI-1). The effect of such a disturbance in the temperature structure on the regional air flow is difficult to predict. There is at least a possibility that the fog mass might behave as another topographic feature, diverting relatively fresh air which would otherwise flow into the city area and even producing a ponding of the cold air draining from areas

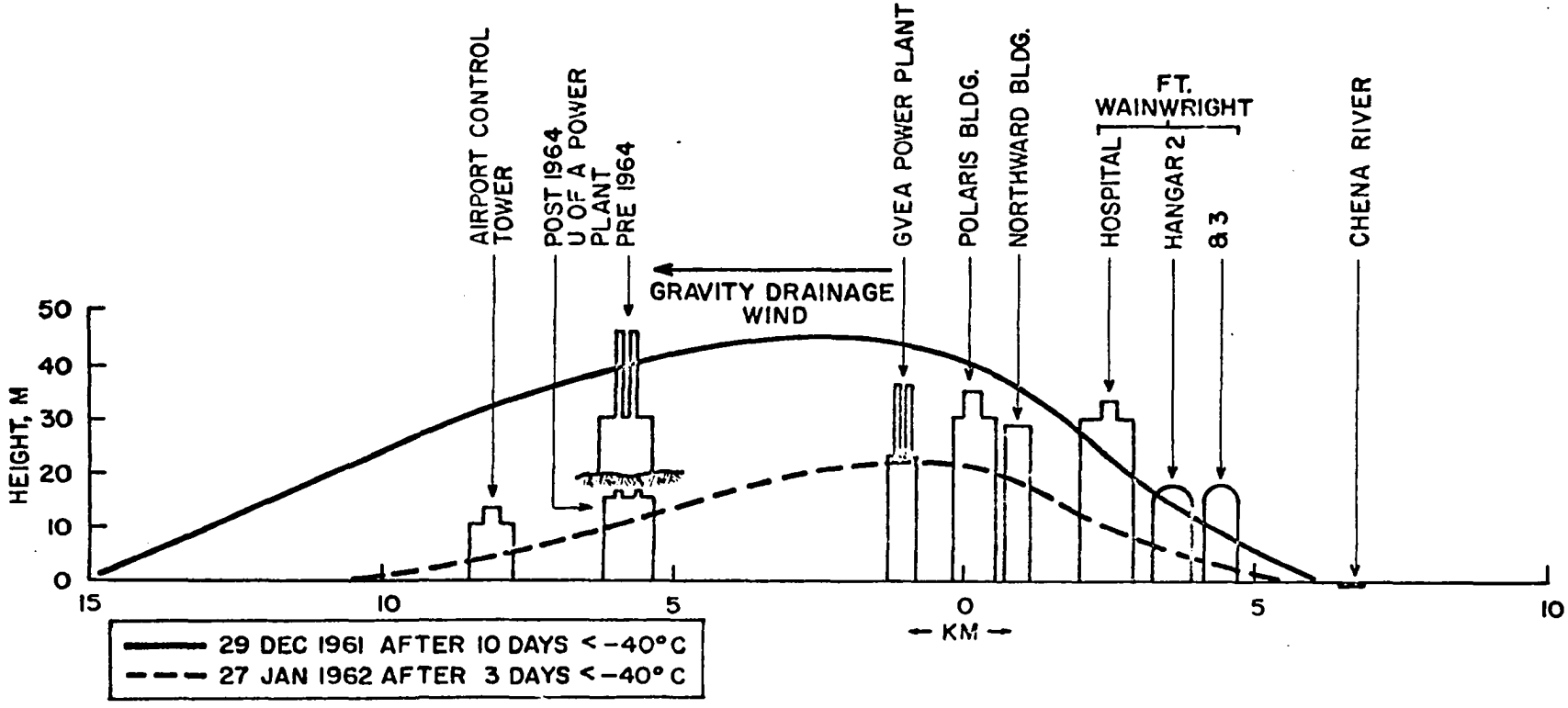

VI-1 Shape of the ice fog mass under moderate (dashed line) and fairly heavy (solid line) ice fog conditions. In most cases the volume within the fog will be nearly isothermal with a sharp inversion at the domed boundary from Benson (1965).

north and west of Fairbanks. There is some informal evidence that the temperature difference between the flats and the lower slope areas north of the city has decreased markedly in recent years, and it is possible that the ice fog may be responsible for the apparent lifting of the inversion in the clear air along the slopes. Much more data is needed before any firm conclusions can be drawn.

5. The Difference Ice Fog Makes

Perhaps the clearest way of emphasizing the overall effect of ice fog on the air pollution potential of the Fairbanks area is to compare the situations with and without ice fog. With moderately dense ice fog, the lapse rate will be convective in the fog layer with an inversion at the top of the fog layer. Man-made heating is balanced by radiation from the fog top. This temperature structure will concentrate any pollutants with effective release heights inside the fog layer. Since the fog height is also determined in part by the altitude at which water vapor is released, the fog top, and hence the confining inversion, will tend to stabilize just above the highest level of water vapor input. Thus one of the worst possible temperature structures for air pollution potential is produced automatically by the fact that the air cannot hold the water vapor released by human activities. On the other hand, radiation and especially scattering by ice crystals will also work to trap most of the man-made heat beneath the inversion, from which it will eventually be radiated away.

If all the water vapor normally released into the Fairbanks area were somehow eliminated without affecting the release of any other substances, the situation would be quite different. The strong ground

inversion normally formed under clear skies in winter at high latitudes would dominate the thermal structure. This would result in concentration of auto exhaust near the ground, while almost all other pollutants would be kept away from street level. The man-made heat addition term would have to be split into two fractions. Heat normally added by radiation from heated solid or liquid surfaces, which under ice fog conditions would be trapped by the fog, would be radiated directly outward without fog and for the most part lost to the area. Furthermore, this radiation would be from surfaces warmer than the fog top. Heat added in the form of heated gases would rise above the city while the gases were cooling due to radiation by the water vapor and CO_2 contained in them. If the volume of heated air were large, relatively clean air from the surrounding areas would constantly move in toward the core area to replace the rising air. Since enough heat would probably be added with such pollutants as car exhaust to weaken the city ground inversion somewhat, the inflow of cold, clean air would tend to lift even the automobile-polluted air above the street level.

In summary, radiation from ice fog crystals has two major effects. First, it produces one of the worst possible thermal structures for air pollution. It is questionable whether human beings could live through a severe ice fog event in a sizeable industrial city of middle latitudes if it were placed at the location of Fairbanks. Any major industrial development of the area will require serious consideration of this air pollution potential if Fairbanks is to remain inhabitable. On the other hand, the temperatures in downtown Fairbanks are probably a good deal warmer than they might be, due partly to the effects of ice fog in altering the surface radiation balance.

REFERENCES

Atwater, Marshall A., 1966, Comparison of Numerical Methods for Computing Radiative Temperature Changes in the Atmospheric Boundary Layer, J. of Appl. Met., v.5, pp. 824-831.

Benson, Carl S., 1965, Ice Fog - Low Temperature Air Pollution Defined with Fairbanks, Alaska as Type Locality, Geophy. Inst. Rep. UAG R-173.

Benson, Carl S. and George W. Rogers, 1965, Alaskan Air Pollution - the Nature of Ice Fog and its Development and Settlement Implications, Proceedings of the 16th Alaskan Science Conference, Juneau.

Bowling, S. A., 1967, A Study of Synoptic-Scale Meteorological Features Associated with the Occurrence of Ice Fog in Fairbanks, Alaska, M.S. Thesis, Univ. of Alaska.

Bowling, S. A., Takeshi Ohtake and Carl S. Benson, 1968, Winter Pressure Systems and Ice Fog in Fairbanks, Alaska, J. of App. Met., v.7, 961-968.

Brooks, Douglas Lee, 1950, A Tabular Method for the Computation of Temperature Change by Infrared Radiation in the Free Atmosphere, J. of Met., v.7, pp.313-321.

Brooks, F. A., 1952, Atmospheric Radiation and its Reflection from the Ground, Jour. of Met. v.9, pp.41-52.

Brunt, D., 1932, Notes on Radiation in the Atmosphere,I, QJRMS 58, pp. 389-418.

Chandrasekhar, S., 1960, Radiative Transfer, Dover, N.Y., 393 pp.

Deirmendjian, D., 1960, Atmospheric Extinction of Infra-red Radiation, QJRMS, v.86, pp.371-381.

Dines, L. H. G. 1931, Temperature Observations in Fog at Kew Observatory, The Meteorological Magazine, v.65, No. 780, pp.277-280.

Dobson, G. M. B., 1948, Some Meteorological Aspects of Atmospheric Pollution, QJRMS, v.74, No. 320, pp. 133-143.

Dwight, Herbert Bristol, 1961, Tables of Integrals and other Mathematical Data, 4th Ed. Macmillian Co., New York, 331 pp.

Elsasser, Walter M., 1943, Heat Transfer by Infrared Radiation in the Atmosphere, Havard Meteorological Studies #6, Milton, Mass. 107 pp.

Elsasser, Walter M., and Margaret F. Culbertson, 1960, Atmospheric Radiation Tables, Meteorological Monographs, v.4, No.23, A.M.S.

Fleagle, R. G., W. H. Parrott and M. L. Barad, 1952, Theory and Effects of Vertical Temperature Distribution in Turbid Air, J. of Met., v. 9, pp. 53-60.

Ford, Lester R., 1955, Differential Equations, McGraw Hill, New York, Toronto, London, xii + 291 pp.

Godson, Warren L., 1965, The Role of Radiative Flux Divergence in the Surface Boundary Layer, First Canadian Conference on Micromet. Toronto.

Goody, R. M., 1964, Atmospheric Radiation, I Theoretical Basis, Oxford, Clarendon Press, Oxford Monographs on Meteorology, 436 pp.

Griggs, M., 1968, Emissivities of Natural Surfaces in the 8-14 Micron Spectral Region, J.G.R. v. 73, pp. 7545-7551.

Grosheva, L. A., 1966, On the Influence of Radiation on the Transformation of Low Cloudiness. Leningrad Glavnaia Geofizicheskaia Observatoriia, Trudy No. 187 pp. 77-81.

Gotaas, Yngvar, and Carl S. Benson, 1965, The Effect of Suspended Ice Crystals on Radiative Cooling, J. App. Met. v. 4, No. 4, pp. 446-453.

Havard, Jesse Boyd, 1960, On the Radiational Characteristics of Water Clouds at Infrared Wavelengths, Ph.D. Thesis, Univ. of Wash., Seattle.

Henmi, Teizi, 1969, Some Physical Phenomena Associated with Ice Fog, M.S. Thesis, University of Alaska.

Henyey, L. G. and J. L. Greenstein, 1941, Diffuse Radiation in the Galaxy, Astrophy. Jour., 93, pp. 70-83.

Hewson, E. W., 1943, The Reflection, Absorption, and Transmission of Solar Radiation by Fog and Cloud, QJRMS, v. 69, pp.47-62.

Houghton, J. T., 1966, The Effect of Contamination on Spectroscopic Determinations of Stratospheric Water Vapour, QJRMS., 92, pp 281-283.

Huffman, Paul, 1968, Size Distribution of Ice Fog Particles, M. S. Thesis, University of Alaska.(see also Ohtake and Huffman, 1969).

Ingersoll, Andrew P., 1969, The Runaway Greenhouse: A History of Water on Venus, Jour. of the Atmos. Sciences, v.26, No. 6, pp. 1191-1198.

Irvine, William M., 1965, Multiple Scattering by Large Particles, Astrophy. Jour., v.142, 1563-1575.

Irvine, William M., 1968, Multiple Scattering by Large Particles, II. Optically Thick Layers, Astrophy. Jour. v.152, pp. 823-834.

Irvine, William M. and James B. Pollack, 1968, Infrared Optical Properties of Water and Ice Spheres, Icarus 8, pp. 324-360.

Jahnke, Eugene and Fritz Emde, 1945, Tables of Functions with Formulae and Curves, Dover, New York, 304+76 pp.

King, Jean I. F., 1968, Infrared Radiative Transfer in the Terrestrial Atmosphere, J. Quant. Spect. Rad. Transf. v.8, pp. 1-16.

Kondrat'yev, K. Ya., 1965, Radiative Heat Exchange in the Atmosphere, Pergamon Press, Oxford, 411 pp.

Kourganoff, V. 1952, Basic Methods in Transfer Problems: Radiative Equilibrium and Neutron Diffusion, Dover, N.Y., 281 pp.

Kraus, E. B., 1947, Note on Fog and Atmospheric Pollution, QJRMS. v.73, pp. 188-190.

Kuhn, P. M., M. S. Lojko and E. W. Petersen, 1969, Infrared Measurements of Variations in Stratospheric Water Vapour, Nature, v.223 pp.462-464.

Kuhn, William R. and Julius London, 1969, Infrared Radiative Cooling in the Middle Atmosphere (30-110 km), Jour. of the Atmos. Sciences, v.26, pp. 189-204.

List, Robert J., 1949, Smithsonian Meteorological Tables, Smithsonian Institution Press, Washington, 527 pp.

Moller, Fritz, 1951, Long-Wave Radiation, Compendium of Meteorology, American Met. Soc., Boston, Mass., pp. 34-49.

Murcray, Wallace B., 1963, Infrared Radiation from the Atmosphere over the Arctic Ocean, Science, v.141, pp. 802-804.

Murcray, D. G., F. H. Murcray and W. J. Williams, 1966, Further Data Concerning the Distribution of Water Vapour in the Stratosphere, Q.J.R.M.S., 92, pp. 159-161.

Myrup, Leonard O, 1969, A Numerical Model of the Urban Heat Island, J. of Appl. Met., v8, pp. 908-918.

Ohtake, Takeshi, 1970, Report on Ice Fog Crystals, Final Report AP-00449, Geophysical Institute, University of Alaska. (in press).

Ohtake, Takeshi and Paul J. Huffman, 1969, Visual Range in Ice Fog, Jour. of Applied Meteorology, v.8, pp. 499-501.

Petrova, L. V. and E. M. Feigelson, 1966, Radiative Heat Exchange for Developing Clouds, Izvestia (Eng.Edition) Academy of Science, USSR, Atm. & Oceanic Physics,v.2, No. 4, pp.205-213.

Pick, D. R. and J. T. Houghton, 1969, Measurements of Atmospheric Infrared Emission with a Balloon-Borne Multifilter Radiometer, Q.J.R.M.S., 95, pp.535-543.

Pollack, James B., 1969a, Temperature Structure of Nongray Planetary Atmospheres, Icarus 10, 301-313.

Pollack, James B., 1969b, A Nongray CO_2-H_2O Greenhouse Model of Venus, Icarus 10, 314-341.

Potter, John F., 1969, Effect of Cloud Scattering on Line Formation in the Atmosphere of Venus, J. Atm. Sciences, v.26, pp. 511-517.

Robinson, E., and G. B. Bell, Jr., 1956, Low-Level Temperature Structure under Alaskan Ice Fog Conditions, Bull. Am. Met. Soc.v.37, pp.506-513.

Rodgers, C. D. and C. D. Walshaw, 1966, The Computation of Infrared Cooling Rate in Planetary Atmospheres, Q.J.R.M.S.,v.92, pp. 67-92.

Sagan, Carl and James B. Pollack, 1967, Anisotropic Nonconservative Scattering and the Clouds of Venus, J G.R., v.72, pp. 469-477.

Sagan, Carl, 1969, Gray and Nongray Planetary Atmospheres: Structure, Convective Instability and Greenhouse Effect, Icarus v.10, pp.290-300.

Samuelson, R. E., 1965, Radiative Transfer in a Cloudy Atmosphere NASA Technical Report TR-215, Washington.

Samuelson, R. E., 1969, The Thermal Radiation Field Emitted by Anisotropically Scattering Cloudy Planetary Atmospheres, Icarus 10, pp.258-273.

Sekera, Zdenek, 1968, Radiative Transfer and the Scattering Problem, J. Quant. Radiat. Transf. v.8, pp. 17-24.

Shekhter, F. N., 1966, Several Questions on Thermal Radiation in a cloudy Atmosphere. Geofizicheskaia Observatoriia, Trudy, No. 187: 82-103,1966.

Simpson, G. C., 1927, Some Studies in Terrestrial Radiation, Memoirs of the Royal Meteorological Society, v.2, No. 16, pp.69-95.

Simpson, G. C., 1928a, Further Studies in Terrestrial Radiation, Memoirs of the Royal Meteorological Society, v.3, No. 21, pp. 1-26.

Simpson, G. C., 1928b, The Distribution of Terrestrial Radiation, Memoirs of the Royal Met. Soc. v.3, No. 23, pp. 53-78.

Sobolev, V. V., 1963, A Treatise on Radiative Transfer, Trans. by S. I. Gaposchkin, D. Van Nostrand, Princeton, 319 pp.

Strom Gordon H., 1962, Atmospheric Dispersion of Stack Effluents, Air Pollution v. I ed. Arthur C. Stern, Academic Press, N. Y. pp. 118-197.

Thuman, W. C. and E. Robinson, 1954, A Technique for the Determination of Water in Air at Temperatures below Freezing, J. of Meteorology 11, 214-219.

Van de Hulst, H. C., 1957, Light Scattering by Small Particles, New York, John Wiley & Sons.pp470.

Weller, Gunter E., ed. 1969, Ice Fog Studies in Alaska, UAG R-207. Geophysical Institute, University of Alaska.

Wendler, Gerd, 1969, Heat Balance Studies during an Ice Fog Period in Fairbanks, Alaska, Monthly Weather Review, v.97, pp. 512-520.

Wexler, H., 1936, Cooling in the Lower Atmosphere and The Structure of Polar Continental Air, Monthly Weather Review, v.64, No. 4.

Yamamoto, Giichi, 1952, On a Radiation Chart, Science Reports of the Tohoku University Fifth Series (Geophysics), v. 4,pp. 9-23.

Yamamoto, Giichi and Gaishi Onishi, 1953, A Chart for the Calculation of Radiative Temperature Changes, Science Reports of the Tohoku Univ. Fifth Series (Geophysics), v. 4, pp. 108-115.

Zdunkowski, W., D. Henderson and J. V. Hales, 1965, The Influence of Haze on Infrared Radiation Measurements Detected by Space Vehicles, Tellus, v. 17, No. 2, pp. 147-165.

Zdunkowski, Wilford, Donald Henderson, and J. Vern Hales, 1966, The Effect of Atmospheric Haze on Infrared Radiative Cooling Rates, J. Atm. Sciences, v. 23, pp. 297-304.